Mechanisms of epileptogenesis in animal models of developmental brain lesions

Dissertation

zur
Erlangung des Doktogrades (Dr. rer. nat)
der
Mathematisch-Naturwissenschaftlichen Fakultät
der
Rheinischen Friedrich-Wilhelms-Universität Bonn

vorgelegt
von

Barbara Karoline Robens
aus
Kattowitz

Bonn, 2016

Angefertigt mit Genehmigung der Mathematisch-Naturwissenschaftlichen Fakultät der Rheinischen Friedrich-Wilhelms-Universität Bonn

1. Gutachter: Prof. Dr. Albert Becker

2. Gutachter: Prof. Dr. Albert Haas

Tag der Promotion: 18.11.216

Erscheinungsjahr: 2016

Eidesstattliche Erklärung

Diese Dissertation wurde im Sinne der Promotionsordnung vom 17.06.2011 am Institut für Neuropathologie der Universität Bonn unter der Leitung von Prof. Albert Becker angefertigt.

Hiermit versichere ich, dass ich die vorgelegte Arbeit selbstständig und ohne unzulässige Hilfe Dritter gemäß der Promotionsordnung vom 17.06.2011 verfasst habe. Nur die angegebenen Quellen wurden in dieser Arbeit genutzt. Abschnitte die direkte Zitate enthalten, wurden als solche gekennzeichnet.

Alle elektrophysiologischen Messungen wurden von Robert Maresch durchgeführt. Die Analyse der elektrophysiologischen Daten erfolgte durch Robert Maresch und Tony Kelly aus dem Institut für experimentelle Epileptologie von Prof. Heinz Beck der Uni Bonn. Die Resultate wurden mit deren Genehmigung in dieser Arbeit verwendet.

Abbildung 2.2 wurde von Prof. Albert Becker aufgenommen und mit seiner Genehmigung in dieser Arbeit verwendet.

Einige Teile dieser Arbeit wurden bereits in Form von wissenschaftlichen Fachartikeln veröffentlicht und entsprechende Abbildungen wurden in dieser Arbeit ebenfalls verwendet:

Robens, B, Grote, A, Pitsch, J, Schoch, S, Cardoso, C, & Becker, A. J. (2016) Minute amounts of hamartin wildtype rescue the emergence of tuber-like lesions in conditional Tsc1 ablated mice. Neurobiology of Disease.

Ort, Datum	Barbara Karoline Robens

Contents

1 Summary

Developmental brain lesions, including glioneuronal tumors (GNT) and malformations of cortical development (MCD), are among the most common causes for pharmaco-resistant epilepsy. Despite substantial differences, their shared major hallmark are dysplastic neurons characterized by abnormal dendritic arborization. However, the exact molecular mechanisms underlying dysplastic neurons and epileptogenesis in these devastating disorders are still largely unknown. This lack in our knowledge significantly hinders the development of novel therapeutic approaches. Therefore, the goal of this study was to gain more insight into various aspects of the pathogenesis of tuberous sclerosis (TSC), focal cortical dysplasia type IIb (FCDIIb) and gangliogliomas (GG) with an emphasis on the mechanisms underlying the emergence of dysplastic neurons.

We generated a mouse model for developmental brain tumors by embryonic, focal p53 knockout as well as BRAF-V600E and Akt expression. Our first finding is that a compromised progenitor cell population is sufficient to induce GG resembling tumors harboring dysplastic neurons. As of yet, there were no GG animal models available, thus our mouse model provides an excellent basis for future in depth analysis of these complex tumors as well as potential drug testing.

In a second experimental setup we analyzed the so far unclear pathogenetic mechanisms underlying the formation of cortical tubers, a hallmark of TSC. These are composed of large dysplastic neurons and giant cells that are histomorphologically virtually indistinguishable from abnormal cells found in FCDIIb lesions. We found that developmental expression of TSC-associated mutations, but not the FCDIIb-associated allelic variants, of the tuberous sclerosis complex1 (*TSC1*) gene results in the formation of dysplastic neurons in mice. Respective TSC1-silenced cortical neurons expressing the mutated *TSC1* gene product hamartin^{R692X} or hamartin^{R786X} showed cellular features reminiscent of dysplastic neurons, stressing their pathogenic potential. Intraventricular *in utero* electroporation (IUE) of *TSC*1-R692X and varying concentrations of wildtype *TSC1* revealed that already minimal amounts of functional hamartin are sufficient to prevent the emergence of dysplastic neurons from tuber-like lesions. This strong rescuing capacity stresses substantial silencing of both *TSC1* alleles as critical pathogenetic mechanism for the manifestation of cortical tubers and provides a promising basis for gene therapy approaches.

Our next finding suggests loss of the cytoskeleton regulating protein Ste20 like kinase (SLK) as a common pathological event in the emergence of dysplastic neurons across distinct glioneuronal lesions. We find reduced SLK protein levels in dysplastic neurons of highly epileptogenic FCDIIb and GGs. Accordingly, shRNA mediated *SLK* silencing in developing cortical neurons results in impaired neurite growth and arborization of higher order dendrites together with a progressive and selective loss of inhibitory synapses in mice older than 15 days. A functional impairment of neuronal inhibition was reflected by a higher propensity for chemically evoked epileptic seizures. These results indicate SLK loss as a key

factor underlying the development of dysplastic neurons and, hence, as a contributor to the emergence of hyperexcitability in epileptogenic brain lesions. Our data suggest, that the SLK mechanistic pathway is in part regulated by the upstream LIM-domain binding (LDB) proteins, transcriptional co-activators with reduced expression in the abnormal neuronal component of GGs. *LDB1* and *LDB2* knockdown in developing mouse neurons results in a reduction of neuronal arbor morphology, reminiscent of dysplastic neurons, that is rescued by SLK overexpression but not *vice versa*.

The present study provides novel insights into the mechanisms of epileptogenesis and the emergence of dysplastic neurons in glioneuronal brain lesions, setting the stage for the development of targeted treatment methods and drug testing.

2 Introduction

Epilepsy is a syndrome characterized by unpredictable, recurrent seizures affecting approximately 50 million people of all ages and is therefore regarded as one of the most common neurological disorder worldwide [1, 2]. It is a spectrum disorder with a wide range of causes as well as seizure types that can vary greatly in frequency and severity [3, 4]. Seizures are commonly regarded as the result of a transient, abnormal, excessive or synchronous neuronal activity in a population of neurons [4, 5]. Up to 60% of patients have focal epilepsies from which around 30% are pharmaco-resistant, probably due to the multiple underlying pathogenetic mechanisms [6]. Epilepsy can be classified by etiology as symptomatic, idiopathic or cryptogenic epilepsy [7]. Among these, developmental brain lesions are the most common causes for drug-resistant, focal, symptomatic epilepsy frequently diagnosed in children and young adults [8–12]. They are characterized by locally restricted loss of cortical lamination, abnormal cell growth and differentiation [8, 11, 13–23]. Within this group of glioneuronal brain lesions two major forms can be distinguished: The neoplastic glioneuronal tumors (GNT) and the non-neoplastic malformations of cortical development (MCD) [24]. Even though their molecular-genetic basis is diverse and pathologic mechanisms are far from completely understood, some similarities have been identified. The major shared functional, pathological feature of the extremely epileptogenic GNT and MCD are dysplastic neurons. As these neurons or their emergence may have a key role in epileptogenesis and thus, for severe drug-resistant epilepsy, they are particularly interesting as a basis for new therapeutic strategies [24]. Uncovering the mechanisms underlying their formation and hyperexcitability will increase our knowledge of epileptogenesis possibly common among glioneuronal lesions and help to identify therapeutic targets. The gradual process whereby the brain develops recurrent seizures that become more frequent and severe is referred to as epileptogenesis [25, 26]. More precisely, epileptogenesis is defined as "... the development and extension of tissue capable of generating spontaneous seizures, resulting in a) development of an epileptic condition and/or b) progression of the epilepsy after the condition is established" [27, 28]. Thus, during this process changes occur in the structure and physiology of the brain that result in the development of epilepsy. Even if these changes are poorly understood they are thought to include reorganization of neuronal networks, reorganization of the molecular architecture of individual neurons, aberrant release of neurotransmitters and inhibition/excitation imbalance, abnormal neurogenesis, axonal sprouting, inflammation and cell death [1, 29].

Surgical resection of the lesion is currently the treatment of choice for medically intractable epilepsy [30–32], but is often due to perilesional pathologic changes of the brain no cure to epilepsy [32–36]. To overcome these known limitations of modern medicine, new treatment options need to be identified. Therefore, determining mechanisms of disease development that include the emergence of dysplastic neurons is indispensable for the development of effective and targeted therapy strategies.

2.1 Glioneuronal tumors

GNTs can be classified as a subgroup of long-term epilepsy associated tumors (LEAT), a term recently introduced by Luyken et al. [11, 37]. LEATs are low grade tumors, characterized by slow growth and they are mostly located in cortical areas, especially in the frontal and temporal lobe [11]. By definition these tumors are mostly diagnosed in young patients with a history of drug-resistant epilepsy for more than two years [11, 24, 37]. Drug-resistant complex partial seizures are often the only clinical manifestation [24]. The two most common forms of LEAT are the GNT gangliogliomas (GG) and dysembryoplastic neuroepithelial tumors (DNT) [38].

2.1.1 Gangliogliomas

GGs are the most common neoplastic tumors causing chronic focal epilepsy [11, 13, 37–39]. They are highly differentiated, benign tumors composed of a mixture of dysplastic neurons and a proliferative glial component [40]. Most GGs are WHO grade I neoplasms and their benign character allows a favorable prognosis after surgical resection and seizure freedom. To avoid uncontrolled seizures and morbidity or the rare risk of malignant transformation, lesionectomy is recommended early after diagnosis [38]. However, resection of the tumor itself is often not sufficient for seizure freedom, due to epileptogenic peritumoral changes [32–36]; e.g. excitatory and inhibitory pathways were shown to be altered in the perilesional cortex. In some cases also focal cortical dysplasias (FCDs), that were reported to coexist with GGs, are responsible for persisting seizures after surgical removal of the tumor [11, 13, 41].

Histologically, GGs can be differentiated from other tumors by Haematoxylin and eosin (HE) staining, revealing nodular or compact aggregates of dysplastic neurons with overt ganglioid morphology with often enlarged, distorted somata and prominent Nissl substance as well as a vesicular nucleus which is often bi- or multi-nucleated [11, 42]. Typically, GGs are positive for the neuronal markers chromogranin A, neurofilament and MAP-2 but not NeuN and show a strong perisomatic synaptophysin staining [42]. In 80% of GGs cases abnormal appearing neurons are surrounded by precursor cell marker CD34 underlining the developmental origin of GGs [42]. Still, no specific marker was found to differentiate dysplastic from normal neurons, therefore, these cells are usually identified by their abnormal size or shape [13] (Fig 2.2 c, d). The neoplastic glial portion, consisting of astrocytes and in part oligodendrocytes is found in varying proportion and distribution [13].

2.1.2 Pathogenesis of gangliogliomas

Until today pathomechanisms leading to GG formation and focal hyperexcitability remain uncertain, though many theories have been hypothesized. The differentiated biphasic glioneuronal architecture, focal nature, coexistence of FCDs and the presence of the CD34 stem cell marker colocalizing with glial cells and neurons underlines the immature phenotype of the tumor cells and the developmental origin of GGs [8, 11, 13, 14, 24, 42]. Furthermore, alterations in pathways critical for cell size and growth control, cortical development and neuronal migration, have been reported. These findings point to a compromised or dysplastic precursor lesion with subsequent neoplastic transformation due

to a second hit in the glial component [13, 15, 16, 40]. However, they also allow for a second theory, as GGs may as well arise from a single neoplastic progenitor cell harboring somatic mutations that gives rise to neuronal and glial cell types [43]. Thus, the resulting tumor cells are monoclonal in origin and subsequently differentiate to form neoplastic glial and dysplastic neuronal elements. Nevertheless, abnormal, dysplastic and hyperexcitable neurons within the lesioned cortex are considered to provoke synchronized discharges and hence, to be responsible for epileptic seizures. In addition to the peculiar cellular composition, tumor size, location, and peritumoral changes contribute to epileptogenesis [24].

Mutational events have been suggested as a possible cause for GGs. A systematic analysis of two key players in the reelin pathway, doublecortin (DCX) and cyclin-dependent kinase 5 (CDK5), revealed no mutations in these genes but reduced expression [44–46]. These proteins play important roles in neuronal development, cellular migration processes and modification of the cytoskeleton, thus, their reduced expression may explain GG formation [40]. Reduced expression of several other genes was further demonstrated by microarray analysis of GG tissue compared to adjacent tissue. In theses studies the authors found altered expression of mRNAs encoding proteins involved in regulation of the chromatin state, intracellular signal transduction, inflammation, cell adhesion, cell cycle and proliferation, development and differentiation [47–49]. One of the most reduced transcripts in GGs in one of these studies was LDB (LIM-domain-binding) 2. It is a transcriptional co-activator that interacts with the LIM-HD (LIM-homeodomain) proteins and LIM-only proteins [47]. Their interaction was shown to be important for neuronal development [50].

Only recently the activating mutation of the BRAF (proto-oncogene B-Raf or v-Raf murine sarcoma viral oncogene homolog B1) oncogene on position V600 was detected in more than 50% of GGs [51, 52]. BRAF is a member of the Raf (Rapidly accelerated fibrosarcoma) family of serine/threonine protein kinases and is a key molecule in the mitogen-activated pathway that regulates a variety of cellular functions, such as proliferation, cell-cycle arrest, terminal differentiation, and apoptosis [53]. Mutated BRAF-V600E is associated with high pS6 (phosphorylated ribosomal protein S6) immunoreactivity [24, 54], a protein that is phosphorylated upon mammalian target of rapamycin (mTOR) activation. Subsequent experiments demonstrated that in BRAF-V600E mutated cells, BRAF signaling leads to activation of downstream proteins and results in excessive mTOR activity [55, 56].

The mTOR pathway is a highly conserved signaling cascade that integrates information from multiple sources in response to cues from nutrient and energy levels, growth factors, synaptic activity, maturity or senescence (see Figure 2.1) [17]. Key molecules in the mTOR pathway include Akt (protein kinase B; PKB), PI3K (phosphatidylinositol 3-kinase), PTEN (phosphatase and tensin homolog) and LKB1 (liver kinase B1). They modulate the downstream tumor suppressor complex containing the *TSC1* and *TSC2* gene products hamartin and tuberin, which in turn inhibit mTOR kinase activity [57]. Active mTOR leads to phosphorylation of various downstream molecules including S6K1 (ribosomal protein p70S6 kinase 1), S6 (ribosomal S6 protein), or 4E-BP (eukaryotic translation initiation factor 4E binding protein 1). Their activation regulates cell growth, proliferation, differentiation, metabolism and ion channel-, neurotransmitter, and receptor expression [58, 59]. Accordingly, pathologies with mTOR hyperactivation, also referred to as “mTorpathies” [60], share similar characteristics such as abnormal cell size, differentiation, proliferation and epileptic seizures [58, 59, 61–64]. These mTorpathies include not only GGs but also FCD and TSC (see more details in chapter 2.2.3). Furthermore, numerous acti-

vating mutations or aberrant activation of other proteins that result in excessive mTOR activity have been associated with these disorders [16, 65–68]. Thus, hyperactivated mTOR signaling represents a feature that may be regarded as a pathogenic link between these diverse disorders. However, their molecular pathogenesis and possible common pathologies have only recently begun to be elucidated. Several open questions remain to be answered as deregulation of the mTOR pathway is certainly only one aspect in the pathology of these complex disorders.

Somatic BRAF-V600E mutations were already known in several other tumors, including melanomas and malignant gliomas [66] and specific BRAF-V600E inhibitors (e.g. Vemurafenib) are currently in clinical trials for treatment of these pathologies [69]. This demonstrates that a more detailed knowledge of pathogenetic mechanisms underlying lesion formation is crucial to enable more targeted therapeutical approaches.

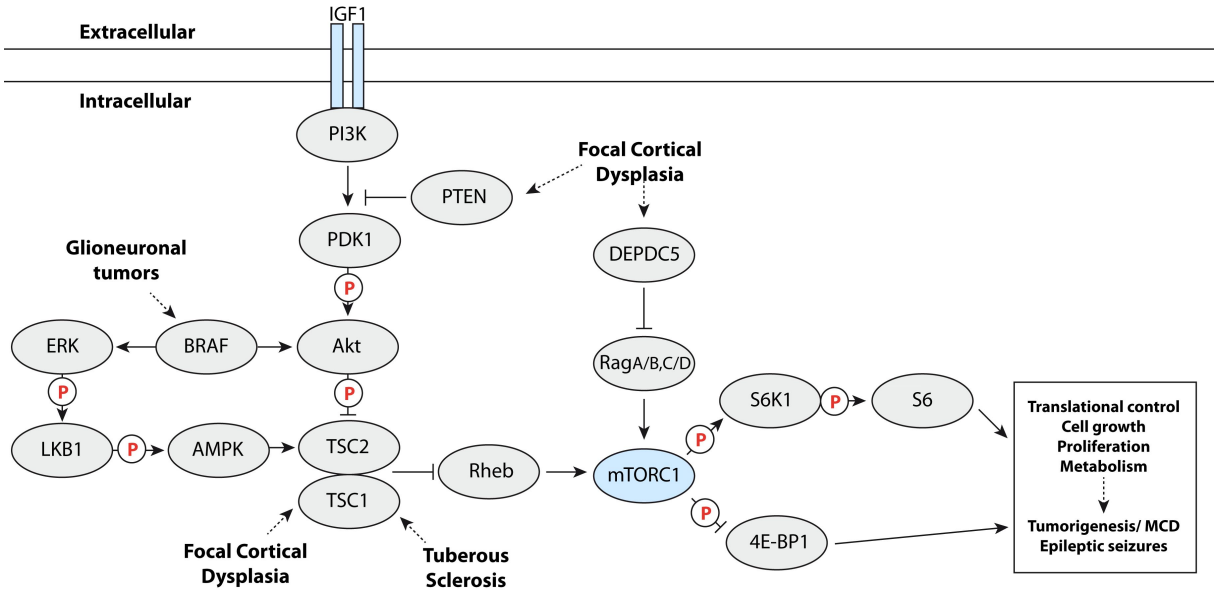

Figure 2.1: **Overview of the mTOR pathway.** The mTOR pathway integrates various signals from extracellular cues that activate the IGF1 tyrosin-receptor kinase. As a result, the mTOR complex 1 (mTORC1) is either activated by the PI3K/PDK1/Akt pathway or by the BRAF/ERK/LKB/AMPK pathway via modulation of the TSC1/TSC2 complex and Rheb GTPase. Activation of the DEPDC5 (DEP domain containing protein 5) pathway inhibits mTOR kinase activity. This leads to regulation of mTOR downstream targets including S6K1, S6, 4E-BP1, which control among other processes protein biosynthesis, cell growth, proliferation and metabolism. Mutations in some of these genes have been implicated with either GNT, FCD and/or TSC by disturbing mTOR mediated cellular control mechanisms. These alterations result in pathological changes including tumorigenesis, malformation of cortical development or epileptic seizures.

2.2 Malformations of cortical development

MCDs, sometimes also referred to as disorders of cortical formation or developmental cortical malformations, represent a complex, inhomogeneous group of brain disorders and are one of the most common non-neoplastic entities in pediatric epilepsy [70]. Besides refractory, pharmacoresistant epilepsy comprising 25 - 40% of all drug-resistant childhood epilepsies, patients suffer from developmental delay, cognitive impairment as well as motor and sensory deficits [71, 72]. Typically formation of MCDs is thought to occur during embryogenesis as a consequence of a disruption of uncertain cause in at least one of the three crucial periods of cortical ontogenesis: cell proliferation, neuronal migration or

post-migrational cortical organization. These disruptions result in abnormal cells and structure of the cortex [12, 73]. The most common forms of MCD include focal cortical dysplasia (FCD), tuberous sclerosis (TSC), double cortex syndrome, lissencephaly, and hemimegalencephaly [73]. FCD and TSC are prototypic examples of MCDs caused primarily by disruptions in proliferation and differentiation of early glio-neuronal precursor cell populations [74], however, such early disturbances may also affect subsequent developmental stages of cortex formation.

2.2.1 Focal cortical dysplasia (FCD)

The International League Against Epilepsy (ILAE) proposed a classification system based on histopathological features sub-classifying isolated and associated forms of FCD into type I, II, and III [75]. Isolated FCD type I is characterized by alterations in cortical lamination often causing severe epilepsy with early seizure onset and psychomotor retardation in young patients [76]. Depending on the pattern of cortical delamination three subtypes are distinguished FCDI a – c. FCDII cases include both, cortical dyslamination and cytoarchitectural abnormalities and the presence of dysplastic neurons in FCDIIa and additionally balloon cells in FCDIIb. Dysmorphic neurons with their abnormal shape, size and orientation are immunohistochemically visualized by HE (Fig. 2.2a, b) [76]. Most balloon cells have multiple nuclei and are positive for glial markers vimentin, GFAP-δ, but also for CD34 or the stem cell markers Pax6, ER81 and Otx1 [21], demonstrating that these cells have immature neuronal and glial features [10]. Both FCDII types exhibit the most severe cytological alterations, i.e. strong enlargement of cells and dysmorphism [10]. The clinical phenotype depends strongly on age and onset of seizures as well as the cortical location of the lesion. FCD type III represents the combination of FCD together with epileptogenic principal lesions.

2.2.2 Tuberous sclerosis (TSC)

TSC is a multi-organic, autosomal, dominant syndrome with a highly variable phenotype and an incidence of one in 6000 people. Currently approx. one million individuals worldwide are affected [77, 78]. Common symptoms are hamartomas or benign tumor-like growths in multiple organ systems including skin, eyes, heart, kidneys, lungs and the brain. In the brain hamartomas are referred to as cortical tubers, the hallmark of TSC. They occur in nearly all patients and represent the major clinical burden. About 90% of affected individuals suffer from severe epilepsy that is drug-resistant in two-thirds of those individuals [79, 80]. Cortical tubers are developmental brain malformations that are formed at around week 10 or 20 of human gestation in one or more focal areas of the temporal or frontal region of the cerebral cortex [81]. They are believed to be the epileptogenic foci [77]. Histopathologically tubers are characterized by loss of normal cortical layering and composed of heterogeneous cell types. These include dysmorphic neurons with abnormal axonal and dendritic patterns, large giant cells (GC) and proliferative astrocytes with aberrant morphology, processes and enlarged cell body [82–85]. GCs are histologically indistinguishable from balloon cells in FCDIIb lesions. Both exhibit strong enlargement of the cell body [75] and express neuronal and immature glial markers. These findings indicate a failure to differentiate before migration to the cortex [83].

2.2.3 Pathogenesis of focal cortical dysplasia & tuberous sclerosis

Both, cortical tubers and FCDIIb share remarkably similar histopathological features, which has inspired scientist to find a pathogenetic link between these two entities. Enlarged and dysplastic cellular components in TSC, FCD and even GGs are united by abnormal mTOR pathway activation, that indicates a common underlying pathogenesis in these distinct lesions [18, 19, 23]. Therefore, the identification of the exact pathogenetic and/or molecular mechanisms responsible for lesion formation or epileptogenesis is critical as they may serve as a substrate for new treatment options for multiple disorders [24, 86].

The exact causes of FCD are not known. Environmental insults were considered as potential FCD causes, however, FCD is often unilateral indicating that rather somatic de novo mutations play a role in their formation [86, 87]. In fact, several individual genes up- or downstream of the mTOR cascade were demonstrated to be mutated or differentially activated not only in FCDIIb but also cortical tubers: Akt, PDK1, PTEN, eIF4G, S6, DEPDC5 [18, 19, 88–91] (see Fig. 2.1). Furthermore LOH or various allelic variants of *TSC1* have been found in FCD patients, suggesting that *TSC1* deregulation and thus aberrant mTOR activation accounts for cellular abnormalities [10, 92, 93]. In FCDIIb patients a *TSC1* allelic variant with a base transition from C to T (2415C to T; His732Tyr) on exon 17 was more frequently found than in control patients [94]. *In vitro* expression of this *TSC1* variant was shown to impair binding of the *TSC1* gene product hamartin to the *TSC2* gene product tuberin potentially resulting in defective tumor suppressor function [93].

In TSC patients the pathogenetic mechanisms are, compared to FCDs better understood. Inactivating mutations in one of the TSC genes, *TSC1* or *TSC2*, coding for hamartin or tuberin respectively, are found in 75-90% of cases [95–98]. Loss of the TSC1/2 tumor suppressor function results in mTOR pathway activation as cause for the formation of the hyperexcitable brain lesion. More than 1000 unique allelic variants with nonsense-, missense-, insertion-, and deletion mutations of *TSC1* or *TSC2* in nearly all exons have been reported [99–103]. In particular, two truncating *TSC1* mutations were frequently found in different cohorts of TSC patients, *TSC*1-R692X and *TSC1*-R786X [101, 103, 104]. The expression of the truncated TSC1 mutants *in vitro* induced binding deficits of hamartin with tuberin and resulted in an abnormal subcellular distribution of the mutated hamartin. These experiments suggest functional impairment of the hamartin/tuberin tumor suppressor complex and thus abnormal mTOR activity [93].

On average, somatic and germline *TSC2* mutations are 3.4 times more common than *TSC1* mutations and often correlated with a more severe clinical phenotype [103, 105]. Even though *TSC1/2* mutations were not found in all TSC patients, it is now assumed that large deletions, somatic mosaicism, or technical limitations account for the rest of patients with no mutation identified [98, 106]. However, there is still debate about the pathogenetic situation of focal cortical tubers and no consensus on the mechanism of cortical tuber formation. Loss of heterozygosity (LOH) has often been observed in extra-cerebral hamartomas [107] or TSC-associated tumors, but only rarely in cortical tubers [108]. Single giant cell sequencing revealed that cortical tubers harbor both germline and somatic mutations, thus supporting a biallelic gene inactivation or a somatic "second hit" event as a potential cause [109–111]. Focally introducing a "second hit" in a *TSC1* heterozygous mouse model resulted in cellular abnormalities reminiscent of theses seen in tubers [112]. In fact, no cortical tubers were found in mice heterozygous for *TSC1* [113–115]. In direct contrast to these findings another group found by deep sequencing of ge-

nomic DNA from whole tubers that "second hit" events in *TSC1* or *TSC2* are rare [116]. Furthermore, the TSC pathway seems to be highly sensitive to gene dosage effects since haploinsufficency impairs neuronal morphology [117]. Thus, further investigation is required to uncover the pathogenetic situation leading to tuber formation.

2.3 A unifying pathological feature of GGs, FCDIIb, and TSC: Dysplastic neurons

Neoplastic gangliogliomas and non-neoplastic lesions from focal cortical dysplasias or tuberous sclerosis patients are quite different in several regards, but as already indicated in chapter 2.2.3 certain similarities exist as well. Among the severe hyperexcitability, histological as well as structural similarities, dysplastic neurons are a striking unifying pathological feature of these glioneuronal lesions [24]. As these dysmorphic neurons are a key morphological hallmark, it remains an open question whether they are the functional substrate conveying the severe drug-resistant epileptic phenotype. Dysplastic neurons are characterized by abnormal dendritic arborization, cytomegaly, sometimes bi- or multinucleation and their abnormal localization and clustered appearance within the cortex [13] (Fig. 2.2). In the context of cytomegaly, deregulation of the mammalian target of rapamycin (mTOR) pathway is frequently reported in dysplastic neurons among the spectrum of glioneuronal lesions [24]. Even though dysplastic neurons are the common key cell type of developmental brain lesions, the molecular mechanisms leading to their emergence or hyperexcitability remain largely unresolved.

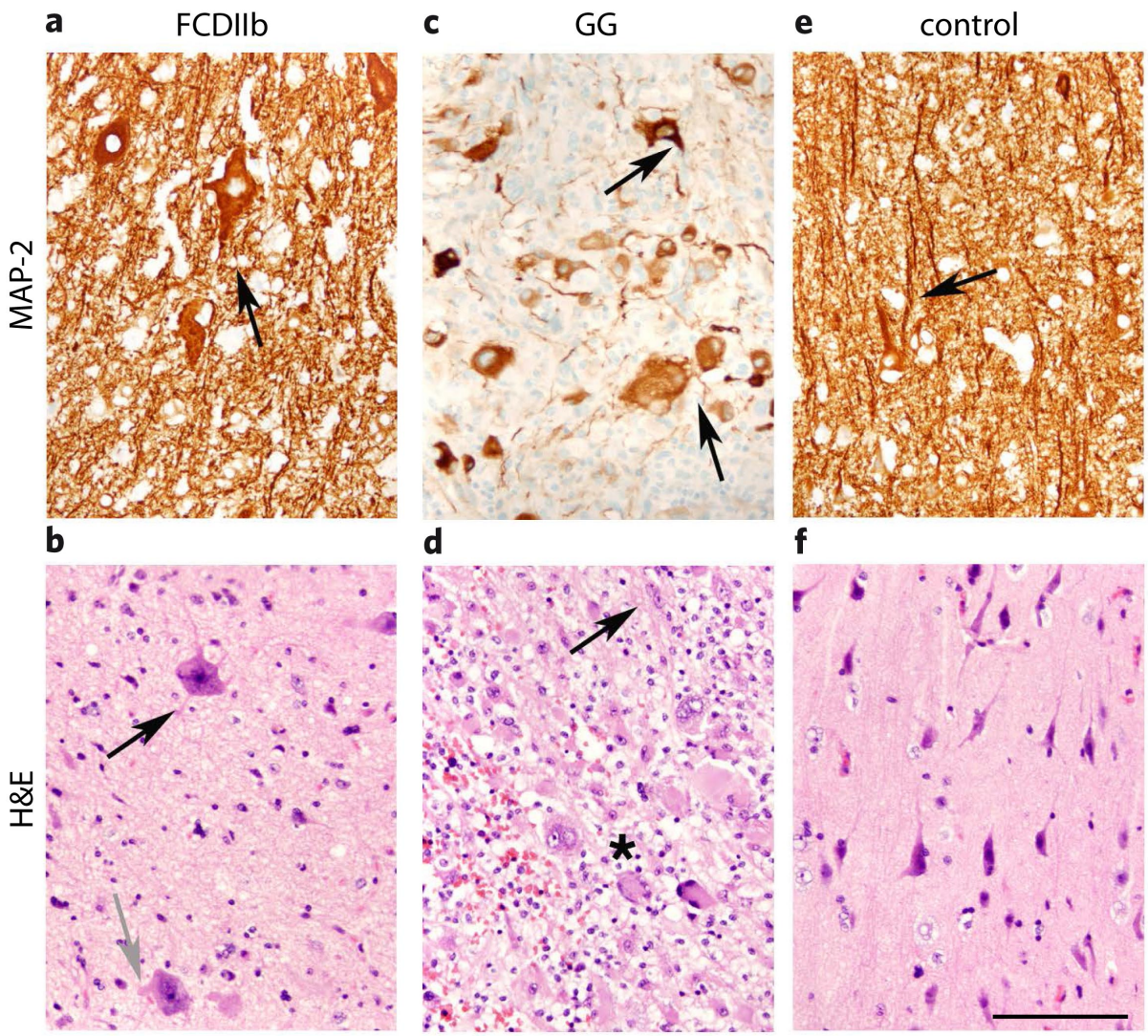

Figure 2.2: **Dysplastic neurons in FCDIIb and GGs.** Human FCDIIb and GG specimens were stained with antibodies against MAP-2 or HE. (a, b) Dysplastic neurons are large, irregularly oriented and have abnormally thin (black arrow) or strong processes (grey arrow). (c, d) They are highly enlarged and present with shortened processes with aberrant, varying diameter (black arrow). Dysplastic neurons often appear clustered (asterisk) and bi-nucleated (black arrow). (e, f) In contrast, normal cerebral cortical structures harbor neurons with clear organoid organization and delicate processes (black arrow). Scale bar 100µm. Image courtesy of Prof. Albert Becker.

2.4 Animal models for GGs, FCDIIb, and TSC

In order to study developmental brain lesions or test potential therapeutics, numerous attempts to generate adequate animal models have been made over the past decades. However, there is still no good animal model to reproduce FCD with all its traits including lamination defects and varying cellular abnormalities. Several different approaches exist to induce FCD-like lesions by disruption of cell proliferation, excitotoxicity or environmental injuries in embryonic or newborn rodents (see table 2.1 for details and references; table modified from [118]). Even though most of these models replicate abnormal cortical lamination and heterotopic and/or dysmorphic neurons, a major downside is that they have a low incidence of spontaneous seizures (10-20% of all animals).

More recently also genetic models have been demonstrated to induce FCD-like lesions. Most of them include mutations affecting the mTOR pathway that have been linked to FCD such as *Pten* and *Tsc1/2 [10, 92, 93, 119].* But also alterations in other genes unrelated to mTOR were found aberrantly expressed in FCDs, such as *Lrp12* (low-density lipoprotein receptor-related protein 12), a protein associated with formation of the cortical plate, neuronal polarity, migration and growth control [120]. Even though most of these animal models exhibited spontaneous seizures, the cellular abnormalities were not spatially restricted to a certain cortical area, a key hallmark of FCD. However, since our knowledge of FCDs is rather limited and there are no ideally suited animal models that precisely replicate all FCD features, the TSC mouse model is currently the best model to study epileptogenesis in MCDs [24, 121].

Table 2.1: Mouse models of FCD

FCD model	Epilepsy	Pathology
In utero x-ray irradiation [122]	$\leq$20% spontaneous seizures	diffuse cortical and hippocampal disorganization, dysmorphic neurons
In utero freeze lesion [123]	Interictal spikes/increased kindling	cortical disorganization (in 42% cases), randomly oriented neurons
In utero exposure of MAM [124, 125]	$\leq$20% spontaneous seizures	cortical disorganization
In utero exposure to BCNU [126, 127]	hyperexcitability	cortical disorganization, dysmorphic neurons
Neonatal focal ibotenate excitotoxicity [118]	hyperexcitability	cortical disorganization
Genetic models: PTEN [128, 129]	severe seizures in 100% cases	cortical disorganization, dysplastic neurons, macrocephaly, large neurons, premature death
Genetic models: TSC [24, 74]	spontaneous seizures	cortical disorganization, large and dysmorphic neurons, premature death
Genetic models: LRP12 [120]	decreased threshold to evoked seizures	cortical disorganization, abnormal neuronal morphology

The Eker rat was the first animal model for TSC. These rats carry spontaneously occurring germline mutations of *TSC2* rendering them *TSC2*-null. In less then half of the Eker rats subcortical and subependymal hamartomas were observed [130] and in some rare cases also cortical tubers but none had spontaneous seizures [131]. The TSC-mouse model was further optimized to reproduce the human phenotype more carefully. All of these new mouse models are based on (conditional) mutations or loss of *TSC1* or *TSC2.* To induce a robust phenotype, usually both alleles are silenced. In heterozygous mice, seizures only occurred in young postnatal mice and stopped after approximately 9 - 18 days of age [131]. Homozygous *TSC1* or *TSC2* knockout mice are embryonic lethal, therefore viable mouse models with Cre-mediated homozygous *TSC1* or *TSC2* inactivation were designed. In these mice expression of Cre under the control of specific promoters leads to *TSC1* or *TSC2* loss in certain central nervous system (CNS) cell populations, such as neurons (synapsin-, CamKII-, Dlc5/6-promoter), astrocytes (GFAP-promoter) or neuronal progenitors (GFAP2-, Emx1-, nestin-promoter) (see table 2.2 for details and references; table modified from [74]). Again, one significant downside in most of these models is that they cause diffuse abnormalities throughout the entire brain and fail to recapitulate localized cortical tubers. A focal approach with a higher degree of temporal and spatial specificity to mimic the pathological situation

in humans more closely, was generated by intra ventricular *in utero* electroporation of heterozygous *TSC1*$^{fl/mut}$ mice with Cre. This TSC mouse model represents the so far most realistic model with increased cerebral excitability and a tuber-like cortical malformation with typical immunohistochemical features. Still also this model has its limitations since no spontaneous seizures were reported in these mice [74].

Table 2.2: Mouse models for TSC

TSC model	Epilepsy	Pathology	Reference
TSC1/*TSC2* KO in astrozytes	epileptic seizures	diffuse, macrocephaly, astrogliosis, cellular hypertrophy, increased astrocyte proliferation, neuronal dispersion, premature death	[132–136]
TSC1/*TSC2* KO in radialglia	epileptic seizures	diffuse cortical disorganization, macrocephaly, astrogliosis	[137–139]
*TSC1*KO in neurons	epileptic seizures	diffuse cortical disorganization, macrocephaly, abnormal neuronal morphology, enlarged and dysplastic neurons, premature death	[140–142]
TSC1 KO in interneurons	decreased threshold to evoked seizures	diffuse cortical disorganization, abnormal neuronal morphology, enlarged and dysplastic neurons, ectopic GABAergic interneurons	[143]
TSC1 KO in neuronal progenitors	epileptic seizures	diffuse cortical disorganization, macrocephaly, astrogliosis, cellular hypertrophy, abnormal neuronal morphology, premature death	[144–146]
Focal *TSC1* KO in fl/mut mice	decreased threshold to evoked seizures	focal cortical disorganization, abnormal neuronal morphology, cellular hypertrophy, tuber-like lesions	[112]
Adult *TSC1* KO	epileptic seizures	Rare giant cells	[147]

As for GGs, so far no animal model exists. Based on the current literature, the Eker rat is the only animal model that developed anaplastic gangliogliomas, in only one out of 19 rats [130]. Typically, models focusing on other brain tumors, such as gliomas, rather rely on human cell lines [148], human primary cell cultures maintained in nude, i.e. immunocompromised mice, or on a rat cell line [149]. In some cases tumor cells are injected into the brains of nude mice or rats, resulting in tumor growth within days with low epilepsy incidence [149]. Obviously, these models are not suited for the study of complex developmental tumors.

Overall, animal models provide invaluable insight into disease pathogenesis, however, the existing animal models do not recapitulate hallmarks of the lesion seen in human TSC, FCD, or GG patients.

2.5 Basic mechanisms of cortex development

Mammalian brain development starts with neurulation from the ectoderm to the neural tube, which is the origin of all cells from the central nervous system [150]. Different stages crucial to generate a func-

tional laminated cortex can be discriminated: cell proliferation, migration, differentiation, expansion in size, complexity and synaptogenesis [150]. The cortex differentiates from the most anterior region of the neural tube that consists of neuroepithelial cells (NEC) [151, 152]. In the germinative ventricular zone (VZ) which lines the ventricle, they extend long processes throughout the entire cortical wall and divide symmetrically [152, 153]. At the onset of neurogenesis some NECs begin to differentiate into radial glia (RGC) that can be identified by their expression of GLAST and BLBP [154–156] (see Fig. 2.3). Pioneer neurons are generated (such as Cajal-Retzius cells) that form the pre-plate [157]. Asymmetrical devisions generate a new RGC and either directly a neuron or an intermediary type of progenitor cell (IPC) [150, 155, 158]. IPCs from the VZ delaminate to the subventricular zone (SVZ) juxtaposed to the basal surface of the VZ [158–160]. After symmetrical devision the IPCs terminally divide into two neurons [158]. Any alterations of this proliferative pool of IPCs that give rise to all projection neurons of the cortex will have a significant impact on the final neuronal output and may result in lamination disorders such as FCD, microlissencephaly or hemimegalencephaly [12, 72]. Primary neurons born in the SVZ split the pre-plate into the marginal zone and the subplate [150, 161, 162]. Newborn projection neurons migrate from the SVZ to their layer of destination in the cortical plate in an inside-out pattern towards the cortical surface [159]. The later-born neurons therefore migrate past the deeper-layer neurons born earlier, shaping the complex laminar cytoarchitecture of the cortex [150]. At first, newborn neurons have a multipolar morphology and later, as they start to migrate a bipolar morphology with a leading and a tail process [163–165]. They migrate along the basal process of the RGC ultimately resulting in the formation of columnar, radial units within the laminated cortex [160]. Disorders affecting the expression of cytoskeleton components or motor proteins impair neuronal migration and thus, will lead to various brain morphogenic disorders such as lissencephaly, sub-cortical band heterotopia or double cortex syndrome [12, 72, 166, 167].

Within the cortical plate glutamatergic, excitatory projection neurons form the six-layered cortex [159]. Together with interneurons they compose the two major classes of neurons that populate the cortex [168]. Unlike excitatory projection neurons, interneurons are largely inhibitory, connect locally within the cortex and originate from progenitors of the subpial proliferative zone called ganglionic eminence [169, 170]. In C57Bl/6 mice, the sequence of different layer projection neurons is well characterized: At around E10.5 the first cortical neurons forming the subplate are born, followed by layer VI neurons around E12.5, layer V at E13.5, layer IV around E14.5 and layer II/III around E15.5 [150, 171]. Each layer is comprised of different types of neurons with different expression patterns or axonal projections. The deeper layer neurons from layer VI and V are mainly corticofugal neurons projecting to subcortical brain areas such as the thalamus, brain stem or the spinal cord. Neurons from layer IV to II are predominantly intracortical neurons that project locally or to the contralateral hemisphere [171]. Layer IV is also referred to as a cortical hub for intracolumnar information processing and converges the majority of the sensory information. It represents a highly interconnected layer that amplifies and redistributes thalamo-cortical inputs [172–174]. At birth neurogenesis and axo-dendritic network formation are largely complete while maturation of glial cells (such as astrocytes and oligodendrocytes), myelination, synaptogenesis, and synapse pruning are still in progress [150, 175]. Proper neurogenesis and migration together with adequately timed gliogenesis are critical for proper neural circuit formation and thus brain function [150].

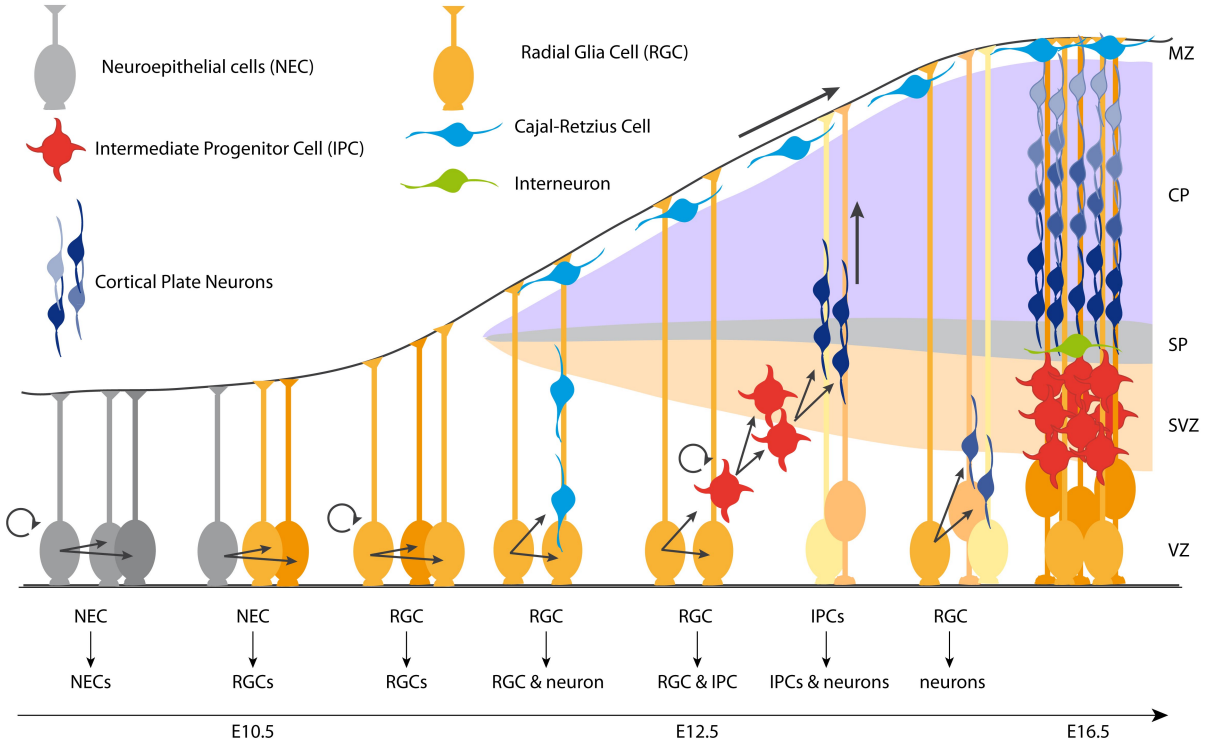

Figure 2.3: **Development of the mouse cortex.** During mouse cortex development neuroepithelial cells (NECs) divide and generate radial glia cells (RGCs) that divide into primary neurons. These include Cajal-Retzius cells that migrate to the marginal zone (MZ) and later on intermediate progenitor cells (IPCs) populating the sub ventricular zone (SVZ) starting at E12.5. IPCs generate cortical layer neurons that migrate through the intermediate zone or subplate (IZ/SP) to their designated layer. Figure modified from [150].

2.5.1 Axon and dendrite outgrowth

During or shortly after neuronal migration first axonal and then dendritic outgrowth starts, a process known as neuronal polarization. Initially, neurons start to form lamellipodia, which then further develop into short processes, the neurites. One of the neurites elongates rapidly and becomes the future axon, whereas the others start to grow later and acquire their characteristic dendritic branch-pattern [176]. Their growth is guided by local or long-range environmental, chemical cues that can either attract or repulse the growth cone (enlargements on a growing neurite tip). This induces reorganization of the cytoskeleton in growth cones and leads to forward movement and extension of the neurite. Microtubules and actin filaments are the major structural components of the cytoskeleton, underlying neurite growth and morphology. Their dynamic rearrangement, especially actin assembly and disassembly is pivotal for motility of the growth cone and the leading edge and consequently for neurite elongation and branching [177]. High F-actin (filamentous actin) turn-over furthermore loosens the actin meshwork and allows microtubules and other proteins to enter distal parts of the growth cone, thereby promoting neurite elongation [178, 179]. Cytoskeleton remodeling is regulated by hundreds of accessory proteins converging intrinsic and extrinsic signals on these filaments, thereby regulating their dynamic assembly and location [180].

A major regulator of actin and microtubule dynamics is the Rho family of GTPases such as RhoA, Rac1 (Ras-related C3 botulinum toxin substrate 1) and Cdc42 (Cell division control protein 42 homolog). RhoA and Rac1 have opposing effects in controlling the orientation, growth and stability of cytoskele-

ton filaments. While Rac1 activation induces actin disassembly, thus, promoting growth and branching, RhoA has mainly growth inhibiting effects [181, 182]. Rac1 activates the Arp (actin-related protein) 2/3 complex that binds actin filaments and leads to actin polymerization and PAK (p21-activated kinase), which leads to phosphorylation of the actin depolymerizing factor cofillin, while RhoA activates formins inducing unbranched filament extension [183–185]. Rac1 and RhoA also influence dynamics and (+)-end capture of microtubules [186]. Besides GDP-GTP exchange by Rho family GTPases, also phosphorylation by various kinases of integrins or microtubule- and actin-associated proteins regulate their stability and orientation and thus axon and dendrite growth or branching [187–192].

In axons, microtubules are usually uniformly oriented with their fast-growing (+)-ends away from the cell body towards the leading edge, providing a protrusive force for outgrowth, while dendrites contain microtubules with both orientations [193]. It has been suggested, that these differences influence the manner in which organelles or proteins are transported along neurites. The stability of microtubules is regulated by accessory proteins that protect filaments from depolymerization. Tau is associated with axonal microtubules while in dendrites MAP (microtubule associated protein) 2 complements microtubules [194] (see Fig. 2.4).

Unlike axons, dendrites harbor Golgi outposts that are required for local dendritic branching. A reduction in Golgi outposts in dendrites reduces branching with a shift from distal to proximal branching [195]. A tightly controlled temporal and spatial interplay between the cytoskeleton, motor protein based transport and organelles is a important mechanism for cytoskeleton organization and thus for neuronal process formation.

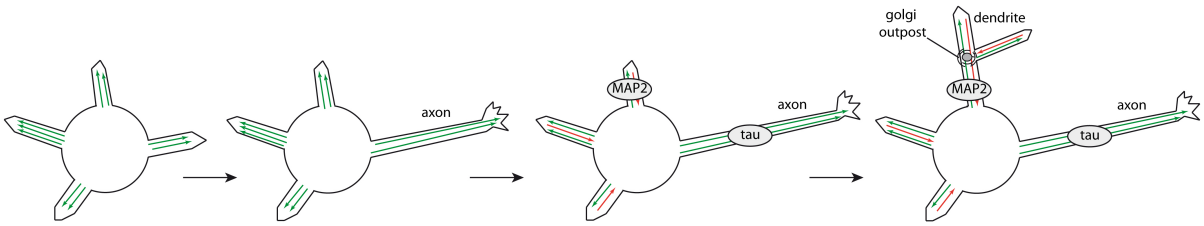

Figure 2.4: **Neurite outgrowth in cultured neurons.** In a dissociated neuronal culture, neurons start to form lamellipodia from which one is determined to become the axon whereas the remaining processes differentiate later into dendrites. While in axons the microtubule polarity is mostly (+)-end distal complemented with tau proteins, dendrites have a mixed orientation of microtubules with MAP-2 as associated proteins and Golgi outposts that are required for dendritic branching. Figure modified from [196].

The pattern of a dendritic arbor in different neurons is not only regulated by cytoskeleton remodeling but also by cell surface receptors that guide outgrowth and transcription factors [197]. Furthermore, the distinct protein expression levels in different neuron classes determine dendrite morphology by regulating branching, thus transcriptional programs are the driving force of neuronal growth [198–200]. The complex interplay of cytoskeleton remodeling and transcription regulation during neuronal polarization are still not fully understood. However, one particular interesting group of highly conserved and ubiquitous transcriptional co-factors are the LIM-domain binding (LDB) proteins LDB1 and LDB2. They mediate the action of the transcription factors LIM-HD (LIM homeodomain) and LMO (LIM-only) proteins that have been associated with a myriad of developmental processes and especially with neuronal specification and cytoskeletal organization [201, 202]. Experiments on zebrafish (*Danio rerio*) and *C.elegans* showed that LDB proteins (or their orthologs) regulate axon outgrowth and neurite branching

[203, 204]. These multi adapter proteins are also important regulators of radial migration and subtype specification of cortical neurons [205, 206].

2.5.2 Synapse development and maintenance

An important step in circuit formation is synapse development including pre- and postsynaptic specializations, synapse pruning and stabilization. Overproduction of synapses takes place in the postnatal period. Less productive or effective connections will be eliminated due to insufficient electrical activity, a process called pruning [207, 208]. In humans, pruning of weak or unused synapses continues about 15 years, a process that is much faster in mice, and includes nearly 50% of all synapses [150]. The remaining synapses are stabilized and require constant maintenance to stay functional [208, 209].

In the embryo, connections are established and influenced by spontaneous activity patterns, thus synapse formation generally starts after birth when synaptic connections are exposed to activity dependent changes caused by interactions with the environment and learning [150, 210]. Once a growing tip has reached its final target it transforms into a presynaptic terminal [150, 211]. Further specializations into specific presynaptic structures generally take place at the axonal, or somatic compartment and specifications of postsynaptic structures along the dendrite [211–214]. The interaction and stability of pre- and postsynapse is mediated by cell-surface molecules, such as cadherins, integrins, neurexins and neuroligins [215–218]. While mature presynapses are mostly characterized by the presence of the active zone and neurotransmitter filled synaptic vesicles [211], the postsynapse is enriched with neurotransmitter receptors. These receptors are incorporated into the membrane and anchored by a dense scaffold-protein-cytomatrix complex [219, 220]. Scaffolding molecules act as anchoring elements that are critical for the organization of functional synapses. They ensure accurate accumulation of neurotransmitter receptors in exact apposition to the presynaptic active zone. Furthermore, they maintain the position of receptors, which is a prerequisite for accurate synaptic transmission [221, 222]. The excitatory postsynapse harbors large numbers of glutamate receptors within the post synaptic density (PSD) that are activated by the glutamate neurotransmitter released from the presynapse. Furthermore, the PSD of excitatory postsynapses consists of stabilizing scaffold proteins such as PSD95, homer and shank, cytoskeleton proteins (mainly actin filaments), adhesion molecules, receptor interacting proteins, protein kinases and phosphatases [219, 220]. Most mature glutamatergic, excitatory postsynapses are organized in tiny actin-rich protrusions on the dendrite, called dendritic spines [223]. Excitatory cortical neurons also receive input from GABAergic, inhibitory interneurons that form synaptic connections onto the axon, cell body or along the dendritic shaft [224]. In contrast to the well characterized excitatory postsynapse, only few information is available on the inhibitory postsynapse. These synapses are formed earlier in development than excitatory synapses [225, 226]. $GABA_A$ receptors ($GABA_A$Rs) of the inhibitory postsynapse directly bind to and are clustered by the scaffolding protein gephyrin that forms a submembranous, hexagonal lattice anchored to the actin and microtubule cytoskeleton (see Fig. 2.5) [221, 227, 228]. Scaffolding of gephyrin in neurons and thus, proper synaptic $GABA_A$R clustering critically depends on the dynamic rearrangements of microtubules and actin filaments [229, 230]. Membrane targeting of gephyrin is mediated by collybistin (Cb), a guanine nucleotide exchange factor (GEF) that catalyzes GDP-GTP exchange on the small GTPase Cdc42 of the Rho family. The assembly of GABAergic postsynapses is triggered by the activation of Cb by NL2, allowing Cb to be recruited to the

membrane, where it facilitates the synaptic accumulation of gephyrin and $GABA_A$Rs [231]. Cb and NL2 are not only crucial for the initial synaptic localization of gephyrin and thus, the establishment of the inhibitory postsynapse, but also for constant maintenance and stability in adult neurons [232–235]. In humans, mutations of Cb, NL2 or gephyrin have been linked to epilepsy, X-linked mental retardation, aggressive behavior, anxiety, autism or hyperekplexia [221, 236–241].

Besides $GABA_A$Rs, NL2 and Cb several other gephyrin-interacting proteins have been identified, although the function of their interaction is largely unknown [242]. Actin-associated proteins (for example Mena/VASP) are thought to connect gephyrin to actin filaments while dynein light chains are implicated in motor-depended transport of gephyrin to the membrane along the cytoskeleton [230, 243, 244]. Nonetheless, modification of the core components of this synapse type by phosphorylation represents one key regulatory mechanism. The formation and stability of postsynapses critically depends on adequate phosphorylation that regulates scaffold clustering, trafficking and binding properties [221, 242, 245, 246]. However, the exact mechanisms that regulate the inhibitory synapse are still only poorly characterized.

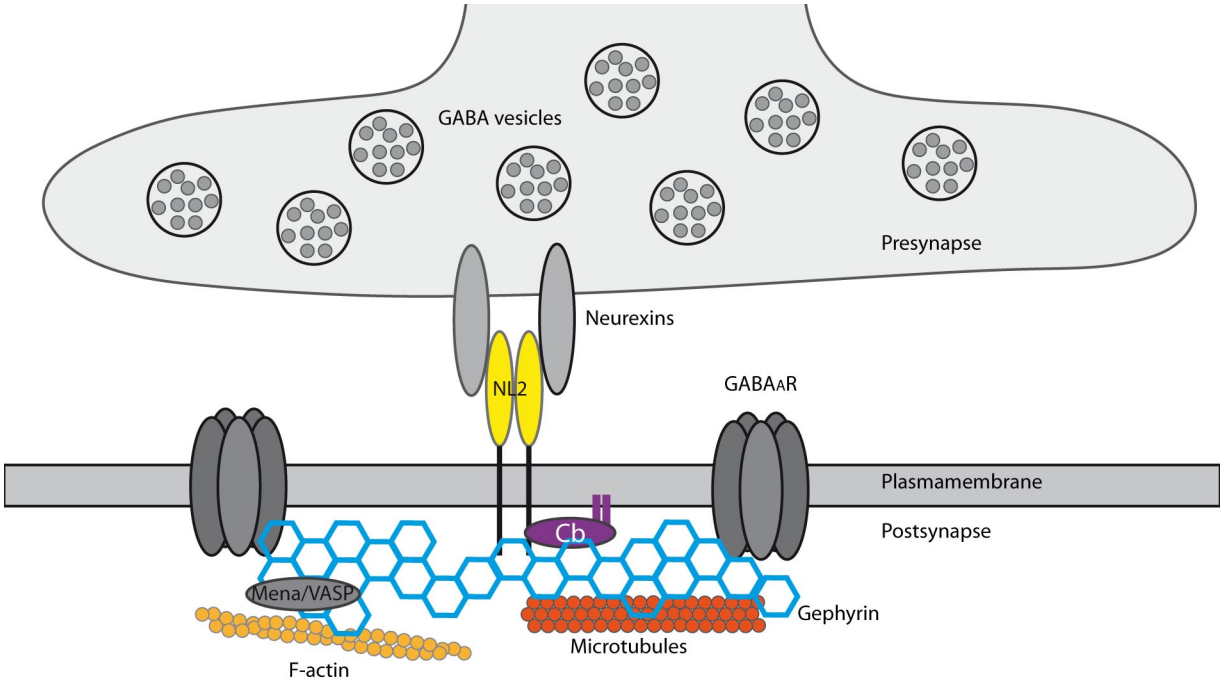

Figure 2.5: **Overview of the inhibitory postsynapse**. The inhibitory postsynapse of the CNS is mainly composed of $GABA_A$Rs that are anchored and stabilized by a scaffold composed of gephyrin, collybistin (Cb) and neuroligin-2 (NL2). This scaffold is connected to the presynapse via interaction of NL2 and neurexins. Moreover, NL2 and gephyrin are in tight association with and the cytoskeletal components, including actin and tubulin. Figure modified from [221].

2.6 Ste20 like kinase (SLK)

Kinases are highly dynamic molecular switches and regulate a multitude of various cellular processes, including regulation of neurite development as well as synapse formation and long-term stability. One large family of serine/threonine kinases particularly involved in these processes is the Ste20 (Sterile 20) protein kinase family. With its more than 60 members this kinase family is divided into two mammalian

subfamilies based on phylogenetic relationships: PAKs (p21-activated kinases) and GCKs (germinal center kinases). These kinases are characterized by the conserved kinase domain and a non-catalytic domain that enables interactions with other molecules and regulatory proteins of the cytoskeleton [247]. Cytoskeleton rearrangement and thus, regulation of growth and cell migration is the major function of these kinases. However, their regulatory mechanisms remain largely unknown.

One particular kinase of this family is the Ste20 like kinase (SLK). SLK is basically ubiquitously expressed but highly enriched in adult and developing cortical neurons [248]. It consists of an N-terminal serine/threonine kinase catalytic domain, a consensus SH3 binding site, a C-terminal ATH (AT1-46 homology domain) domain and an M-NAP (microtubule and nuclear associated protein) homology domain [249, 250]. Gene-trap mediated SLK truncation that results in less efficient phosphorylation leads to reduced cell proliferation and developmental defects that consequently result in lethality around E12.5 - E15 [248]. This finding implies an important role of SLK in embryonic and possibly also brain development, however, nothing is known about SLKs function in the CNS.

SLK is one of the less well characterized Ste20 kinases and initial insights into SLKs functions were gained from experiments in fibro- and myoblasts or other cell lines only within the last 15 years. In these cells SLK is predominantly expressed at the periphery at scaffold structures of weak cellular adherence but is also present in the cytosol [249]. SLK was shown to be part of a signaling pathway mediating JNK1 (Jun terminal kinase 1) activation and apoptosis [249–251]. Furthermore, SLK is needed for efficient cell migration, a process in which SLK induces cytoskeleton rearrangements by regulating actin fiber disassembly, microtubule dynamics and orientation, and focal adhesion turn over [252–254]. Focal adhesions are protein complexes that mediate cellular adherence to the substratum, including integrins, paxillin, vinculin and FAK (focal adhesion kinase) [254, 255]. In cultured, migrating fibroblasts, the induction of SLKs kinase activity requires FAK and MAPK (mitogen activated protein kinase)-dependent pathways and the recruitment to the leading edge requires Src family kinases [253, 254]. The exact molecular mechanisms are still unclear, but is was suggested that SLK is recruited to the leading edge of migrating fibroblasts by a microtubule-dependent process. This induces a redistribution of SLK to local sites of adhesion using actin fibers or microtubules. At these sites, recruited SLK phosphorylates signaling components, regulating growth and migration [254].

Furthermore, SLK was shown to phosphorylate Rac1 and RhoA, two major regulators of cytoskeleton dynamics. Rac1 activation by SLK leads to actin fiber disassembly in various cultured, non-neuronal cells [249, 256], while RhoA is inhibited by SLK phosphorylation at Ser188. This promotes adhesion- and F-actin disassembly, further demonstrating SLKs important role for cytoskeletal remodeling and cell motility [257]. Other known downstream substrates of SLK are paxillin, dynactin and ezrin, proteins involved in cytoskeleton dynamics and myelin basic protein, histone H3 and histone H1 [250, 258–261]. Consistent with a role in cytoskeleton rearrangements, SLK was also shown to be involved in cell cycle progression. SLK knockdown or expression of a kinase inactive mutant inhibited fibroblast proliferation *in vitro* by interfering with microtubule dynamics during mitosis [262]. In contrast to phosphorylation, direct binding of SLK and LDB (LIM-domain binding protein) 1 and 2 in fibroblasts resulted in SLK inactivation that was highly dependent on the relative stoichiometry of LDB-proteins. These results identified LDB transcriptional co-activators as potential SLK regulators and demonstrated a kinase independent SLK mechanism in migrating cells [263].

In summary, SLK is a key player for cell motility and growth in non-neuronal cell lines that regulates cytoskeleton reorganization and cross talk between actin and microtubules. These functions suggest a potentially similar molecular mechanism in neurons, however, to date SLKs function in these cells remains unknown.

3 Aims of the study

Developmental brain lesions including gangliogliomas (GGs), tuberous sclerosis (TSC) or focal cortical dysplasias (FCDs) are devastating conditions affecting mostly young patients suffering from pharmacoresistant epilepsy. Until today their treatment is difficult and often accompanied with major side effects. Even though significant progress has been made in this research field over the last years, the molecular pathogenesis of developmental lesions is still only poorly understood. This is to a large extent due to the lack of adequate animal models that reliably replicate all crucial aspects of the individual condition. For the identification of novel and targeted therapeutical options it will be essential to uncover the specific mechanisms of epileptogenesis in these disorders and to create suitable mouse models.

The major unifying hallmark of these highly epileptogenic glioneuronal lesions are dysplastic neurons, which are characterized by abnormal dendritic arborization. So far, the molecular mechanisms leading to their formation or hyperexcitability are largely unknown. Deregulation of several candidate genes that may be implicated in their emergence have been identified by various approaches. Expression analysis or immunohistochemical stainings on human GG specimens revealed strongly reduced expression of Lim-domain binding (LDB2) transcripts and increased levels of phosphorylated Protein kinase B (Akt) compared to the surrounding brain tissue. Furthermore, mutational analyses found specific sequence alterations of the tuberous sclerosis complex 1 (*TSC1*) gene to be frequent in TSC or FCD type IIb (FCDIIb) patients as well as one particular Raf murine sarcoma viral oncogene homolog B1 (BRAF) mutation (BRAF-V600E) in GGs. The aim of this study is to analyze the molecular mechanisms of epileptogenesis underlying the most common developmental brain lesions GG, TSC and FCDIIb, with a specific focus on dysplastic neurons possibly induced by deregulation of the mentioned candidate genes.

Our first goal is to establish a novel mouse model for GGs by expressing the mutated BRAF-V600E together with a constitutively active form of Akt in p53-null developing cortical neurons. With this experimental approach we will identify the contribution of these molecular alterations to the manifestation of dysplastic neurons and consequently the so far uncertain etiology of GGs. Furthermore, a GG mouse model will enable detailed research of the neoplasm as well as drug testing.

The second goal is to analyze the pathogenetic mechanisms underlying the formation of dysplastic neurons within cortical tubers. To increase our understanding of the etiology and cellular composition of cortical tubers from TSC patients, we will investigate morphological and structural effects of TSC1 loss at distinct developmental time windows or progenitor cell populations. A further goal is to identify the pathogenetic potential of disease associated *TSC1* gene variants to induce dysplastic neurons. By analyzing the gene dosage required for the formation of tuber-like lesions harboring dysplastic neurons, we intend to clarify the controversy about their pathogenetic situation.

The next goal is to find out, whether the emergence of dysplastic neurons has a shared molecular cause

across the different types of glioneuronal lesions that possibly even accounts for the severe epileptic phenotype. It was previously shown that reduced levels of LDB2 result in an abnormal arborization of the dendritic tree in cultured neurons. So far, it is unresolved if a decrease in LDB2 levels *in vivo* causes alterations resembling dysplastic neurons. In non-neuronal cells LDB2 engages in a functionally important interaction with its family member LDB1 and the Ste20 like kinase (SLK). However, virtually nothing is known about SLKs function in the mammalian brain. It remains an open question, whether the SLK/LDB1/2 complex plays a role in neurite morphology and whether deregulation of these proteins may contribute to the emergence of dysplastic neurons. Therefore, our third goal is to study the role of SLK in developing neurons *in vitro* and *in vivo*. In non-neuronal cells, SLK was shown to be an important regulator of cytoskeleton dynamics, a process critical at various stages of neuronal development and especially for normal dendritic arborization. Thus, we aim to analyze the effect of SLK silencing or overexpression on neurite development and synapse formation. Moreover, with our experiments we want to answer the question, whether neuronal SLK loss *in vivo*, as present in FCDIIB and GG patients, results in the emergence of dysplastic neurons and thus, a hyperexcitable brain lesion.

In a similar set of experiments, we aim to analyze whether also loss of LDB2 and LDB1 interferes with normal neuronal development and mirrors dysplastic neurons. We will further examine whether spatially restricted cortical, silencing of both LDB proteins during mouse development has the potential to induce an epileptic condition.

In summary, this study provides novel insights into the emergence of dysplastic neurons and thus, developmental brain lesions and underlying mechanisms of epileptogenesis that may represent a basis for new targeted and effective treatment methods.

4 Material

4.1 Equipment

Equipment	Model	Company
Acrylamid electrophoresis system	Mini-PROTEAN 3 Electrophoresis System	BioRad
Agarose electrophoresis system	SUB-CELL GT	BioRad
Analytical balance	BP210S	Sartorius
Autoclave	HSP Laboklav	Steril Technik AG
Balance	SBC53	SCALTEC
Blotting paper	white	Whatman, GE Healthcare
Cell culture hood	MSC-Advantage	Thermo Scientific
Centrifuge	Function line	Heraeus
Centrifuge	5415C	Eppendorf
Centrifuge	Mikro 22R	Hettich
Centrifuge	Mikro 200R	Hettich
Centrifuge	Rotina 220R	Hettich
Confocal laser scanning microscope	Eclipse Ti	Nikon
Controller	Micro4 Controller, 4-Channel	World Precision Instruments
Electrode forceps	7mm	
Electroporator	CUY21SC	Nepa Gene
Filter system (IUE)		Harvard Apparatus
Gas anesthesia		Harvard Apparatus
Gel documentation system	AlphaImager	Alpha Innotech
Glass capillaries	1.2mm	Drummond Scientific
Heating pad		
Incubator (cells/cell culture)	HERAcell 150 / 150i	Thermo Scientific
Incubator (media/cell culture)	Modell 100	Memmert
Incubator small	Inkubator 1000, Unimay 1010	Heidolph
Incubator small Incubating	Mini shaker	VWR
Infrared imaging system	Odyssey	Li-cor
Inverse microscope	Axio Observer 1A	Zeiss
Inverse microscope	Axiovert 40 CF	Zeiss

Microinjector	Picospritzer III	General Valve Corporation
Micro glass capillary puller	PC-10	Narishige group
Microtome	Microm HM 335 E	Microm
Nitrocellulose membrane	Protran 0.4 mm	Whatman, GE Healthcare
PCR-Cycler	UNOII	Biometra
PCR-Cycler	T3	Biometra
PCR-Cycler	T3000	Biometra
pH-meter	pHMeter 766	Calimatic Knick
Power Supplies Agarose	PHERO-stab.500	BIOTEC-FISCHER
Power Supplies Agarose	Power Pack 25	Biometra
Real time PCR (Taqman)	9700HT	ABI Prism
Rotor	Type 70 Ti	Beckman Coulter
Shaker plate	Polymax 1040	Heidolph
Spectrophotometer	ND-1000	NanoDrop
Thermo shaker	MKR13	HLC
Thermo shaker	Thermomixer compact	Eppendorf
Ultrasonicator	Processor UP50H	Hielscher
Ultrasonicator	Labosonic 2000	B.Braun
Vibratome Microm	HM 650V	Thermo Scientific
Vortex	Vortex-Genie 2	Scientific Industries
Vortex	Reax control	Heidolph

Table 4.1: Equipment used for this study

4.2 Chemicals

Chemical	**Company**
4',6-diamidino-2-phenylindolindole, dihydrocholoride (DAPI)	Life technologies
6 x loading buffer	Fermentas
Acrylamide	Roth
Agarose	peqLab
Ammoniumpersulfate (APS)	Roth
Ampicillin	Roth
Aqua ad injectabilia	Delta Select
Bovine serum albumin (BSA)	Sigma-Aldrich
Buprenovet	Bayer
Calcium chloride	Sigma-Aldrich
Chloroform	Roth
Complete Mini Protease Inhibitor	Roche
Direct PCR Tail Lysis Reagent	PeqLab
EDTA	Calbiochem

Eosin	Roth
Ethanol	Fluka
Ethidiumbromide	Merck
Fast Green	Sigma-Aldrich
Fetal calf serum (FCS)	Life technologies
Gabrilen	Mibe
Gelatin from cold water fish skin	Sigma-Aldrich
Glucose solution 5 %	Fresenius
HEPES	Sigma-Aldrich
Hemalaun solution (Mayer)	Merck
HCl 2N	Merck
Isofluorane	Sigma-Aldrich
Isopropanol	Fluka
Jasplakinolide	Thermo Fischer Scientific
Kanamycin	Sigma-Aldrich
Ketamine (Ketavet)	Pfizer
Luria Broth-Agar	LabM/idg
Luria Broth-Medium	LabM/idg
Magnesium chloride	Merck
Methanol	Merck
Mowiol 4-88	Roth
Normal goat serum (NGS)	Gibco
Paclitaxel (taxol)	Sigma-Aldrich
Paraformaldehyd	Roth
PBS	Biochrom AG
Penicilin	Sigma-Aldrich
Pentylenetetrazol (PTZ)	Sigma-Aldrich
Phalloidin (Acti-stain 555 fluorescent phalloidin)	Cytoskeleton
Phalloidin (Phalloidin-iFluor 647 Conjugate)	Biomol/Rockland
Propidium iodide	Sigma-Aldrich
Protease inhibitor cocktail (complete)	Roche
Ringer solution	Braun
RNAse away	Molecular BioProducts
Saccharose	Sigma
Sodiumchloride	Roth
Sodiumdodecylsulfate (SDS)	Roth
Sodiumhydrogenphosphate	Merck
ß-Marcaptoethanol	Roth
TEMED	Roth
Tris-Base	Sigma
Tris-HCl	Roth
Triton-X-100	Roche

Vectashield mounting medium	Vector Laboratories
Xylazine (Rompun)	Bayer
Xylol	Merck

Table 4.2: Chemicals used for this study

4.3 Antibodies

Primary antibodies

Antibody	**Dilutions**	**Company**
β-actin mouse (ab6276)	1:5000	Abcam
Acetylated Tubulin (T7451)	1:1000	Sigma-Aldrich
Annexin V (R-20, sc-1929)	1:200	Santa Cruz
Chromogranin A (M086901)	1:500	DAKO
Cleaved Caspase-3 (9661T)	1:200	Cell Signaling Technology
Cre recombinase (ab137240)	1:100	Abcam
CUX1 (CDP, M-222, sc-13024)	1:200	Santa Cruz
FoxP2 (ab1307)	1:200	Abcam
GFAP (G3893)	1:500	Sigma-Aldrich
hrGFP (monoclonal) (240241)	1:5000	Agilent Vitality
LDB1 (ab96799)	1:400	Abcam
MAP-2 (MAB3418)	1:500	Millipore
NeuN (A60, MAB377)	1:400	Millipore
Neurofilament (M076229)	1:500	DAKO
p53 (ab26)	1:200	Abcam
pS6 (Ser240/244, D68F8 XP, 5364S)	1:600	Cell Signaling Technology
pS6 (Ser235/236, 2211L)	1:600	Cell Signaling Technology
S100 (Z031101)	1:1500	DAKO
SLK (anti rabbit)	1:800	Donated by Prof. Luc Sabourin (Ottawa)
Vimentin (ab5733)	1:2000	Millipore

Table 4.3: List of primary antibodies

Secondary antibodies

Antibody	**Dilutions**	**Company**
Alexa Fluor 405 goat anti mouse	1:200	Life Technologies
Alexa Fluor 405 goat anti rabbit	1:200	Life Technologie
Alexa Fluor 488 goat anti mouse	1:200	Life Technologies
Alexa Fluor 488 goat anti rabbit	1:200	Life Technologie
Alexa Fluor 568 goat anti mouse	1:200	Life Technologie
Alexa Fluor 568 goat anti rabbit	1:200	Life Technologie

Alexa Fluor 568 donkey anti goat	1:200	Life Technologie
Alexa Fluor 647 goat anti mouse	1:200	Life Technologie
Alexa Fluor 647 goat anti rabbit	1:200	Life Technologie
Alexa Fluor 647 goat anti chicken	1:200	Life Technologie
IRDye 680-anti mouse IgG	1:20000	LI-COR Odyssey
IRDye 680-anti rabbit IgG	1:20000	LI-COR Odyssey
IRDye 800-anti mouse IgG	1:20000	LI-COR Odyssey
IRDye 800-anti rabbit IgG	1:20000	LI-COR Odyssey

Table 4.4: List of secondary antibodies

4.4 Cell culture media and reagents

Cell culture medium	**Company**
B27	Gibco
Basal Medium Eagle (BME)	Life technologies
Dulbecco's Modified Eagle's Medium (DMEM)	Gibco
Fetal calf serum (FCS)	Life technologies
Hank's Buffered Salt Solution (HBSS)	Gibco
Iscove's Modified Dulbecco's Medium (IMDM)	Gibco
L-Glutamine	Gibco
Minimum essential medium (MEM)	Sigma-Aldrich
Penicillin-Streptomycin	Gibco
Phospate saline buffer (PBS)	Gibco
Poly-D-Lysin	Sigma-Aldrich
Trypsin-EDTA	Gibco

Table 4.5: Culture media used for this study

4.5 Kits

Kit	**Company**
BigDye® Terminator v3.1 Cycle Sequencing Kit	Applied Biosystems
DNA Clean and Concentration kit	Zymo Research
Dynabeads® mRNA DIRECT™ Micro Kit	Life technologies
EndoFree Plasmid Maxi Kit	Quiagen
GeneJET™ Plasmid Miniprep Kit	Thermo Scientific
High Capacity cDNA Reverse Transcription Kit	Applied Biosystems
PureLink™ HiPure Plasmid Filter Maxiprep Kit	Life technologies
RevertAid First Strand cDNA Synthesis Kit	Thermo Scientific
SYBR ® Green RT-PCR Mix	Applied Biosystems
Zymoclean DNA Clean&Concentrator kit	Zymo Research

Zymoclean Gel DNA recovery kit	Zymo Research

Table 4.6: Kits used in this study

4.6 Oligo nucleotides

4.6.1 Cloning Primers

Enzymes were obtained from fermentas.

Plasmid	Direction	Primer 5'-sequence-3'	Enzyme	Vector
2A-Cherry	fw	GCGACCGGTCTCGAGGAGCTAT CTAGAGTG	AgeI	pB-CAG-GFP
2A-Cherry	rev	GCGGCGGCCGCCTACTTGTACAG CTCGTCCATGC	NotI	pB-CAG-GFP
CAG-Cre-GFP	fw	GCGGAATTCATGTCCAATTTACT GACCGTACA	EcoRI	pB-CAG-GFP
CAG-Cre-GFP	rev	GCGCCCGGGCCATCGCCATCTTC CAGCAGG	XmaI	pB-CAG-GFP
Cherry-2A-BRAF-V600E-KD	fw	GCGACCGGTgACCATGGACTTGA TTAGAGACCAAGG	AgeI	CAG-Cherry-2A
Cherry-2A-BRAF-V600E-KD	rev	GCGGCGGCCGCTCAGTGGACAG GAAACGCAC	NotI	CAG-Cherry-2A
hSLK-mut-GFP	fw	GCGGAATTCACCATGTCCTTCTT CAATTTCCGTAAGA	EcoRI	pB-CAG-GFP
hSLK-mut-GFP	rev	GCGACCGGTTGATCCGGTGGAA TGCAAGC	AgeI	pB-CAG-GFP
hSLK-mut-mCherry	fw	GCGGAATTCACCATGTCCTTCTT CAATTTCCGTAAGA	EcoRI	CAG-Cherry
hSLK-mut-mCherry	rev	GCGGCGGCCGCCTACTTGTACAG CTCGTCCATGC	NotI	CAG-Cherry
mCherry	fw	GCGACCGGTATGGTGAGCAAGG GCGAGG	AgeI	pB-CAG-GFP
mCherry	rev	GCGGCGGCCGCCTACTTGTACAG CTCGTCCATGC	NotI	pB-CAG-GFP
mCherry-2A-GFP	fw	GCGGAATTCACCATGATGGTGA GCAAGGGCGA	EcoRI	pB-CAG-GFP
mCherry-2A-GFP	rev	GCGGGTACCGCTCCAGGGCCGG GATTCTCCTCC	KpnI	pB-CAG-GFP
mLDB1-mCherry	fw	GCGGAATTCATGCTGGATCGGG ATGTGG	EcoRI	CAG-Cherry

mLDB1-mCherry	rev	GCGACCGGTCCCTGGGAAGCCTGTGACGTG	AgeI	CAG-Cherry
mLDB1-mut-mCherry	fw	GCGGAATTCATGCTGGATCGGGATGTGG	EcoRI	CAG-Cherry
mLDB1-mut-mCherry	rev	GCGACCGGTCCCTGGGAAGCCTGTGACGTG	AgeI	CAG-Cherry
mLDB2-mCherry	fw	GCGGGATCCATGTCCAGCACACCACATGA	BamHI	CAG-Cherry
mLDB2-mCherry	rev	GCGACCGGTCCCTGGGAAGCCTGGGGTG	AgeI	CAG-Cherry
mLDB2-mut-mCherry	fw	GCGGGATCCATGTCCAGCACACCACATGA	BamHI	CAG-Cherry
mLDB2-mut-mCherry	rev	GGCGACCGGTCCCTGGGAAGCCTGGGGTG	AgeI	CAG-Cherry
mSLK-GFP	fw	GCGCCCGGGATGTCCTTCTTCAATTTCCGTAAG	XmaI	pB-CAG-GFP
mSLK-GFP	rev	GCGACCGGTCCTGACCCAGTGGAATGTAAG	AgeI	pB-CAG-GFP
mSLK-mCherry	fw	GCGCCCGGGATGTCCTTCTTCAATTTCCGTAAG	XmaI	CAG-Cherry
mSLK-mCherry	rev	GCGACCGGTCCTGACCCAGTGGAATGTAAG	AgeI	CAG-Cherry
mSLK-K63R-GFP	fw	GCGCCCGGGATGTCCTTCTTCAATTTCCGTAAG	XmaI	pB-CAG-GFP
mSLK-K63R-GFP	rev	GCGACCGGTCCTGACCCAGTGGAATGTAAG	AgeI	pB-CAG-GFP
mSLK-K63R-mCherry	fw	GCGCCCGGGATGTCCTTCTTCAATTTCCGTAAG	XmaI	CAG-mCherry
mSLK-K63R-mCherry	rev	GCGACCGGTCCTGACCCAGTGGAATGTAAG	AgeI	CAG-mCherry
myrAkt-2A-mCherry	fw	CGACCATGGGGTGTATTAAATCGAAACGGAAAGACAACCTTC	KpnI	CAG-2A-mCherry
myrAkt-2A-mCherry	rev	GAGGCGGCCGCTTAGGCTGTGCCACTGGCTGA	NotI	CAG-2A-mCherry

shLDB1-hrGFP	top	TTTGCACGCTACTTCCGAAGCATTTCTCGAGAAATGCTTCGGAAGTAGCGTGTTTTT	BamHI	pAAV-U6-shRNA-CBA-hrGFP
shLDB1-hrGFP	bottom	CTAGAAAAACACGCTACTTCCGAAGCATTTCTCGAGAAATGCTTCGGAAGTAGCGTG	HindIII	pAAV-U6-shRNA-CBA-hrGFP
shLDB2-hrGFP	top	CGACGGACCAAAGCGATACATTCAAGAGATGTATCGCTTTGGTCCGTCTTTTTGGAAA	BamHI	pAAV-U6-shRNA-CBA-hrGFP
shLDB2-hrGFP	bottom	TTTCCAAAAAGACGGACCAAAGCGATACATCTCTTGAATGTATCGCTTTGGTCCGTCG	HindIII	pAAV-U6-shRNA-CBA-hrGFP
shSLK-hrGFP	top	GATCTCGGGTTGAGATTGACATATTAATAGTGAAGCCACAGATGTATTAATATGTCAATCTCAACCTTTTGGAAA	BamHI	pAAV-U6-shRNA-CBA-hrGFP
shSLK-hrGFP	bottom	GCTTTTCCAAAAGGTTGAGATTGACATATTAATACATCTGTGGCTTCACTATTAATATGTCAATCTCAACCCGA	HindIII	pAAV-U6-shRNA-CBA-hrGFP
shSLK-mRFP	top	CGCGTGGTTGAGATTGACATATTACTCGAGTAATATGTCAATCTCAACCTTTTTTAT	MluI	pLVTHM-mRFP
shSLK-mRFP	bottom	CGATAAAAAAGGTTGAGATTGACATATTACTCGAGTAATATGTCAATCTCAACCA	ClaI	pLVTHM-mRFP
TSC1-WT-2A-mCherry	fw	GCGGGTACCATGGCCCAACAAGCAAATGTC	KpnI	CAG-2A-mCherry
TSC1-WT-2A-mCherry	rev	GCGACCGGTGCTGTGTTCATGATGAGTCTCA	AgeI	CAG-2A-mCherry
TSC1-R692X-2A-mCherry	fw	GCGGGTACCATGGCCCAACAAGCAAATGTC	KpnI	CAG-2A-mCherry
TSC1-R692X-2A-mCherry	rev	GCGACCGGTGAGGGTGCGGATCTCATCT	AgeI	CAG-2A-mCherry
TSC1-H732Y-2A-mCherry	fw	GCGGGTACCATGGCCCAACAAGCAAATGTC	KpnI	CAG-2A-mCherry
TSC1-H732Y-2A-mCherry	rev	GCGACCGGTGCTGTGTTCATGATGAGTCTCA	AgeI	CAG-2A-mCherry

TSC1-R786X-2A-mCherry	fw	GCGGGTACCATGGCCCAACAAG CAAATGTC	KpnI	CAG-2A-mCherry
TSC1-R786X-2A-mCherry	rev	GCGACCGGTGTCATGCTGCAGCT GTCTGA	AgeI	CAG-2A-mCherry

Table 4.7: Primers used for cloning.(fw: forward; rev:reverse)

4.6.2 Sequencing Primers

Template	Direction	Primer 5'-sequence-3'
Akt	fw	ATGGGGAGCAGCAAGAGCAA
		GCTCACCCAGTGACAACTCA
		GATTGTGTCTGCCCTGGACT
		GCAGCACCGGTTCTTTGCC
		AGTTCGAGATCGAGGGCGA
		ACCCCGAGGACGGCGC
BRAF	fw	TGTTGAATGTGACAGCACCTAC
		AATGCAAGATAAAAATCCATACAGCT
hSLK	fw	AATCTTTGGATCCTCATTGAATTTTG
		GAATTAAATCCAATGCGAGTGCT
		TCAACAGCAAAATTCTTAATGAAAAAC
		TTACAAAGGAAGACACCCAAGAG
		AGTGAAGTTCAGGATGCTTCTAAA
		TTACAGATAGTGATTCCAAAACTGAA
		GAGAGAGTGCCTGAATAACAAG
		GCCAATGTCCGCGAACTGC
mSLK	fw	TGCTGTGATGCTTGAACTTGAG
		TGAGCCCCCAACATTAGCAC
		GGATGAGCATGCAAGTGATGT
		ACCAGTGATAGAAGCAGTGAG
		CAGAAAGTGCCCGTTAAAGCA
		CGGGAGCTGAGGCTTCTTC
		AATTTGGGAGCTTGAAGAGCGA
		CACCTGTTGGTTGAACATGAGA
mLDB1	fw	CCCTCGACTGTGACCAGG
		ACGACAGCAGCCCAGCAAA
		GGAACAGCAAGCCTCCATC
mLDB2	fw	ATATCACAACTCATCCATCACAGT
		AGAACCCACAAGGCAACCGA
		AACCTCCCGCCACGCAAG

GFP	fw	ATGGTCCTGCTGGAGTTC
CAG-X	fw	CTTCTGGCGTGTGACCGG
		GAAGCGGTGCGGCGCC
mCherry	rev	ATGATGGCCATGTTATCCTCCT
pLVTHM-mRFP	fw	ATTTAGGTGACACTATAG
TSC1	fw	TTCGTCTCCTTTTTGCGTTCTC
		CACAGACAACACCATCTTCTGAA
		CCTCCCCCGTATGATCATCT
		CAGACTGATACAGCAGGGAG
		GAGGACTGCAGGAACATGATT
		GCAGGTTGGAGAAAGATGGC
		ATTCCCCTGAACCTAGATGGC

Table 4.8: Sequencing primers.(fw: forward; rev: reverse)

4.6.3 Genotyping primers

Genotype	**Primer 5'-sequence-3'**
$p53^{fl/fl}$	GGTTAAACCCAGCTTGACCA
	GGAGGCAGAGACAGTTGGAG
$TSC1^{fl/fl}$	AGGAGGCCTCTTCTGCCTACCC
	TGGGTCCTGACCTATCTCCTA
	CAGCTCCGACCATGAAGTG

Table 4.9: Primers used for genotyping of TSC1 and p53 mice.

4.6.4 Primers for quantitative real-time PCR

Gene	**Primers**	**Company**
SLK	TTCGGGAACTGCACCAGCT	Life Technologies
	CTTCTTCCTGGGTCTCAGCT	
β-actin	ATGCTCCCCGGGCTGTATT	Life Technologies
	CTCCATGTCGTCCCAGTTGG	

Table 4.10: Primers used for quantitative real time RT-PCR

4.7 Enzymes

Enzyme	**Company**
DNase I	Roche
FastAP	Life technologies
Pfu DNA Polymerase	Life technologies

PNK	Life technologies
Proteinase K	PeqLab
Econo Taq DNA Polymerase	Life technologies
T4 Ligase	Thermo Scientific
Trypsin	Gibco

Restriction Enzymes	**Company**
EcoRI, XbaI, XmaI, AgeI, KpnI, NotI, BamHI, MluI, ClaI, HindIII	Thermo Scientific

Table 4.11: List of Ezymes used in this study

4.8 Plasmids

Generated plasmids

Name	**Insert**	**Vector**
CAG-mCherry-2A-GFP	mCherry-2A	pB-CAG-GFP
CAG-mCherry	mCherry	pB-CAG-GFP
CAG-2A-mCherry	2A-mCherry	pB-CAG-GFP
CAG-Cre-GFP	Cre	pB-CAG-GFP
CAG-Cherry-2A-BRAF-V600E-KD	BRAF-V600E-KD	CAG-mCherry-2A
CAG-mCherry-2A-GFP	mCherry-2A	pB-CAG-GFP
CAG-hSLK-mut-GFP	hSLK-mut	pB-CAG-GFP
CAG-hSLK-mut-mCherry	hSLK-mut	CAG-mCherry
CAG-mLDB1-mCherry	mLDB1	CAG-mCherry
CAG-mLDB1-mut-mCherry	mLDB1-mut	CAG-mCherry
CAG-mLDB2-mCherry	mLDB2	CAG-mCherry
CAG-mLDB2-mut-mCherry	mLDB2-mut	CAG-mCherry
CAG-mSLK-GFP	mSLK	pB-CAG-GFP
CAG-mSLK-mCherry	mSLK	CAG-mCherry
CAG-mSLK-K63R-GFP	mSLK-K63R	pB-CAG-GFP
CAG-mSLK-K63R-mCherry	mSLK-K63R	CAG-mCherry
CAG-myrAkt-2A-mCherry	myrAkt	CAG-2A-mCherry
U6-shLDB1-hrGFP	shLDB1	pAAV-U6-shRNA-CBA-hrGFP
U6-shLDB2-hrGFP	shLDB2	pAAV-U6-shRNA-CBA-hrGFP
U6-shSLK-hrGFP	shSLK	pAAV-U6-shRNA-CBA-hrGFP
U6-shSLK-mRFP	shSLK	pLVTHM-mRFP
CAG-TSC1-WT-2A-mCherry	TSC1-WT	CAG-2A-mCherry

CAG-TSC1-R692X-2A-mCherry	TSC1-R692X	CAG-2A-mCherry
CAG-TSC1-H732Y-2A-mCherry	TSC1-H732Y	CAG-2A-mCherry
CAG-TSC1-R786X-2A-mCherry	TSC1-R786X	CAG-2A-mCherry

Table 4.12: Constructs generated during this study

Plasmids generated prior this study

Plasmids with shLDB1 (sh216), shLDB2 (sh916), shSLK within the pAAV-U6-shRNA-CBA-hrGFP vector.

Plasmids kindly provided by other labs

pCAG_PSD95.FingR-eGFP-CCR5TC; AddGene Plasmid #46295 and pCAG_GPHN.FingR-eGFP-CCR5TC; AddGene plasmid #46296, was a gift from Don Arnold [264].

SLK K63R (Prof. Luc Sabourin, Ottawa Hospital Research Institute, Canada), pB-CAG-GFP, pB-CAG-pBase (Joe LoTurco, University of Connecticut, USA), GLAST-Cre, Nestin-Cre, BLBP-Cre, GFAP-Cre (Carlos Cardoso, INSERM, Institut de Neurobiologie de la Méditerranée, Marseille, France),

5 Methods

The approved nomenclature fore gene symbols is used throughout the text. Gene symbols are abbreviated and italicized (http://www.genenames.org). This nomenclature would require that human gene symbols are written with capitalized letters, and that in mouse gene symbols only the first letter is capitalized. However, we refrain from doing so in order to keep the appearance simple and uniformly.

All patients included in this research project gave informed and written consent for additional studies. Procedures were carried out in accordance to the Helsinki Declaration and were approved by the local ethics committee.

5.1 Molecular biological methods

5.1.1 Polymerase chain reaction (PCR) and agarose gel electrophoresis

PCR is a technique to amplify DNA from cDNA templates. The DNA-polymerases used in this study are Pfu-Polymerase and EconoTaq-Polymerase. To avoid mutations the Pfu polymerase is used for cloning since it has proof reading properties. The EconoTaq is used for genotyping as proof reading is not required for this approach. Typically a reaction mix for cloning contains 36.4µl a.dest, 5µl 10x$MgSO_4$-containing Pfu-buffer (Life technologies), 3µl 25mM $MgSO_4$ (Life technologies), 0.6µl dNTPs (Life technologies), 1.5µl 10pmol/µl forward primer, 1.5µl 10pmol/µl reverse primer, 1µl Pfu polymerase (Life technologies) and 1µl cDNA. A reaction for genotyping contains 2µl a.dest, 5µl 2xEcono-mix (Life technologies), 1µl forward 10pmol/µl primer, 1µl 10pmol/µl reverse primer and 1µl tail-lysate.

Double stranded DNA samples are then amplified in a thermocycler. A typical amplification program with Pfu polymerases for a 1000 base pair long DNA fragment consists of an initial 10min denaturation period at 94°C, followed by 35 cycles of 1min 94°C, 50sec primer annealing at 58°C and 2min elongation at 72°C (Pfu amplifies 500 base pairs/min), completed by a final 10min elongation phase. Amplification of 300 base pair long DNA fragments with Econo Taq consists of an initial 10min denaturation period at 95°C, followed by 35 cycles of 50sec 95°C, 50sec 58°C and 60sec 72°C, completed by a final 10min elongation phase. Amplified DNA fragments were complemented with 6x loading dye (Life technologies) and separated on a 1% agarose gel containing 2% ethidium bromide for 30 – 60 min and 150V. For an estimation of band size, GeneRuler 1kB DNA ladder was also loaded on the agarose gel. DNA bands were visualized by UV-light, cut out of the gel for further vector generation and purified with the Zymoclean Gel DNA recovery kit.

5.1.2 Cloning

For the generation of new plasmids template cDNAs were amplified by PCR with appropriate primers (all primers including restriction enzyme recognition sequences used are listed in chapter 4.6.1). Primers and shRNA oligomers were ordered online (Invitrogen Life Technologies). shRNAs were designed based on sequences in the RNAi Codex database (http://cancan.cshl.edu/cgi-bin/Codex/Codex.cgi). Before ligation into their final vectors, the shRNA oligomers were annealed in 100mM Tris pH7.5, 1M NaCl and 10mM EDTA solution for 10min at 95°C. Samples were cooled down slowly to room temperature and phosphorylated by addition of PNK (polynucleotide kinase, Life technologies) and 10xkinase buffer (Life technologies). After purification by ice-cold ethanol precipitation oligomers were ready for ligation. Final vectors and purified PCR amplicons were digested with appropriate enzymes (see primer list with used enzymes in chapter 4.6.1 and vector list in chapter 4.8 for details; buffers were used as recommended by the manufacturer: https://www.thermofisher.com/de/[...]/double-digest-calculator-thermoscientific.html). All vectors were additionally dephosphorylated to avoid self-ligation by adding 1µl of FastAP (fast alkaline phosphatase, Life technologies) to each reaction and finally both, vectors and PCR amplicons were purified with the Zymoclean DNA Clean&Concentrator kit. A ligation mix contained 1µl T4 DNA ligase (Life technologies), 2µl 10xT4 DNA ligase buffer (Life technologies), 50ng vector DNA, a molecular ratio of 1:3 PCR amplicon DNA and a.dest was filled up to achieve an end volume of 20µl. The DNA mix was incubated at 16°C for 20 – 24h. For amplification of newly generated plasmids, chemically competent 5-alpha *E.coli* were incubated with 20µl ligation reaction for 20min on ice. After a 45sec long heat shock, bacteria-DNA mix was incubated for another 2min on ice. Afterwards, 200µl sterile LB-medium was added and the bacteria were incubated for 60min at 37°C and 800rpm. Bacteria were plated on LB-agar plates containing the appropriate antibiotics as selection marker (100µg/ml ampicillin or kanamycin) and incubated over night at 37°C. To test for positive clones, single colonies were picked with a pipette tip and allowed to grow in 4ml antibiotics containing LB-medium for 12 – 16h at 200rpm and 37°C. Afterwards, bacteria was pelleted and plasmid DNA was isolated and purified with the GeneJet Plasmid Miniprep Kit following the manufacturer's instructions. Correct insertion of PCR amplicons was verified by sequencing reactions (BigDye Terminator v3.1 Cycle Sequencing Kit PCR sequencing reaction, performed according the manufacturer's instructions; sequencing reaction carried out at the Life&Brain GmbH in Bonn). By transfection of the newly generated plasmids into HEK293T cells, we tested for robust expression and/or correct subcellular localization of fluorescent proteins.

For *in utero* electroporation or transfection of primary cultured cortical neurons, plasmids were amplified in 200ml LB-medium-bacteria cultures and isolated with the EndoFree Plasmid Maxi Kit following the manufacturer's instructions.

5.1.3 Genotyping

To verify the correct genotype of the used *TSC1*$^{fl/fl}$ and *p53*$^{fl/fl}$ mice, small tail pieces were cut from three week old mice. To extract DNA, tails were incubated on a thermo shaker in lysis solution (Direct PCR Tail Lysis Reagent, PeqLab) containing 1% proteinase K for 2 – 18h at 55°C. Proteinase K was inactivated by 85°C for 60min and the crude tail DNA mix was then used for further PCR amplification.

5.1.4 mRNA isolation, cDNA synthesis and real-time PCR

mRNA was isolated from cultured neurons transduced with rAAV crude extracts by using the Qiagen RNA Mini Kit according to the manufacturer's instructions. For each condition, neurons from four wells of a 24-well plate were combined for RNA isolation. Reverse transcription and cDNA synthesis were performed using the RevertAidH Minus First Strand cDNA Synthesis Kit (Thermo scientific) with oligo dT primers as recommended by the manufacturer. Similarly, instructions of the manufacturer were followed for real-time PCR using the SYBR Green PCR kit (Life technologies). Therefore, 3µl Sybr Green were mixed with 1.25µl cDNA, 0.3µl 5'primer, 0.3µl 3'primer and 1.4µl DEPC-water. In an ABI Prism 9700HT system (PE Applied Biosystems, USA) samples were first heated to 95°C for 10min and then amplified by 40 cycles of 95°C for 15sec, 59°C for 60sec, 72°C for 40sec. Gene expression was calculated as $2^{-\Delta ct}$(Δ cycle threshold value (ct) = ct of the analyzed gene - ct β-actin). relative to an internal reference gene (β-actin).

5.2 Cell culture

5.2.1 Cell culture with human embryonic kidney (HEK) cells

HEK293T cells were continuously cultured in DMEM (supplemented with 10% FCD and 1% Pen/Strep) in a T75 tissue culture flask at 37°C in an incubator with 5% CO_2. These actively dividing cells were passaged as soon as they reached 70 – 80% confluency. Therefore, culture medium was replaced with 5ml PBS as a washing step and then incubated in 2ml trypsin-EDTA (Gibco) to detach the cells from the bottle ground. After 1 – 2min 5ml DMEM was added to stop the lysis reaction. Cells were singularized by pipetting up and down. Cell density was assessed using a Neubauer counting chamber. For HEK293T cell transfection, 50000 cells per well of a 24-well plate were seeded. For further cultivation, approximately 1mio. cells were left in the culture flask and 12ml DMEM was added.

5.2.2 Transfection of HEK cells

HEK293T cells were transfected with the calcium phosphate method 24h after plating. Three hours before transfection, culture medium of HEK293T cells plated in 24-well plates was replaced with 1ml IMDM (containing only 5% FCS) per well. DNA (500ng/µl) was mixed with 50µl 250mM $CaCl_2$. While mixing on a vortex 55µl 2xHEBES phosphate-buffer (50mM HEPES, 280mM NaCl, 1.5mM Na_2PO_4 - pH7.1) was added dropwise. 50µl of the DNA mix was added per well and the DNA-$CaPO_4$ precipitate was allowed to form. After 14 – 18h IMDM was replaced with fresh culture medium. After 48h transfected HEK293T cells were harvested for protein extraction. In the case that HEK293T cells were transfected for verification of newly generated plasmids, cells were 4% PFA fixed an analyzed with a fluorescence microscope (Zeiss Axio Observer.A1, A-Plan 10X 0.25NA objective).

5.2.3 Production of crude recombinant adeno-associated virus (rAAV) extracts

For production of recombinant adeno-associated viruses (rAAVs), HEK293T cells were plated in 10cm culture dishes. 24h after plating, culture medium was replaced with IMDM and 5% FCS. The DNA-$CaCl_2$

mix for one 10cm-dish contained 5.5µg endotoxin free AAV plasmid DNA, 11.0µg pFdelta6 plasmid, 2.64µg pRV1 plasmid, 2.75µg pH21 plasmid, 145µl 2.5M $CaCl_2$ and 1ml a.dest. While mixing, 1.15ml 2xHEBES phosphate-buffer was added dropwise. The DNA-CaP mix was added to the culture medium and IMDM was replaced with culture medium 14 – 18h later. After 48h AAV containing HEK293T cells were harvested for virus extraction. Therefore, cells were detached from the culture plate by adding 1ml trypsin-EDTA. Culture medium and lysed cells were collected in a 15ml falcon tube and spun for 4min at 2000rpm. The supernatant was discarded and the cell pellet was resuspended in 500µl PBS. After three freeze-thaw cycles, cells were lysed and the AAV particles were separated from cell debris by full speed centrifugation for 3min. The supernatant, containing the crude AAV particles was stored at 4°C for short-term use and at -80°C for long-term use.

5.2.4 Primary neuronal cell culture

Primary cortical neurons were dissected from embryo brains of pregnant (E17 – E19) mice or rats. Both cortical hemispheres were removed and kept in ice-cold HBSS (calcium and sodium free Hank's Buffered Salt Solution). Meninges were removed and each isolated cortical hemisphere was reduced to small pieces. After three washing steps with 5ml ice-cold HBSS, the brain pieces were incubated for 10min in 4.5ml HBSS (supplemented with 500µl trypsin) at 37°C. Afterwards the pieces were washed again three times with HBSS supplemented with 1mg/ml 200µl DNAse I and with 800µl warm BME (Eagle's Basal Medium). To mechanically isolate and singularize neurons, brain pieces were gently triturated using 1ml pipette tips. Cell density was then assessed in a Neubauer counting chamber. For subsequent transfection or transduction, cortical neurons were plated at a density of 55000 cells/well on poly-D-lysine (0.01%) coated glass cover slips in a 24well-plate. Culture medium contained NB (NeuroBasal) supplemented with B27 and L-Glutamine and cells were maintained in a humidified incubator at 37°C with 5% CO_2. Culture medium was replaced with 1ml fresh NB medium/well 24h later.

5.2.5 Transfection and transduction of primary neuronal cultures

Two – four days after preparation (DIV1 – 4) cortical neurons were transfected using the calcium phosphate method as described in [265]. Neuronal medium was collected, stored at 37°C and replaced by warm MEM (Minimum Essential Medium Eagle). A transfection mix for two wells contained 5µg endotoxin free plasmid DNA and 60µl 250mM $CaCl_2$. Same molecular ratios were used when transfecting shRNAs together with overexpression plasmids. While mixing on a vortex, 65µl 2xBBS (BES-buffered saline; 280mM NaCl, 1.5mM Na_2HPO_4, 50mM BES, pH 7.1) was added drop-wise. After adding 60µl of the DNA-containing mix per well, neurons were incubated for 30 – 50 min at 37°C with 2.5% CO_2. As soon as a prominent calcium-phosphate precipitate formed, cells were washed twice with HBS (HEPES-buffered saline; 135mM NaCl, 4mM KCl, 1mM Na_2HPO_4, 2mM $CaCl_2$, 1mM $MgCl_2$, 10mM glucose, 20mM HEPES, pH 7.35), twice with BME and in the end the previously removed and stored medium was added to the cells. At DIV4, 6, 14, or 21 neurons were 4% PFA fixed and either mounted on glass slides or used for immunocytochemistry. For cell death assays, 5mM propidium iodide was added to neurons before PFA-fixation. For transduction, 20 – 40µl of crude rAAV extract was added to neurons one day after plating (DIV1). Neurons were harvested on DIV14 and used for mRNA expression

analysis.

5.3 Biochemical methods

5.3.1 SDS-Page and western blotting

To harvest proteins form HEK293T cells, the culture medium was removed 48h after transfection, replaced with cold PBS and the cells were detached from the culture dish using a cell scraper. Cells were collected in a 1.5ml tube and pelleted by full speed centrifugation for 3 min at 4°C. The pellet was resuspended in lysis buffer (4mM HEPES, 150mM NaCl, 1% Triton X-100, protease inhibitor cocktail) and sonicated for 1 – 3sec. This was followed by a second full speed centrifugation at 4°C for 3 min to pellet the cell debris. The protein concentration of the supernatant was measured using a Nanodrop. For SDS PAGE 50µg protein per sample supplemented with 6x Laemlibuffer (TRIS-hydrochlorid 378mM, 30% glycerol, 12% SDS and 0.06% Bromphenolblue, 10% β-mercaptoethanol) were denatured at 95°C for 5min and then loaded on a 10% acrylamide gel. After separation proteins were transferred onto a nictrocellulose membrane by western blotting for 3h at 4°C and 200mA or over night at 4°C and 45mA. Subsequently, the membrane containing the proteins was incubated on a rocking plate in 3% cold-water fish gelatin in PBST (PSB with 0.1% Triton X-100) to block unspecific binding sites. After 1h blocking the membrane was incubated for 3h in primary antibodies that were diluted in the blocking solution. Unbound antibodies were removed by three washings steps for 5min with PBST. Secondary fluorescent-labeled IRDyes anti mouse 800nm or anti rabbit 680nm IgG antibodies were diluted (1:20000) in PBST and incubated for 1h. After three washing steps with PBST the IRDyes were detected with the infrared Odyssey imaging system.

5.4 Immunochemical methods

5.4.1 Immunocytochemistry

For immunofluorescence analysis primary cultured cortical neurons were fixed by incubation in 4% PFA for 15min. Residual PFA was removed by three washing steps with PBS and one washing step with PBST (0.1% Triton X-100 in PBS). This was followed by 1h incubation with blocking solution (10% FCS, 1% NGS, 0.3% Triton X-100 in PBS). After overnight incubation with primary antibodies in blocking solution at 4°C, neurons were again washed with PBS and incubated with Alexa Fluor® secondary antibodies diluted in PBS for 45min. For some experiments, secondary antibody solution was supplemented with fluorescently labeled phalloidin. Afterwards, neurons were washed three times with PBS and mounted on glass slides with mowiol.

5.4.2 Immunohistochemistry

For co-immunofluorescence analysis PFA-perfused mouse brains were cut on a Microm HM 650V vibratome to 80µm brain slices. For immunohistochemical stainings, free floating brain slices were washed three times in PBST (PBS with 0.1% Triton X-100) and incubated in blocking solution (0.1%

Triton X-100, 0.1% Tween 20, 4% BSA in Tris-buffered saline (TBS) pH 7.7) for 1h at room temperature. Primary antibodies were diluted in blocking solution and incubated at 4°C over night on a rocking platform. Afterwards, the brain slices were washed again three times in PBST and the secondary fluorescently labeled Alexa Fluor antibodies diluted in PBST were incubated for 1h at room temperature. After three washing steps brain slices were mounted on glass slides with vectashield.

For immunofluorescence analyses, human GG and FCDIIb paraffin tissue sections, diagnosed according to the current WHO classification by an experienced neuropathologist (Prof. Albert Becker) [266] were used. Discrimination of lesion versus adjacent non-lesioned 'control' CNS tissue based on hematoxylin & eosin (HE)-staining. Paraffin was removed by incubation in xylol for 20min, 100% ethanol for 2min, 96% ethanol for 2min, 75% ethanol for 2min, 50% ethanol for 2 min and a.dest for 2min.

For HE staining, brain sections were incubated in hematoxylin for 6 - 8min to label cellular nuclei. Hematoxylin was removed by rinsing the sections for 10min with fresh water. Afterwards specimens were incubated in 10% eosin (supplemented with 0.001% glacial acetic acid) for 10min, that was removed by rinsing with water for 3min and followed by 5 min incubation in 80% ethanol, 5min 100% ethanol and 5 min xylol. HE stained brain sections were mounted with corbit and dried in at 37°C for 30min.

For immunofluorescence analyses of paraffin embedded *in utero* electroporated mouse brains, brains were cut into 3µm thick slices on a microtome and mounted on glass slides. After paraffin was removed (as described earlier in this section) sections were incubated in 0.1% citric buffer (pH 6.0) in a microwave for 20min. After this antigen retrieval step, brain slices were cooled down to room temperature, washed three times for 5min in PBS, placed in a sealed, humid chamber and incubated in blocking solution (5% FCS, 1% NGS in PBS). Primary antibodies were diluted in blocking solution and incubated over night at room temperature. Afterwards the sections were washed three times with PBS, incubated in Alexa Fluor secondary antibodies diluted in PBS for 2h at 37°C, washed again three times and mounted with vectashield.

5.5 Microscopy and imaging analysis

All specimens were imaged with a confocal microscope (Nikon Eclipse Ti confocal microscope - Nikon Instruments) and analyzed for different parameters. All images used for figures were edited and created in Adobe Photoshop CS6 or Adobe Illustrator CS6.

5.5.1 Neurite quantification and Sholl Analysis

Confocal images of mRFP or hrGFP expressing primary cortical neurons were made and analyzed using the NeuronJ plug in for ImageJ. For morphometric quantifications each neuron was reconstructed manually by tracing their neurites from branch point to the tip. For axon length determination, only the axon with its branches was reconstructed from DIV6 neurons. For quantification of different order dendrites, the whole dendritic tree was reconstructed at DIV14. Each branch of a single neuron was designated as either primary, secondary or tertiary, depending on its branch point origin. Dendrites originating from the soma were termed primary, dendrites branching out of primary dendrites were considered secondary and those growing out of secondary were accordingly defined as tertiary

dendrites. The absolute number of all different order dendrites was determined for each neuron and summarized as the mean number of dendrites. Furthermore, the length of each reconstructed dendritic subunit was measured by NeuronJ and also summarized as the mean value.

Single *in utero* electroporated neurons were analyzed in a similar fashion. As IUE usually resulted in densely packed clusters of electroporated neurons, only neurons from layer IV in the outer borders of the IUE area that were mostly isolated were selected. For Sholl analysis, each traced neuron was overlaid with rings of 10 or 50μm intervals with the neurons soma being the center. Then the number of intersections with neurites for each circle was assessed by the Sholl analysis tool of ImageJ [267, 268].

5.5.2 Fluorescence intensity analysis

To analyze immunohistochemical stainings from human surgical specimens, confocal maximum intensity projection images of z-stacks were taken and analyzed by NIS Elements Nikon software. The auto-detect function of the software automatically recognized and set MAP-2 positive neurons as region of interest (ROI). Fluorescence intensity of SLK or LDB1 in MAP-2 positive neurons within the and outside the GG was determined. Vimentin staining was used to help distinguish GG- from adjacent control brain tissue. In the case of FCDIIb analysis, only highly enlarged, dysplastic neurons positive for MAP-2 were selected for determination of SLK fluorescence intensity. As a control, normal sized MAP-2 positive neurons without apparent pathological changes of morphology, in an area with maximal distance from dysmorphic neurons were chosen and automatically detected by the software. Single cell SLK fluorescence intensity was read out for each ROI and subtracted by background fluorescence of individual images. The mean fluorescence intensity for lesioned vs. non-lesioned brain area was summarized as the mean value.

5.5.3 Analysis of colocalization

Colocalization of MAP-2 and GFAP with LDB1 was analyzed in neurons from human GG specimens, colocalization of SLK with gephyrin or PSD95 in primary transfected cortical neurons and colocalization of DAPI, NeuN, Cux1 and FoxP2 with ectopic neurons in brains electroporated with shSLK. For that purpose confocal maximum intensity projection images of z-stacks were taken and analyzed with the NIS Elements Nikon software. In order to analyze overlap, or positive colocalization, the fluorescence signal recorded for each ROI (MAP-2 positive neurons in GGs, gephyrin or PSD95-positive synapses or DAPI, NeuN, Cux1 or FoxP2) in each channel was subtracted by the corresponding background value of each individual image. We defined an overlap as positive or colocalized when the fluorescence signal of the ROI for PSD95, gephyrin, MAP-2, GFAP, DAPI, NeuN, Cux1 or FoxP2 overlaps with the ROI for SLK, LDB1 or hrGFP expressing ectopic neurons with more than three-times the fluorescence intensity of the background. Thus all SLK, LDB1 or hrGFP fluorescence intensity values lower than three-times the value of the background were determined as negative or not colocalized.

5.5.4 Quantification of synapse density

Confocal maximum intensity projection images of z-stacks of brains *in utero* electroporated with mRFP or shSLK together with GFP-fused gephyrin-, or PSD95-FingRs were taken and analyzed with two dif-

ferent methods. In a first manual analysis all GFP-labeled synapses on a mRFP expressing dendritic branch were counted. Afterwards the complete dendritic tree was reconstructed and the length was read out using the ImageJ plug-in NeuronJ as described before. The corresponding number of gephyrin- or PSD95 positive postsynapses per 100µm dendrite was summarized as the mean value. This approach was verified by using an automatic quantification method. A custom made MATLAB algorithm (provided by Carsten Robens, Institute for Applied Physics, Bonn, Germany) calculated the number of GFP-labeled synapses per µm dendrite overlapping at least 50% with the red fluorescent dendritic processes. Brain slices from mice at different ages (P5, P15, P30, P60 $\pm$1 day) were analyzed and compared.

5.5.5 Analysis of growth cone size

For the analysis of growth cone size, confocal maximum intensity projection micrographs of z-stacks from PFA-fixed transfected cortical neurons were analyzed with the NIS Elements Nikon software. ROIs were laid around individual growth cones that were identified by morphology, location and the presence of strong phalloidin fluorescence signals. We distinguished between growth cones from axons and from future dendrites. The size of each individual ROIs was measured and their mean size was compared to the mean size of control growth cones.

5.5.6 Analysis of gephyrin cluster size and fluorescence intensity of synaptic antibody staining

For the determination of gephyrin cluster size, z-stack maximum intensity projections of confocal micrographs of phalloidin/antibody labeled neurons transfected with gephyrin-GFP-FingRs and mRFP/shRNAs were analyzed with ImageJ. First, only the green, gephyrin-GFP channel was used. For each image, the background was subtracted using the 'subtract background' function. A rolling ball radius of 1/3 pixel width of the image (in our case 340) was used. For each image the lower threshold level was set to 20%. With the 'analyze particles' function of ImageJ, the program automatically recognized all round objects, larger than 2 pixels (corresponding to a length of 0.44µm or an area of 0.088µm^2). The size of each particle was determined by the program. The particles represent gephyrin positive synapses only from transfected cortical neurons. The outline of each particle was converted in to a ROI and overlaid on the channels for acTubulin, phalloidin and mRFP of the corresponding image. The fluorescence intensity was read out only for the ROI that represents the gephyrin positive synapse. The values for the fluorescence intensity of acTubulin and phalloidin were normalized to the corresponding mRFP fluorescence intensity within the same ROI. The mean fluorescence intensity for control and shSLK transfected neurons was summarized from all synapses of all analyzed neurons. For a more detailed illustration of the distribution of synapses with distinct fluorescence intensities, values were binned and plotted as a histogram. As the number of synapses was different in both conditions, all values were expressed as percentage of the absolute number of analyzed synapses.

5.5.7 Analysis of *TSC1* knockout neurons

To test for pathological mTOR pathway activation, confocal maximum intensity projection images of z-stacks were taken from brain slices of TSC1$^{fl/fl}$ mice *in utero* electroporated with distinct, indicated

plasmids. These brain slices were immunolabeled with antibodies against phospho-S6 Ribosomal Protein (pS6) and depending on the experiment also against NeuN, S100, GFAP and/or vimentin. mCherry expressing cells were automatically recognized by the ROI auto-detect function of the NIS Elements Nikon software and parameters such as fluorescence intensity or cell size were generated for each ROI. In each condition the individual results of each neuron (that was bright enough to be recognized by the software) was included into the analysis and summarized as the mean value. Analysis was carried out as described in [269].

5.5.8 Cortical positioning of electroporated neurons

For *TSC1*$^{fl/fl}$ mice: The final position of cortical neurons *in utero* electroporated at different time points was analyzed by defining the borders of the six-layered cortex based on NeuN staining. The percentage of all electroporated neurons within each layer was calculated manually. As an additional control, the mean distribution of all electroporated neurons within the cortex was determined by measuring the distance of each individual neuron to the upper border of layer I. Analysis was carried out as described in [269].

For wildtype mice *in utero* electroporated with control vs. shRNAs: The percentage of ectopic neurons was determined by manually counting all electroporated neurons within layer II/III and IV versus neurons located in deeper layers. As described before, layers were distinguished by NeuN staining.

5.5.9 Assessment of tumor "malignancy" and Kaplan-Meier curve

In order to estimate survival time of tumor bearing mice, usually the time until death is noted and illustrated in a Kaplan-Meier survival plot. However, the induced tumors of our GG model had a highly malignant progression that was apparent by rapid weight loss. To avoid unnecessary suffering, every mouse that lost more than 20% body weight in less than 24h was sacrificed, since it would most certainly die within the next 48h. The day of sacrifice was included in the Kaplan-Meier curve.

5.5.10 Band analysis after western blot

In order to analyze relative protein levels after western blot, band fluorescence intensity was quantified using ImageJ. The fluorescence intensity of the protein of interest was normalized to the respective loading control, the house keeping gene β-actin. For better comparison the resulting ratios were normalized to the respective overexpression condition (in the case of the shRNA assays, this condition was SLK-, LDB1-, LDB2-overexpression respectively).

5.6 Intraventricular *in utero* electroporation in mice

All procedures including animals were performed in accordance with the guidelines of the Bonn University Medical School Care Committee. Mice were kept in an animal facility, with a maximum of 4 animals per cage. All animals had continuous access to fresh water and food, and were kept under the control of an alternating 12-hour light or dark cycle.

In utero electroporation was performed as published in [120, 269]. Male and female mice were allowed to mate for 10 - 12h, and the day of mating was defined as embryonic day zero (E0). For all *in utero* electroporations CD1/C57Bl/6 hybrid female mice were used, as these have a considerably higher pup survival rate. C57Bl/6 mice have poor mother instincts and as a consequence most of their pups die within 24h after birth. C57Bl/6 *TSC1*$^{fl/fl}$ and *p53*$^{fl/fl}$ mice were crossed with CD1 mice for three generations. For accelerated backcrossing, C57Bl/6 specific SNPs were sequenced from the F2 and F3 offsprings genome. Mice with the lowest C57Bl/6 -specific SNP score were used for further breeding to either generate homozygous WT mice or homozygous *TSC1*$^{fl/fl}$ and *p53*$^{fl/fl}$ mice. Thus, our mice have a mixed genetic background, however, we refer to them as CD1 mice in the following, since the CD1 background is predominant. SNP sequencing estimated a 90% CD1 and 10% C57Bl/6 genetic content after the third generation. Only for PTZ experiments C57Bl/6 mice were used, because CD1 mice are more sensitive to PTZ and are therefore not ideally suited for these experiments.

Time pregnant CD1 or C57Bl/6 mice (E14, E16, E17, E18) were injected with buprenovet (0.05mg/kg) and gabrilen (5mg/kg) 30min prior to the procedure. Mice were anesthetized with isoflurane (induction 3.5%; surgery 2.5%) and placed on a heating pad (41°C). The uterine horns were exposed from the abdominal cavity by laparotomy. Each embryo was injected once with 2 – 4µl DNA (3 - 5µg/µl, supplemented with 0.1mg/ml of the dye Fast Green that was used as a visual control) into one lateral ventricle trough the uterine wall using a previously pulled and beveled glass capillary and a microinjector. This was followed by electroporation by discharging a 4000 µF capacitor charged to 45V with a CUY21SC square-wave electroporator (5 electrical pulses with a duration of 50ms in 950ms intervals) and a 2-panel electrode (7mm electrodes) that was placed between the eyes of the embryo to target cortical ventricular progenitors in the motor- and somatosensory cortex. Embryos and intestines were constantly rinsed with warm ringer solution supplemented with 1% penicillin/streptomycin. After the procedure, animals were allowed to give birth. Their offspring was either first subjected to PTZ assays or immediately anesthetized with ketamine/xylazine (100mg/kg and 10mg/kg respectively) and then sacrificed by cardiac 4% PFA perfusion. The brain was removed carefully, kept in 4% PFA at 4°C for two days and then stored in PBS at 4°C.

5.7 PTZ experiments

Mature (P45-50) C57Bl/6 mice *in utero* electroporated at E14 were injected intraperitoneally with pentylenetetrazole (PTZ, 10mg/kg) and hyperexcitability of the brain was assessed as described in [120]. PTZ was solved in PBS and all mice were repetitively injected in 10-minute intervals until the occurrence of the first generalized seizure. Two parameters of semiological seizures were determined: The nature of seizures of each individual mouse was rated according to a modified Racine score [270], and the time point of the occurrence of the first Racine score IV and V seizure. After the experiment all mice were sacrificed by 4% PFA heart perfusion.

5.8 Statistical analyses

The following statistical tests were applied: two sided paired Student's t-test (quantification of onset of PTZ-induced seizures, SLK/LDB1 expression in human ganglioglioma or FCDIIb tissue, real-time PCR, S100-, acTubulin- and phalloidin fluorescence intensity, number of ectopic cells in shSLK *in utero* electroporated brains, number of different order dendrites *in vivo*, and electrophysiological measurements), One-way ANOVA with Bonferroni post-correction (quantification of different order dendrites *in vitro*, axon length, synapse density, knockdown efficiency of shRNAs, cell size and pS6 fluorescence intensity), fisher's exact test (quantification of differences between the severity of PTZ-induced seizures), Chi-squared test (quantification of the final positioning of neurons in cortical layers), Two-way ANOVA with Bonferroni post-correction (quantification of the final positioning of neurons in cortical layers), and Mann-Whitney U-test (quantification of Sholl analysis, distribution of fluorescence intensities of acTubulin and phalloidin, distribution of neurons in $TSC1^{fl/fl}$ mouse brains). All standard errors are indicated as the 'standard error of the mean' (SEM).

6 Results

6.1 Establishing a ganglioglioma mouse model

GGs are among the most common neoplasms causing chronic, focal epilepsy especially in children and young adults, but to date no adequate animal model has been established to study this tumor entity in more detail. In order to analyze their pathogenic origin as well as mechanisms leading to the emergence of dysplastic neurons in these highly epileptogenic neoplasms, we aimed to generate a GG mouse model. Therefore, we intraventricularly *in utero* electroporated (IUE) $p53^{fl/fl}$ mice at 14 days post fertilization (E14; Fig. 6.1a) with a specific DNA mix containing CAG-Cre-GFP, CAG-myrAkt-2A-mCherry, CAG-mCherry-2A-BRAF-V600E-KD and CAG-pBase plasmids.

IUE of CAG-Cre-GFP at E14 into the lateral ventricle of $p53^{fl/fl}$ mice suppresses expression of the major tumor suppressor gene *Tp53* (encoding the protein p53) in cortical progenitor cells within the proliferative zones destined for cortical layer II/III and IV. Mutations in the *TP53* gene, encoding the tumor suppressor protein p53, are abundantly identified in several brain tumors including medulloblastomas, oligodendrogliomas, high-grade astrocytomas, and glioblastomas [271]. Most genetically engineered mouse models for these brain tumors use a combination of *TP53* knockout together with expression of an activated, pro-survival protein [271]. To drive GG specific tumor formation, we co-electroporated a constitutively active, membrane targeted Akt, mimicking phosphorylated Akt. Abnormal Akt phosphorylation is often reported in GG tissue [16, 272]. Furthermore, we co-electroporated the kinase domain (KD) of BRAF carrying a point mutation at position V600 that leads to a transition from valine to glutamate. Mutated BRAF-V600E was demonstrated in more than 50% of GGs and is - similar to phosphorylation by Akt - associated with high pS6 immunoreactivity (IR) in respective tumor cells and thus, mTOR pathway activation [24, 51, 52, 54]. To avoid that the plasmids are lost in dividing cells the piggyBac transposase pBase was also co-electroporated. This enables permanent integration of the genes into the genome at inverted terminal repeats (ITRs) that flank Cre, BRAF-V600E-KD and myrAkt. By IUE at E14 we aimed to mimic the focal, cortical character in a restricted number of cells and the presumed developmental origin of the dysplastic lesion. By expression of the plasmid mix in p53-silenced neuronal precursor cells, we expect to generate a developmental brain tumor with cellular features resembling those of GG patients. These features include enlarged, multi-nucleated dysplastic neurons together with prominent chromogranin A, neurofilament, MAP-2 and vimentin IR.

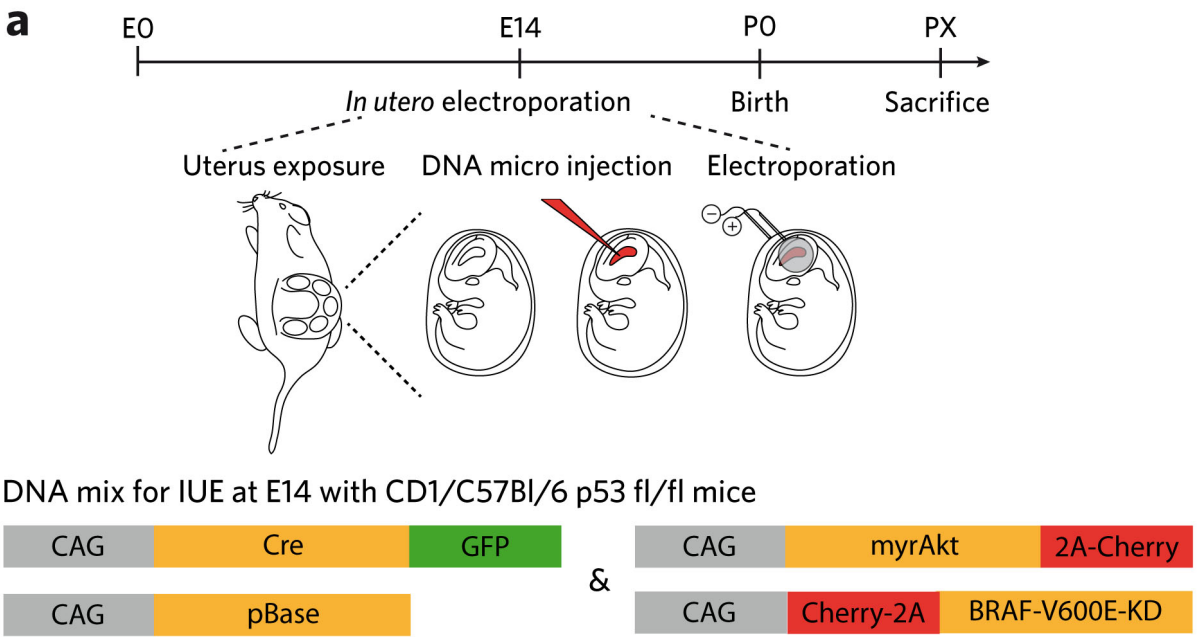

Figure 6.1: **Intraventricular *in utero* electroporation of p53$^{fl/fl}$ mice.** (a) At E14, embryos of time pregnant mice were *in utero* electroporated with a mix of plasmids: CAG-Cre-GFP, CAG-myrAkt-2A-mCherry, CAG-mCherry-2A-BRAF-V600E-KD and CAG-pBase plasmids.

6.1.1 Cerebral tumor characterization

For our study we obtained the C57Bl/6 Trp53tm1Brn/J (provided by The Jackson Laboratory, USA) mouse strain that enables Cre-recombinase (Cre) mediated p53 knockout. However, we observed that C57Bl/6 mice often have small litters ($\leq$ 7 pups) with low pup-survival rates, especially after the stressful surgery. To enhance pup survival and thus, litter size, we transferred the floxed p53 locus from C57Bl/6 mice into the CD1 background, since these mice have larger litter sizes and excellent mother instincts. We crossbred C57Bl/6 Trp53tm1Brn/J mice with CD1 mice for three generations, which was sufficient to increase pup survival dramatically (91.0$\pm$6.1% to previously 10.9$\pm$7.6%). By using female CD1 p53$^{fl/fl}$ mice and C57Bl/6 male p53$^{fl/fl}$ mice for our GG mouse model we combined most of the positive traits of the CD1 mouse line (large litter size, very high survival) and the C57Bl/6 mouse line (high electroporation efficiency). At E14, embryos were *in utero* electroporated with the plasmid mix (pBase, mCherry-tagged BRAF-V600E-KD, myrAkt and CAG-Cre-GFP to knockout p53, Fig. 6.1).

Mice electroporated with all four plasmids developed after 33 - 75 days unilateral, rapidly growing tumors, most often localized in rather medial than lateral parts of the brain. The enlargement of the dorsal part of the brain due to the large tumor volume was visible in living mice as an occipital deformation (Fig. 6.2a). At this stage, mice were less active and started to loose weight rapidly. They were sacrificed as soon as they lost more than 20% body weight within 24h. The resulting tumors showed high variability in volume and vascularization (Fig. 6.2b - d). In most cases, strong vascularization with intraventricular haemorrhage was observed (Fig. 6.2b). While some tumors occupied nearly the whole hemisphere (Fig. 6.2c), others were smaller, less vascularized and clearly circumscribed (Fig. 6.2d, Fig. 6.3a).

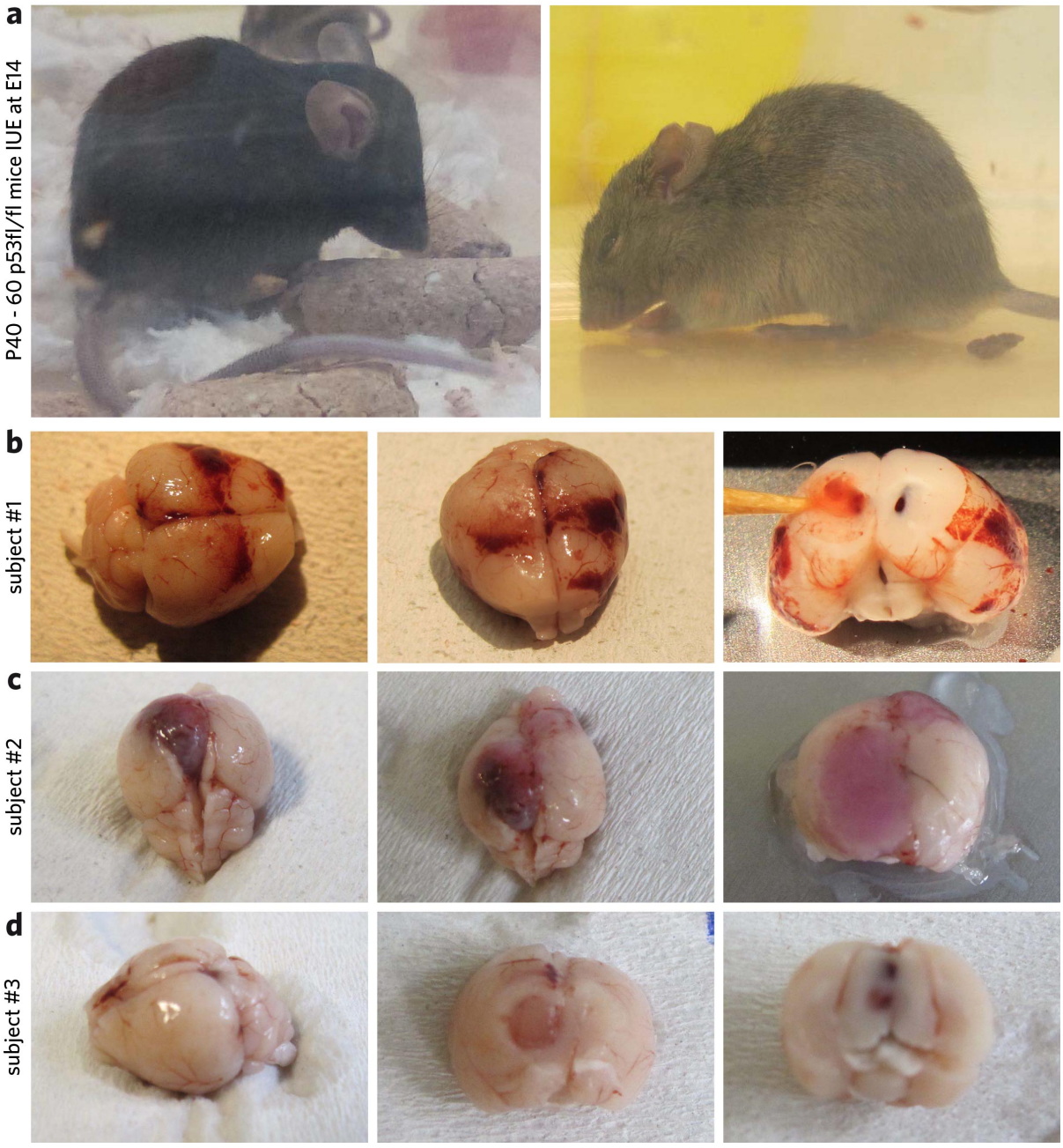

Figure 6.2: **Expression of BRAF-V600E-KD and myrAkt in p53 knockout cells induces brain tumors.** (a) Electroporated mice older than 30 days started to develop head deformations with a pronounced swelling of the back of the head, most often accompanied with reduced behavioral activity, feeding and rapid weight loss. Exemplary pictures of brain tumors from different mice: (b) Brains of affected mice showed most often strong vascularization and blood-filled lateral ventricles. (c) The size of the resulting tumor varied greatly between individuals. While in some cases the tumor occupied most of one hemisphere, (d) it was smaller and less vascularized in others.

HE staining of paraffin embedded brain sections clearly defining tumor versus non-tumor cells revealed cellular abnormalities, such as enlarged, dysplastic neurons with irregular orientation and sometimes even bi-nucleated cells (Fig. 6.3b, c). These tumors were also visible in 80µm thick vibratome brain sections of 4% PFA-perfused mice as red-fluorescing tumor-cell aggregates (Fig. 6.3c). Immunohistochemical stainings of respective brain slices of one exemplary mouse with a circumscribed tumor is shown in (Fig. 6.3d, e). It harbored dysplastic and bi-nucleated neurons that resembled cellular compo-

nents of GGs and revealed only a few p53-positive cells within the tumor. This was in strong contrast to the proximal non-tumor, peri-lesional brain tissue or the contralateral cortex (Fig. 6.3d, e; dashed line separates tumor from non-tumor tissue, upper part is tumor, lower part is non-tumor tissue). MAP-2 staining was strong and abundant on the contralateral hemisphere and at the vicinity of the tumor, whereas MAP-2 fluorescence was weak within the tumor (Fig. 6.3d). However, the weak MAP-2 signal outlined highly enlarged and aberrantly oriented neurons within the tumor as already seen in the HE staining. Similarly, only a few GFAP positive glial cells were observed within this particular tumor, whereas the peri-lesional tissue as well as the contralateral hemisphere showed strong GFAP signal with a large number of astrocytes (Fig. 6.3e). However, tumor characteristics varied significantly between litter mates, including immunoreactivity for glial and neuronal cell types.

Mortality rates of mice developing tumors were highly variable and no clear correlation between tumor size and time of death could be determined. Tumor-bearing animals began to die at P33, however, at day 75, all remaining mice were sacrificed for analysis (Fig. 6.3f; mice from two different litters, n = 13 mice). Out of thirteen $p53^{fl/fl}$ mice *in utero* electroporated with the cocktail of tumor-inducing plasmids, only two did not develop tumors until the time point of analysis at P75. As a control, mice heterozygous for the p53 flox-locus ($p53^{fl/wt}$ mice) were electroporated with the same combination of plasmids, CAG-Cre-GFP, myrAkt-mCherry and BRAF-V600E-KD-2A-mCherry and pBase. At P75, none of these mice showed clear signs of tumor growth, including head deformations or weight loss and were therefore sacrificed (Fig. 6.3f; mice from two different litters, n = 11 mice). Only in three out of eleven mice, small tumor-resembling, red-fluorescent masses (as shown in Fig. 6.3c) were observed by fluorescence microscopy. This observation indicates that these mice have a reduced risk for tumor formation or slower tumor growth kinetics and that the rapid malignant course of the tumors in the $p53^{fl/fl}$ mice may be due to p53 knockout. Together, these results suggest that loss of p53 together with a mutated form of the BRAF kinase domain and a constitutively active Akt induces fast growing tumors harboring enlarged and dysplastic neurons.

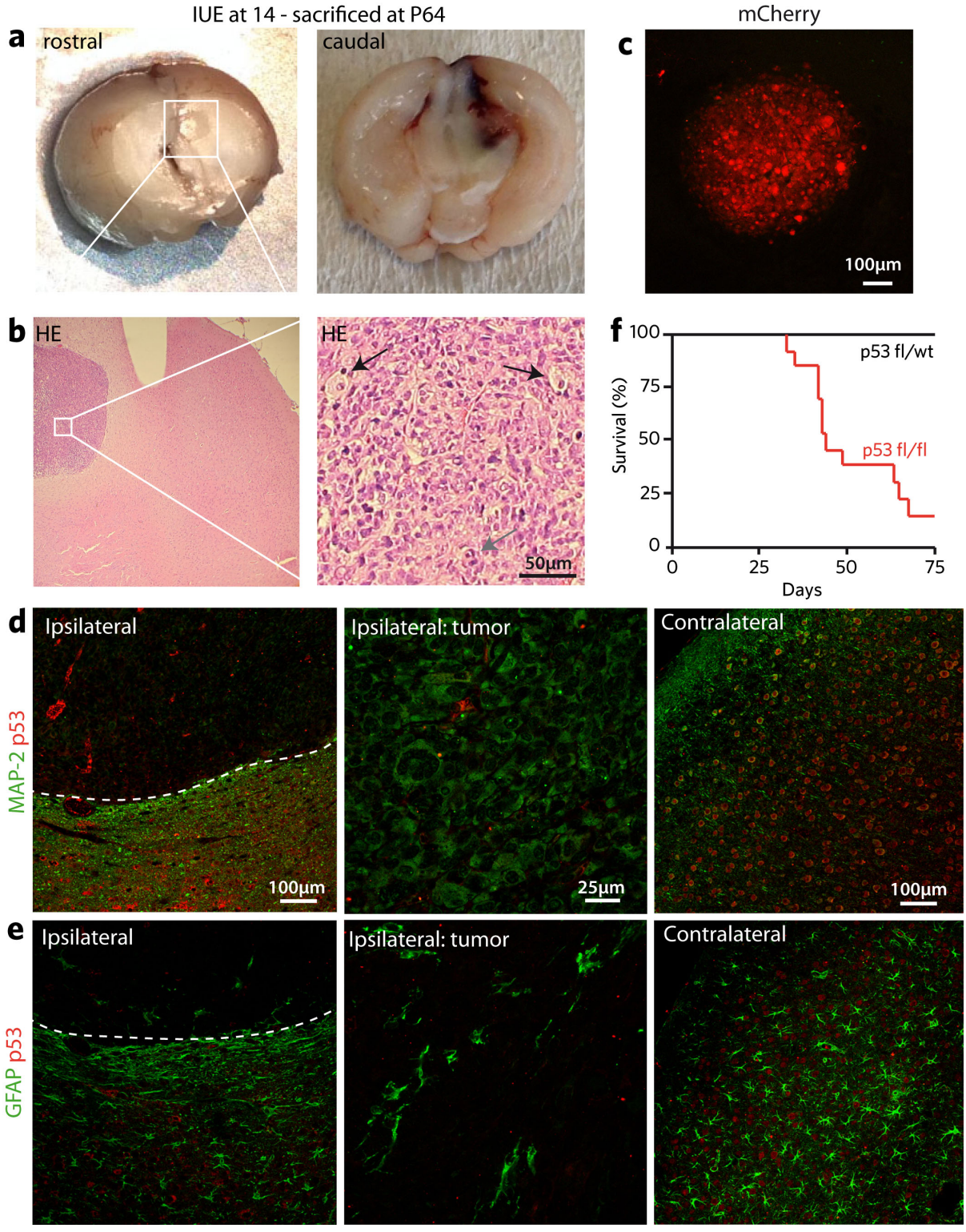

Figure 6.3: **Cellular characteristics of tumor cells and high mortality of mice with tumors.** (a) Exemplary brain with a rather small tumor and moderate vascularization induced by IUE at E14 with CAG-Cre-GFP, pBase, myrAkt-mCherry and Cherry-BRAF-V600E-KD. (b) HE staining revealed cellular abnormalities such as enlarged cell bodies (black arrow) or sometimes bi-nucleated cells (grey arrow). (c) Exemplary confocal image of a brain section with a small tumor with strong mCherry fluorescence. (d) Antibody staining against MAP-2 and p53 in an exemplary mouse harboring a tumor with GG-resembling features revealed low p53 and MAP-2 IR but large and aberrantly oriented cells within the tumor. This was in strong contrast to the peri-lesional and contralateral tissue. Here, MAP-2 positive neurons colocalized with the tumor suppressor protein p53. (e) A low abundance of GFAP positive astrocytes was detected within the tumor compared to peri-lesional and contralateral tissue with substantially more astrocytes. Dashed lines indicate tumor borders, upper part is tumor and lower part of the micrograph is peri-lesional brain. All scale bars as indicated. (f) Kaplan-Meier curve shows the survival pattern of heterozygous mice versus mice homozygous for $p53^{fl/fl}$ (n = 13 $p53^{fl/fl}$ and n = 11 $p53^{fl/wt}$ mice from two different litters).

Even though the induced tumors appeared to be heterogeneous, immunohistochemical stainings revealed certain cellular similarities, partly resembling those of GGs. Typically, cells within GGs show strong IR for chromogranin A, neurofilament (NF) and MAP2 [42], while GFAP and vimentin staining is found in varying proportion and distribution but is most often also highly increased [13]. In a first and preliminary, non-quantitative analysis, most tumors demonstrated highly enlarged cells with strong vimentin and chromogranin A IR (Fig. 6.4a, b, f). MAP-2, neurofilament (NF) and GFAP staining on the other hand was varying throughout the group. Around 1/3 of the tumors presented with weak GFAP or MAP-2 signals while 2/3 showed strong GFAP, NF, or MAP-2 IR (Fig. 6.4c, d, e). Furthermore, HE and MAP-2 staining clearly identified enlarged, dysplastic cell components within the tumor with random orientations (Fig. 6.4a, d). Two of the thirteen $p53^{fl/fl}$ mice, that did not develop tumors, only showed strong infiltration of GFAP-positive astrocytes in most parts of the brain.

Overall, the induced tumors appeared heterogeneous in terms of immunoreactivity, size, and growth kinetics. While one population of tumors showed typical characteristics of GGs the other rather resembled gliomas, suggesting that the exact composition, location or number of progenitor cells electroporated with the plasmid-mix defines the resulting tumor type. Nevertheless, these results indicate that GGs develop from a mutual mutated progenitor cell population.

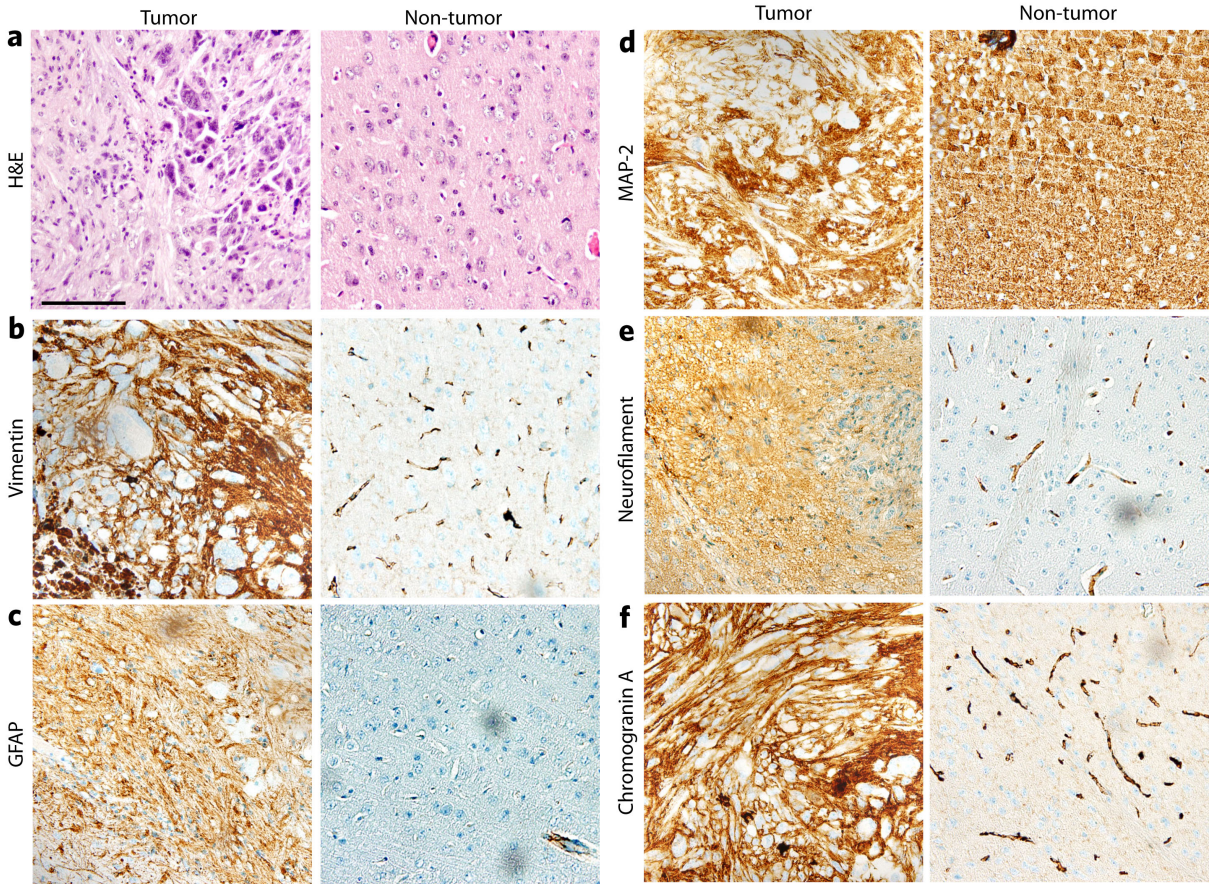

Figure 6.4: **Representative IHC micrographs of the predominant tumor type.** (a) Representative micrographs of the prevalent tumor entity localized in the area around the lateral and medial septal nucleus. It shows enlarged and irregularly oriented cellular components, (b) strong vimentin, (c) GFAP, (d) MAP-2, (e) neurofilament, (f) and chromogranin A IR, which is in contrast to contralateral non-tumor brain tissue; Scale bar 100µm.

6.2 Analysis of dysplastic neurons within tuber-like lesions in an improved TSC mouse model

Tuberous sclerosis (TSC) is an autosomal-dominant inherited, multi-organic disorder characterized by dysplastic lesions in the brain, the so-called cortical tubers [273]. They are composed of giant cells and large dysplastic neurons that closely resemble balloon cells and cytomegalic dysplastic neurons in FCDIIb cases. Thus, a common pathogenic pathway was proposed [24]. In TSC and FCDIIb patients different *TSC1* mutations or allelic variants have been described. However, it is unclear whether these are leading to the emergence of dysplastic neurons or not [94, 101, 103, 104]. Moreover, there is still no consensus on the pathogenetic situation within cortical tubers of TSC patients. While extracerebral neoplasms frequently have loss of heterozygosity (LOH), such events are rarely detected in cortical tubers [107, 108]. Somatic second-hit events in *TSC1* heterozygous patients may therefore account for cortical tubers and their dysplastic neurons, especially since no tubers have been reported in mice heterozygous for *TSC1* [109–111, 113, 114]. However, another study showed that second hits are rare in cortical tubers [116]. Despite of a multitude of different studies on TSC and various existing TSC animal models, fundamental and crucial information about genetic causes of the emergence of dysplastic neurons and thus cortical tubers are still unclear or missing. Here, we use an improved mouse model based on a recently developed TSC model [112] to analyze the pathological situation of TSC associated brain lesions and their functional hallmark, dysplastic neurons.

6.2.1 Establishing an improved TSC mouse model

Focal *TSC1* knockout by *in utero* electroporation generates a focal lesion that mimics more closely the pathologic situation in human patients than any other TSC mouse model, however, this model is still only rarely used [112]. Most researchers utilizing TSC mouse models use the common C57Bl/6 mouse strain because it is a highly homogenous, inbred laboratory mouse strain. The C57Bl/6 TSC1tm1Djk/J strain provided by The Jackson Laboratory is an established mouse model for Cre-mediated *TSC1* knockout and thus, for research on tuberous sclerosis. For our study, we aimed to knockout *TSC1* in a focal cortical area, in a subset of precursor cells, during mid-corticogenesis. This is achieved by *in utero* electroporation of Cre. The resulting lesion is investigated postnatally at P24 - 30. As mentioned in chapter 6.1.1, to enhance pup survival and thus, litter size, we aimed to use CD1 *TSC1*$^{fl/fl}$ mice. Since there are no CD1 *TSC1*$^{fl/fl}$ mice available, we generated *TSC1*$^{fl/fl}$ mice with the CD1 background (CD1 *TSC1*$^{fl/fl}$ mice) by crossbreeding CD1 mice with C57Bl/6 TSC1tm1Djk/J mice for three generations. Thereby, we established an improved TSC mouse model for IUE by mating CD1 *TSC1*$^{fl/fl}$ female mice with C57Bl/6 *TSC1*$^{fl/fl}$ male mice.

First, CD1 *TSC1*$^{fl/fl}$ x CD1 *TSC1*$^{fl/fl}$ mice were IUE at E14 with CAG-Cre-GFP and mCherry or mCherry alone as a control to validate that also in this genetic background, Cre mediates efficient *TSC1* deletion that results in the activation of the mTOR pathway, as it has been reported in the C57Bl/6 background [112]. At P24 - 30, mice were sacrificed and coronal sections were analyzed for typical markers of aberrant mTOR activity such as strong pS6 IR and increased cell volume/soma size [112]. Most electroporated neurons positive for NeuN were observed within the motor- and somatosensory cortex ranging from layer II/III to IV. In accordance, strong pS6 IR was observed only in the ipsilateral cor-

tex of mice *in utero* electroporated with CAG-Cre-GFP together with the volume dye mCherry (Fig. 6.5a, c), but not on the contralateral hemisphere (Fig. 6.5b) or after IUE of the volume dye alone (Fig. 6.5d, mCherry/*TSC1*$^{fl/fl}$ 483.2±10.6a.u. vs. mCherry/Cre^{+}/*TSC1*$^{-/-}$ 1339.5±39.1a.u.; One-way ANOVA with Bonferroni post correction ***$p \leq 0.001$, N = 7 − 8 mice with n = 23 − 30 cells each). Furthermore, soma size of individual Cre-positive *TSC1* knockout neurons was increased (Fig. 6.5c) compared to neurons electroporated with mCherry alone (Fig. 6.5d; mCherry/*TSC1*$^{fl/fl}$ 163.7±3.0μm^2 vs. mCherry/Cre^{+}/*TSC1*$^{-/-}$ 391.9±5.3μm^2; One-way ANOVA with Bonferroni post-correction ***$p \leq 0.001$, N = 7 − 8 mice with n = 41 − 60 neurons each).

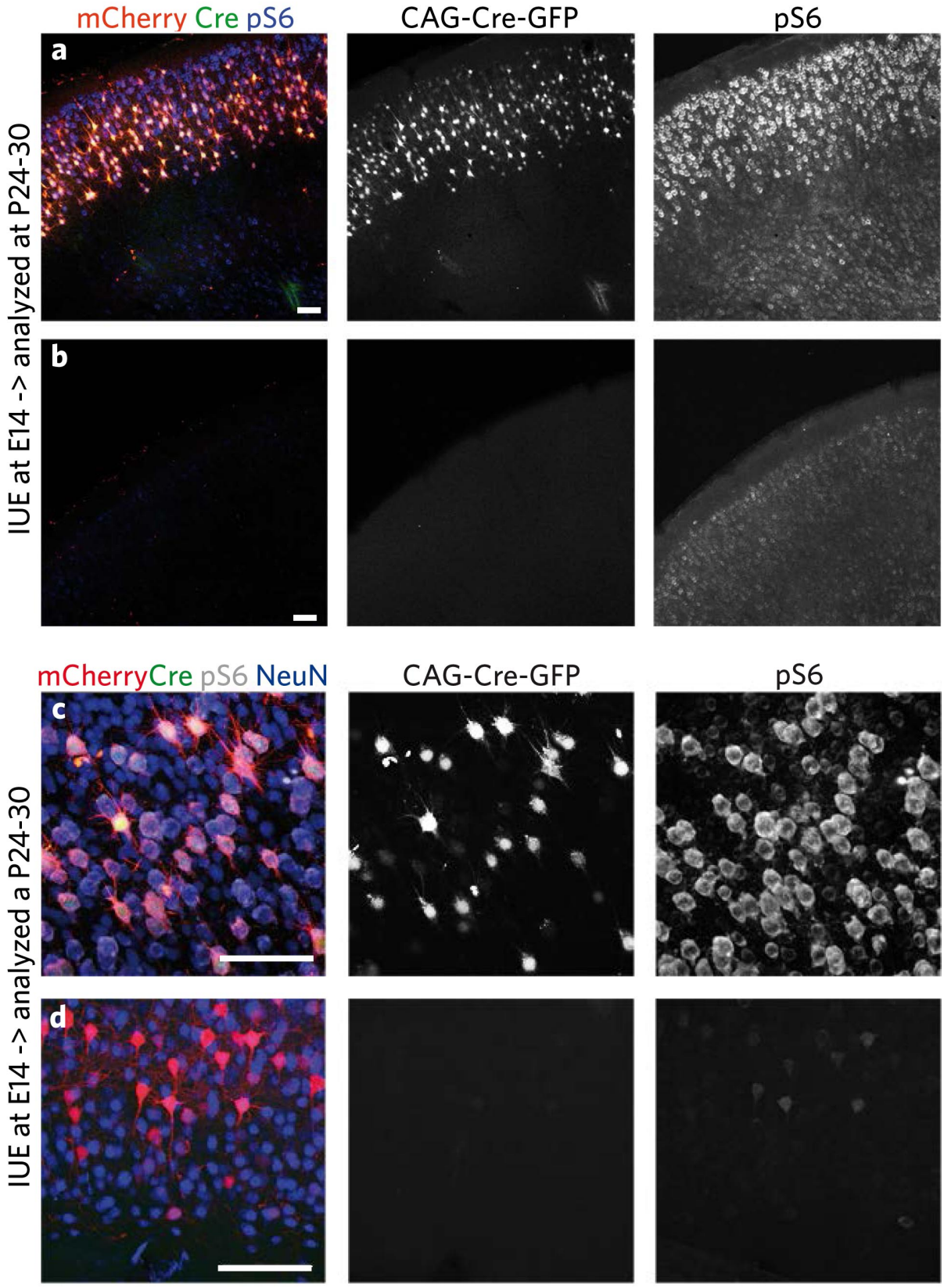

Figure 6.5: **Enhanced mTOR pathway activation following Cre expression in CD1 *TSC1*$^{fl/fl}$ mice.** (a) Brain slices of CD1 *TSC1*$^{fl/fl}$ mice (E14) *in utero* electroporated with either CAG-Cre-GFP and mCherry or only mCherry as a control were stained against pS6 at P24 - 30. Neurons from the ipsilateral cortex with strong Cre-GFP and mCherry expression had a high pS6 immunoreactivity, (b) unlike the contralateral, non-electroporated hemisphere that had only low pS6 IR; Scale bar 100µm. (c) Cre- and mCherry-electroporated neurons were NeuN-positive, appeared larger and had strong pS6 IR. (d) In contrast, neurons from the ipsilateral cortex, electroporated with only mCherry had only weak pS6 fluorescence intensity and appeared normal sized; Scale bar 100µm. Image inspired by Robens et al., 2016 [269].

Recent studies on C57Bl/6 *TSC1*$^{fl/fl}$ mice demonstrated that Cre mediated, aberrant activation of the mTOR pathway in neurons results in excessive branching and a thickening of dendrites [110, 274]. To examine if we observe similar changes of neuronal morphology upon *TSC1* knockout in CD1 *TSC1*$^{fl/fl}$ mice, we performed morphometric analyses of single CAG-Cre-GFP or control *in utero* electroporated neurons. Sholl analysis is a method to quantify the complexity of neuronal arbors. The number of neurite intersections with concentric circles originating from the soma and increasing in diameter is counted for each individual neuron. Analysis of respective neurons revealed a significantly increased number of intersections of neurites with Sholl circles, suggesting dendritic overgrowth upon Cre-mediated *TSC1* knockout (Fig. 6.6a, b). This was in contrast the physiological neuronal arbors of mCherry electroporated neurons (Fig. 6.6a, c; Mann-Whitney U-test ***p≤0.001, n = 5 control, n = 8 *TSC1* knockout neurons). Furthermore, Cre-induced *TSC1* knockout resulted in an increased neurite diameter (Fig. 6.6d, e).

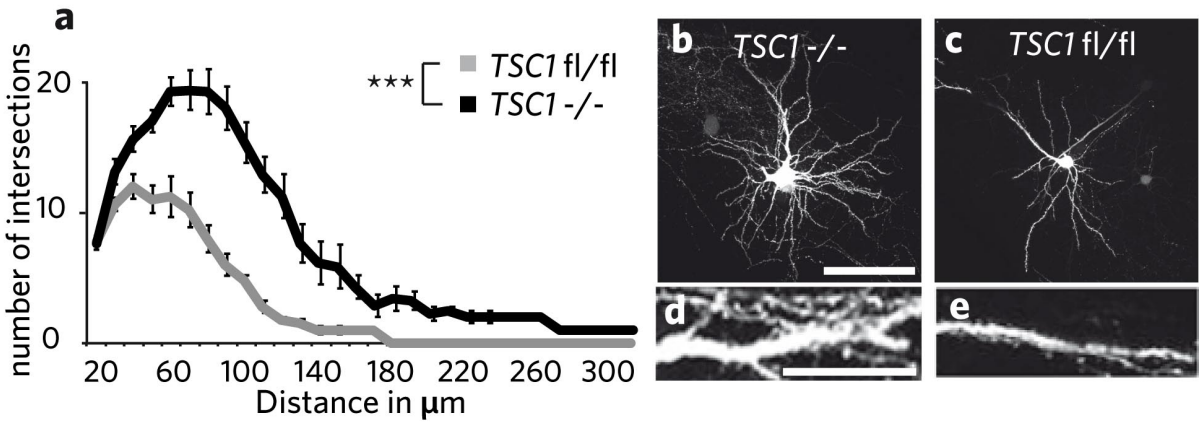

Figure 6.6: **Altered neuronal morphology upon Cre expression in CD1 *TSC1*$^{fl/fl}$ mice.** (a) Sholl analysis revealed an increased number of intersections in (b) dysplastic *TSC1* knockout neurons compared to (c) control neurons; Scale bar 100µm (Mann-Whitney U-test: ***p≤0.001, n = 5 control, n = 8 *TSC1* knockout neurons). (d, e) A larger neurite diameter was observed in Cre-electroporated *TSC1* knockout neurons compared to mCherry control neurons; Scale bar 25µm. Image inspired by Robens et al., 2016 [269].

CAG-Cre-GFP *in utero* electroporation and subsequent expression did not result in considerable astrocyte infiltration or any other signs of gliosis (not shown). Together, these results demonstrate that Cre-mediated knockdown of *TSC1* in the CD1 background causes phenotypically identical changes as observed in C57Bl/6 *TSC1*$^{fl/fl}$ mice. These experiments demonstrate the functionality of this mouse line for further studies.

6.2.2 Embryonic *TSC1* knockout leads to altered final positioning of cortical neurons

Abnormal neuronal polarity or morphology have been indicated to alter migration characteristics in developing cortical neurons during corticogenesis [165, 275]. Since neuronal morphology is altered upon Cre-mediated *TSC1* knockout (i.e. enlarged neuronal cell bodies) in our experimental setup, we asked whether these changes interfere with their migration properties or final positioning within the cortical plate. We *in utero* electroporated mice with CAG-Cre-GFP and mCherry at different embryonic

stages (E14 - 18) and analyzed their cortical localization at P24 - 30. Electroporation with only mCherry at E14 revealed that neurons were mostly located in layer II/III (66.7±8.3%) but also in part in upper layer IV (33.3±8.3%). In contrast, TSC1 ablated neurons were localized in more or less similar numbers in layer II/III (39.7±8.0%) and IV (54.4±6.9%) and also in part in even lower layers (5.9±2.3%; Fig. 6.7a, b, g). Nearly all control neurons electroporated at E16 clustered at the uppermost part of layer II/III (93.4±2.6%), whereas *TSC1* knockout neurons were aberrantly dispersed throughout layers II/III, with only 35.2±7.2% neurons in the upper half of layer II/III, 50.4±3.9% in the lower layer II/III and 14.4%±6.9 in layer IV (Fig. 6.7c, d, g). Electroporation of CAG-Cre-GFP at E17 resulted in a wider dispersion of enlarged *TSC1* knockout neurons mainly from the middle to the external border of layer II/III: 37.6±8.0% neurons were found in the upper part of layer II/III, 56.7±6.8% in lower layer II/III and 5.7±3.5% in layer IV. In strong contrast, neurons electroporated at E17 with the control plasmid mCherry formed a very delicate, homogenous band at the external border of layer II (91.6±3.4%), as expected at such relatively late time points of embryonic development (Fig. 6.7e, f, g). No electroporated cells were observed in the cortex when IUE was carried out at E18 (data not shown).

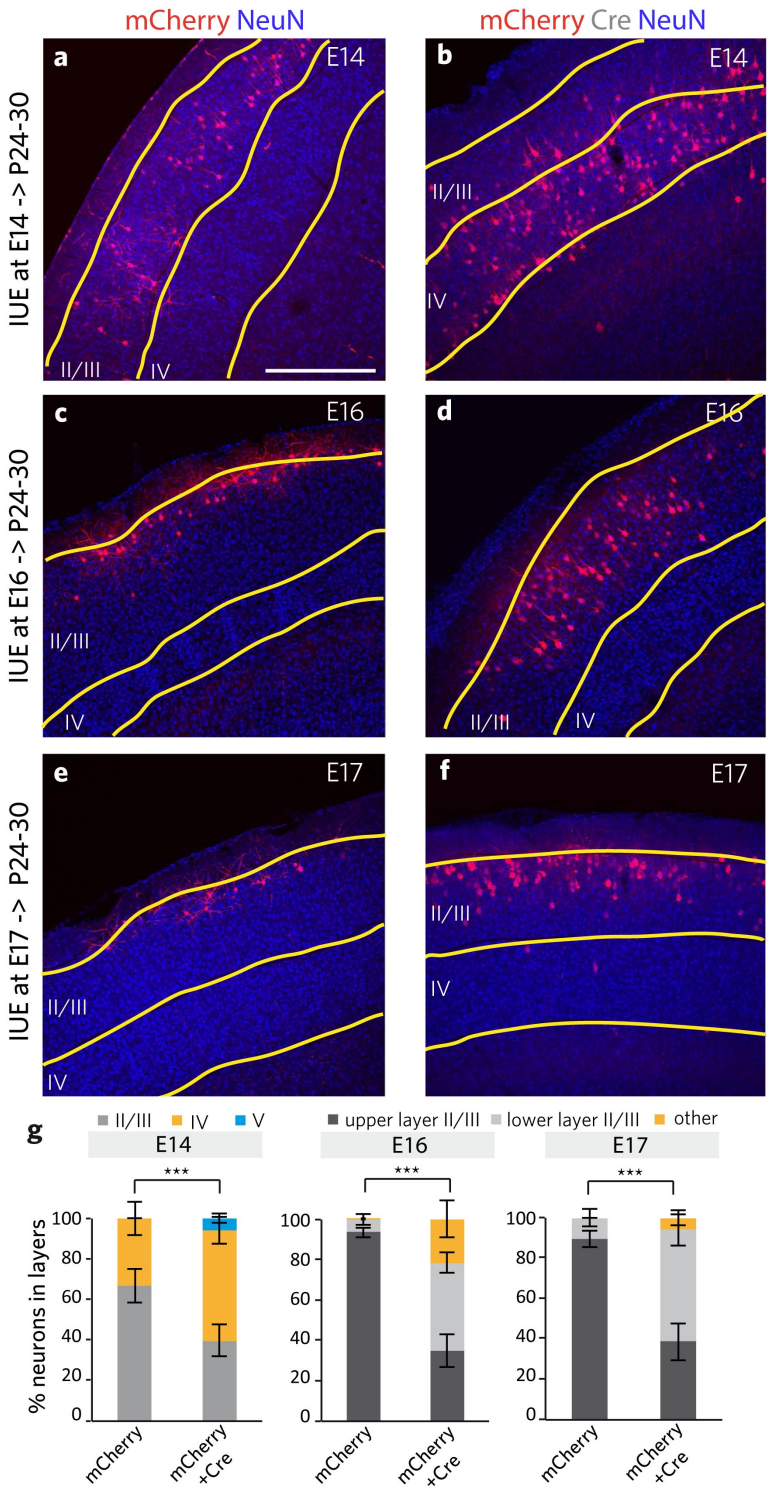

Figure 6.7: **Cre-induced *TSC1* knockout affects final cortical positioning of developing neurons.** (a) At E14, E16, and E17 $TSC1^{fl/fl}$ mice were *in utero* electroporated with either CAG-Cre-GFP and mCherry or mCherry alone as control and analyzed at P24 - 30. After control IUE at E14, approximately 1/3 of all control electroporated neurons were located in upper layer IV and 2/3 in layer II/III with an even distribution throughout this layer. (b) In contrast, more Cre-expressing *TSC1* knockout neurons were located in layer IV (54.4%) than in layer II/III (39.7%). (c) At E16, most control neurons were located at the upper third of layer II/III (93.4%), (d) while *TSC1* knockout cells were widely dispersed throughout most parts of layer II/III with only a few in layer IV. (e) IUE at E17 with the control plasmid mCherry led to clustering of neurons around the border of layer II/III and layer I (91.6%) with only a small number of electroporated cells (a, b, e, 25.8±12 cells per 80µm slice in contrast to >100-300 cells per slice at E14). (f) TSC1 ablated neurons appeared evenly dispersed all over layer II/III, in lower parts of layer II/III (56.7%) and at upper cortical layer II/III (37.6%). (g) Quantification of the percentage of neurons in each layer (N = 4 – 16 mice analyzed, all electroporated neurons in a brain slice were analyzed; E14: n = 32 – 249 neurons per brain slice, E16: n = 24 – 301 neurons per slice and for E17: n = 9 – 103 neurons per slice; Two-way ANOVA with Bonferroni post-correction and Chi-square test: ***$p \leq 0.001$; Scale bar 400µm). Image inspired by Robens et al., 2016 [269].

These results were corroborated by measuring the distance from each electroporated neuron to layer I in order to quantify their distribution in the cortex. Again, the distribution of *TSC1* knockout neurons was significantly different compared to age-matched control electroporated animals (Fig.6.8 a). Upon Cre-expression at different embryonic stages, the position of individual neurons is more dispersed towards deeper cortical layers (E14: mCherry/$TSC1^{fl/fl}$ 286.2±5.8µm vs. mCherry/$Cre^{+}/TSC1^{-/-}$ 413.0±4.9µm; E16: mCherry/$TSC1^{fl/fl}$ 79.5 ±4.0µm vs. mCherry/$Cre^{+}/TSC1^{-/-}$ 245.3 ±5.8µm; E17: mCherry/$TSC1^{fl/fl}$ 53.5±5.8µm vs. mCherry/$Cre^{+}/TSC1^{-/-}$ 116.9±6.3µm; Mann-Whitney U-test ***p≤0.001, N = 4 – 11 mice, all neurons on a brain slice were analyzed). Together, these results suggest that *TSC1* knockout results in defective final positioning independent of the developmental stage.

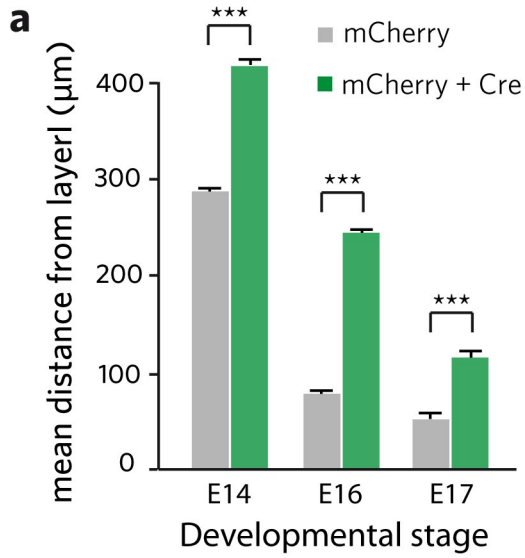

Figure 6.8: ***TSC1* knockout neurons have an increased mean distance to cortex layer I**. (a) Cre-mediated *in utero* knockout of *TSC1* at E14, E16, and E17 resulted on average in a significantly larger distance of most neurons to the upper layer of the cortex at P24 - 30 (N = 4 – 16 mice analyzed, all electroporated neurons in a brain slice were analyzed; E14: n = 537 mCherry/$TSC1^{fl/fl}$ neurons and n = 1258 mCherry/$Cre^{+}/TSC1^{-/-}$ neurons, E16: n = 352 mCherry/$TSC1^{fl/fl}$ neurons and n = 886 mCherry/$Cre^{+}/TSC1^{-/-}$ neurons, E17: n = 106 mCherry/$TSC1^{fl/fl}$ neurons and n = 509 mCherry/$Cre^{+}/TSC1^{-/-}$ neurons; Mann-Whitney U-test: ***p≤0.001).

6.2.3 Induction of dysplastic neurons within tuber-like lesions is not restricted to a certain time point in embryonic development

TSC1 knockout at E14 resulted in tuber-like lesions with prominent dysplastic neurons, as demonstrated by the aberrant dendritic morphology, increased pS6 IR, increased cell size and ectopically located neurons within the cortex. We therefore asked next, whether the emergence of dysplastic neurons depends on a certain developmental stage and if the exact time point of TSC1 loss influences their phenotype. We *in utero* electroporated mice at E16, E17, and E18 and quantified soma size of individual neurons as an indicator for increased mTOR pathway that is characteristic for dysplastic neurons within tuber-like lesions. We observed *TSC1* knockout neurons of P24 - 30 mice to be strongly increased in size when CAG-Cre-GFP was electroporated at E16 (Fig. 6.9a) or E17 (Fig. 6.9b). Co-electroporation of CAG-Cre-GFP and the mCherry expressing *TSC1* plasmid successfully rescued the morphological effects of *TSC1* knockout at E16 and E17. No mCherry expressing neurons were observed when IUE was carried out at E18. A detailed quantification showed that *TSC1* knockout at E16 and E17 equally increased soma size

two-fold, compared to control electroporated neurons of age matched mice. Co-electroporation of *TSC1* rescued the Cre-mediated effect on soma size back to control levels (Fig. 6.9c; N = 3 - 6 mice, for E16: n = 22 – 33 neurons per brain slice and for E17: n = 9 – 23 neurons per brain slice; for E16: mCherry/$TSC1^{fl/fl}$ 153.2±4.2µm^2 vs. mCherry/Cre$^+$/$TSC1^{-/-}$ 409.6±9.4µm^2 vs. mCherry/Cre$^+$/$TSC1^+$ 179.7±7.2µm^2; E17: mCherry/$TSC1^{fl/fl}$ 157.3±3.0µm^2 vs. mCherry/Cre$^+$/$TSC1^{-/-}$ 424.6±10.2µm^{2}vs. mCherry/Cre$^+$/$TSC1^+$ 162.2±5.7µm^2; One-way ANOVA with Bonferroni post-correction ***p≤0.001). No morphological differences of neurons electroporated at different time points were observed. These results indicate that the formation of dysplastic neurons is independent of the exact embryonic time point of TSC1 loss. On the other hand, their emergence can be rescued by TSC1 expression at all time points investigated.

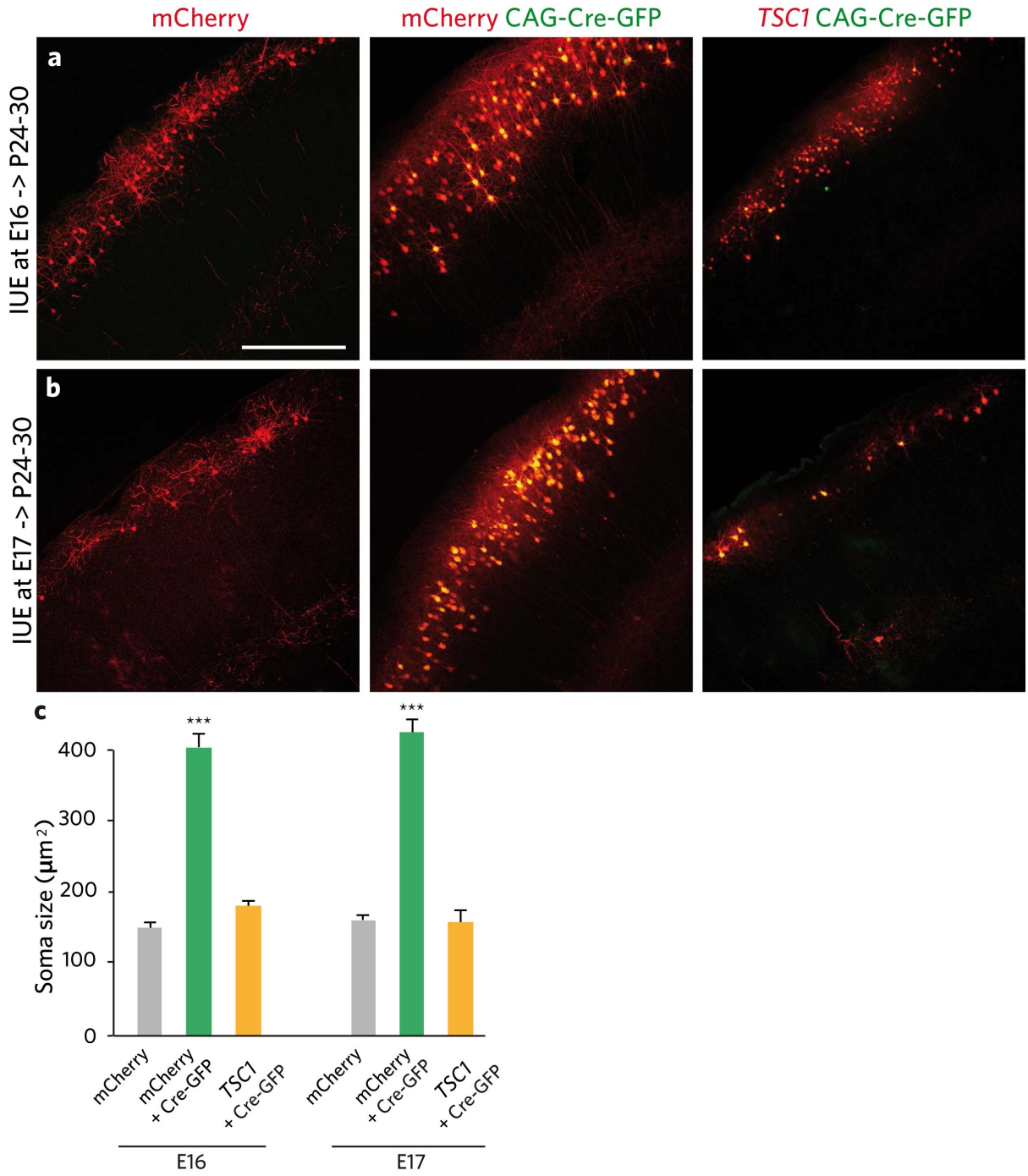

Figure 6.9: ***TSC1* knockout at different embryonic stages does not affect the emergence of dysplastic neurons caused by TSC1 loss.** (a) *TSC1*$^{fl/fl}$ mice were electroporated with mCherry, mCherry&Cre or mCherry&*TSC1*-mCherry at E16 or (b) E17 and analyzed at P24 - 30; Scale bar 400µm. (c) Quantification of their soma size revealed a significant increase in neuron size in Cre-electroporated mice, in contrast to neurons of mice electroporated with mCherry or the rescue construct. The increase of soma size following Cre expression was similar when electroporating at E16 or E17 (N = 3 - 6 mice; for E16: n = 22 – 33 neurons per brain slice and for E17: n = 9 – 23 neurons per brain slice; One-way ANOVA with Bonferroni post-correction: $^{***}p \leq 0.001$). Image inspired by Robens et al., 2016 [269].

6.2.4 Focal cortical expression of distinct *TSC1* variants results in tuber-like lesions

The *in vitro* expression of two stop mutants of the *TSC1* gene frequently found in TSC patients, encoding hamartin^{R692X} and hamartin^{R786X}, was recently shown to result in an aberrant subcellular distribution

and substantial binding deficits with the *TSC2* gene product tuberin. Similarly, the expression of a polymorphism that is frequently found in FCDIIb individuals, hamartin^{H732Y}, also results in abnormal cellular distribution and impaired hamartin-tuberin heteromer formation *in vitro* [93]. It is so far unresolved whether these alterations of the *TSC1* gene leading to the described functional changes result in the emergence of dysplastic neurons as found in cortical tubers or FCDIIb lesions. To address this possibility, we *in utero* electroporated these different mCherry labeled *TSC1* variants or an mCherry-*TSC1* wildtype (WT) plasmid as a control, together with CAG-Cre-GFP at E14. At P24 - 30, soma size and pS6 fluorescence intensity were quantified and used as an indicator for mTOR-pathway upregulation and thus dysplastic neuron formation. Since we already showed in chapter 6.2.1 that TSC1 loss at E14 results in a substantial increase of these two parameters in dysplastic neurons, they are a valid read-out for assessing the extend of lesion formation.

Electroporation of *TSC1*-WT or *TSC1*-H732Y had no effects on cell size or S6 phosphorylation (Fig. 6.10a, b). Occasionally, enlarged cells with strong pS6 IR were observed within the cortex of respective mice. These cells, however, were negative for mCherry (and thus negative for *TSC1*-WT or *TSC1*-H732Y), indicating that expression of either *TSC1*-WT or the *TSC1*-H732Y variant in a *TSC1*-null background rescues the Cre-mediated effect on neuronal cell size and increased S6 phosphorylation in a comparable fashion. In contrast, expression of the truncated variants *TSC1*-R692X or *TSC1*-R786X did not rescue the Cre-mediated effect. Individual mCherry expressing neurons showed strong pS6 IR with dramatically increased cell size (Fig. 6.10c, d). Also neighboring cells with only low mCherry or Cre-GFP expression had strong pS6 signals. Detailed quantification demonstrated that, in comparison to only mCherry electroporated cortical neurons, expression of *TSC1*-WT&Cre or *TSC1*-H732Y&Cre had no effect on pS6 fluorescence intensity or soma size. In direct contrast, expression of CAG-Cre-GFP&mCherry resulted, as mentioned in chapter 6.2.1, in a strong increase in pS6 fluorescence intensity and soma size that was comparable to expression of *TSC1*-R692X&Cre or *TSC1*-R786X&Cre. Compared to control-, or *TSC1*-WT&Cre-, or *TSC1*-H732Y&Cre-electroporated neurons, Cre&mCherry-, or *TSC1*-R692X&Cre-, or *TSC1*-R786X&Cre-expressing neurons had a two-fold increase in pS6 fluorescence intensity and soma size (Fig. 6.10e, f; Fluorescence intensity: N = 6 mice with n = 33 – 41 neurons each; mCherry/*TSC1*$^{fl/fl}$ 483.2 $\pm$10.6a.u vs. mCherry/Cre^{+}/*TSC1*$^{-/-}$ 1339.5 $\pm$39.1a.u, mCherry/Cre^{+}/*TSC1*-WT 420.7 $\pm$6.4a.u, mCherry/Cre^{+}/*TSC1*-H732Y 427.8 $\pm$8.7a.u, mCherry/Cre^{+}/*TSC1*-R692X 1237.1 $\pm$22.0a.u, mCherry/Cre^{+}/*TSC1*-R786X 1210.9 $\pm$35.7a.u; One-way ANOVA with Bonferroni post-correction $^{***}p\leq0.001$; Soma size: N = 6 mice with n = 50 – 65 cells each; mCherry/*TSC1*$^{fl/fl}$ 163.7 $\pm$3.0µm^2 vs. mCherry/Cre^{+}/*TSC1*$^{-/-}$ 391.9 $\pm$5.3µm^2; mCherry/Cre^{+}/*TSC1*-WT 154.8 $\pm$3.0µm^2, mCherry/Cre^{+}/*TSC1*-H732Y 173.0 $\pm$2.7µm^2, mCherry/Cre^{+}/*TSC1*-R692X 431.6 $\pm$ 4.7µm^2, mCherry/Cre^{+}/*TSC1*-R786X 339.5 $\pm$5.9µm^2; One-way ANOVA with Bonferroni post-correction $^{***}p \leq0.001$). Thus, IUE of different disease-associated *TSC1* variants has distinct phenotypes, suggesting that *TSC1*-R692X and *TSC1*-R786X variants may be involved in the emergence of dysplastic neuron and thus, tuber-like lesions. On the other hand the *TSC1*-H732Y variant, whose expression resulted in a normal neuronal morphology and weak pS6 fluorescence intensity similar to *TSC1*-WT, may not be relevant for the formation of dysplastic neurons in FCDIIb lesions.

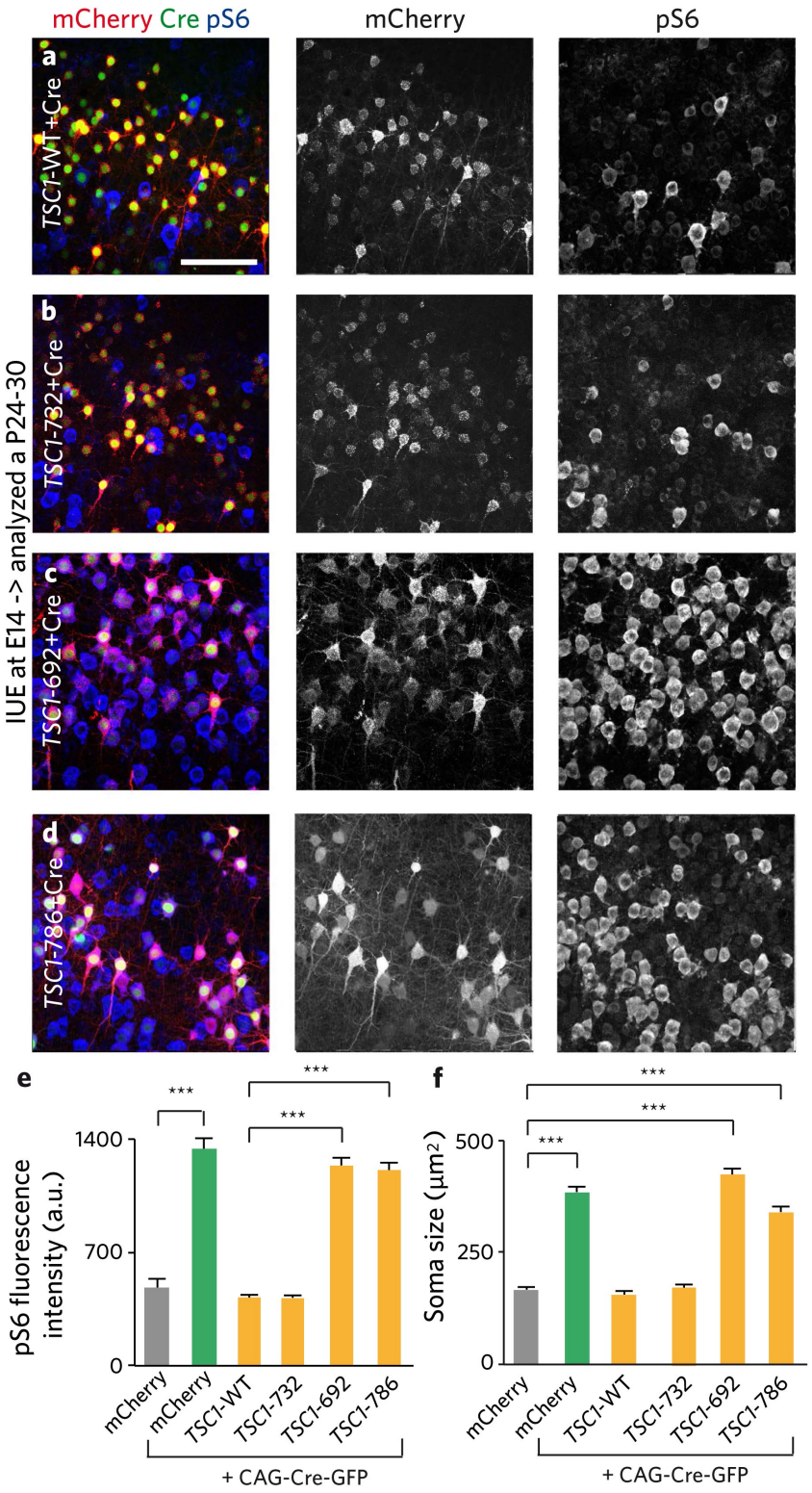

Figure 6.10: **Distinct phenotypes upon expression of *TSC1* allelic variants**. (a - d) $TSC1^{fl/fl}$ mice were *in utero* electroporated at E14 with CAG-Cre-GFP and either *TSC1*-WT-mCherry, *TSC1*-H732Y-mCherry, *TSC1*-R692X-mCherry or *TSC1*-R786X-mCherry. Brain slices from P24 - 30 mice were stained with pS6 antibodies. (a) Single cells expressing Cre (green) and *TSC1*-WT (red) or (b) *TSC1*-H732Y appeared normal-sized and had a low pS6 IR. Occasionally, neighboring cells had strong pS6 IR but without any considerable mCherry expression. (c) Co-electroporation with CAG-Cre-GFP and *TSC1*-R692X or (d) *TSC1*-R786X resulted in enlargement of the soma and high pS6 signals, even in Cre-negative, neighboring cells. (e) pS6 fluorescence intensity was significantly increased in Cre&mCherry-, *TSC1*-R692X&Cre- or *TSC1*-R786X&Cre-electroporated neurons compared to mCherry-, *TSC1*-WT&Cre- or *TSC1*-H732Y&Cre-electroporated neurons. (f) Soma size was significantly increased in Cre&mCherry-, *TSC1*-R692X&Cre- or *TSC1*-R786X&Cre-expressing neurons compared to control neurons (N = 6 mice with n = 50 – 65 cells each; One-way ANOVA with Bonferroni post-correction: ***$p \leq 0.001$; Scale bar 100µm). Image inspired by Robens et al., 2016 [269].

6.2.5 Minimal amounts of wildtype *TSC1* are sufficient to prevent dysplastic neuron and tuber-like lesion formation

Even though it is established that TSC is caused by inactivating mutations of *TSC1* or *TSC2* genes, there is still debate about the pathogenetic situation of cortical tubers. Classical second hit events have been proposed to explain the formation of cortical tubers, while another study claims that second hits are rare events in tubers. To clarify this controversy, we analyzed which relative concentration of wildtype *TSC1* is necessary to rescue the emergence of dysplastic neurons mediated by *TSC1* knockout together with expression of one of the truncated, lesion-inducing *TSC1* variants, *TSC1*-R692X. *TSC1*$^{fl/fl}$ mice were *in utero* electroporated at E14 with a mixture of CAG-Cre-GFP, *TSC1*-R692X-mCherry and *TSC1*-WT-mCherry successively decreasing the concentration of *TSC1*-WT DNA from 10:1 to 1:1, 1:10 or 1:20 (Fig.6.11 a). Again, soma size was analyzed as an indicator for abnormal mTOR activity. No significant change in soma size was measured for the concentrations 10:1, 1:1 or 1:10 compared to each other or to mCherry or *TSC1*-WT&Cre electroporated neurons. Very low concentrations of *TSC1*-WT (1:20) resulted in a slight but significant increase in soma size (Fig.6.11 b; N = 6 - 7 mice with n = 52 – 65 neurons each; mCherry/*TSC1*$^{fl/fl}$ 163.7±3.0µm^2; mCherry/Cre$^+$/*TSC1*$^{-/-}$ 391.9±5.3µm^2; mCherry/Cre$^+$/*TSC1*-WT:*TSC1*-R692X: 1:1, 171.8±3.8µm^2; 10:1 167.8±4.5µm^2; 1:10 162.3±3.2µm^2; 1:20 280.9±6.3µm^2; One-way ANOVA with Bonferroni post-correction ***$p \leq 0.001$). However, this affected only individual neurons that may have only received the Cre&*TSC1*-R692X plasmids but not the *TSC1*-WT plasmid due to its low concentration. Only single neurons appeared enlarged, while most neighboring and mCherry expressing cells appeared normal sized. Nevertheless, these results indicate that already low amounts of functional *TSC1*-WT are sufficient to rescue the *TSC1* knockout or *TSC1*-R692X mediated phenotype of enlarged, dysplastic neurons. Thus, our results clearly favor Knudson's second hit hypothesis of biallelic gene inactivation responsible for tuber formation.

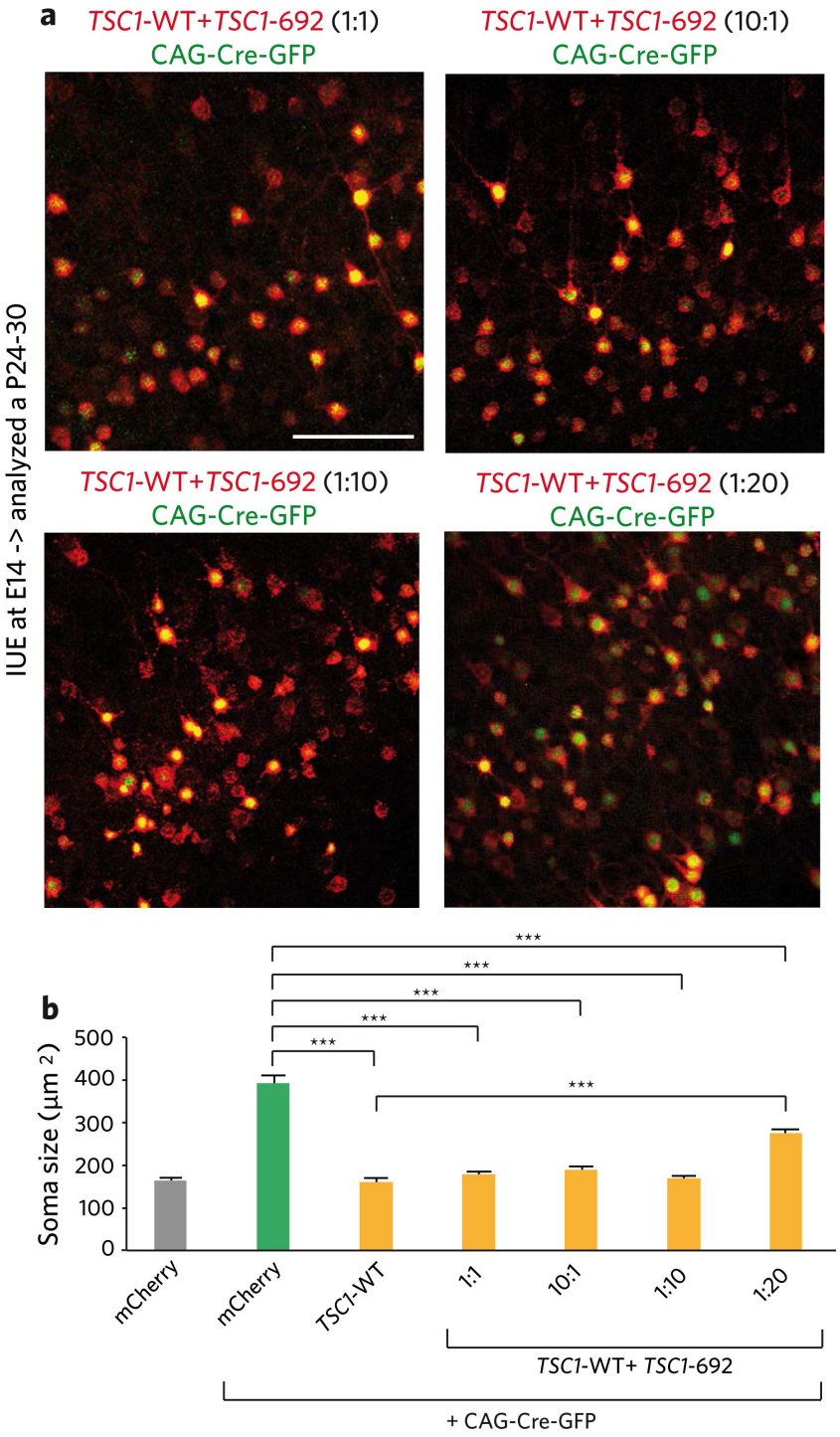

Figure 6.11: **Low concentrations of *TSC1*-WT prevent the emergence of dysplastic neurons and the tuber-like *TSC1* knockout phenotype.** (a) $TSC1^{fl/fl}$ mice were electroporated with a combination of CAG-Cre-GFP, *TSC1*-R692X-mCherry and varying amounts of *TSC1*-WT-mCherry plasmid. (b) At P24 - 30, soma size was comparable to mCherry or *TSC1*-WT&Cre electroporated neurons for the ratios 1:1, 10:1 and 1:10 of *TSC1*-WT and *TSC1*-R692X. A higher dilution of *TSC1*-WT down to 1:20 resulted in a slight but significant increase in the mean soma size compared to the other ratios or the control (N = 6 - 7 mice with n = 52 – 65 neurons each, One-way ANOVA with Bonferroni post-correction: ***$p \leq 0.001$; Scale bar 100µm). Image inspired by Robens et al., 2016 [269].

6.2.6 *TSC1* knockout in different precursor cell populations

Dysplastic neurons or giant/balloon cells within cortical tubers or FCDIIb lesions often show a mixed neuro-glial composition and have immature neuronal and glial features [10]. This finding supports their origin from intermediate progenitor cells. Thus, neurons and glial cells may both be involved in lesion formation. However, their cell lineage has not been fully defined yet. To address this issue, we aimed to *in utero* electroporate mice at E14 - 15 with mCherry as a volume dye and different Cre constructs under the control of distinct, cell type specific promoters. This will enable us to knockout *TSC1* only in a certain subset of precursor cells and analyze possible occurring cytoarchitectural differences and characterize the contribution of distinct progenitor cell types involved in dysplastic neuron formation, and thus tuber development. We used the brain lipid-binding protein (BLBP) or Glast promoter to target radial glia precursor cells, GFAP for astrocytes and Nestin for immature neurons. All used promoter-Cre sequences were flanked by piggyBac transposase recognition sequences to allow for genomic integration by co-electroporation of the pBase transposase. We noticed that the resulting phenotype was similar for all used Cre constructs: electroporated cells appeared enlarged compared to mCherry electroporated control cells, showed a typical neuronal morphology and were positive for NeuN (Fig. 6.12a - f; N = 2 - 7 mice with n = 13 – 43 neurons each). No cells with glial morphology were observed within the cortex when electroporating at E14 - E15, even though CAG-Cre was expressed under the control of the astroglial GFAP promoter (Fig. 6.12e). This indicates that the used GFAP promoter was leaky, allowing also neurons to express Cre, and/or that electroporated and dividing glial cells lost their fluorescent markers and subsequently also Cre. Since we cannot control for leakiness of the other used promoters (IUE of these also showed no electroporated glial cells), these results can not be used for interpretation of the involved cell lineage. Nevertheless, these experiments corroborate our previous results that *TSC1* knockout in neurons causes a tuber-like lesion with enlarged, dysplastic neurons.

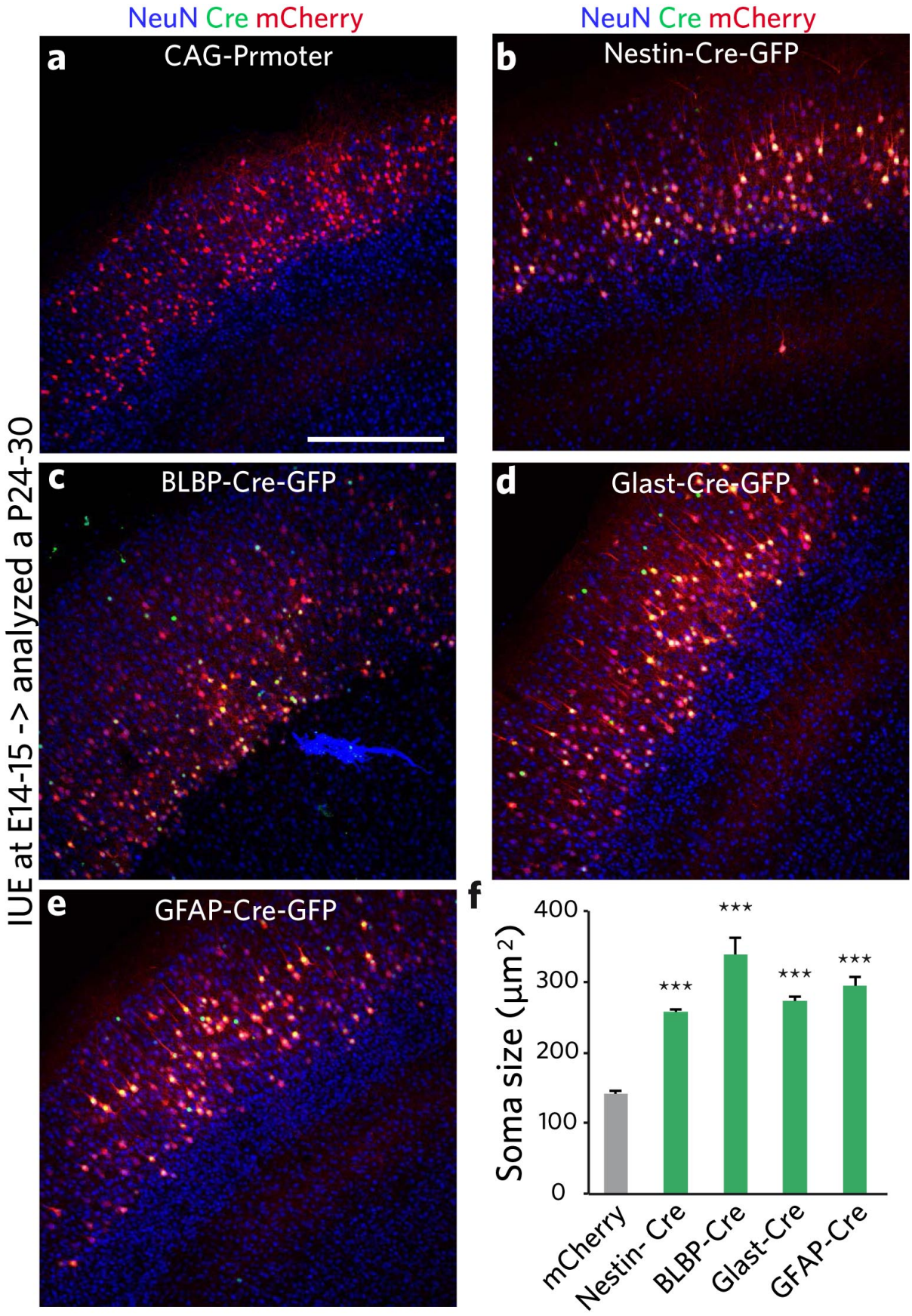

Figure 6.12: **Cell type specific expression of Cre results in increased soma size.** (a) *TSC1*$^{fl/fl}$ mice were *in utero* electroporated between E14 - 15 with pBase together with control mCherry plasmids, (b) Nestin-Cre, (c) BLBP-Cre, (d) Glast-Cre, and (e) GFAP-Cre. (f) Quantification was performed at P24 - 30 and showed that soma size was significantly increased when different promoter-Cre constructs were electroporated compared to control electroporation. No gross differences in cellular composition or soma size were seen when comparing the different promoter-Cre constructs (N = 2 - 7 mice with n = 13 – 43 neurons each, One-way ANOVA Bonferroni post-correction: ***$p \leq 0.001$; Scale bar 400µm).

Since some of the used promoter-Cre constructs appear to be leaky or unspecific and did not result in electroporated, cortical glial cells, we *in utero* electroporated time pregnant *TSC1*$^{fl/fl}$ mice with CAG-Cre&mCherry at E16 - 17, the time point when glial cells are generated more abundantly. Brain slices of P24 - 30 mice were stained with antibodies against neuronal NeuN (Fig. 6.13a) or vimentin, GFAP, and S100 to label immature and mature glial cells (Fig. 6.14a - c). We observed mCherry^{+}, electroporated glial cells only in a specific brain area located near the lateral ventricular wall within the lateral septal nucleus. Cre-expressing glia cells were never positive for the neuronal marker NeuN (Fig. 6.13a) but for vimentin (Fig. 6.14a) or S100 (Fig. 6.14b) and occasionally for GFAP.

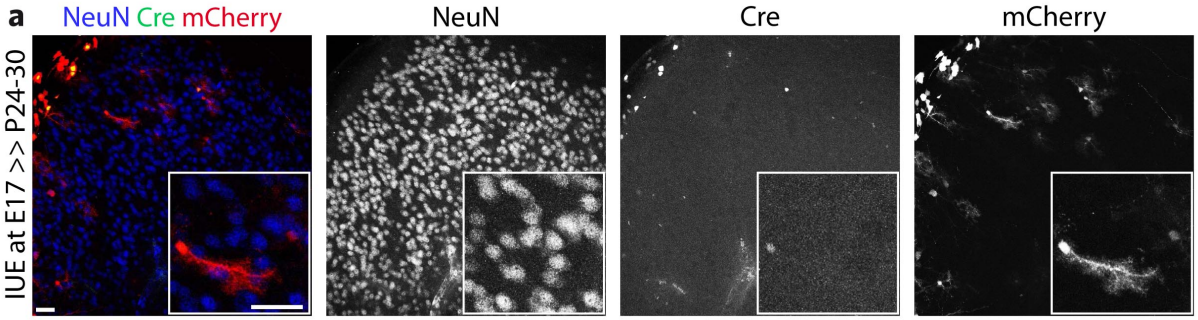

Figure 6.13: **Cre-expressing glial cells are negative for NeuN.** (a) Brain slices of P24 - 30 mice, electroporated at E16 - 17, were stained with NeuN antibodies. Electroporated, Cre- and mCherry-positive glia cells were negative for the neuronal marker NeuN; insets show areas of higher magnification within the same picture; Scale bar 100µm.

Compared to controls (Fig. 6.14c), brain slices from Cre-electroporated mice had a 77.9% increased overall S100 fluorescence intensity (N = 2 - 4 mice, with 3 brain slices each, all glia cells on a brain slice were analyzed; Student's t-test, $^{***}p \leq 0.001$); a characteristic that was also observed within cortical tubers of TSC patients. These results indicate that the rarely found *TSC1* knockout glia cells outside the cortex may not be giant cells, since they are only positive for glial but not neuronal markers, however, studies also found GC expressing only glial markers [276].

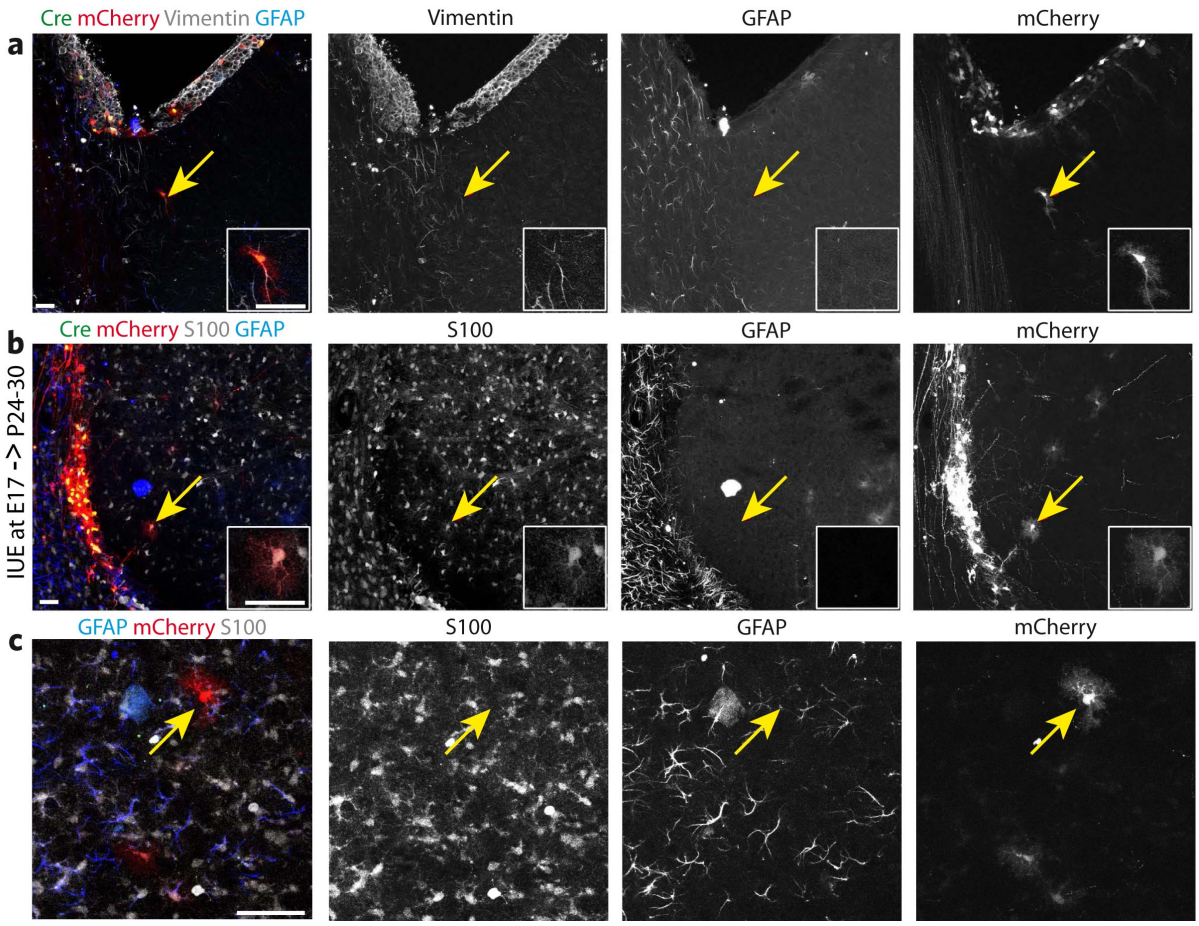

Figure 6.14: ***TSC1* knockout glia cells outside the cortex are exclusively positive for glial markers.** (a) At E16 - 17, $TSC1^{fl/fl}$ mice were *in utero* electroporated with mCherry or Cre&mCherry and brain slices of P24 - 30 mice were stained with vimentin and GFAP or (b) S100 and GFAP antibodies. Electroporated glial cells were only found within the lateral septal nucleus. In Cre-electroporated mice, glia cells were positive for vimentin and S100 but only occasionally for GFAP; yellow arrows. (c) Control electroporated cells were mainly S100 positive; insets show areas of higher magnification; Scale bar 100µm.

6.3 The role of SLK for normal cortex development

6.3.1 Loss of SLK expression in dysplastic neurons of FCDIIb and GGs

The unifying functional characteristic of glioneuronal developmental brain lesions are dysplastic neurons with their distinctive aberrantly shaped dendritic tree. This phenotype suggests impaired cytoskeletal dynamics arising during brain development. In order to analyze whether the occurrence of such abnormal neurons can have a common cause in all of the different lesions and possibly even account for the severe epileptic phenotype, we analyzed whether the Ste20 like kinase SLK, strongly expressed in the embryonic cortex and known to be critically involved in cytoskeleton remodeling and migration of fibroblasts, has a role in their emergence. So far, nothing specific is known about SLKs function in neurons. However, recent data generated in various non-neuronal cell lines indicate a role for SLK in cytoskeletal rearrangements and migration. Both are essential developmental processes potentially altered in dysplastic neurons of developmental brain lesions.

In order to answer this question, we first analyzed SLK expression in two of the most common glioneu-

ronal lesions, i.e. GGs and FCDIIb that represent a neoplastic and non-neoplastic entity, respectively. We performed co-immunohistochemical stainings on human FCDIIb tissue with antibodies against SLK and the neuronal marker MAP-2. We found nearly no SLK immunoreactivity (IR) in enlarged, dysplastic neuronal elements in comparison to normal-sized neurons located in columnar organized cortical areas (Fig. 6.15a). Quantification revealed a 78% lower SLK IR in dysplastic neurons compared to non-lesioned control neurons (Fig. 6.15b, control 249.4$\pm$10.1a.u. vs. FCDIIb 55.8$\pm$5.7a.u.; N = 10 different patients with a total of n = 159 control and n = 94 dysplastic neurons, Student's t-test ***$p \leq 0.001$). Correspondingly, analyzing dysplastic neurons in human GG tissue also revealed a reduced SLK IR in neurons within the GG (identified by strong vimentin staining) in comparison to adjacent control tissue (Fig. 6.15c). Here, we found a 20% lower SLK IR within the GG in comparison to control neurons (Fig. 6.15d, control 567.3$\pm$5.6a.u. vs. GG 458.9$\pm$3.6a.u.; N = 8 different patients with a total of n = 453 control cells and n = 551 cells within the GG; Student's t-test ***$p \leq 0.001$). These results indicate reduced SLK protein levels in dysplastic neurons of tow substantially different entities of developmental brain lesions, FCDIIb and GGs. Furthermore, SLK is rather localized in neuronal than glial vimentin-positive cells. This finding suggests that decreased levels of SLK would more likely impact neuronal than glial cells, suggesting a role for SLKs in the emergence of dysplastic neurons.

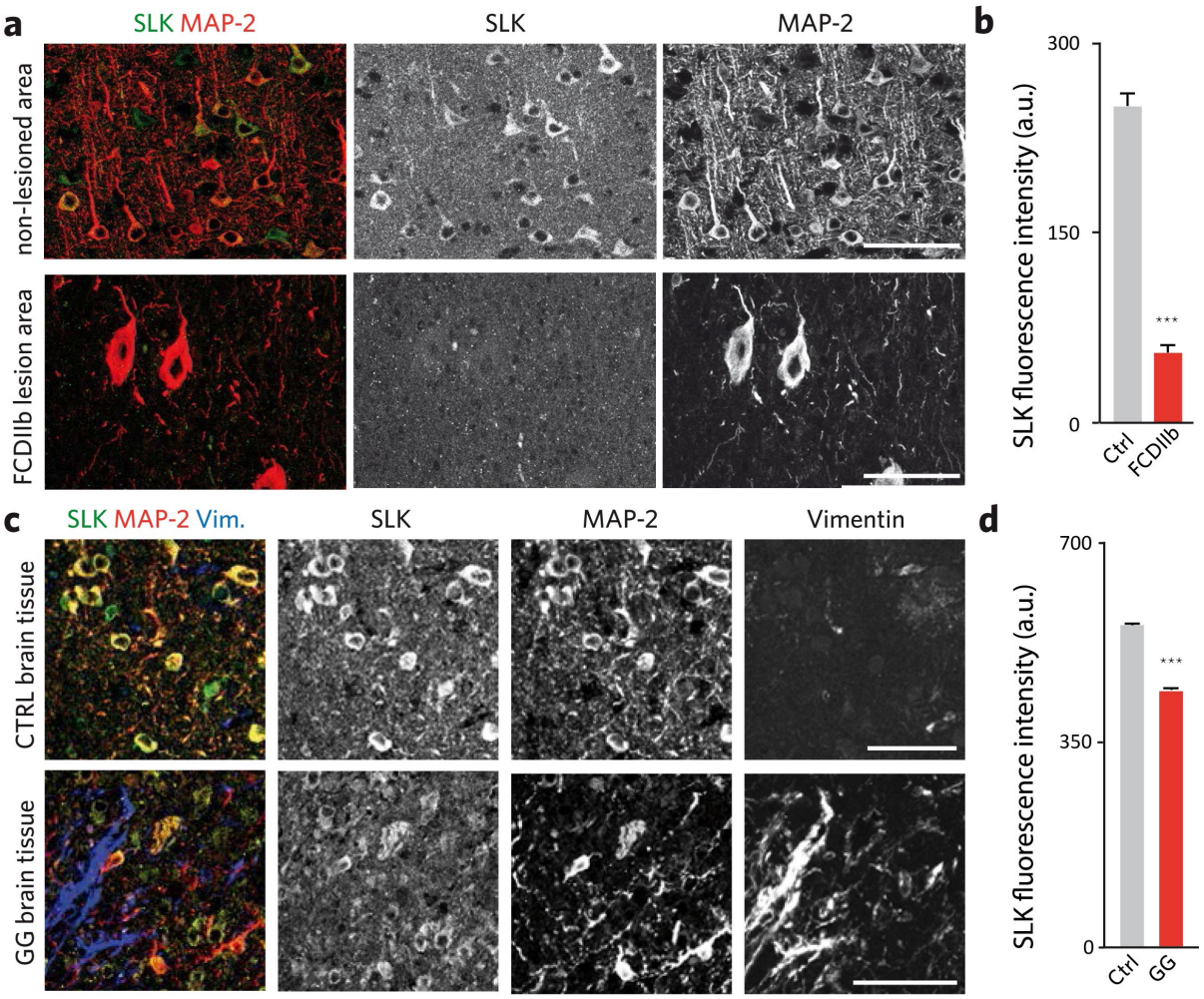

Figure 6.15: **Reduced SLK protein levels in dysplastic components of FCDIIb and GGs.** (a) Paraffin embedded brain slices of human FCDIIb specimens were co-stained with SLK and MAP-2 antibodies. (b) SLK IR in enlarged, dysplastic neurons was significantly lower compared to normal-sized neurons located in an columnar organized cortical area. (c) Human GG brain tissue co-immunohistochemically stained with SLK, MAP-2 and vimentin antibodies (N = 10 different patients with a total of n = 159 control and n = 94 dysplastic neurons, Student's t-test, ***$p \leq 0.001$). (d) Quantification revealed a 20% reduction of SLK IR within the area of the GG with a high number of vimentin positive glial cells in comparison to neurons in the adjacent control tissue, negative for vimentin (N = 8 different patients with a total of n = 453 control cells and n = 551 cells within the GG, Student's t-test, ***$p \leq 0.001$). Scale bar 100µm.

6.3.2 RNAi mediated *SLK* knockdown

The reduction of SLK protein in human dysplastic neurons implies SLK deregulation as a potential pathological factor contributing or leading to the emergence of dysplastic neurons and thus, to lesion formation. The aberrant dendritic morphology of such dysplastic neurons is their major morphological characteristic. We therefore asked whether SLK - with its reported ability to regulate both actin filament dynamics [249, 256] and microtubule orientation in fibroblasts [252, 253, 256] - may be necessary for the establishment of a normal dendritic arbor. No such studies have been performed in neurons yet. However, the robust expression of SLK in the developing cortex suggests a critical function for young neurons, especially since gene-trap mediated truncation of SLK results in embryonic lethality at the time of onset of cortex development.

One of the best ways to analyze the specific functional role of a protein is to knockdown or increase

its expression. We used RNA interference (RNAi), which is an RNA-mediated gene silencing process, achieved by delivery and subsequent cellular expression of short hairpin RNA (shRNA) containing plasmids. In our studies all used shRNA vectors also encode a fluorescent protein (hrGFP or mRFP) that is expressed under the control of an independent, ubiquitous promoter. This allows for reliable detection of shRNA expressing cells.

We designed specific shRNAs to target mouse and rat *SLK* mRNA sequences, which mediates targeted protein down-regulation in both species. To asses effects of SLK overexpression and to exclude off-target effects of the shRNA, a human *SLK* (hSLK) variant with silent point mutations within the shRNA target sequence was generated (hSLK-mut, further referred to as hSLK). Efficient *SLK* knockdown by the shRNA and rescue by hSLK expression was confirmed by immunoblotting protein homogenates of HEK293T cells co-transfected with the respective plasmids: *SLK* shRNA (shSLK) was transfected together with a murine, non-resistant *SLK* or in combination with the resistant *hSLK* (Fig. 6.16a). The quantification confirmed efficient mouse *SLK* knockdown by shSLK, since the detected SLK protein level was significantly reduced down to 2.1% in comparison to cells only transfected with mouse *SLK*. In addition, introducing the silent point mutations into the human *SLK* sequence rendered this *hSLK* plasmid resistant to the shRNA. Its expression was unchanged despite shSLK co-transfection (Fig. 6.16b). To verify shRNA efficiency also in neurons, paraffin embedded brain slices from mice with *in vivo* expression of various plasmids were stained with SLK antibodies. As a control, the empty hrGFP expressing U6 RNAi vector (further referred to as control), without *SLK* shRNA was transfected. Control- and non-electroporated neurons showed moderate SLK IR, whereas SLK staining was virtually absent in shSLK expressing cortical neurons (Fig. 6.16c). Rescue by coexpression of shSLK together with the shRNA resistant hSLK on the other hand resulted in strong SLK IR in respective cells. In a third approach, successful SLK down-regulation by shRNAs was assessed *in vitro* in primary cortical neuronal cultures. Neurons were previously transduced with crude AAV particles enabling efficient transgene expression of up to 90 - 95% of all neurons. Their mRNA was harvested 14 days later and *SLK* expression was analyzed in a semi-quantitative approach by real-time PCR. In comparison to U6 hrGFP control neurons, shSLK expressing cells showed a 81.3% reduction of *SLK* mRNA transcripts (Fig. 6.16d). These results demonstrate potent knockdown of mouse *SLK* by shSLK expression that can be rescued by coexpression of hSLK in different experimental set-ups *in vitro* and *in vivo*.

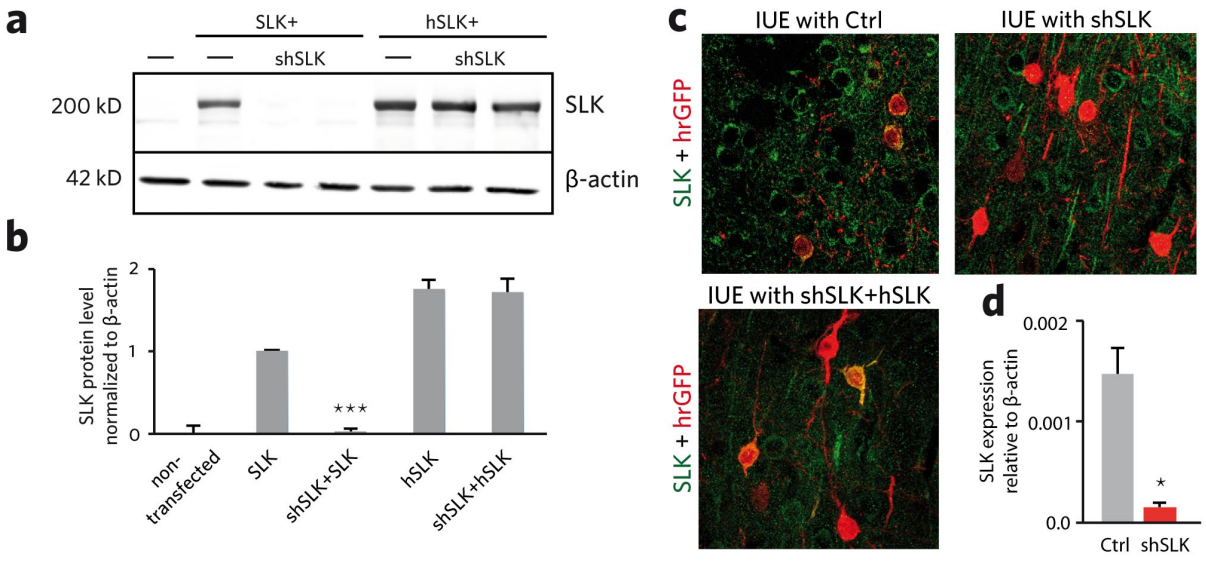

Figure 6.16: **Assaying the RNAi mediated *SLK* knockdown efficiency *in vitro* and *in vivo*.** (a) Western blot of HEK293T cells transfected with indicated plasmid combinations. SLK protein was detected when SLK was overexpressed and when hSLK alone or in combination with shSLK was expressed. Effective protein transfer and equal protein amounts are indicated by positive β-actin signal for all samples. (b) Quantification of mean protein band intensity from N = 3 independent experiments normalized to β-actin and afterwards normalized to SLK band intensity (N = 3, One-way ANOVA with Bonferroni post-correction, ***p$\leq$0.001). Co-transfection of *SLK* shRNA and mouse *SLK* (SLK) reduced SLK signal by 97.8% compared to cells that only expressed SLK. (c) After intraventricular *in utero* electroporation of the empty U6 hrGFP-expressing control vector (red), transfected- and non-transfected neurons had moderate SLK IR (green). Conversely, SLK IR in hrGFP-tagged shSLK expressing neurons was lost. Neurons expressing both, shSLK and the shRNA resistant hSLK, had strong SLK IR; Scale bar 50µm. (d) Semi-quantitative real-time PCR with mRNA extracted from shSLK transduced mouse cortical neurons confirmed potent *SLK* knockdown in comparison to U6 control transduced neurons (n = 6 hrGFP controls, n = 8 shSLK, *p$\leq$0.05, Student's t-test).

6.3.3 *SLK* knockdown in neurons results in impaired neurite morphology *in vitro*

Considering the abnormal dendritic arbor of dysplastic neuronal components of FCDIIb or GGs, we tested the effect of *SLK* knockdown in primary cortical neurons with the established *SLK* shRNAs by transfection at DIV 2 - 4. At DIV14, neuronal morphology was imaged, reconstructed and analyzed (Fig. 6.17a). At the time point of analysis, most neurons exhibited strongly branched dendritic arbors with no gross difference between groups. A detailed quantification of different order dendrites revealed no change in first (red) or second order (green) dendrites. However, the number of third order dendrites (blue) was significantly reduced upon SLK loss (Fig. 6.17b) down to 58.8% in comparison to control transfected neurons (control 30.8$\pm$2.0 vs. shSLK 18.1$\pm$1.4 third order dendrites per neuron; n = 11 control, n = 12 shSLK; One-way ANOVA with Bonferroni post-correction, ***p$\leq$0.001). To investigate whether SLKs kinase activity is required for normal dendritic growth, neurons were transfected with an *SLK* plasmid carrying a K63R mutation, rendering SLK kinase null. K63R-SLK expression resulted in a reduction of the distal dendrites similar to shSLK expression (18.7$\pm$2.1 third order dendrites per neuron; n = 12 K63R-SLK; One-way ANOVA with Bonferroni post-correction, ***p$\leq$0.001). Coexpression of shRNA resistant hSLK not only rescued the shRNA-mediated dendritic impairment but also increased the number of third order dendrites significantly (Fig. 6.17b, shSLK+hSLK 43.5$\pm$1.4 third order dendrites per neuron; n = 9 shSLK+hSLK; One-way ANOVA with Bonferroni post-correction, ***p$\leq$0.001). Overall, the individual dendrite length was unchanged in proximal or distal dendrites (Fig. 6.17c), indi-

cating a reduced total volume of the dendritic tree in comparison to controls due to loss of SLK kinase activity.

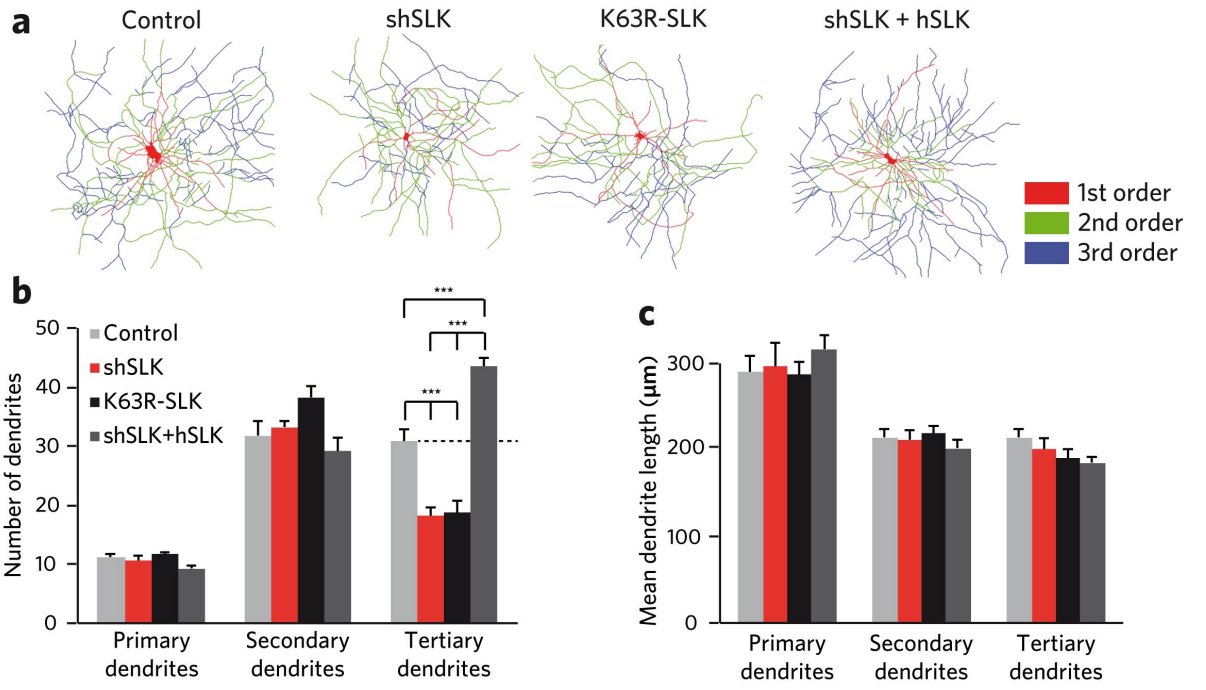

Figure 6.17: **SLK silencing in cortical neurons leads to a reduced number of higher-order dendrites.** (a) At DIV4, rat cortical neurons were transfected with different plasmids and the morphology of their dendritic arbor was reconstructed at DIV14; different colors indicate different order dendrites. (b) The total number of proximal, primary and secondary dendrites was similar in all conditions, whereas the abundance of third order dendrites was significantly reduced after *SLK* knockdown or expression of the kinase dead K63R-SLK. Expression of hSLK together with shSLK counteracted the loss of tertiary dendrites. (c) Mean dendrite length was unchanged compared to control neurons in all tested groups (N = 3 independent experiments, n = 9 – 12 neurons per condition, One-way ANOVA with Bonferroni post-correction, ***$p \leq 0.001$, stars indicate statistically significant difference compared to hrGFP control).

Growth of dendrites and axons is regulated by common regulatory pathways, but is also influenced by mechanisms specific to axons or dendrites that allow for the specification into distinct compartments. To assess whether proper dendritic scaling or the growth promoting effects mediated by SLK are specific for dendrites or whether SLK is generally required for normal neurite growth, we analyzed the consequence of SLK loss or overexpression on axon growth. Therefore, neurons were transfected at DIV2 and axon length was determined at DIV6. 24h after plating, cultured primary neurons form short neurites from which only one - the future axon - starts to grow rapidly, while the other neurites start to grow and develop into dendrites not before DIV 4 - 5. Thus, at DIV6 the axon can be easily discriminated from dendrites as a single long branch (Fig. 6.18a). Quantification of confocal micrographs showed that loss of SLK led to a reduction of axon length by 50.4% in comparison to control neurons (Fig. 6.18b; control: 4766±499µm vs. shSLK 2027±255µm; n = 11 control, n = 19 shSLK; One-way ANOVA with Bonferroni post-correction, ***$p \leq 0.001$). Expression of the kinase dead K63R-SLK showed a similar reduction of axon length (control: 4766±499µm vs. K63R-SLK 2362±220µm; n = 12 K63R-SLK; One-way ANOVA with Bonferroni post-correction, ***$p \leq 0.001$). These effects were not seen when the shRNA resistant hSLK was coexpressed with shSLK (control: 4766±499µm vs. hSLK+shSLK 5296±355µm; n = 10 shSLK+hSLK; One-way ANOVA with Bonferroni post-correction, not significant). Our results indi-

cate that SLK regulates general growth regulatory processes needed for normal dendritic arborization and axon growth. These results furthermore imply, that SLK loss may be a contributing factor in the emergence of dysplastic neurons.

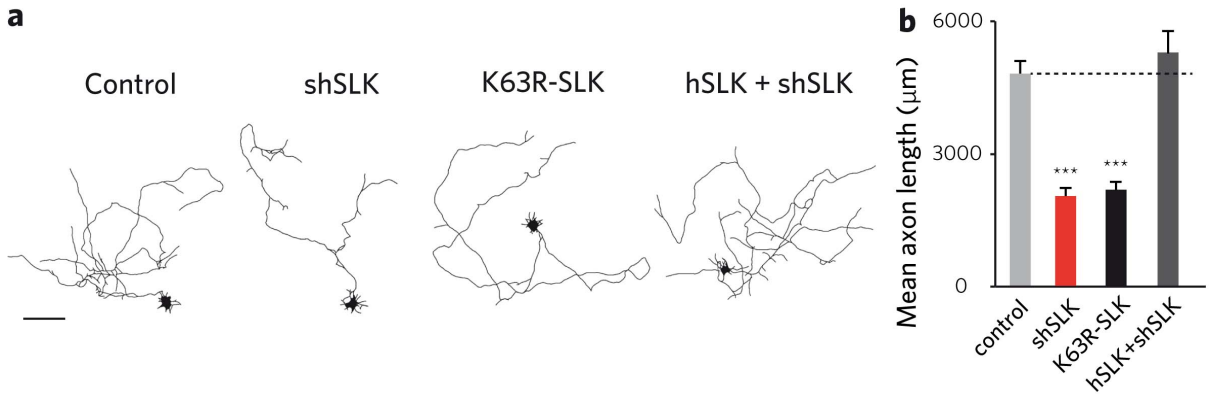

Figure 6.18: ***In vitro* knockdown of *SLK* results in reduced axon length**. (a) Embryonic rat cortical neurons were transfected at DIV2, PFA-fixed and reconstructed at DIV6; Scale bar 100µm. (b) Axon length was reduced by approximately 50% when *SLK* was knocked down or when the kinase dead K63R-SLK was overexpressed. Coexpression of hSLK together with shSLK slightly increased axon length (N = 3 independent experiments with 10 - 19 neurons each, One-way ANOVA with Bonferroni post-correction, ***$p \leq 0.001$, stars indicate statistically significant difference compared to hrGFP control).

6.3.4 Focal cortical loss of SLK results in impaired cortex development

In order to analyze if loss of SLK expression in developing neurons of mouse embryos surrounded by a functional neuronal network causes similar changes in neurite morphogenesis *in vivo*, we knocked down *SLK* in cortical neuronal progenitors by shRNA expression during embryonic development. To mimic the focal, cortical character in a restricted number of cells and the developmental origin of dysplastic lesions, we delivered shSLK or control plasmids by intraventricular *in utero* electroporation (IUE) at E14 (Fig. 6.19a). By IUE of shSLK at E14 into one lateral ventricle, SLK protein expression will be prevented in cortical progenitor cells within the proliferative zones destined for layer II/III and IV. At the time point of analysis (P30 - 35), hrGFP expressing plasmids were spread throughout the somatosensory and in part the motor- and cingulate cortex layer II/III and IV, ranging approximately from Bregma 2.0 to -1.0 (Fig. 6.19b).

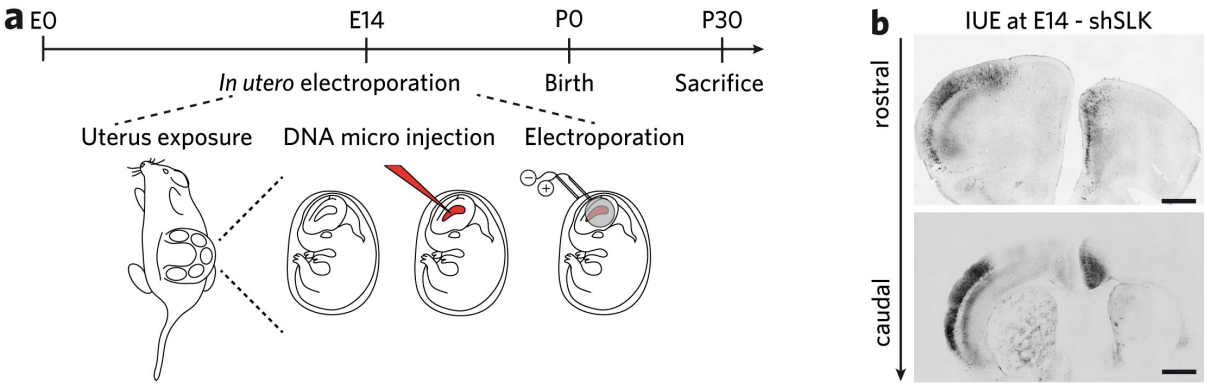

Figure 6.19: **Intraventricular *in utero* electroporation.** (a) At E14, embryos of time pregnant mice were *in utero* electroporated with hrGFP-labeled shRNAs or control plasmids. (b) Exemplary brain slice of a 4-week old mouse, depicting the distribution of hrGFP-expressing electroporated neurons in cortical layers, from rostral to caudal; Scale bar 1000µm.

Brain slices from control or shSLK electroporated mice were immunohistochemically stained with neuronal (NeuN) and astroglial (GFAP) markers. Both markers showed a similar, inconspicuous pattern in both groups, without any signs of astrogliosis or infiltration of reactive astrocytes (Fig. 6.20a). Cortical lamination in shSLK IUE mice appeared partially altered. Approximately 10±2% of all electroporated neurons were ectopically positioned in deeper cortical layers in about 66% of all analyzed animals (Fig. 6.20b; N = 4 mice each with n = 1081 control and n = 1286 shSLK cells; $^{**}p \leq 0.01$, Student's t-test, N = 22 mice were analyzed for ectopically localized neurons). Remarkably, none of these cells were positive for NeuN (labeling mature neurons) despite their obvious neuronal shape. All neurons showed robust DAPI signal, a fluorescent dye that binds to the DNA and thus stains the nucleus of vital cells. Nearly all ectopic cells were negative for birthdate-specific marker expression, such as Cux1 or FoxP2 that specifically label layer II/III&IV or layer V&VI neurons respectively (Fig. 6.20c, d, e).

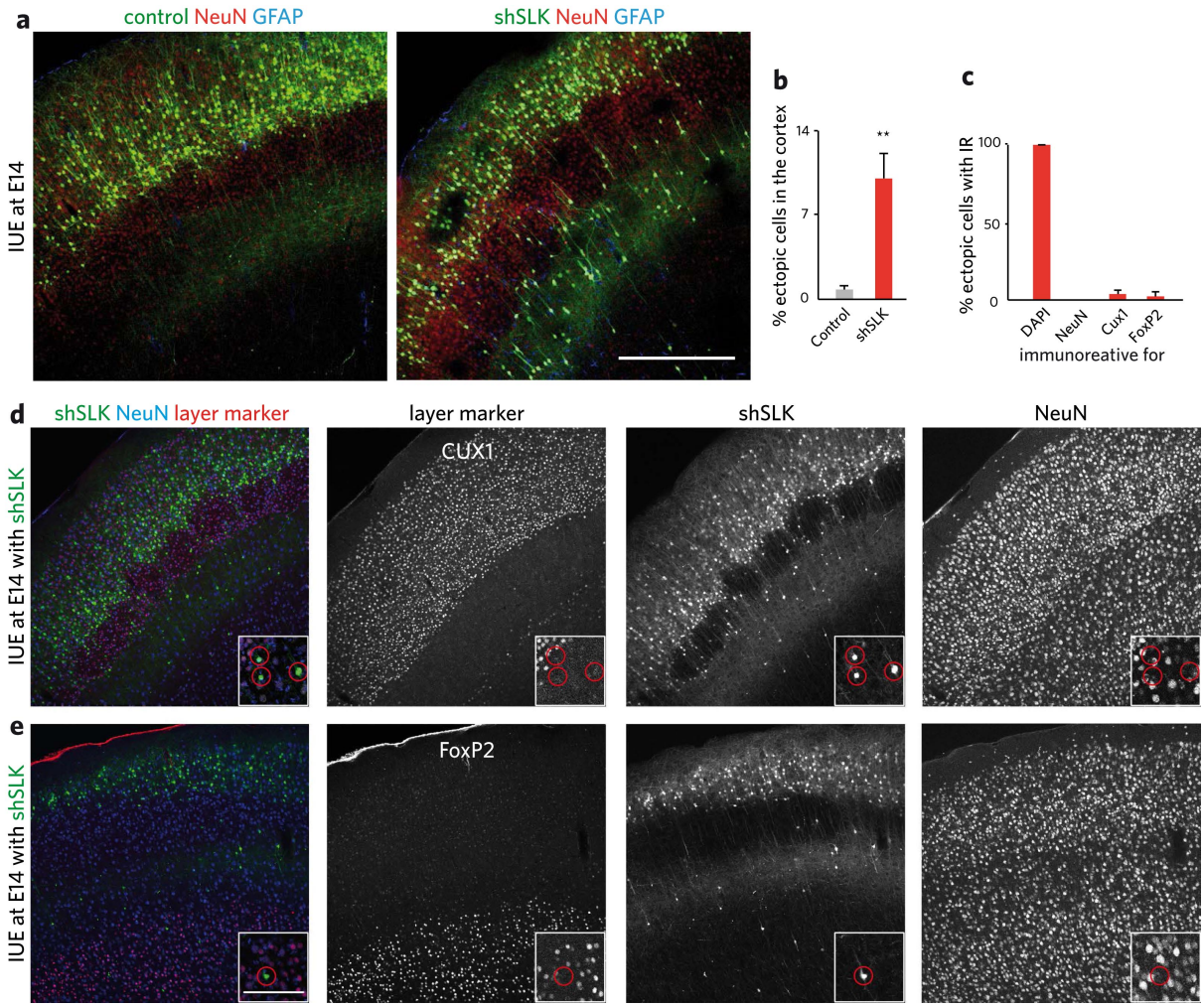

Figure 6.20: **Partially disrupted cortical architecture after *SLK* knockdown *in vivo*.** (a) Brain slices of *in utero* electroporated mice were immunohistochemically stained with NeuN and GFAP antibodies; Scale bar 400µm. (b) In most mice electroporated with shSLK, on average 10% of all neurons, were observed to be ectopically localized in deeper cortical layers (N = 4 mice each with n = 1081 control and n = 1286 shSLK cells; **p≤0.01, Student's t-test). (c) Ectopic cells were positive for DAPI, negative for NeuN and nearly all were negative for the layer specific markers (d) Cux1 and (e) FoxP2 (N = 4 mice each; Scale bar 20µm).

Subsequently, we selected single *in utero* electroporated cortical neurons at the edge of the electroporated area, mainly located in the upper parts of layer IV, to examine their morphology (Fig. 6.21a). Similar to the *in vitro* results (Fig. 6.17), reduction of SLK protein levels by shSLK expression *in vivo* caused a significant and selective reduction in the number of distal dendrites (Fig. 6.21b, reduction of first order dendrites by 12.4%, second order dendrites 24.7% and third order dendrites by 76.5%; N = 2 – 3 mice from different litters with n = 7 control and n = 9 shSLK neurons, Student's t-test; ***p≤0.001 for third order dendrites). This analysis was complemented by morphometric Sholl analysis. Quantification corroborated our previous results and revealed a substantial reduction of dendritic tree complexity in shSLK electroporated neurons compared to hrGFP-expressing control neurons (Fig. 6.21c, N = 2 – 3 mice from different litters with n = 7 control and n = 9 shSLK neurons, Mann-Whitney U-test; ***p≤0.001). For unknown reasons *in utero* electroporation of the kinase dead K63R-SLK variant in different expression vectors did not result in expression at P3 or P30. Mice were co-electroporated with K63R-SLK-2A-mCherry and hrGFP and at both time points (P3 and P30) only hrGFP expression was

detectable.

Our results demonstrate that *in vivo* loss of SLK in cortical precursors results in ectopic cortical localization in a subset of neurons and substantial morphological alterations that reflect the nature of dysplastic neurons. These observations suggest that SLK plays a considerable role in the regulation of neurite growth or branching and final neuronal positioning or migration that may be disrupted in dysplastic neurons of developmental brain lesions.

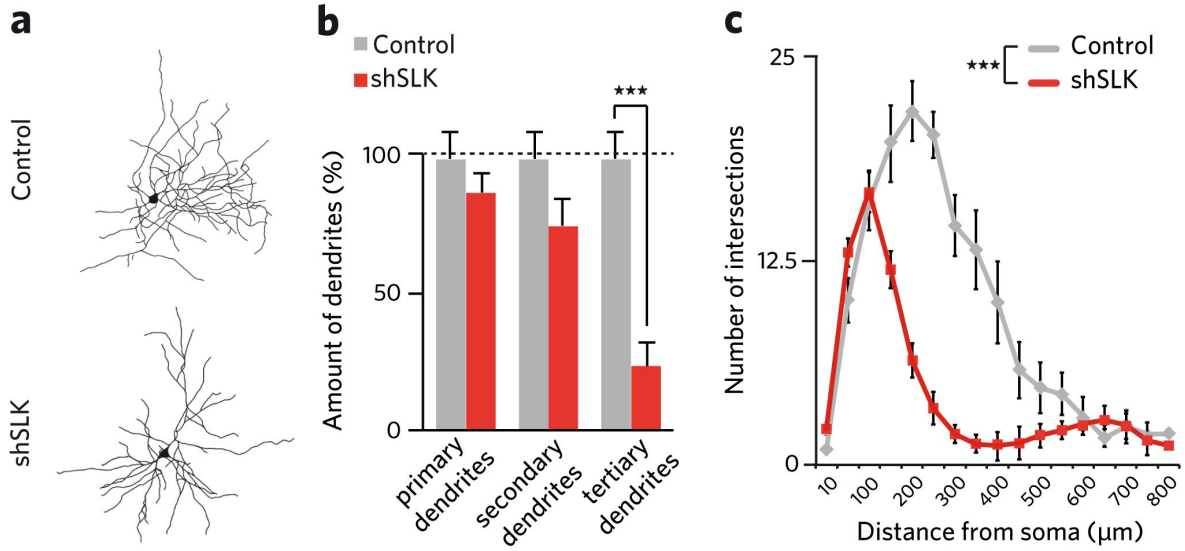

Figure 6.21: ***In vivo* knockdown of *SLK* leads to impaired dendritic morphology of cortical neurons.** (a) High magnification confocal micrographs of reconstructed, multipolar, cortical neurons electroporated with either hrGFP-expressing control- or shSLK plasmids. (b) Quantification of the number of different order dendrites in control- or shRNA-electroporated brains revealed a strong reduction of third order dendrites in the absence of SLK. (c) Sholl analysis of single neurons demonstrated a reduced number of intersections in SLK silenced cortical neurons, in comparison to control neurons (N = 2 – 3 mice from different litters with n = 7 control and n = 9 shSLK neurons; Student's t-test for dendrite numbers and Mann-Whitney U-test for Sholl analysis; ***$p \leq 0.001$).

6.3.5 SLKs specific subcellular localization

The specific subcellular localization of a protein allows for speculations about its functions. As there are no information about the localization of SLK in neurons we stained cultured cortical neurons at DIV14 with antibodies against SLK and the dendritically enriched MAP-2. In fibroblasts, SLK has been shown to colocalize with microtubules during adhesion and migration. It is unclear whether this is also the case in neurons. We observed endogenous SLK to be present in all major compartments of the neuron, including axon, MAP-2 labeled dendrites and particularly in the cell body (Fig. 6.22a). Co-labeling with the F-actin binding GFP-labeled toxin phalloidin revealed a high degree of overlap with SLK not only in neurites but also in neurite tips/growth cones (Fig. 6.22b, c).

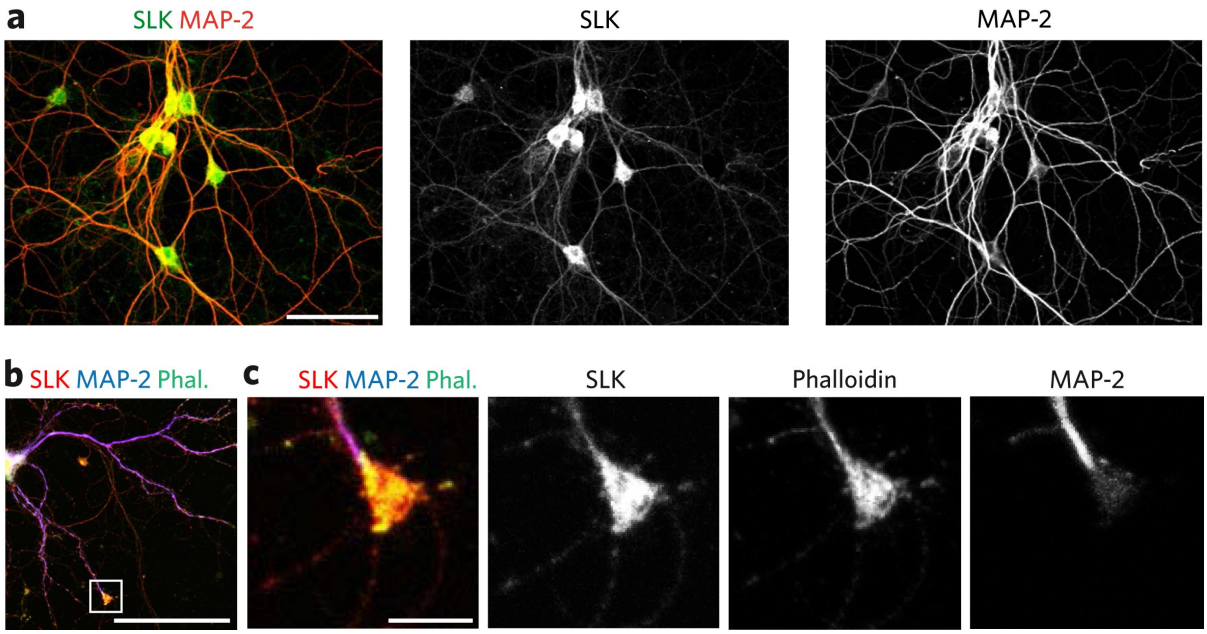

Figure 6.22: **SLK colocalizes with dendritic markers and phalloidin.** (a) Embryonic rat cortical neurons were PFA-fixed at DIV14 and stained against MAP-2 or SLK; Scale bar 50µm. (b) mRFP-transfected cortical neurons were stained with SLK and MAP-2 antibodies and labeled with GFP-phalloidin at DIV14; Scale bar 50µm. (c) Close-up of the growth cone; Scale bar 6µm.

Several other members of the Ste20 kinase family (TAO, MINK and TNIK) have been reported to be localized at and functionally relevant for synapses. Thus, we analyzed whether SLK is also present at the synapse by transfecting neurons at DIV4 with a volume dye (mRFP) and GFP-labeled PSD95- (Fig. 6.23a) or gephyrin-GFP-FingRs (Fig. 6.23c). FingR stands for fibronectin intrabodies generated with mRNA display. They are expression regulated GFP-fused mRNAs that bind to endogenous PSD95 or gephyrin with high affinity. At DIV21 only little spatial overlap of SLK with PSD95 (a marker for excitatory synapses, concentrated at the tips of dendritic spines) or spines was found (Fig. 6.23b). SLK IR was measured in only 28.4±15.1% of all $PSD95^{+}$ synapses. In contrast, SLK labeling had a high degree of overlap with $gephyrin^{+}$ punctae (97.7±1.8%) located on dendritic shafts (Fig. 6.23d). These results indicate that SLK is present in and probably important for inhibitory synapses but rather not for excitatory synapses.

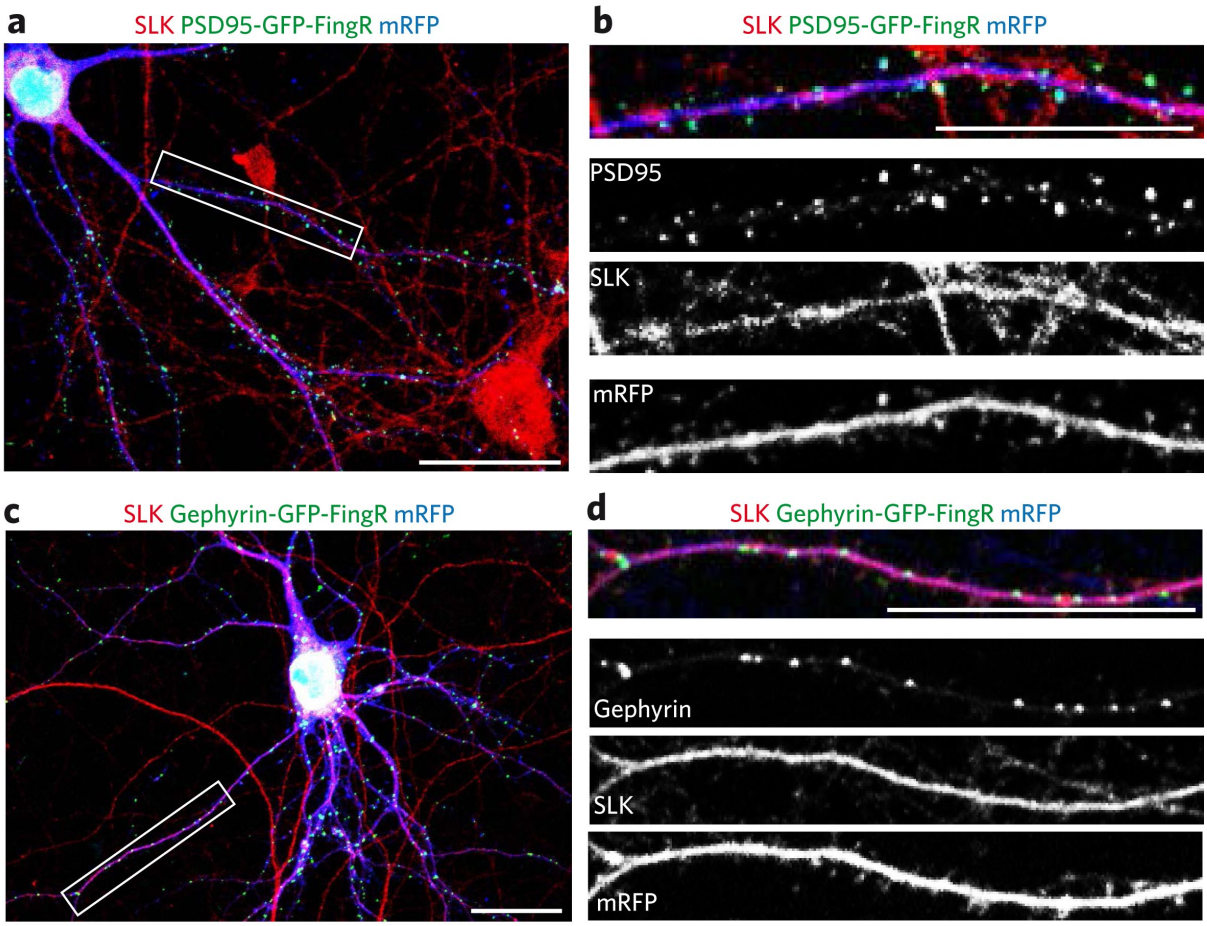

Figure 6.23: **Overlapping expression of SLK with gephyrin at inhibitory postsynapses.** (a) At DIV4, rat cortical neurons were transfected with mRFP and PSD95-GFP-FingRs and stained with SLK antibodies at DIV21; Scale bar 25µm. (b) Only little spatial overlap between SLK and PSD95-GFP or spines was observed; Scale bar 25µm. (c) Rat cortical neurons were transfected at DIV4 with mRFP and gephyrin-GFP-FingRs and stained against SLK at DIV21; Scale bar 25µm. (d) The gephyrin-GFP signal overlapped spatially with dendritic SLK staining; Scale bar 25µm.

6.3.6 SLK silencing results in progressive juvenile inhibitory postsynapse loss

To further explore the possibility of a specific function of SLK for inhibitory synapses, mouse embryos were *in utero* electroporated at E14 with control- or shSLK plasmids together with either gephyrin- (Fig. 6.24a) or PSD95-GFP-FingRs (Fig. 6.24d). In this case, the control plasmid was the empty mRFP-expressing plasmid and the shRNA was an mRFP-expressing shSLK. Synapse density was assessed at different time points after birth by counting the GFP-labeled inhibitory or excitatory postsynapses along the dendrites. Detailed quantification revealed no change in synapse density at early ages, P5 and P15. However, starting at P30 gephyrin$^+$ synapse density was significantly decreased after shSLK mediated *SLK* knockdown. Moreover, without SLK the synapse density seemed to progressively decrease, since neurons at P15 harbored significantly more synapses than neurons at P60, unlike in the controls (Fig. 6.24b; P5: n = 19 control, n = 21 shSLK, P15: n = 15 control, n = 24 shSLK, P30: n = 12 control, n = 11 shSLK, P60: n = 10 control, n = 10 shSLK; gephyrin-positive synapses/100µm at P5: mRFP control 6.5±0.6 vs. shSLK 4.7±0.5; P15: mRFP control 17.0±1.7 vs. shSLK 17.5±1.0; P30: mRFP control 22.8±2.4 vs. shSLK 13.1±1.3; P60: mRFP control 25.6±3.0 vs. shSLK 11.9±1.4; One-way

ANOVA with Bonferroni post-correction, ***$p \leq 0.001$). This postnatal reduction of inhibitory synapses was preceded by a developmental impairment that led to the formation of less third order dendrites, starting at P15 (Fig. 6.24c; P15: n = 8 control, n = 12 shSLK, P30: n = 15 control, n = 14 shSLK, P60: n = 9 control, n = 10 shSLK; no third order dendrites at P5, third order dendrites/neuron: P15: mRFP control 6.6±0.9 vs. shSLK 1.1±0.4; P30: mRFP control 14.9±1.1 vs. shSLK 3.5±0.7; P60: mRFP control 7.5±1.3 vs. shSLK 2.3±0.4, One-way ANOVA with Bonferroni post-correction, ***$p \leq 0.001$). In direct contrast, knockdown of *SLK* did not affect the number of $PSD95^{+}$postsynapses, which was unchanged at all investigated time points compared to control (Fig. 6.24e; P5: n = 9 control, n = 9 shSLK, P15: n = 7 control, n = 7 shSLK, P30: n = 19 control, n = 14 shSLK, P60: n = 9 control, n = 7 shSLK). Together, these results corroborate the hypothesis that SLK is important for the development of higher order dendrites. They furthermore suggest that SLK plays a role in the stability of inhibitory postsynapses but not for their initial formation.

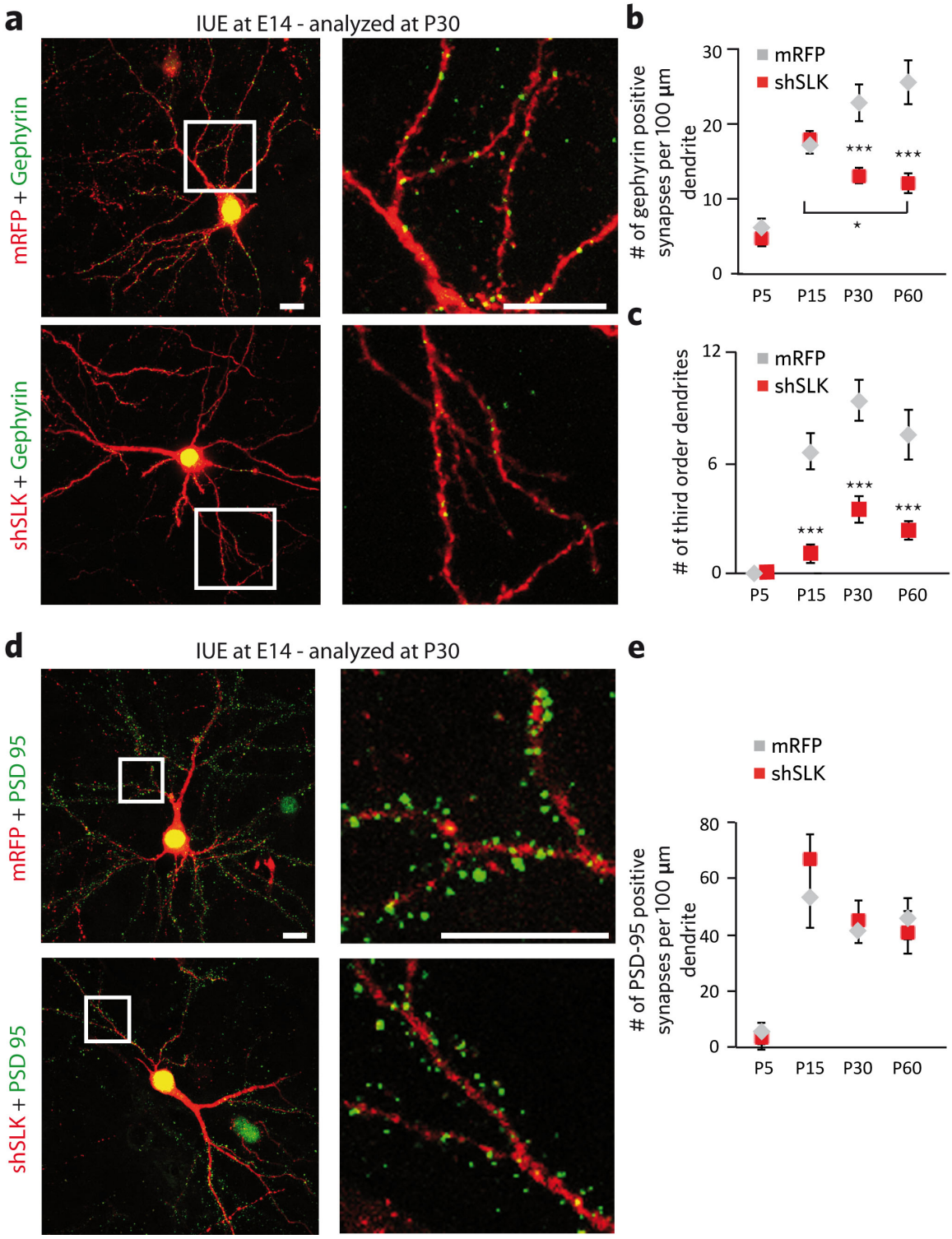

Figure 6.24: ***SLK* knockdown leads to reduced inhibitory postsynapse density *in vivo*.** (a) Exemplary neurons of P30 mice *in utero* co-electroporated at E14 with control or shSLK and GFP bound gephyrin-FingRs; white squares indicate areas of higher magnification seen in the right panel. (b) Synapse density was unchanged at P5 or P15 but significantly reduced at P30 and P60 when electroporating shSLK. (c) The number of distal dendrites was reduced in shSLK expressing cortical neurons from P15 to P60 (N = 2 – 4 mice from different litters with n = 2 – 4 different neurons per animal, One-way ANOVA with Bonferroni post-correction; ***$p \leq 0.001$). (d) Exemplary images of cortical neurons electroporated with PSD95-GFP-FingRs and mRFP-control or shSLK from P30 mice; right panel shows area within the white square at higher magnification. (e) PSD95-positive postsynapse density was similar at P5, P15, P30 or P60 in both groups (N = 3 – 4 mice from different litters with n = 2 – 4 different neurons per animal, $p \geq 0.05$, One-way ANOVA with Bonferroni post-correction; unless indicated otherwise, stars indicate statistically significant difference compared to mRFP control; Scale bar 100 µm).

6.3.7 Reduced inhibition upon *SLK* knockdown

A reduction of inhibitory postsynapses may translate into reduced inhibition and may thus lead to an imbalance of excitation/inhibition of the neuronal network. To test for that possibility time pregnant mice were *in utero* electroporated at E14 with U6 hrGFP control or shSLK plasmids. At the age of P30 - 40 mice were sacrificed and patch-clamp recordings were performed on acute brain slices by Robert Maresch in the department of epileptology in Bonn (Lab of professor Heinz Beck). In hrGFP-expressing neurons from cortical layer II/III (Fig. 6.25a, b), spontaneous miniature excitatory postsynaptic currents (mEPSC) and spontaneous miniature inhibitory postsynaptic currents were recorded (mIPSCs, Fig. 6.25c, d). Analysis, performed by Robert Maresch and Tony Kelly (Lab of professor Heinz Beck), revealed a reduced mIPSC frequency in shSLK neurons (Fig. 6.25e; frequency reduced by 43.5%; n = 11 control, n = 12 shSLK neurons; hrGFP control 10.0$\pm$1.1Hz vs. shSLK 5.7$\pm$1.1Hz; *p$\leq$0.05, Student's t-test) which is in good agreement with the selective loss of inhibitory synapses (Fig. 6.24). The amplitude of the spontaneous mIPSCs was unchanged (Fig. 6.25f). Frequency and amplitude of mEPSCs were unchanged as well (Fig. 6.25g, h), further corroborating our findings of stable excitatory synapse density in shSLK neurons (Fig. 6.24). Furthermore, the input resistance was unaffected in shSLK neurons compared to controls, while the cell capacitance was significantly reduced (Fig, 6.25i, j; n = 11 control, n = 12 shSLK neurons; control 153.2$\pm$9.7pF vs. shSLK 115.9$\pm$12.5pF, *p$\leq$0.05, Student's t-test. The reduced cell capacitance is consistent with a smaller neuronal surface as reflected by a reduction of axon length (Fig. 6.18) and dendritic complexity (Fig. 6.21). Together, these results show that the observed morphological changes induced by SLK loss are also reflected by a functional impairment.

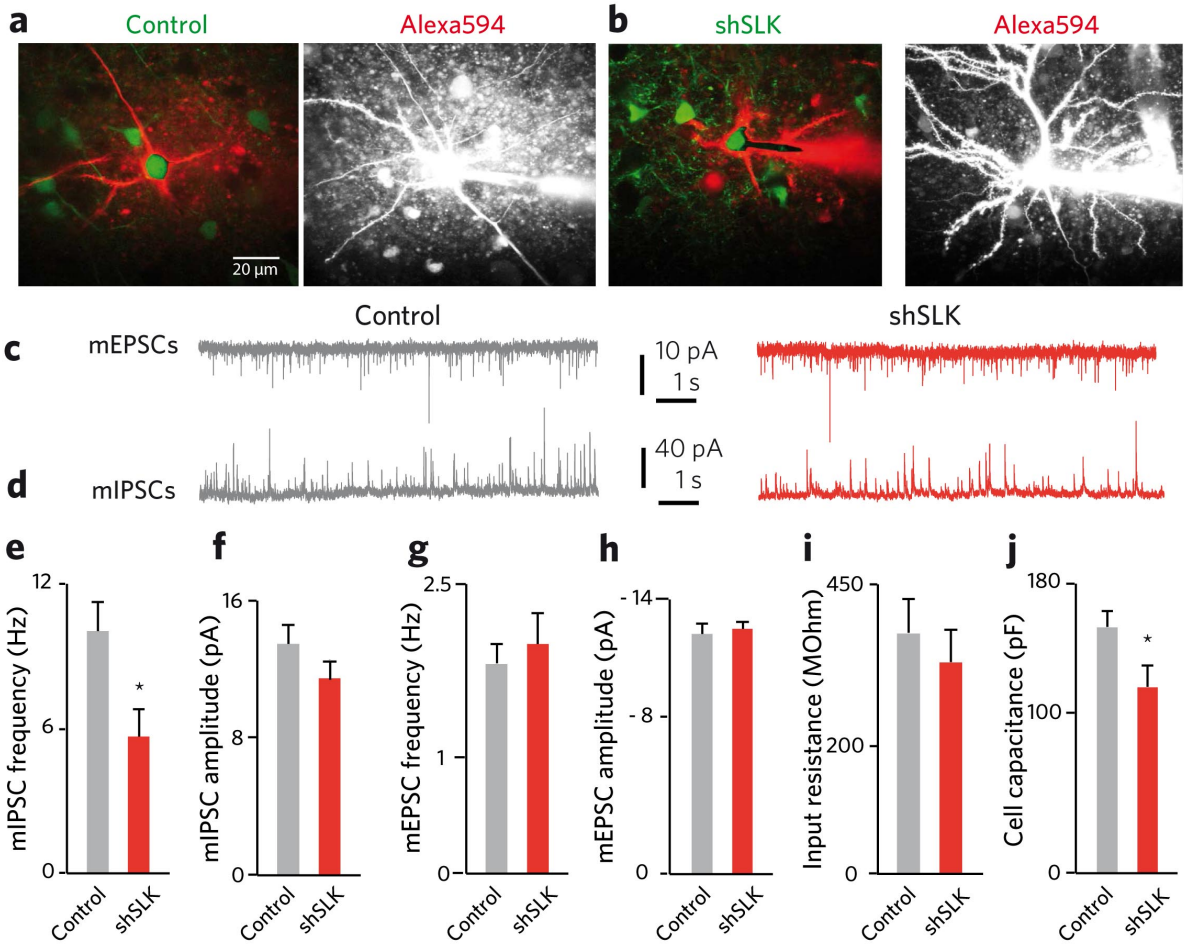

Figure 6.25: **Reduced mIPSC frequency and cell capacitance following SLK loss**. (a) In cortical neurons from layer II/III, electroporated with control or (b) shSLK, (c) mEPSCs and (d) mIPSCs were recorded. (e) Upon SLK loss mIPSC frequency was significantly reduced, whereas (f) mIPSC amplitude, (g) mEPSC frequency (holding potential -60mV) and (h) amplitude remained on control levels. (i) Input resistance was unchanged as well, however, (j) cell capacitance was significantly reduced in shSLK expressing neurons (N = 4 – 6 mice with n = 11 – 12 neurons, *p≤0.05, Student's t-test, stars indicate statistically significant difference compared to hrGFP control). Image courtesy of Robert Maresch, Tony Kelly and Heinz Beck. Experiments performed by Robert Maresch, analysis performed by Robert Maresch and Tony Kelly.

6.3.8 Focal *SLK* knockdown leads to increased PTZ-induced seizure severity

Reduced inhibitory synapse density and reduced inhibition, together with an aberrant cortical lamination and impaired dendritic morphology after SLK loss suggest a severe impairment in local cortical circuitry. To test whether these pathological changes - mirroring key features of dysplastic neurons and associated lesions - are sufficient to induce a hyperexcitable brain lesion, we subjected control- or shSLK electroporated mice to repetitive pentylenetetrazol (PTZ) injections. PTZ binds to and inhibits $GABA_A$Rs. Thus, with increasing dosage, PTZ induces epileptiform seizures in healthy mice that can be rated by their severity (I - V) according to Racine [270]. We continuously injected low doses of PTZ every 10 minutes until animals encountered generalized, Racine Score V seizures (Fig. 6.26a). We observed that chemically evoked seizures were more severe in shSLK electroporated mice in comparison to controls expressing the U6 hrGFP vector. Most control mice usually first encountered rather mild Racine IV seizures while shSLK IUE mice showed in most cases more severe Racine V seizures as their first seizure event (Fig. 6.26b; IV: 64.8% of control mice vs. 18.18% of shSLK mice, V: 35.3% of control

mice vs. 81.8% of shSLK mice; n = 17 control, n = 11 shSLK mice; Fisher's exact test, *p≤0.05). In contrast, seizure onset time was not affected by *SLK* knockdown (Fig. 6.26c). Together, these results indicate that a focal cortical loss of SLK, characterized by malpositioned and aberrantly arborized neurons with impaired inhibition, may indeed lead to the emergence of dysplastic neurons and translate into a hyperexcitable phenotype.

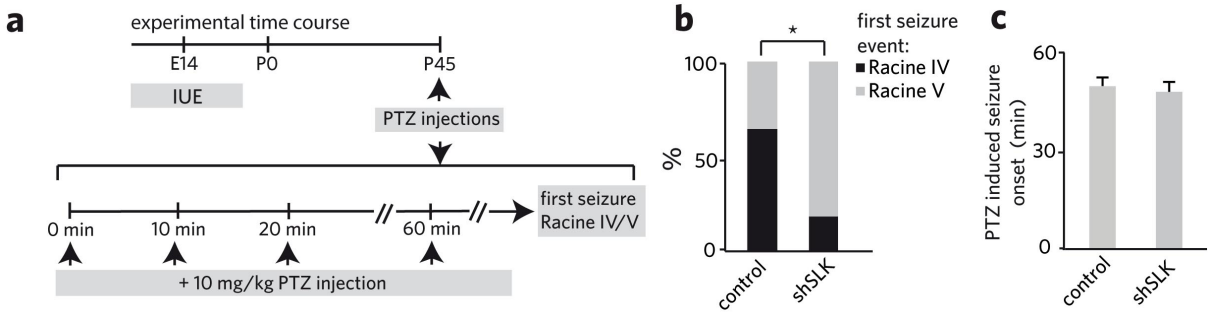

Figure 6.26: **Increased PTZ-induced seizure propensity after *SLK* knockdown.** (a) *In utero* electroporated mice were injected repetitively with PTZ at P40 – 45. (b) Mice *in utero* electroporated with control plasmids had predominantly Racine Score IV seizures as their first epileptic event, while shSLK mice showed more severe seizures rated as Racine Score V. (c) No change in the onset time of the first PTZ induced seizure-like event was observed in shSLK mice compared to control mice (N = 3 – 5 different litters with n = 17 control and n = 11 shSLK mice; Fisher's exact test; *p≤0.05).

6.3.9 *In vitro* analysis of SLK interaction with the cytoskeleton

The hyperexcitable phenotype of developmental, locally restricted SLK loss in mice is most possibly a consequence of the combination of the progressive loss of inhibitory synapses and the altered neuronal morphology. Adequate cytoskeleton dynamics and actin-microtubule cross talk are required for both, neurite growth and synapse stability [176, 177, 229, 230]. In order to investigate whether SLK regulates these processes by direct interaction with the cytoskeleton, a function of SLK that has been reported in fibroblasts [254], we analyzed different cytoskeleton-related parameters.

First, we determined the consequences of *SLK* knockdown on growth cone size. SLK was shown to be recruited to the leading edge of spreading fibroblasts where it facilitates actin depolymerization, a process needed for efficient cell migration [254]. Actin depolymerization within the growth cone is also critical for growth and extension of neurites. We therefore first analyzed whether *SLK* knockdown or SLK overexpression affects the size of the growth cone. This parameter is regarded as a measure for "normal" cytoskeleton remodeling in growing structures. To that end, neurons were transfected with control, shSLK, *SLK*, or the kinase dead K63R-*SLK* plasmid at DIV1 and growth cone size was measured three days later at DIV4. For visualization of the growth cone, 4%-PFA fixed neurons were stained with antibodies against acetylated tubulin (acTubulin) and red-labeled (Actin-stain 555) phalloidin (Fig. 6.27a - d). Acetylated tubulin is more stable and provides a stronger pushing force needed for growth. Growth cones of control neurons had a similar F-actin staining pattern (assessed by phalloidin red-fluorescence), shape, and size as shSLK transfected neurons (Fig. 6.27a - d). SLK overexpression or the presence of the kinase dead K63R-SLK had no effect on growth cone size as well (Fig 6.27e, two independent experiments with n = 10 - 24 growth cones each, One-way ANOVA with Bonferroni post-correction). This result indicates that SLK may not be regulating the gross morphology of the growth cone in expanding axons and thus, impairment in neurite growth upon SLK silencing seems to be

independent from growth cone functionality.

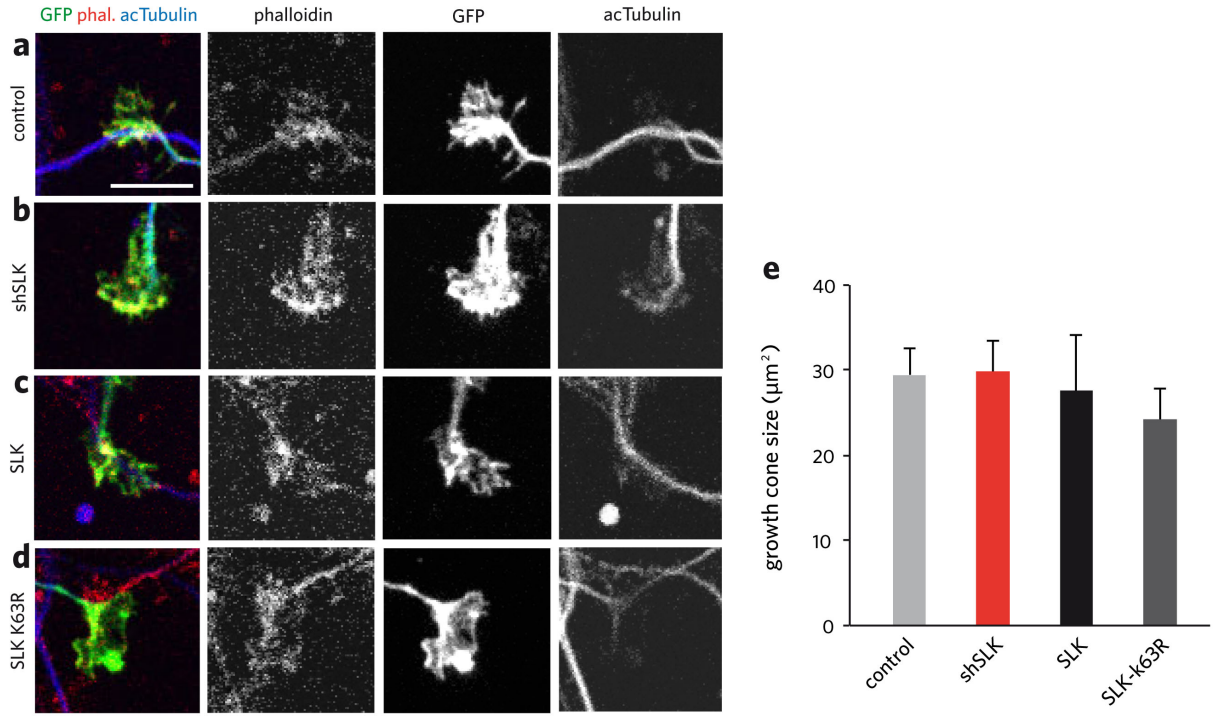

Figure 6.27: **Growth cone size unchanged upon *SLK* knockdown or overexpression.** (a) Neuronal cultures were transfected with control-, (b) shSLK-, (c) SLK-, (d) or K63R-SLK plasmids at DIV1; Scale bar 6µm. (e) At DIV4, the size of the growth cone was measured and revealed no significant differences between the groups (N = 2 independent experiments, with n = 10 - 24 growth cones per condition, One-way ANOVA with Bonferroni post-correction).

The size and stability of the inhibitory postsynapse depends on a proper regulation of the cytoskeleton scaffold and correct actin and microtubule cross-talk, both properties that have been associated with SLK in fibroblast cultures [254]. If SLK is needed for the stability of the postsynapse by regulating local cytoskeleton dynamics, the reduced synapse density may be explained by SLK loss. To test whether SLK regulates synapse stability in neurons, we assessed the fluorescence intensity of phalloidin and acTubulin within gephyrin-GFP positive inhibitory postsynapses of control or *SLK* knockdown neurons. Neurons were transfected at DIV3 with the mRFP-expressing control vector or the mRFP-labeled shRNA against *SLK* together with gephyrin-GFP-FingRs. At DIV21, neurons were stained with antibodies against acTubulin and F-actin was visualized by iFluor647-phalloidin application (Fig. 6.28a, b). The fluorescence intensity of acTubulin or phalloidin was normalized to the mRFP signal within each gephyrin$^+$ synapse. We found that synaptically localized fluorescence intensity of both, acTubulin and phalloidin was dramatically reduced in shSLK transfected neurons compared to control neurons (Fig. 6.28c, e; n = 10 neurons per condition with 2196 synapses in controls and 2190 synapses in shSLK transfected neurons). In both groups, gephyrin-GFP positive punctae clearly colocalized with the microtubule marker acTubulin or the F-actin marker phalloidin but within inhibitory synapses of SLK silenced neurons significantly more synapses had low acTubulin or phalloidin fluorescence intensities (Fig. 6.28d, f, Mann-Whitney U-test, $^{***}p \leq 0.001$).

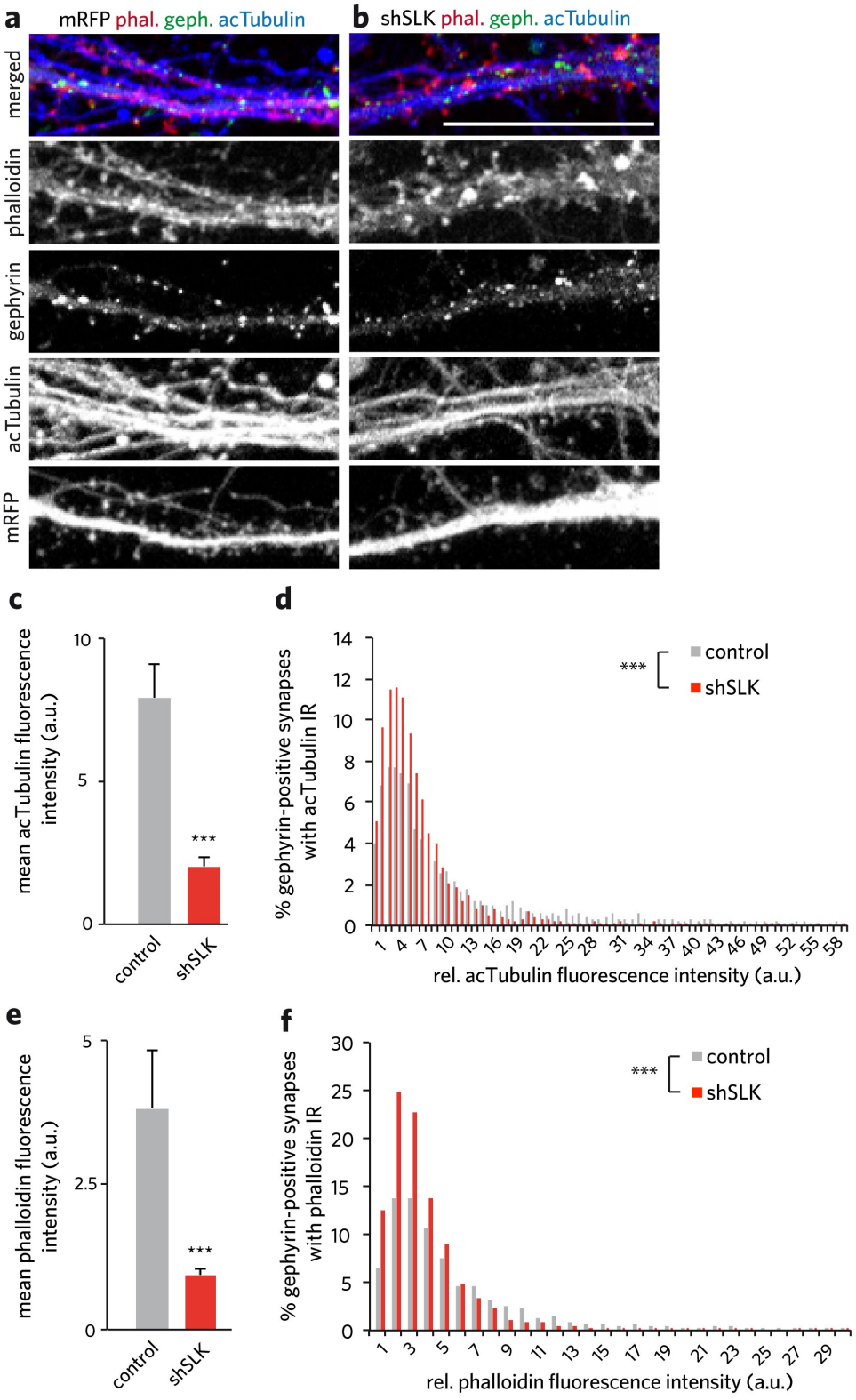

Figure 6.28: **Knockdown of *SLK* reduces fluorescence intensity of synaptically localized components of the cytoskeleton**. (a) Cortical neurons were transfected at DIV3 with gephyrin-GFP-FingRs and an mRFP-expressing control plasmid or (b) shSLK and stained with iFluor647-phalloidin and antibodies against acTubulin at DIV21; Scale bar 25µm. (c) The fluorescence intensity of synaptically localized acTubulin was significantly lower in shSLK transfected neurons compared to control neurons. (d) The histogram illustrates the significant difference in the abundance of different acTubulin fluorescence intensities for both groups normalized to mRFP or mRFP-shSLK respectively. (e) *SLK* knockdown resulted in a reduced synaptic phalloidin fluorescence intensity compared to control neurons. (f) The histogram illustrates the statistically significant difference in the abundance of different phalloidin fluorescence intensities in control or shSLK transfected neurons normalized to mRFP or mRFP-shSLK respectively (n = 10 neurons per condition with 2196 synapses in controls and 2190 synapses in shSLK transfected neurons, Mann-Whitney U-test, ***$p \leq 0.001$).

The size of gephyrin clusters is regulated by their phosphorylation status [228], therefore loss of phosphorylation that may be mediated by SLK at inhibitory synapses can affect gephyrin cluster size. To examine this hypothesis, we analyzed the size of gephyrin-GFP punctae in neurons transfected with a control vector or shSLK together with gephyrin-GFP-FingRs at DIV3 (Fig. 6.28a, b). At DIV21, the size of gephyrin-GFP punctae was measured in control and *SLK* knockdown neurons. We observed no changes in synapse size upon *SLK* knockdown (Fig. 6.29a; n = 10 neurons for each condition with 2185 synapses in control and 2056 synapses in shSLK transfected neurons, Student's t-test, $p \geq 0.05$). The histogram illustrates the abundance of gephyrin$^+$ synapses with different sizes, which is similar in both groups (Fig. 6.29b). Taken together, these results suggest that in cultured neurons SLK may indeed interfere with or regulate the stability of cytoskeletal components within the inhibitory postsynapse even though gephyrin cluster size was not affected.

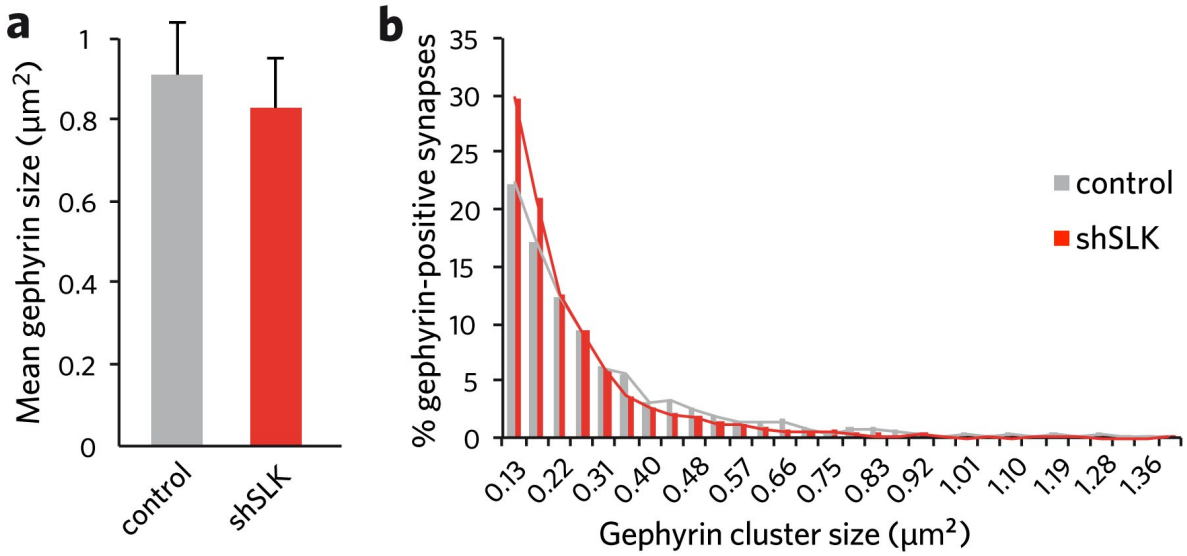

Figure 6.29: **Knockdown of *SLK* does not alter gephyrin-cluster size.** (a) The mean gephyrin cluster size was similar in control or SLK depleted neurons. (b) No significant changes in the abundance of different-sized gephyrin clusters were observed (n = 10 neurons for each condition with 2185 synapses in control and 2056 synapses in shSLK transfected neurons).

6.4 The role of LDB1 and LDB2 for normal cortex development

6.4.1 Reduced LDB1 protein levels in dysplastic neurons human GG cases

The transcriptional co-activator LDB2 was shown to be one of the most reduced transcripts in human GGs compared to adjacent control tissue (assessed by microarray analysis) [47]. Therefore, we aimed to analyze whether LDB loss may be involved in the formation dysplastic neurons and thus, an epileptogenic, developmental brain lesion.

In mammals, two LDB family members exist which have partially overlapping and redundant functions. They have been implicated in cell-fate determination, development and cytoskeletal organization [277, 278], important cellular processes that may be altered in dysplastic neurons. Furthermore, both were demonstrated to functionally interact with SLK. Thus, also LDB1 expression in GG tissue was assessed by immunohistochemical staining of GG tissue with LDB1 antibodies to explore the pos-

sibility, that also LDB proteins play a role in the emergence of dysplastic neurons (Fig. 6.30a). Co-immunohistochemical reactions with antibodies against LDB1 and NeuN (neuronal marker) revealed a significantly reduced nuclear LDB1 fluorescence intensity in ganglioglioma compared to adjacent control brain tissue (Fig. 6.30b; N = 3 different GG patients with a total of n = 274 control cells and n = 496 cells within the GG; Student's t-test $p \leq 0.001$). Vimentin antibody-labeling of astrocytes was used to discriminate lesioned cortex versus non-lesioned cortex. LDB1 fluorescence colocalizes with the neuronal protein NeuN but barely with the astroglial protein GFAP (Fig. 6.30c). Detailed quantification showed that only 7% $GFAP^+$ astrocytes overlapped with $LDB1^+$ cells while 99% $NeuN^+$ cells overlapped with $LDB1^+$ cells indicating that LDB1 was preferentially expressed in the dysplastic neuronal compartment of these lesions. Consequently, only 5% of $LDB1^+$ cells overlapped with $GFAP^+$ and 66% of $LDB1^+$ cells with NeuN, implying that LDB1 is also expressed in another cell type. This cell type may be an immature, tumor specific cell population, neither positive for NeuN nor GFAP (Fig. 6.30d).

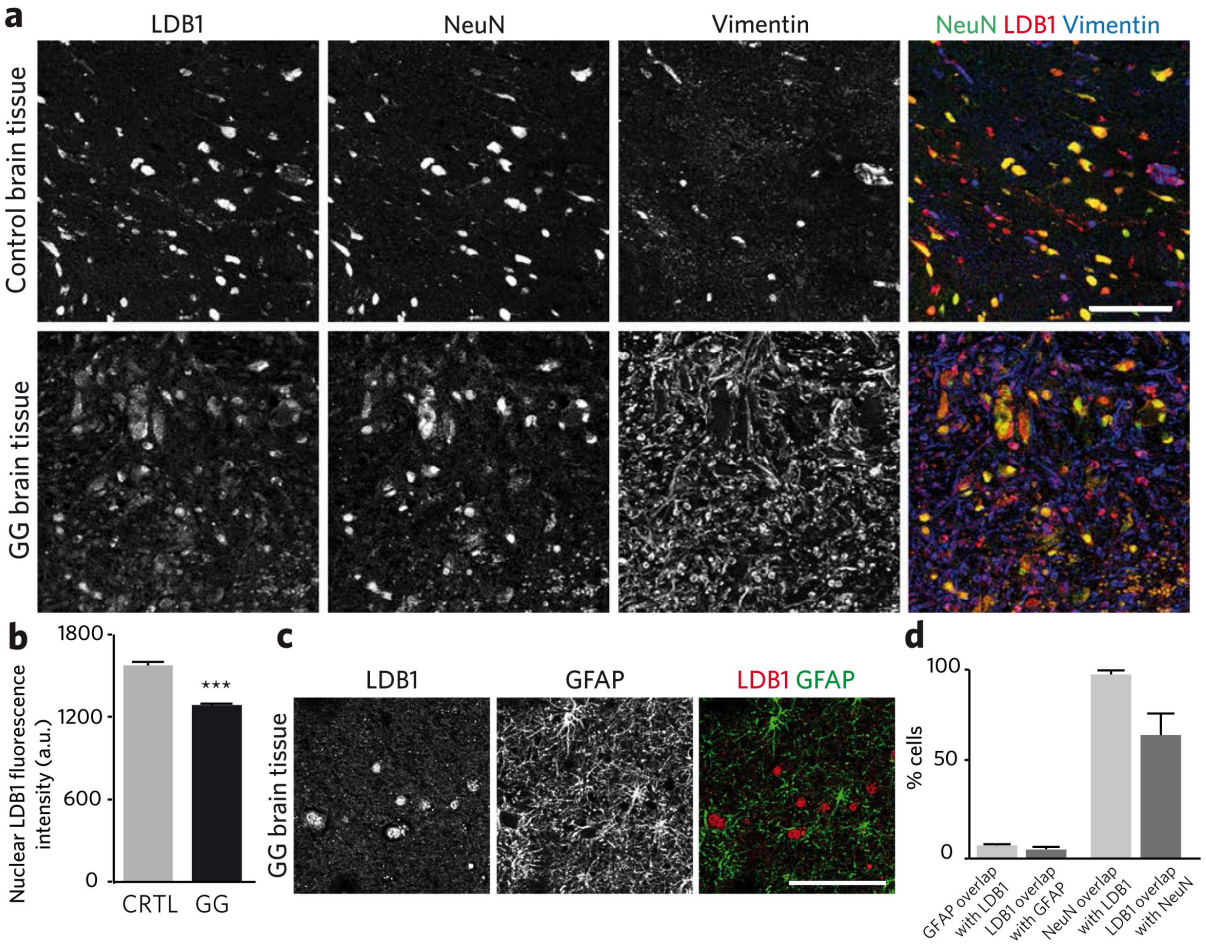

Figure 6.30: **Low LDB1 protein expression in human GGs.** (a) Human brain tissue was stained with LDB1, NeuN and vimentin in order to compare LDB1 protein levels in GG and adjacent control tissue. Scale bar 100µm. (b) The mean nuclear LDB1 fluorescence intensity was significantly lower in GG tissue in comparison to adjacent control tissue (N = 3 different GG patients with a total of n = 274 control cells and n = 496 cells within the GG; Student's t-test $^{***}p \leq 0.001$). (c) To analyze if LDB1 is expressed in astroglia, GG brain tissue was colabeled with LDB1 and GFAP. Scale bar 100µm. (d) To identify the major cell types expressing LDB1, the overlap of LDB1 with NeuN or GFAP positive cells was assessed: 7% of all GFAP positive astrocytes and 99% of all NeuN positive neurons overlapped with LDB1. Only 5% LDB1 positive cells overlapped with GFAP and 66% with NeuN (N = 3 different patients with GGs with a total of n = 368 cells positive for LDB1 in NeuN co-stainings, n = 104 cells positive for NeuN, n = 72 cells positive for LDB1 in GFAP co-stainings and n = 229 cells positive for GFAP).

6.4.2 RNAi mediated *LDB*1/2 knockdown

The expression of both, LDB1 protein and *LDB2* transcripts, was reduced in human GGs tissue in comparison to adjacent control tissue. In order to analyze whether these reduced levels of the transcriptional co-activators may have a functional relevance in the emergence of dysplastic neurons, we generated specific shRNAs to knockdown *LDBs*. They were designed to target mouse and rat *LDB1* and *LDB2* mRNA sequences. shRNA-resistant cDNA variants of *LDB1* and *LDB2* were generated for rescue and cross-rescue experiments, by introducing silent point mutations within the shRNA binding site. Knockdown efficiency of the *LDB1* or *LDB2* shRNA was confirmed by immunoblotting of protein homogenates from HEK293T cells, which had been co-transfected with the respective mCherry-tagged expression plasmids and the hrGFP-tagged shRNAs (Fig. 6.31a, b). Transfection of *LDB1* (shLDB1) or *LDB2* (shLDB2) shRNAs with corresponding expression plasmids prevented expression of either LDB1 or LDB2. In contrast, expression of the shRNA-resistant mutated LDB1 *(*LDB1-mut*)* and mutated LDB2 *(*LDB2-mut*)* variants was not affected by the respective shRNAs (Fig. 6.31c, d; N = 3 Western Blots).

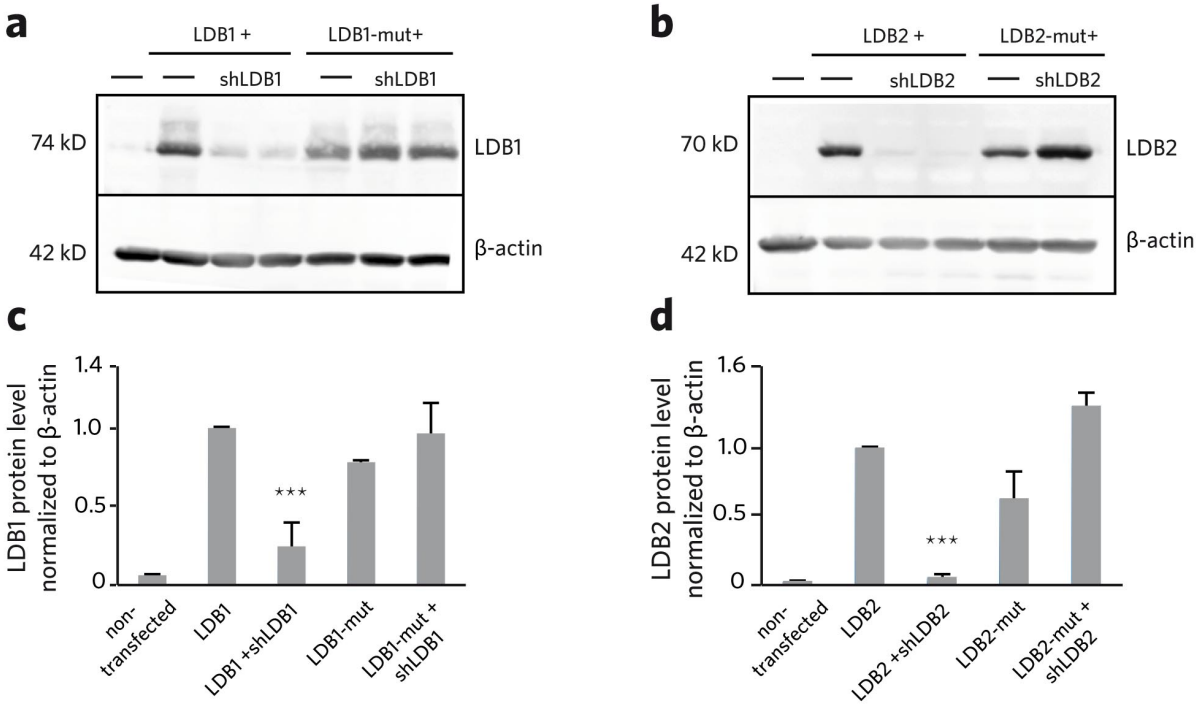

Figure 6.31: **shRNA mediated *LDB1* or *LDB2* knockdown is effective *in vitro*.** Efficiency of *LDB* knockdown was assessed by Western blot. Therefore HEK293T cells were transfected with (a) *LDB1* or (b) *LDB2* plasmids alone or in combination with specific shRNAs. In addition, cells were transfected with resistant mouse *LDB1-mut* or mouse *LDB2-mut* plasmids (carrying silent point mutations) alone or in combination with the murine shRNAs. β-actin was used as a housekeeping gene. (c) shRNAs targeting mouse *LDB1* or (d) *LDB2* knocked down specifically the native mouse *LDB1* or *LDB2,* respectively. Overexpression of the resistant LDB1-mut or LDB2-mut did not result in a significant protein reduction (N = 3 Western Blots, One-way ANOVA with Bonferroni post-correction,***$p \leq 0.001$).

6.4.3 *LDB*1/2 knockdown in neurons results in impaired neurite morphology *in vitro* and *in vivo*

In *Caenorhabditis elegans* or *Drosophila melanogaster,* LDB1 proteins or their orthologs (Chip) were shown to be involved in axon guidance and neurite growth [263, 279], suggesting a similar important

function for normal neuronal growth of LDB proteins in mammalian development. To address the possibility of redundant roles of LDB1 and LDB2 during neuronal growth, we analyzed both proteins. Given that LDB1/2 seem to be reduced in dysplastic neurons with aberrant dendritic morphology, we analyzed the effect of *LDB1* and/or *LDB2* knockdown or overexpression on neurite growth in mammalian cortical neurons. Therefore, the previously validated shRNAs and/or expression plasmids were transfected in cortical neurons at DIV3 and their dendritic morphology was analyzed at DIV14. We found that dendritic arbor formation was affected in the absence of one or both LDBs. Within the neuronal dendritic arbor, different order dendrites can be differentiated: The primary dendrites grow out of the neurons soma, second order dendrites branch from first order dendrites and tertiary dendrites branch from secondary dendrites (Fig. 6.32a, different colors indicate different order dendrites). Quantification of the number of first and second order dendrites did only detect a slight but not significant change in the absence of LDB1/2 (not shown). However, the total number of tertiary dendrites was significantly reduced by more than 50% (Fig. 6.32b). Coexpression of shRNA-resistant LDB1 resulted in a rescue of this phenotype in *LDB* single and double knockdown neurons, indicating that the shRNA mediated effects on dendritic morphology are not off-target effects. Overexpression of LDB1 had no significant effect on the number of third order dendrites (Fig. 6.32b; n = 7 - 17 neurons, One-way ANOVA with Bonferroni post-correction; $^{*}p \leq 0.05$, $^{***}p \leq 0.001$).

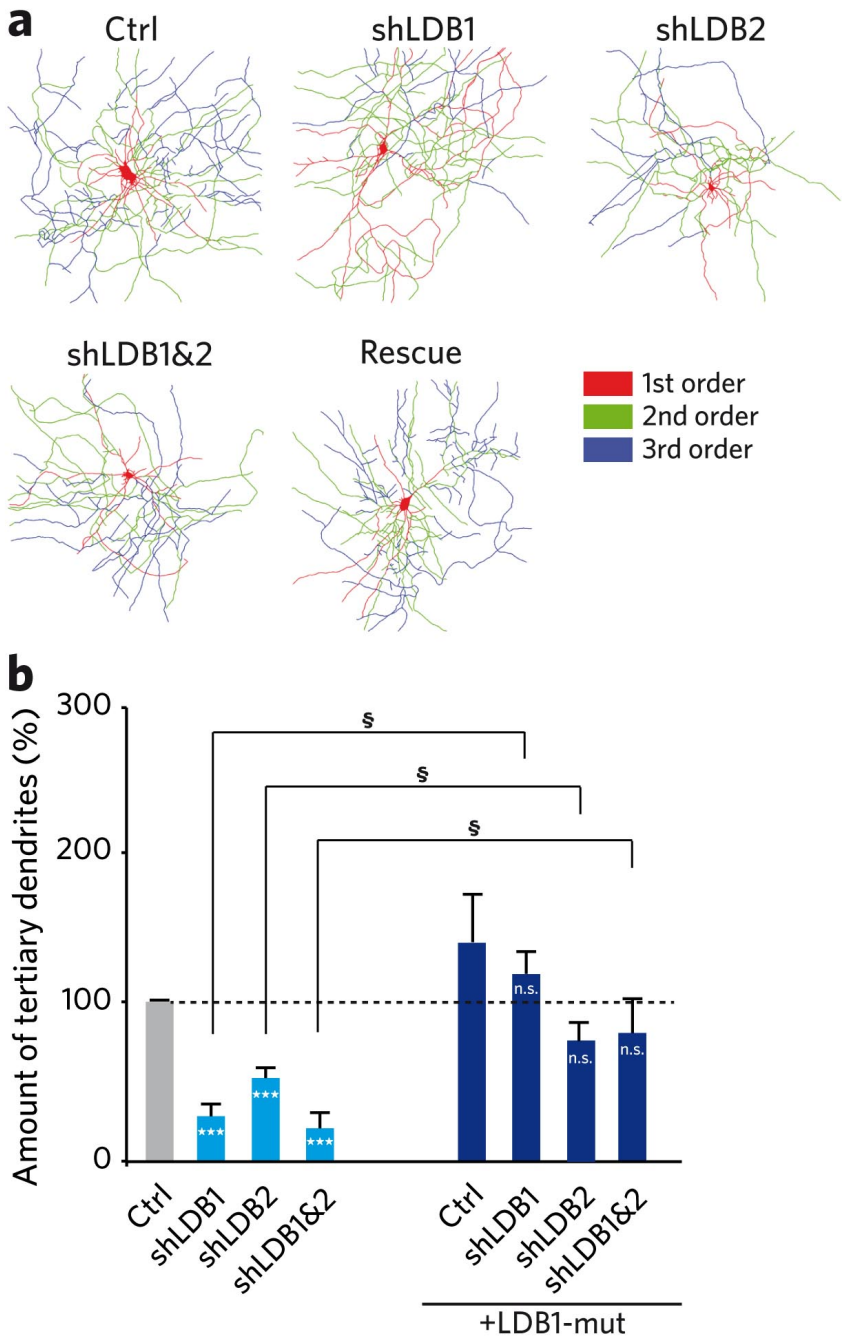

Figure 6.32: **LDB1 and/or LDB2 loss leads to reduced number of third order dendrites.** (a) Rat cortical neurons were transfected at DIV3 with shRNAs together with or without shRNA-resistant LDB1 expression plasmids and analyzed at DIV14. Color-code indicates different order dendrites. (b) Knockdown of either *LDB1* or *LDB2* led to a significant reduction in the number of third order dendrites. Coexpression of LDB1 rescued dendritic branching to control levels (N = 3 independent experiments with 7 - 17 neurons per condition, One-way ANOVA with Bonferroni post-correction; $^{*}p \leq 0.05$, $^{***}p \leq 0.001$, stars indicate statistically significant difference compared to hrGFP control, paragraphs demonstrate significant difference as indicated, n.s. symbolizes non-significant differences).

We demonstrated earlier that SLK is also implicated in branching and/or development of higher order dendrites, therefore, we analyzed whether SLK expression had the potential to restore the effect on dendritic morphology in LDB1/2 silenced neurons. To this end, we transfected neurons with *LDB* shRNAs and *SLK* expression plasmids. Interestingly, SLK expression rescued the shLDB mediated effect on dendrite morphology when only one but not both *LDBs* were knocked down (Fig. 6.33a). Importantly, *SLK*

knockdown was not rescued by LDB1 expression, indicating that SLK may be a downstream effector of LDB in regulating dendrite morphology in developing cortical neurons (n = 7 - 17 neurons; One-way ANOVA with Bonferroni post-correction; *p≤0.05, **p≤0.01, ***p≤0.001).

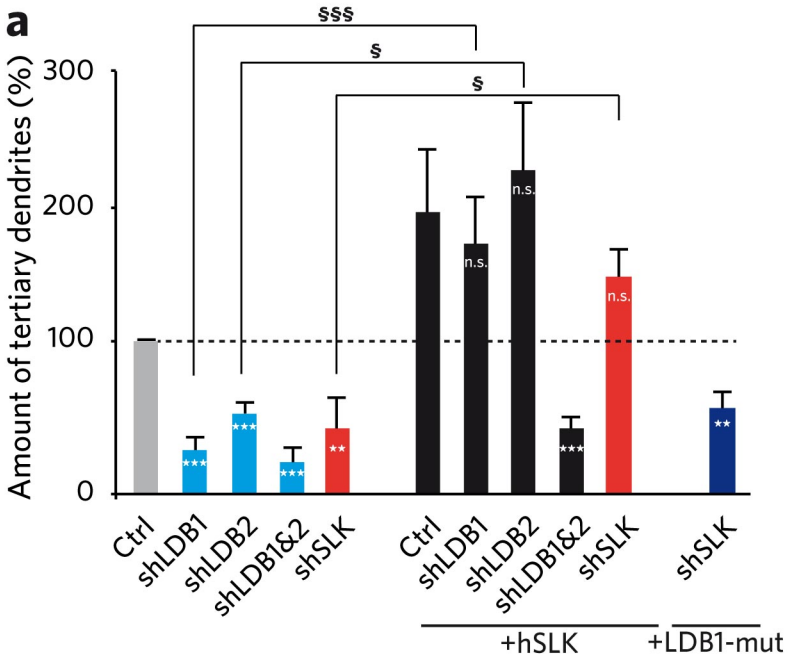

Figure 6.33: **Knockdown of *LDB1* or *LDB2* is rescued by SLK overexpression**. Rat cortical neurons were transfected at DIV3, analyzed and reconstructed at DIV14. (a) The shRNA mediated effect of *LDB1*, *LDB2* or *SLK* knockdown on the number of third order dendrites was rescued by SLK expression. However, SLK expression was not sufficient to rescue the knockdown of both *LDBs*. Expression of LDB1 was not sufficient to rescue *SLK* shRNA mediated effect on dendritic morphology (N = 3 independent experiments with 7 - 17 neurons per condition, One-way ANOVA with Bonferroni post-correction; *p≤0.05, **p≤0.01, ***p≤0.001, stars indicate statistically significant difference compared to hrGFP control, paragraphs demonstrate significant difference as indicated, n.s. symbolizes non-significant differences).

Similar to the experiments with *SLK* shRNAs, we assessed whether LDB proteins are needed exclusively for proper dendritic scaling or also for axon growth. Therefore, the length of axons was measured at DIV6 in neurons that had been transfected at DIV2 with shRNAs or a combination of shRNAs and *LDB* expression plasmids. Also in this experimental design we noticed a reduction in axon length after loss of individual or both LDB proteins (Fig. 6.34a). Whereas primary cortical neurons in the control condition showed normal axon growth and branching, axons of *LDB1* and *LDB2* knockdown neurons exhibited a robust reduction in length (Fig. 6.34b; n = 13 - 26 neurons; One-way ANOVA with Bonferroni post-correction; **p≤0.01, ***p≤0.001). Coexpression of shRNAs with shRNA-resistant LDB1 rescued axon length in LDB1 and LDB2 single- and double-silenced neurons. In contrast, LDB2 expression was only sufficient to rescue *LDB1* or *LDB2* single- but not double knockdown (Fig. 6.34c; n = 9 - 54 neurons; One-way ANOVA with Bonferroni post-correction; **p≤0.01, ***p≤0.001), indicating that LDB1 and LDB2 have only partially overlapping functions in axon growth.

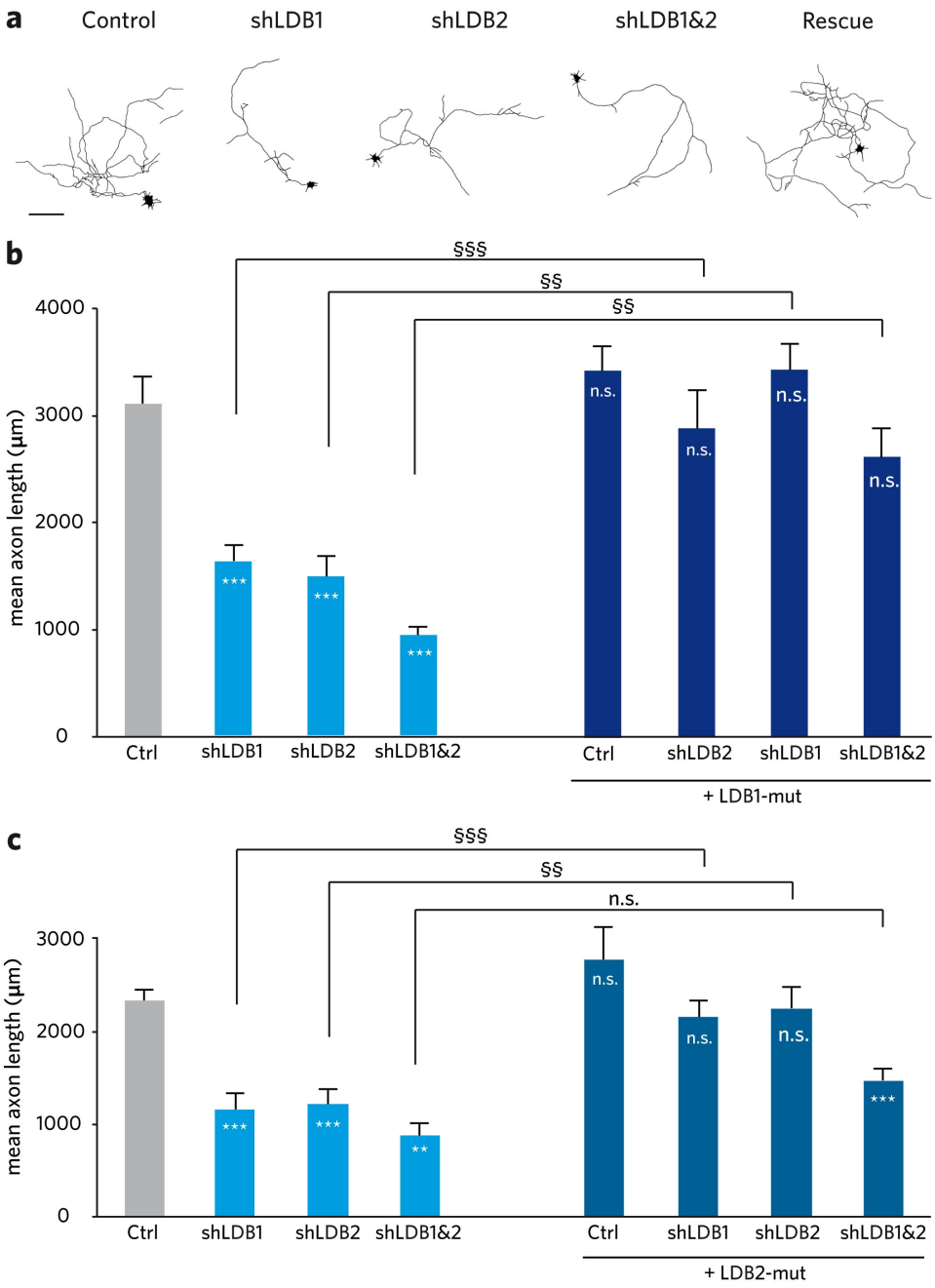

Figure 6.34: ***LDB1* and *LDB2* knockdown results in reduced axon length.** (a) Embryonic rat cortical neurons were transfected at DIV2 with shRNAs targeting *LDB1* or *LDB2* alone or in combination with resistant *LDB1* or *LDB2* expression plasmids, reconstructed and analyzed at DIV6; Scale bar 100µm. (b, c) Quantification of axon length demonstrated a reduction by approximately 50% after *LDB1* and/or *LDB2* knockdown. Coexpression of shRNAs together with LDB1 or LDB2 had no significant effect on axon length in comparison to control. However, co-transfection of *LDB2* and both shRNAs resulted in a reduced axon length in comparison to control (N = 3 independent experiments with 9 - 54 neurons per condition, One-way ANOVA with Bonferroni post-correction, $^{**}p \leq 0.01$, $^{***}p \leq 0.001$, stars indicate statistically significant difference compared to hrGFP control, paragraphs demonstrate significant difference as indicated, n.s. symbolizes non-significant differences).

Similar to the analysis of dendrite morphology, we co-transfected *LDB*1/2 shRNAs with shRNA-resistant human *hSLK* expression plasmids. Axon length in *LDB1* and *LDB2* single knockdown neurons expressing SLK was indistinguishable from control conditions. Double *LDB*1&2 knockdown, however, was again not rescued by SLK expression. Axon length was significantly reduced in comparison to control

transfected neurons, indicating that at least one LDB family member needs to be present to ensure normal axonal growth. Similar to our results obtained in DIV14 neurons, expression of LDB1 or LDB2 did not rescue axon length after *SLK* knockdown (Fig. 6.35a; n = 13 - 54 neurons; One-way ANOVA with Bonferroni post-correction; $^{**}p \leq 0.01$, $^{***}p \leq 0.001$).

These experiments indicate that LDB proteins are important for proper neurite scaling in developing cortical neurons and that LDB and SLK may act in concert during these processes. Consequently, loss of both proteins seems to have to potential to induce dysplastic neurons.

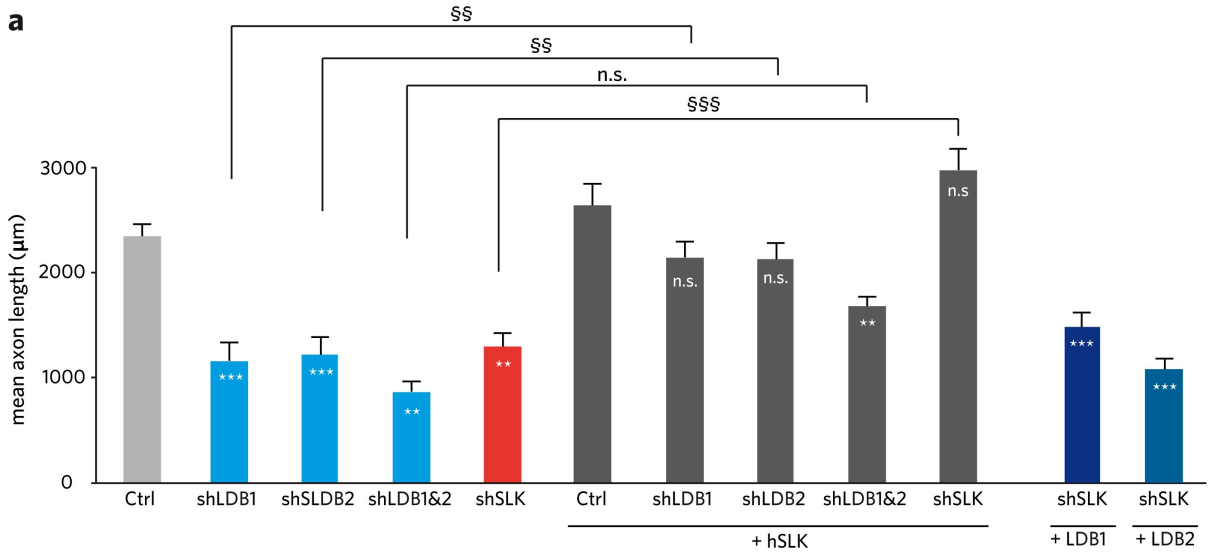

Figure 6.35: **SLK rescues *LDB1* or *LDB2* single, but not double knockdown.** (a) Embryonic rat cortical neurons were transfected at DIV2 and analyzed at DIV6. Co-transfection of *LDB1*, *LDB2* or *SLK* shRNAs in combination with a resistant *SLK* overexpression plasmid had no effect on axon length. However, knockdown of both *LDB1* and *LDB2* with SLK overexpression led to a significant reduction in axon length. Expression of LDB1 or LDB2 did not rescue shSLK mediated effect on axon length (N = 3 independent experiments with 13 - 54 neurons per condition, One-way ANOVA with Bonferroni post-correction, $^{**}p \leq 0.01$, $^{***}p \leq 0.001$, stars indicate statistically significant difference compared to hrGFP control, paragraphs demonstrate significant difference as indicated, n.s. symbolizes non-significant differences).

LDB proteins are highly abundant during corticogenesis but also in the adult cortex and seem to be important for proper neurite scaling in isolated and cultured cortical neurons. In order to examine the relevance of these proteins for normal cortical development within a neuronal network, we knocked down their expression during mouse brain development. To mimic the focal character, presumed developmental origin and associated cortical LDB1/2 reduction of GGs, we used the *in utero* electroporation approach to reduce LDB1 and LDB2 expression only in a restricted number of cells during mid-corticogenesis. Embryos of time pregnant mice (E14) were electroporated with the established shRNAs or control plasmids in one lateral ventricle and cortical development was examined at P30 - 35 (see IUE protocol in Fig. 6.19a). Brain slices of shLDB1&2 electroporated mice showed a similar cortical architecture as control mice. In both groups, NeuN and GFAP labeling was inconspicuous without signs of gliosis or migration deficits (Fig. 6.36a). High magnification images of single IUE multipolar layer IV neurons at the borders of the IUE area revealed a significant reduction in arbor size after *LDB*1&2 knockdown in comparison to control neurons (Fig. 6.36b). Similar to our *in vitro* results (Fig. 6.32), reduction of LDB1&2 levels led to a loss of third order dendrites in comparison to control electroporated neurons, also *in vivo* (Fig. 6.36c; control neurons n = 7; shLDB1&2 neurons n = 6 from N = 2

different litters, Student's t-test; ***p≤0.001). These neuropathological observations were corroborated by morphometric Sholl analysis. Quantification showed in contrast to control electroporated neurons, a reduced number of crossings over the majority of the measured distance in LDB1&2 silenced neurons. These observations indicate a reduced dendritic complexity (Fig. 6.36d; Mann-Whitney U-test; *p≤0.05). Furthermore, they provide *in vivo* evidence for an important role of LDB proteins in the regulation of neuronal growth processes during corticogenesis, that may be altered in dysplastic neurons of developmental brain lesions.

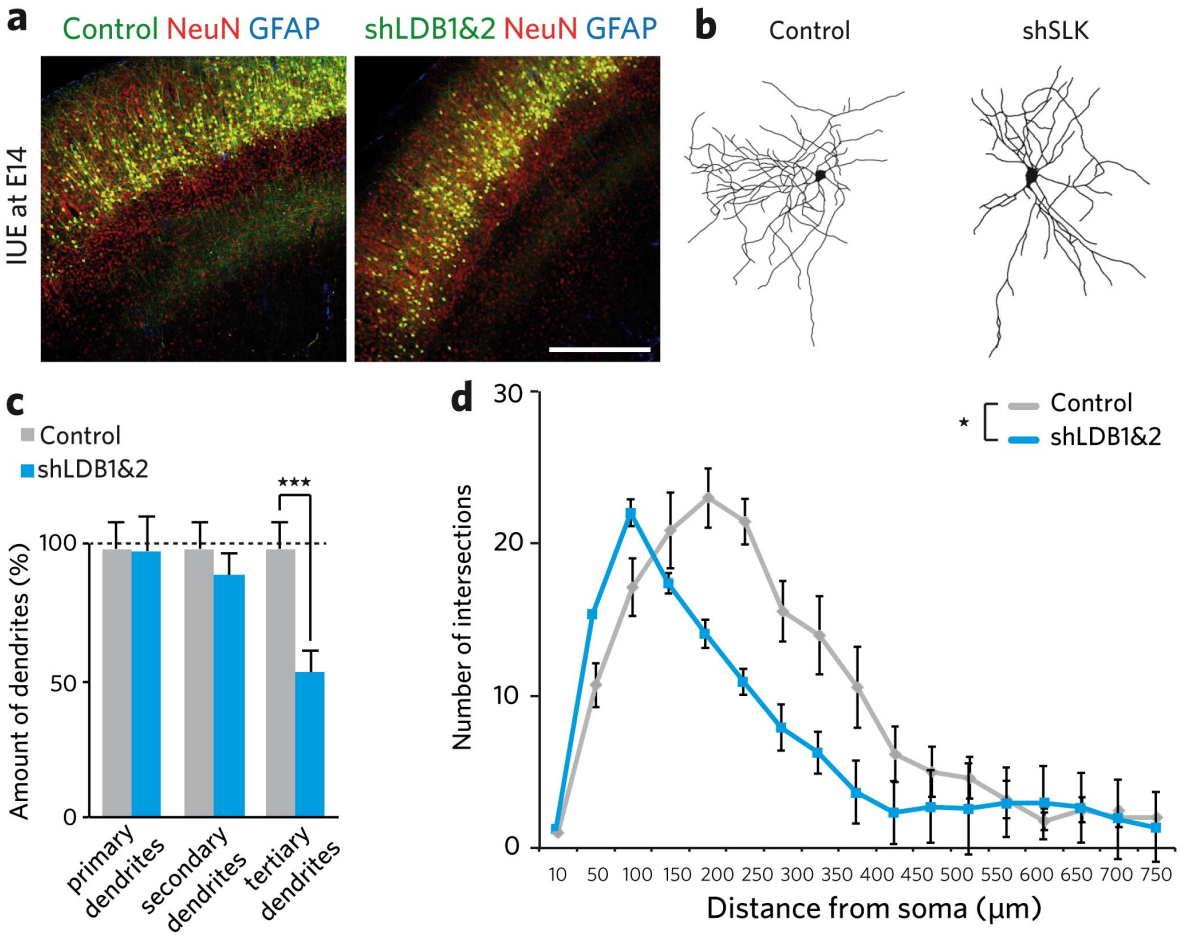

Figure 6.36: **Reduced dendritic complexity upon *LDB*1&2 knockdown**. (a) Embryos of time pregnant mice were *in utero* electroporated at E14 with *LDB1* and *LDB2* shRNAs (shLDB1&2) or control plasmids. Knockdown of both, *LDB1* and *LDB2* had no apparent effect on cortical structure or on the abundance of GFAP-positive astrocytes; Scale bar 400µm. (b) High magnification images of reconstructed, individual, electroporated cortical neurons located in the periphery of the electroporated area. (c) Quantification of the number of different order dendrites in control- or shLDB1&2 electroporated brain slices revealed a robust reduction of distal dendrites after *LDB*1&2 knockdown. (d) Sholl analysis of single neurons demonstrated a reduced number of intersections in LDB1&2 silenced cortical neurons, in comparison to control neurons (control neurons n = 7; shLDB1&2 neurons n = 6 from 2 different litters, Student's t-test, ***p≤0.001; for Sholl analysis: Mann-Whitney U-test, *p≤0.05).

6.4.4 Focal *LDB*1&2 knockdown does not induce a hyperexcitable cortical lesion

We next turned to the question, whether the observed impairment in dendritic and axonal structures of shLDB1&2 IUE mice, as seen in dysplastic neurons of GGs, are also reflected in functional alterations that may contribute to the emergence of an epileptic brain lesion. Since mice from respective IUE

cohorts did not show spontaneous, semiological seizures, we challenged them by subjecting adult (P30 - 50) *in utero* electroporated mice to repetitive low-dose PTZ injections (Fig. 6.37a). Unlike control mice, that most often had rather mild Racine score IV seizures as their first seizure event, animals with focal *LDB*1&2 knockdown had more severe epileptic seizures rated as Racine Score V (Fig. 6.37b). However, this difference in seizure severity and the PTZ-induced seizure onset time were statistically not significant (Fig. 6.37c; control n = 13, shLDB1&2 n = 10 mice, Fisher‘s exact test p = 0.21). This finding indicates that the observed neuropathological alterations in neurite development alone were not sufficient to cause a robust hyperexcitable phenotype.

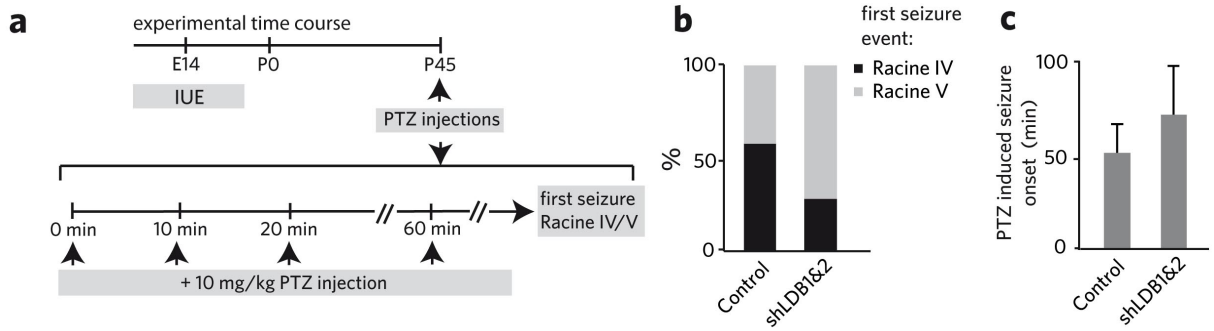

Figure 6.37: **Evoked seizure severity is unchanged upon LDB1&2 loss.** (a) *In utero* electroporated C57Bl/6 mice were subjected to repetitive PTZ injections at P30 - 50. (b) *LDB*1&2 knockdown resulted in slightly, but not statistically significantly increased seizure severity. While control mice suffered most often from Racine score IV seizures, shLDB1&2 IUE mice showed more often Racine score V seizures as their first seizure event. (c) PTZ-induced seizure onset time was similar in both groups (control n = 13, shLDB1&2 n = 10 mice, Fisher‘s exact test, p = 0.21).

7 Discussion

In this study, we analyzed key molecular mechanisms underlying the formation of dysplastic neurons in three of the most common developmental brain lesions, i.e. FCDIIb, TSC and GGs. Dysplastic neurons are a major unifying hallmark of these disorders. Until today underlying mechanisms of their emergence or epileptogenesis were largely unresolved, possibly because they were mainly investigated by immunohistochemical analysis of human biopsy specimens. These, however, do not allow for a dynamic intervention, drug testing or analyses at earlier time points, since human brain tissue is only removed when the patient suffers from severe pharmacoresistant epileptic seizures. To overcome these known limitations, we utilize mouse models that enable the study of this particular dysmorphic neuron and epileptogenic, developmental lesions. We demonstrated that the pathogenetic deregulation of various genes (*BRAF*, *Akt* or *TSC1*) results in the emergence of dysplastic neurons specific for the respective lesion. But we also showed, that these dysplastic neurons, found across substantially distinct neoplastic and non-neoplastic glioneuronal lesions also share a pathological deregulation of SLK as a common contributing factor leading to their formation. The results obtained in this study increase our understanding of the underlying pathologic mechanisms involved in the manifestation of dysplastic neurons, epileptogenesis and thus, developmental brain lesions. These insights can open new avenues for the development of novel therapeutic approaches.

7.1 Focal loss of p53 together with BRAF-V600E and Akt expression induces glioneuronal tumors with dysplastic neurons

Although our knowledge of the biology of cerebral tumors and malformations of cortical development expanded over the past years, only little progress was made in finding new treatment options for these devastating disorders. Development of animal models that reliably replicate human diseases are essential for uncovering the underlying molecular mechanisms of epileptogenesis and the validation of new therapeutical approaches. *In utero* electroporation (IUE) represents an excellent tool to address the effects of different genes or gene variants on restricted brain areas at controlled time points during development and is already in use to create new animal models for epileptogenic brain lesions [280, 281]. However, still no animal models exist that mirrors human gangliogliomas and thus, our knowledge about etiology or pathological mechanisms underlying the formation of dysplastic neurons in this entity is very limited. To gain more insight into gene function in tumorigenesis, molecular mechanisms, cellular origins, disease progression or epileptogenesis we developed a GG animal model. We used *in utero* electroporation of a combination of genes, known to promote tumor growth or reported to be altered in human GG specimens (Fig. 7.1a).

At the current, very early development-stage, our mouse model reliably generates lethal brain tumors

in 84.6% of all mice. However, the induced lesions present high heterogeneity in terms of tumor growth rate, malignancy, immunohistochemically identified cellular features and lethality. Some of the induced tumors showed typical GG features, including enlarged, dysplastic neurons and bi-nucleated cells embedded in an astroglial cellular matrix with sometimes piloid features such as eosinophilic granular bodies and strong chromogranin A immunoreactivity (IR). Thus, this tumor model is the first animal model to reproduce tumors with features resembling gangliogliomas, including dysplastic neurons. These observations demonstrate, that the expression of mutated BRAF-V600E and aberrant activation of Akt leads to the emergence of dysplastic neurons, underlining their pathogenetic potential in human GG cases. However, further improvement and fine tuning of our mouse model is necessary to generate a stable phenotype mainly mirroring benign gangliogliomas. Human GGs also reveal particularly strong immunoreactivity for the stem cell marker CD34. About 74% of GGs are positive for CD34 and the expression of this marker correlates with S-100 protein IR [42]. Another proposed marker to discriminate GGs from other glioneuronal tumors is AMOG (adhesion molecule on glia) [16]. In future experimental approaches to fine tune the model and generate tumors that resemble GGs more closely, these markers could be used for further characterization or discrimination.

Currently, most of the tumors generated with our mouse model resemble gliomas. Gliomas are fast growing, highly malignant brain tumors, properties often mirrored by our mouse model. *TP53* mutations are frequently identified in gliomas [271], suggesting that malignancy is conveyed by p53 loss in our mouse model. This theory is supported by the observation that $p53^{fl/wt}$ mice, electroporated with all four tumor-inducing plasmids, did not develop large and malignant tumors, at least not until day 75. To address this hypothesis in future experiments, electroporation of BRAF-V600E and activated Akt in a wild type mouse with intact *TP53* may generate a less malignant lesion that mirrors GGs more closely. Furthermore, the expression of the respective tumor-inducing plasmids driven by cell type specific promoters may influence the resulting tumor type (as already demonstrated in [280]). This may increase tumor specificity and allow for novel insights into tumor etiology. Complementary experiments should be carried out with BRAF-V600E or activated Akt in combination with shRNAs against *SLK*, to validate SLK loss as a contributing, common factor in the emergence of dysplastic lesions. Since a major hallmark of GGs are epileptic seizures, cortical excitability needs to be assessed in the respective generated tumors.

Importantly, our mouse model helped to identify the etiology of GGs that remained controversial over the past decades. We demonstrated that GGs arise form a genetically compromised precursor cell population, which differentiates into abnormal neuronal and glial tumor elements (Fig. 7.1b). Thus, monoclonal tumor cells arise from a shared precursor cell. This result is in direct contrast to another theory, which proposes that GGs arise from a dysplastic precursor lesion with a subsequent somatic so-called "second-hit" mutation in the proliferative glial component. Thus our experiments clearly favor the theory of somatic mutations in precursor cells as the origin of GGs.

Even though our mouse model at its current stage can not be considered as a reliable GG mouse model, it helped to gain more insight into the origin of dysplastic neurons, the etiology of GGs and sets the stage for future studies on this particular tumor entity. Our model allows for analysis of mechanisms of epileptogenesis, the developmentally-regulated temporal and spatial determinants and the contribution of distinct precursor cell types or gene variants involved in the emergence of dysplastic neurons and

other developmental cerebral tumors. It also provides a promising basis for the development of a more optimized GG mouse model that consistently recapitulates histological hallmarks of GGs that can be used for detailed analysis and testing of putative therapeutical compounds.

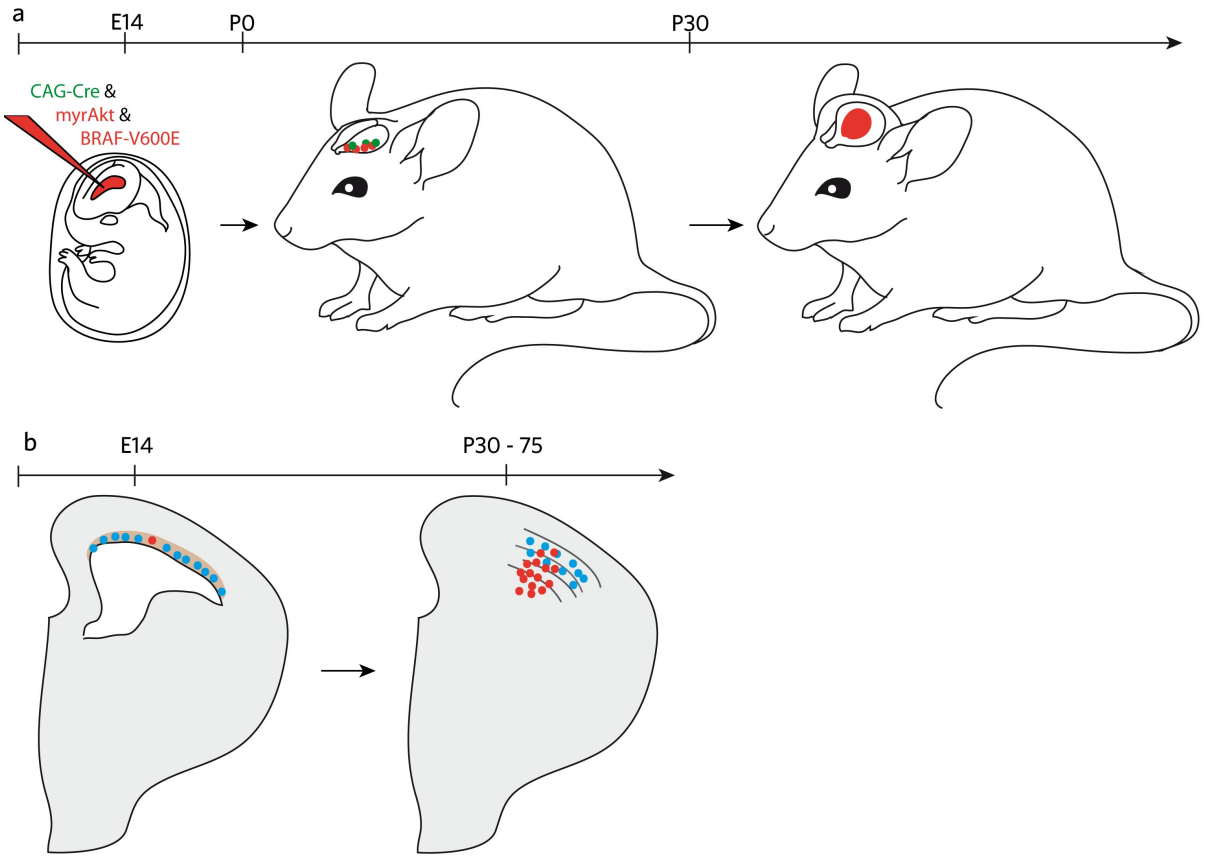

Figure 7.1: **Focal loss of p53 together with BRAF-V600E and Akt expression induces brain tumors with dysplastic neurons and indicates a monoclonal origin of GGs.** (a) $p53^{fl/fl}$ embryos are *in utero* electroporated with mCherry-labeled myrAkt, BRAF-V600E kinase domain and GFP labeled CAG-Cre to knockout p53. After $\geq$ 33 days 85% of all *in utero* electroporated mice start to develop lethal brain tumors from which some show features reminiscent of GGs. (b) A genetically compromised precursor cell in the proliferative zones of the developing brain gives rise to neoplastic glial and neuronal cells that will form the ganglioglioma.

7.2 Analysis of the pathogenetic mechanisms underlying tuberous sclerosis

In order to gain more insight into the pathogenetic background of dysplastic neuron development in TSC patients we optimized the IUE-based TSC mouse model to dramatically enhance litter survival. These newly generated CD1 $TSC1^{fl/fl}$ mice showed similar pathological features as C57Bl/6 $TSC1^{fl/fl}$ mice, including focal lesions containing cytomegalic, dysplastic neurons with strong mTOR pathway activation, aberrant dendritic morphology, and loss of normal cortical lamination. Features closely resembling cortical tubers of human TSC patients (Fig. 7.2b). Even though our improved TSC animal model does not recapitulate all features of human tubers (i.e. astrogliosis or spontaneous seizure activity), it appears suited and facilitates the opportunity to study the underlying mechanisms of *TSC1* deregulation.

First, we analyzed the time frame susceptible for the manifestation of dysplastic neurons comprising cortical tubers. Our experiments showed that loss of both *TSC1* alleles, independent of the time point of TSC1 loss, resulted in the emergence of dysplastic neurons and abnormal final positioning of respective neurons (Fig. 7.2b). Dysplastic neurons were characterized by a dramatic increase of cell size and strong phosphorylation of S6 that indicate excessive mTOR pathway activation. Neuron size and cortical localization were similarly altered in lesions of different mice, caused at distinct developmental time points (E14, E16, E17). These results suggest that there is no specific vulnerable phase or time window during embryonic development for cortical tubers to emerge. Thus, the exact time point of the pathogenetic event leading to tuber formation will most likely not influence the resulting phenotype in humans. This hypothesis is in good agreement with a study that knocked down *TSC1* in newborn mice by intracerebral ventricular AAV injections that still resulted in reduced survival and pathologic findings of enlarged neurons and cortical heterotopias [282]. Furthermore, expression of TSC1 had the potential to rescue the phenotype of dysplastic neurons even very late during cortical development. This result suggests that TSC1 reconstituting therapies may be effective, even in later developmental stages.

The abnormal cortical layering seen in surgical brain specimens of human TSC patients was partially reproduced by our animal model. Focal loss of TSC1 at E14 resulted in an abnormally increased number of neurons in cortical layer IV. This phenotype is probably caused by delayed migration of cortical neurons, since aberrant neuronal morphology or polarity are thought to impair migration characteristics of developing neurons [165, 275]. TSC1 loss may impair the transition from the multipolar to the bipolar morphology in neurons entering the cortical plate. A similar defect of delayed cortical neuron radial migration, induced by impaired neuronal polarity and thus impaired multipolar-bipolar transition, was previously described in an animal model of *in utero TBC1D24* (TBC1 domain family member 24) knockdown in rats [275].

An increased number of cortically integrated neurons in layer IV can foster increased network excitability. Layer IV is regarded as a cortical hub for intracolumnar information processing, since it converges the majority of the sensory information [172, 173]. It is a highly interconnected layer that amplifies and redistributes thalamo-cortical inputs. Thus, an increased number of neurons in this layer may increase integration and recurrent inputs, thereby contributing to the epileptogenic potential of TSC [174]. However, we did not detect spontaneous epileptic discharges in our mouse model, similar to another mouse model of focal cortical *TSC1* knockout [112]. This observation indicates that either the ectopically located dysplastic neurons are not aberrantly integrated into the existing network in this experimental setup or that also other parameters profoundly influence the excitability of the lesion. The size and the exact location of the lesion and its composition of compromised precursor cell populations are examples of such parameters [112, 134, 140]. Finally also the age of the mice was recently shown to be critical for seizure occurrence, as tuberless mice heterozygous for *TSC1* had spontaneous seizures only until 9 - 18 days of age [174]. Alternatively, the time window of observation was too small or hyperexcitability did not result in semiological seizures. But keeping in mind that although almost all TSC patients have epileptic seizures, by far not all of their cortical tubers are epileptogenic [283], stresses that various factors and their interaction substantially influence cortical excitability in a complex manner. The contribution of the altered neuronal positioning to cortical hyperexcitability,

in concert with the mentioned parameters needs to be addressed in future studies. This may be of particular interest, especially since EEG recordings, providing a more detailed analysis and quantification, were not performed in this study. They could reveal different forms of alterations of cortical excitability that did not translate into semiological seizures in our experimental set up.

Since the exact time point of TSC1 loss did not affect characteristics of the resulting dysplastic neurons or the tuber-like cortical phenotype, we next analyzed whether the expression of distinct disease-associated *TSC1* variants induces pathological dysplastic neurons. We analyzed the morphological effects on neurons and possible implications for tubers of the allelic *TSC1* variant coding for hamartin^{H732Y}, frequently found in FCDIIb patients [94]. Furthermore, we expressed variants of *TSC1* with truncating point mutations coding for hamartin^{R692X} and hamartin^{R786X}, abundant in TSC patients [101, 103, 104]. Previous *in vitro* studies in HEK293T (human embryonic kidney) cells demonstrated reduced binding of these hamartin variants with tuberin [93]. These results not only indicate functional impairment of hamartin^{H732Y}, hamartin^{R692X} and hamartin^{R786X}, but also reduced tumor suppressor function. *In utero* expression of the respective truncated hamartin variants *TSC1*-R692X and *TSC1*-R786X in a Cre-mediated *TSC1*-null background resulted in cortical lesions with a morphological phenotype of dysplastic neurons (Fig. 7.2a). This phenotype was indistinguishable from the morphological defects caused by *TSC1* knockout, stressing the pathogenetic potential of these truncated hamartin mutants. Surprisingly, *in utero* expression of Cre and *TSC1*-H732Y rescued the TSC1 loss-induced cytological consequences and did not recapitulate the findings of the recently published HEK293T cell culture experiments [93]. Respective cortical neurons did not show characteristics typical for dysplastic neurons, indicating at least residual functionality of hamartin^{H732Y}. HEK293T cells are human immortalized, mitotically active tumor cells and consequently have a highly active translational machinery with a distinct proteome, including post-translational modifications and composition. Therefore, distinct relative expression levels of the hamartin variants may have been produced in neurons *in vivo* and the previous *in vitro* study. This may have affected the resulting binding efficiency, possibly by binding site competition [93]. Furthermore, it is possible that earlier time points than E14 are required for hamartin^{H732Y} to generate a similar phenotype as *in vitro*. However, our previous experiments demonstrate that the phenotype induced by TSC1 loss is rather time independent. Thus, our results clearly argue for a strong rescuing capacity of hamartin^{H732Y} *in vivo* in an E14 induced *TSC1*-null cellular background. This finding indicates that the *TSC1*-H732Y variant may not be responsible for lesion development in FCDIIb patients.

Binding of hamartin^{H732Y} to tuberin and their co-localization was not completely lost in the *in vitro* experiments with HEK cells, but was only reduced down to 40% and 20%, respectively [93]. The full rescue potential of *TSC1*-H732Y *in vivo*, despite the reported reduced binding to tuberin suggests, that there is still a remaining interaction of hamartin^{H732Y} and tuberin in cortical neurons. This remaining interaction seems to be sufficient for the mutant hamartin to remain functionally active and exert its function together with tuberin as a tumor suppressor. Our finding supports the notion that only a very small amount of functional hamartin is necessary to maintain the wildtype cellular phenotype. Future studies need to address this hypothesis and exploit the intriguing possibility that only minimal *TSC1* concentrations are sufficient to retain the physiological neuronal phenotype, which may not be the case for *TSC2*, possibly providing an explanation for the more severe clinical phenotype observed in TSC patients carrying *TSC2* mutations [106].

To improve our understanding of the etiological basis and the contribution of distinct cellular elements in the emergence of cortical tubers, we aimed to knockout *TSC1* in different progenitor cell types by using various promoter-Cre plasmids in *TSC1*$^{fl/fl}$ mice. Identification of the lineage that is originally compromised provides invaluable insights into understanding tumor mechanisms and the design of therapy options. All Cre-plasmids used for this study were flanked by piggyBac recognition sequences to ensure stable integration into the genome by the pBase transposase. We observed that all Cre-constructs, even GFAP-Cre-GFP, yielded similar results, such as strongly increased soma size of NeuN-positive cells and the absence of electroporated cortical glial cells. These observations imply abnormally enhanced mTOR activity only in neurons, thus, indicating that the promoter constructs used in this experiment are either unspecific or "leaky". Therefore, we can not deduce the contribution of different precursor cell elements to cortical tubers. However, electroporation of CAG-Cre-GFP at E16 - 17 resulted in sparse electroporation of few, single glia cells positive for vimentin or S100 and negative for NeuN in deep, medial brain areas, but not the cortex. Thus, electroporation at E14 with CAG-Cre-GFP driving Cre expression in all cell types did not result in *TSC1* knockout glia cells in the cortex and may therefore not contribute to tuber-like lesion formation. Together these results allow for two different conclusions: First, the piggyBac transposase or the recognition sequences did not work as expected and failed to integrate Cre into the genome of the animals. This results in strong dilution of the Cre plasmid in rapidly dividing glial cells. This assumption is strengthened by the observation that only neurons express Cre-GFP. Unlike glia, they are post-mitotic cells and, therefore, the Cre-plasmids will not be diluted in respective neurons. Second, the tuber-like lesions generated with the cell-type independently expressed CAG-Cre-GFP are composed mainly of *TSC1*-null neurons and may not contain *TSC1*-null glia cells. This observation provides an explanation for the absence of astrogliosis and possibly even the absence of spontaneous seizures in our and previous experiments of focal cortical *TSC1* knockout [112]. Even though animal models of TSC, with exclusively neuronal TSC1 loss, exhibited epileptic seizures, these models do not recapitulate the pathologic situation in TSC patients that have focal/localized lesions. These animal models are based on general, neuronal TSC1 loss across most parts of the brain, instead of a focal neuronal TSC1 loss as seen in cortical tubers [140–142]. Thus, locally restricted neuronal TSC1 loss without local contribution of *TSC1*-null glia cells may not be sufficient to generate an epileptic cortical tuber. Although these series of experiments can not be interpreted in terms of distinct contributing cell types, they still allow for speculations about the necessity of compromised glial cells in cortical tubers to generate epileptic seizures. This intriguing hypothesis needs to be verified in future studies, for example with a functional piggyBac system or cell-type specific promoter-Cre constructs.

Even though cortical tubers are thought to be the origin of recurrent seizures and are therefore extensively studied, the underlying pathogenetic mechanisms leading to their emergence are still controversial [274]. While some studies rarely found biallelic *TSC1* loss using state-of-the-art deep sequencing or loss of heterozygosity (LOH) [108, 116, 284], other studies provided proof for classical somatic second hit events and consequently, biallelic *TSC1* inactivation to explain tuber formation in humans [109–111]. To provide more insight to this debate, we rescued Cre-induced *TSC1* loss in mouse brains by expression of a truncated *TSC1* allele together with varying concentrations of wild type *TSC1.* The cytological consequences of the expression of these three plasmids was analyzed at P24 - 30. We

found that even minimal concentrations of *TSC1*-WT DNA were sufficient to retain a physiological cellular phenotype (Fig. 7.2c). Respective *TSC1* knockout neurons that had received 10-times more non-functional, truncated *TSC1* (*TSC1*-R692X) than functional *TSC1* wildtype showed normal cell size, indicating physiological mTOR pathway activity. Even lower dilutions of *TSC1*-WT down to 1:20 mostly rescued *TSC1*-KO induced cytological consequences. At this *TSC1*-WT concentration, enlarged neurons were observed. However, due to the extremely low *TSC1*-WT concentration these neurons may have only received the truncated *TSC1*-R692X allele and Cre but not the wildtype *TSC1*. Nevertheless, these results generally argue in favor of a bialellic *TSC1* loss or a substantial silencing of the second allele, critical for the manifestation of cortical tubers. Technical limitations or hard-to-detect intronic mutations and/or genetic mosaicism may account for TSC cases with no identified mutations [98, 106]. Alternatively, molecular alterations and post-translational modifications affecting the functionality of the TSC1/TSC2 tumor suppressor complex may occur at a dynamic, epigenetic level. Studies in human TSC associated tumor cells demonstrated complete tuberin reduction induced by promoter methylation [285] or post-translational inactivation of tuberin by non-physiological phosphorylation in cortical tubers [286]. Parallel mechanisms may be operative in respective lesions or contribute to tuber emergence and can not be controlled for or mimicked in our experimental setup.

Pharmacological therapy with mTOR inhibitors rapamycin or everolimus reduce clinical symptoms in TSC patients, however, due to various side effects long-term treatment may not be an option [287]. The strong capacity of wildtype hamartin to rescue the tuber-like phenotype may serve as a basis for future treatment of TSC patients. Gene therapy, locally reconstituting hamartin expression within the restricted area of the cortical tuber, should have significantly less side effects than a systemic treatment. Analogous gene therapeutic approaches have already been demonstrated to be successful in treating manifest, developmental brain lesions in adult rats or young mice as they reduced the size of the cortical malformation, neuron size, excessive mTOR pathway activation and seizure risk [288, 289].

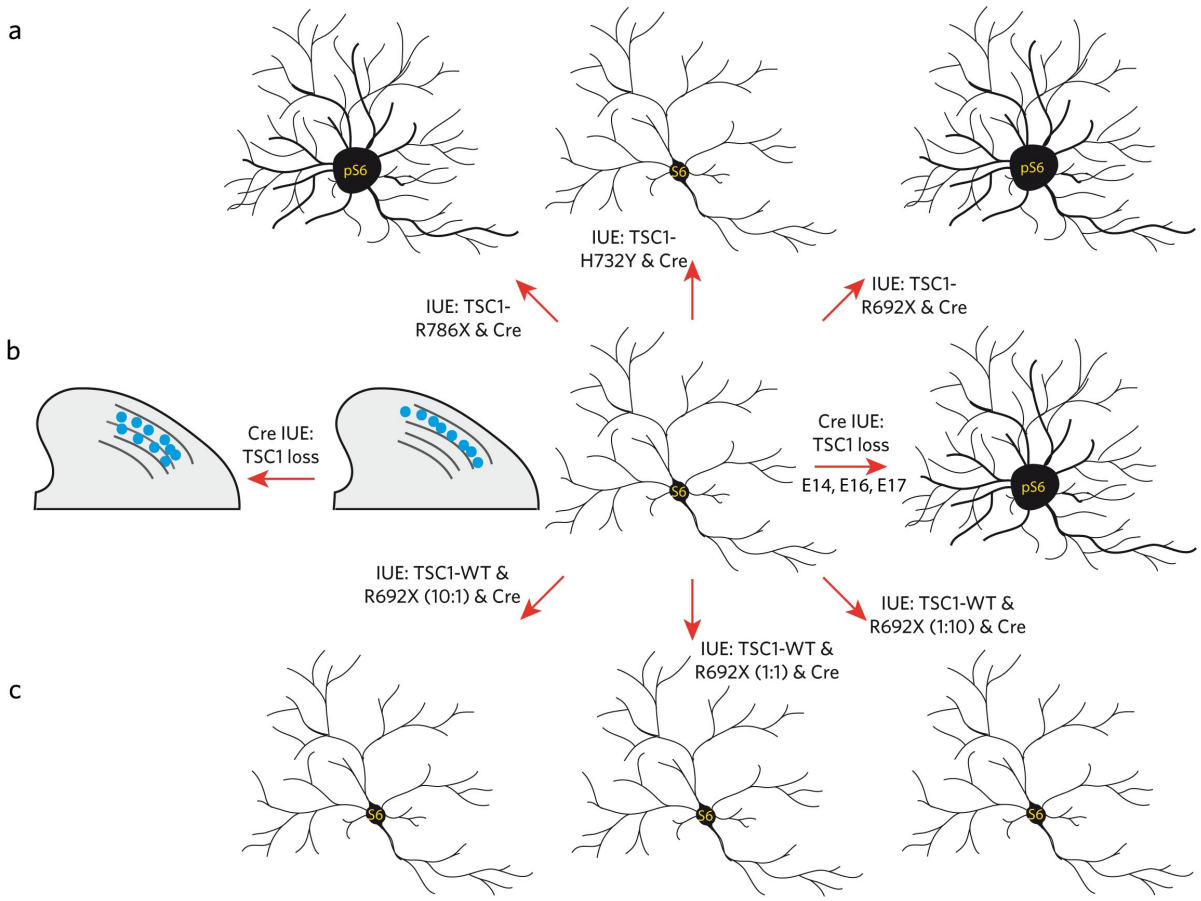

Figure 7.2: **Summary of the main finings.** (a) Expression of Cre and *TSC1*-R786X and *TSC1*-R962X in $TSC1^{fl/fl}$ mice at E14 results in the emergence of dysplastic neurons, characterized by increased pS6 immunoreactivity and soma size, while expression of Cre and *TSC1*-H732Y rescued the Cre-induced *TSC1* knockout phenotype. (b) Upon TSC1 loss, induced by *in utero* electroporation of Cre at E14, E16, and E17, final positioning of dysplastic cortical neurons is altered. (c) The emergence of dysplastic neurons is already prevented by the presence of minimal amounts of *TSC1*-WT.

7.3 SLK is needed for normal cortex development

To find a molecular alteration that is possibly shared by dysplastic neurons from various distinct developmental brain lesions, we analyzed the so far only poorly characterized Ste20 like kinase (SLK) in the context of cellular abnormalities reflected by dysplastic neurons. We found strongly decreased SLK expression in FCDIIb and GG associated dysplastic neurons. Interestingly, knockdown of *SLK* resulted in aberrant neurite growth, resembling the pathologic dendritic morphology of dysplastic neurons. The growth defects caused by *SLK* knockdown, were reflected by a reduction in the average axon length and the amount of third order dendrites *in vitro* and *in vivo* as well as a reduction of neurite intersections in Sholl analysis (Fig. 7.3a). Together these findings can be interpreted as a loss of arbor complexity upon SLK loss. Our corresponding electrophysiological experiments confirmed these findings, as shSLK-silenced neurons had a decreased membrane capacitance. This suggests a reduction of neuronal surfaces due to the reduced axon length and the absolute number of higher order dendrites without considerable changes in dendrite length. The fact that overexpression of the kinase dead SLK mutant K63R resulted in a reduction of third order dendrites and axon length, similar to shSLK expressing

neurons, suggests that the kinase activity of SLK is required for proper neurite growth and branching.

SLK was previously shown to modulate cytoskeleton dynamics in non-neuronal cells, a process that is a prerequisite for normal neurite growth and branching that may be disturbed in dysplastic neurons [254]. Accordingly, cytoskeleton remodeling, especially microtubule assembly and actin (in-)stability, represents the most likeliest underlying mechanism of SLK action during neurite development. Phosphorylation of microtubule associated proteins regulates microtubule stability [176] and SLK was previously shown to co-localize with and regulate the orientation of microtubules [254]. Furthermore, experiments with migrating fibroblasts demonstrated that SLK regulates actin destabilization by phosphorylation of Rac1, a process required for cytoskeleton remodeling and cell growth [256]. Rac1 belongs to the Rho family of GTPases and controls a wide range of cellular processes upon activation, including cytoskeletal rearrangements as well as growth and branching of dendrites [290, 291]. Additionally, it was already demonstrated that dominant negative Rac1 impairs neurite outgrowth and axon specification, underlining the importance of Rac1 regulation for normal neurite development [256]; a process that is possibly mediated by SLK phosphorylation.

It is possible that Rac1 activation of SLK is regulated by the integrin-FAK pathway, upstream of SLK, Rac1 and RohA. Previous experiments with non-neuronal cells demonstrated that SLK controls actin-microtubule interactions [254]. At the leading edge of migrating fibroblasts, cross-talk between actin and microtubules is regulated by integrin signaling pathways [292]. Integrin α and β heterodimers are attached to the extracellular matrix (ECM) and the intracellular actin cytoskeleton. Intracellularly, integrins are linked to the cytoskeleton by various adapter proteins, including focal adhesion kinase (FAK), vinculin, talin, and paxillin [293, 294]. Together this protein complex regulates dynamic rearrangements of actin and its cross-talk with microtubules. In migrating cells, the downstream protein Rac1 directs actin disassembly to induce lamellipodia generation and their elongation [294, 295]. Loss of integrin or Rac1 in neurons leads to reduced size and complexity of the dendritic tree [182, 296]. Together these facts point towards a role of SLK downstream of the integrin/FAK pathway to phosphorylate Rac1 (Fig. 7.3b) [192, 209, 296]. An activation of SLK by the integrin/FAK complex in migrating fibroblasts was previously proposed by Wagner et al. [253].

Moreover, dendrite growth and branching also requires organelles, such as Golgi outposts in dendrites. Less Golgi outposts in dendrites lead to reduced branching mainly in distal dendrites [195]. SLK was previously shown to influence the proper localization of the Golgi complex [252], suggesting that similar defects in Golgi positioning may result in defective branching of cortical neurons following *SLK* knockdown in our model.

Intriguingly, the cortical laminar structure was also impaired in mice electroporated with *SLK* shRNAs. We found varying portions of cells with obvious neuronal morphology, but negative for layer-specific and the neuronal marker NeuN, dispersed throughout all cortical layers. This suggests an immature neuronal cell type that failed to properly differentiate due to SLK loss. Undifferentiated cells, positive for stem cell- or precursor markers are typical features observed in abnormal cellular components of GGs. However, this hypothesis needs to be verified by future experiments that may include immunohistochemical stainings with specific antibodies against immature neurons.

Furthermore, impaired neuronal migration or altered final positioning is in accordance with the previously hypothesized role of SLK in regulating cytoskeleton dynamics via the downstream protein Rac1.

shRNA mediated *in utero* depletion of Rac1 delays the onset or reduces the speed of cortical neuron migration rather than inhibiting it entirely [297]. Accordingly, loss of SLK was shown to affect migration of fibroblasts due to impairments in cytoskeleton dynamics, further emphasizing that similar mechanisms may be operative in neurons as well. Evidence for the importance of Ste20-related kinases for normal neuronal migration by regulation of cytoskeleton dynamics was recently provided [298]: shRNA mediated focal knockdown of *Mst3b* by *in utero* electroporation results in impaired neuronal migration together with reduced neurite length due to loss of RhoA phosphorylation. RhoA is a protein, which is critically involved in cytoskeletal reorganization and is also a known substrate of SLK [257, 298].

Our experiments confirmed F-actin colocalization with SLK in neurites and the growth cone, which strengthens our hypothesis that SLKs interaction with components of the cytoskeleton is involved in regulating neuronal development. However, loss of SLK did not result in growth cone collapse or reduction of its size, features often associated with impaired cytoskeleton dynamics [299]. The results of this experiment suggest an actin- or tubulin-independent regulatory mechanism of SLK to influence neurite growth. However, due to limitations in the optical resolution of our confocal microscope, we can not rule out that more subtle changes in growth cone morphology may have been missed in the current study. These alterations in growth cone morphology may include actin-fiber orientation as well as number and orientation of filopodia, comprising the growing elements of the growth cone. Since we are only able to analyze snapshots of PFA-fixed, static cellular compartments, dynamic changes or abnormalities occurring during active growth periods were not detectable. Therefore, this experiment does not exclude the possibility that SLK regulates neurite growth by cytoskeleton remodeling also in neurons.

In summary, our data confirm that SLK loss may indeed by a unifying feature of dysplastic neurons comprising distinct glioneuronal lesions. They demonstrate that SLK is needed for normal cortex development, since loss of SLK, as present in dysplastic neurons in GG and FCDIIb, impairs neurite morphology and final positioning of cortical neurons within the six-layered cortex. This aberrant neuronal morphology and cortical positioning may affect local circuitry and thereby result in altered neuronal excitability. As these are features often observed in GGs or FCDIIb lesions, our results suggest that SLK loss leads to the emergence of dysplastic, hyperexcitable neurons, thereby, contributing to the pathogenesis of these lesions.

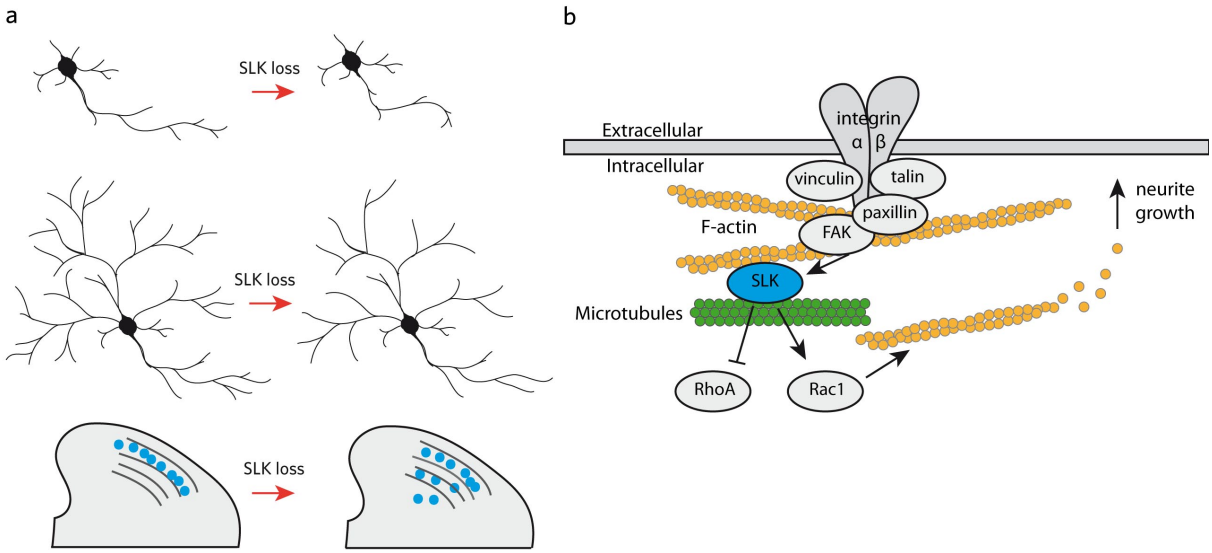

Figure 7.3: **SLK is needed for normal neuron and cortex development**. (a) Summary of the main findings. Upon SLK loss neurons exhibit a dysplastic phenotype. Their axon length is reduced, dendritic tree complexity is reduced and a subset of neurons are ectopically located within deeper layers of the cortex. (b) Possible mechanism of SLK action during neurite growth (Figure modified from [254]). SLK acts downstream of the integrin/FAK pathway to regulate the activity of Rac1 and RhoA. SLK-dependent Rac1 activation during phases of neuronal growth leads to actin disassembly and promotes neurite growth.

7.4 Focal loss of SLK leads to a hyperexcitable neuronal phenotype

Distal dendrites of excitatory neurons harbor large numbers of excitatory synapses, whereas inhibitory synapses are concentrated more proximally [300]. This suggests a preferential loss of excitatory synapses in our *SLK* knockdown model. Surprisingly, we observed the exact opposite. We found a progressive inhibitory synaptopathy in *SLK* knockdown neurons. Inhibitory postsynapses of young mice initially developed normally, but when these mice were older than 15 days, their inhibitory synapse density was significantly reduced. This observation indicates that SLK is required for the stabilization of already formed synapses. Defective dendritic branching in corresponding neurons preceded this phenotype and therefore, can not be a consequence of the latter. Conversely, aberrant arborization affected a dendritic compartment, which does not directly involve inhibitory synapses, whereas the gross morphology of neuronal somata and proximal dendritic processes appeared unaltered. This lack of normal projections and GABAergic synapses translated into reduced miniature IPSC frequency, implying impaired neuronal inhibition. Considering that excitatory synapse density and mEPSCs were unaffected by SLK loss, a hyperexcitable neuronal phenotype should be the net result (Fig. 7.4a). These data indicate that SLK is required specifically in inhibitory synapses, a hypothesis corroborated by the preferential localization of SLK at inhibitory postsynaptic sites.

A molecular hub consisting of $GABA_A$Rs, the cell adhesion molecule neuroligin-2 (NL2), the scaffolding proteins collybistin (Cb) and gephyrin is essential for the formation, plasticity and stability of the inhibitory postsynaptic site [228, 301]. Phosphorylation mediates proper functionality and the correct interaction of these four proteins. This is mandatory for the stability of the postsynaptic scaffold and thus, for functionality of the entire synapse that would be otherwise retracted [221, 228, 242, 246]. Thereby, phosphorylation of gephyrin, collybistin, NL2 or associated proteins constitutes a possible mechanism

by which SLK may act to stabilize the postsynapse (Fig. 7.4b). Given that NL2 and especially gephyrin are highly phosphorylated proteins, we can only speculate about the relevant interactions with the kinase SLK that elicit the impaired stability of inhibitory synaptic structures.

The cytoplasmatic protein Cb is required for the postsynaptic clustering of gephyrin and $GABA_A$Rs in the mammalian forebrain [233]. Accordingly, Cb knockout in adult or embryonic mice leads to a region-specific loss of gephyrin and gephyrin-dependent $GABA_A$R clusters at inhibitory synapses. These mice display an increase in anxiety scores, impaired spatial learning, and generalized seizures [232, 233]. These results indicate that Cb is not only needed for the establishment of the synapse but also for its long-term stability [240]. It is possible, that absence of SLK or phosphorylation by SLK alters the interaction properties of Cb with its postsynaptic partners, which in turn could lead to loss of $GABA_A$ receptors and subsequent inactivation and retraction of the synapse. Since SLK harbors an SH3 binding domain, it is also possible that SLK interacts directly with collybistins SH3-domain and exerts its functions by direct interaction with the scaffold [302]. A kinase independent function has been described for SLK in C2C12 cells before [249].

Alternatively, SLK may be required for the phosphorylation of the adhesion molecule NL2. NL2 triggers the interaction of Cb with the submembranous protein scaffold and thus, synaptic $GABA_A$R accumulation [235]. Local, conditional NL2 knockout in the adult cortex selectively causes a gradual loss of inhibitory synapses with a chronic and delayed time course [303]. The destabilization of already formed inhibitory synapses results in pathological neuronal network function, as these mice exhibit abnormalities in fear memory, anxiety and social interaction behavior [303]. These experiments demonstrate that NL2 is needed for postsynaptic stability, a process that may require NL2 phosphorylation by SLK.

Gephyrin clusters and anchors $GABA_A$Rs by forming a hexagonal lattice that interacts with various proteins and the cytoskeleton [221, 227, 228]. Loss or altered stability of the gephyrin lattice reduces neurotransmitter receptor clusters, thereby impairing synaptic transmission [231, 233, 304]. Modification of gephyrin by phosphorylation induces conformational changes, altered clustering, cluster size, trafficking and interaction with binding proteins [221, 242, 245, 246]. They represent properties that may be regulated by direct phosphorylation of gephyrin by SLK.

In contrast to excitatory postsynapses that mainly contain actin microfilaments [223], gephyrin scaffolding of inhibitory postsynapses depends on the presence of both, the actin and the microtubule cytoskeleton [229, 230]. Their interaction is thought to be critical for postsynaptic localization of gephyrin. Therefore, SLK - as a kinase involved in actin- and microtubule filament cross-talk - may play a selective role in stabilizing exclusively the inhibitory, gephyrin$^+$ postsynapse (Fig. 7.4b). However, in our experiments loss of SLK did not result in a reduction of gephyrin-cluster size, which one could expect when the postsynaptic scaffold is less stable and the involved proteins are lost. Technical limitations and inadequate optical resolution, however, prevent the detection of very subtle alterations in gephyrin size, discrete spatial dislocalization or its very local interaction with other molecules. Furthermore, it was recently shown that homeostatic programs in neurons are triggered when they lose their neurotransmitter receptors that cause an all-or-none reduction of functional synapses. This means that in order to maintain the synaptic strength, these consolidation programs favor less functional synapses with “normal” receptor abundance rather than maintaining all synapses with less receptors [305]. This observation is in good agreement with our finding of reduced synapse numbers with normal size after

SLK loss. Thus, the size of the inhibitory postsynapse may not be the adequate read-out to assess synaptic impairments mediated by SLK silencing. Therefore, we analyzed the relative fluorescence intensity of antibody labeled cytoskeletal elements (F-actin and acetylated tubulin) within the inhibitory synapse. We found that the fluorescence signal of both, F-actin and acTubulin was significantly reduced upon *SLK* knockdown. These results suggest local rearrangement or dissolution of actin filaments and microtubules within the inhibitory synapse or its scaffolding proteins, caused by *SLK* knockdown. This alteration of the cytoskeleton may impair scaffold stability and consequently lead to a retraction of dysfunctional synapses.

Our results further underline that SLK may indeed regulate the stability of the inhibitory synapse by local regulation of the cytoskeleton stability. This could occur via the Rac1/PAK pathway that was very recently demonstrated to be essential for GABAergic postsynaptic stability [306]. In this pathway, Rac1 activation facilitates PAK activation that in turn stabilizes F-actin. This process promotes inhibitory synapse stability. Disruption of their interaction was shown to impair $GABA_AR$ clustering and leads to a decreased strength of synaptic inhibition. Since SLK is known to activate Rac1 (see also chapter 7.3), this particular pathway represents a further possible mechanism of SLK action in regulating synapse integrity (Fig. 7.4b). But we can only speculate that the observed abnormal cytoskeleton rearrangements caused by SLK loss affect the stability of the synaptic gephyrin scaffold. Future experiments need to further explore the possibility of SLKs direct interaction with or phosphorylation of gephyrin or other components of the inhibitory synapse. Especially, the effect of SLK on cytoskeleton dynamics and regulating molecules needs to be addressed, since SLK was proposed to be a downstream mediator of the integrin β pathway and an upstream activator of Rac1 [254], two major regulators of synapse stability [209, 306]. These experiments would provide more insight on how exactly SLK facilitates synaptic stability.

Even though the distal parts of the dendritic arbor were affected by *SLK* knockdown and we observed a reduced number of inhibitory synapses, the density of excitatory synapses and the frequency of mEPSCs remained on control levels over all examined time points. This can be explained by the preferential localization of SLK at gephyrin$^+$ synapses rather then PSD95$^+$ synapses. Consequently, loss of SLK can not alter excitatory synapse formation or stability. A synapse specific function, that is exclusively operative in excitatory synapses, has already been described for the Mst3b Ste20 kinase [298]. In cortical neurons Mst3b was shown to impair specifically excitatory synaptic transmission [298], stressing the emerging functional relevance of Ste20 kinases for synapses and thus, for normal network function.

A combination of reduced inhibition - caused by a loss of inhibitory synapses - together with an aberrant dendritic morphology upon SLK loss will most likely profoundly influence signal integration, hence, network function is impaired. This hypothesis is supported by the increased propensity for PTZ induced seizures in our focal *SLK* knockdown model.

In conclusion, our results demonstrate that loss of SLK, as present in FCDIIb and GG specimens, is a possible shared pathomechanism in focal developmental brain lesions that explains emergence of dysplastic neurons and their striking hyperexcitability. Even though many genes are differentially expressed in those disorders, focal knockdown of only SLK resulted in a phenotype with key features of epileptogenic lesions [24, 307]: aberrant dendritic arborization, impaired neuronal migration, inhibitory synaptopathy and hyperexcitability. Even if SLK loss may not be the only factor mediating

hyperexcitability in dysplastic lesions, this kinase represents a novel, promising substrate for therapies aiming at seizure prevention or suppression.

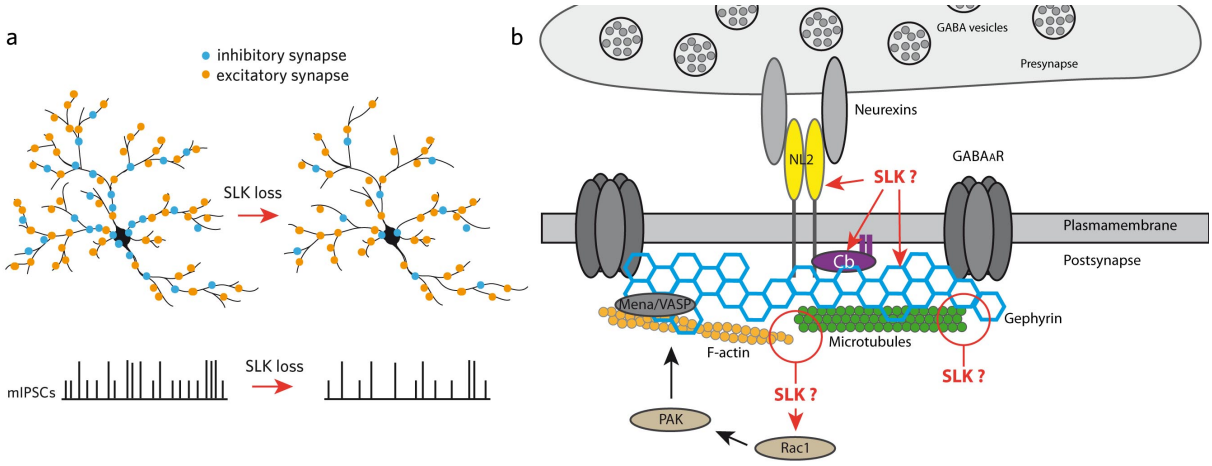

Figure 7.4: **SLK is needed for the stability of inhibitory postsynapses.** (a) Summary of the main findings. Upon SLK loss inhibitory postsynapse density is reduced, while the density of excitatory synapses is unchanged in juvenile mice. This defect is reflected in a reduced mIPSC frequency. (b) Possible mechanism of SLK action within established synapses (Figure modified from [221]). SLK either regulates the function of the core components of the inhibitory synapse NL2, Cb or gephyrin, or influences actin-microtubule cross-talk or microtubule-gephyrin interaction. As in growing neurites, SLK may regulate Rac1 activity that is needed for F-actin stability in synapses.

7.5 Loss of LDB1 and LDB2 leads to aberrant neuronal morphology

Given that SLK loss may be a common pathological event in dysplastic neurons, we next turned to the question whether also loss of the SLK interacting multi-adapter LDB - as present in GGs - plays a role in the emergence of dysplastic neurons. LDB proteins represent a family of nuclear transcriptional co-activators. Their interaction with LIM domain transcription factors during early embryogenesis is critical for cell-fate determination, development and cytoskeletal organization [277, 278, 308]. In cultured fibroblasts, *C.elegans* or *D.melanogaster* LDB1 proteins, or their ortholog (Chip), are required for axon guidance and neurite growth [203, 263, 279, 309, 310], suggesting a critical role for this protein also in the development of mammalian neurons. A significant reduction of *LDB2* transcripts was previously reported [47] and in this study, we also confirmed reduced LDB1 protein expression in dysplastic neurons of gangliogliomas, i.e. one of the most frequent epileptogenic tumor entity with chronic focal epilepsies. To assess, whether this reduction in LDB1 and LDB2 expression contributes to the emergence of aberrantly shaped dysplastic neurons and, hence, hyperexcitability, we analyzed the consequence of LDB1/2 loss in developing neurons.

We observed that loss of the respective proteins led to reduced axon length and a less complex dendritic tree, that can be interpreted as defects in axon and dendrite growth (Fig. 7.5a, b). With respect to neurite development *in vitro,* knockdown of *LDB1* or *LDB2* demonstrated functional redundancy, since loss of each resulted in similar impairments. These impairments were rescued by expression of both LDB family members. Both LDBs were reported to have overlapping, but also clearly distinct functions [205, 310], which becomes most evident in *LDB* knockout mice: While *LDB1* knockout mice are embryonic lethal [277], *LDB2* knockout mice appear healthy and fertile [311].

The impaired neurite morphology upon LDB loss, a morphological key feature of dysplastic neurons in gangliogliomas and other epileptogenic malformations, together with the substantial loss of LDB in gangliogliomas suggest a critical role of these proteins for normal neuronal development. Thus, a lack of LDB1 and/or LDB2 may indeed contribute to the emergence of dysplastic neurons. However, our results indicate that this may be the only or major contributing effect of LDB loss to lesion formation, since in our focal *LDB*1&2 knockdown mouse model cortical migration and excitability appeared mostly unaffected. This observations demonstrates that the abnormal neurite pattern, in a restricted number of neurons caused by focal LDB loss, in itself is not sufficient to render the brain significantly more susceptible to seizures at that age. It is possible that the intrinsic excitability of *LDB* knockdown neurons is reduced or that the neuronal network is locally compromised due to the abnormal dendritic arborization. Consequently, neuronal circuitry is altered, but is not pronounced enough to affect the excitability of an entire network. Hence, LDB loss may contribute to the formation of an epileptogenic lesion, but will most certainly not be the only factor.

Intriguingly, *in vitro LDB*1&2 knockdown had a very similar phenotype as *SLK* knockdown. We therefore analyzed whether these proteins regulate neurite development via a common pathway. With cross-rescue experiments, we observed that SLK indeed rescues *LDB1* or *LDB2* knockdown, but not *vice versa*. This indicates that SLK is a downstream effector of LDB1/2 in the context of neurite growth. Our experiments furthermore demonstrate that neurite development is only rescued as long as at least one LDB family member is still present. This observation corroborates SLK as a potential downstream effector that requires either LDB1 or LDB2 for functional axon or dendrite development. These proteins may either directly affect SLK function, expression or they participate in an alternate, so far unknown regulatory pathway. Axon growth and dendrite branching are neuronal process in which growth dynamics and underlying molecular mechanisms are distinct in several regards [312–314], thus our data indicates that the LDB/SLK pathway has a fundamental upstream role in both processes that, when disturbed may lead to the emergence of dysplastic neurons.

In the leading edge of migrating fibroblasts, the direct interaction of extra-nuclear LDB1, LDB2 and SLK homodimers has been demonstrated [263]. In these non-neuronal cells their interaction leads to reduced SLK kinase activity. This inhibitory effect was highly dependent on the concentration of the individual LDB proteins, indicating that SLK activity is dynamically modulated by the molecular composition of the LDB/SLK complex [263]. Our experiments in neurons, however, indicate a positive regulation of LDB proteins on SLK function. Loss of SLK or the expression of the kinase dead K63R-SLK variant (functionally equal to SLK inhibition or blocked phosphorylation activity), results in impaired neurite development. These results suggest a neuron specific functional interaction of these proteins. However, in contrast to fibroblasts, LDB1/LDB2/SLK interaction in neurons may be indirect, since we never observed LDB1 or LDB2 expression outside the nucleus (data not shown). In addition, SLK is preferentially expressed in the cytosolic compartment of neurons, thus, considerably restricting the possible direct, spatial interaction of LDB1/2 to a very small fraction of total neuronal SLK. Therefore, the more likely scenario is that the transcriptional co-activators LDB1 or LDB2 directly regulate SLK transcription (Fig. 7.5c). As discussed in detail in chapter 7.3, cytoskeleton remodeling represents a possible mechanism of action of LDB and the downstream protein SLK. However, as *SLK* knockdown also results in additional neuronal impairments, not reflected in LDB1&2-silenced cells, LDB proteins

are most certainly not the only molecules regulating SLK activity during distinct cellular processes.

In summary, this data demonstrate that loss of the multi adapter proteins LDB1 and LDB2 - as present in dysplastic cells of human GG patients - contributes to the morphological defects seen in dysplastic neuronal elements of respective developmental lesions. Our results furthermore demonstrate that LDB1/2 proteins regulate normal neurite growth, probably in concert with SLK. Even though *LDB1&2* knockdown does not result in a severe epileptogenic phenotype, the consequence of loss of functional LDB should not be underestimated in the emergence of dysplastic developmental lesions. LDBs underlying downstream pathway should be considered as a basis to derive more targeted anti-epileptic therapy.

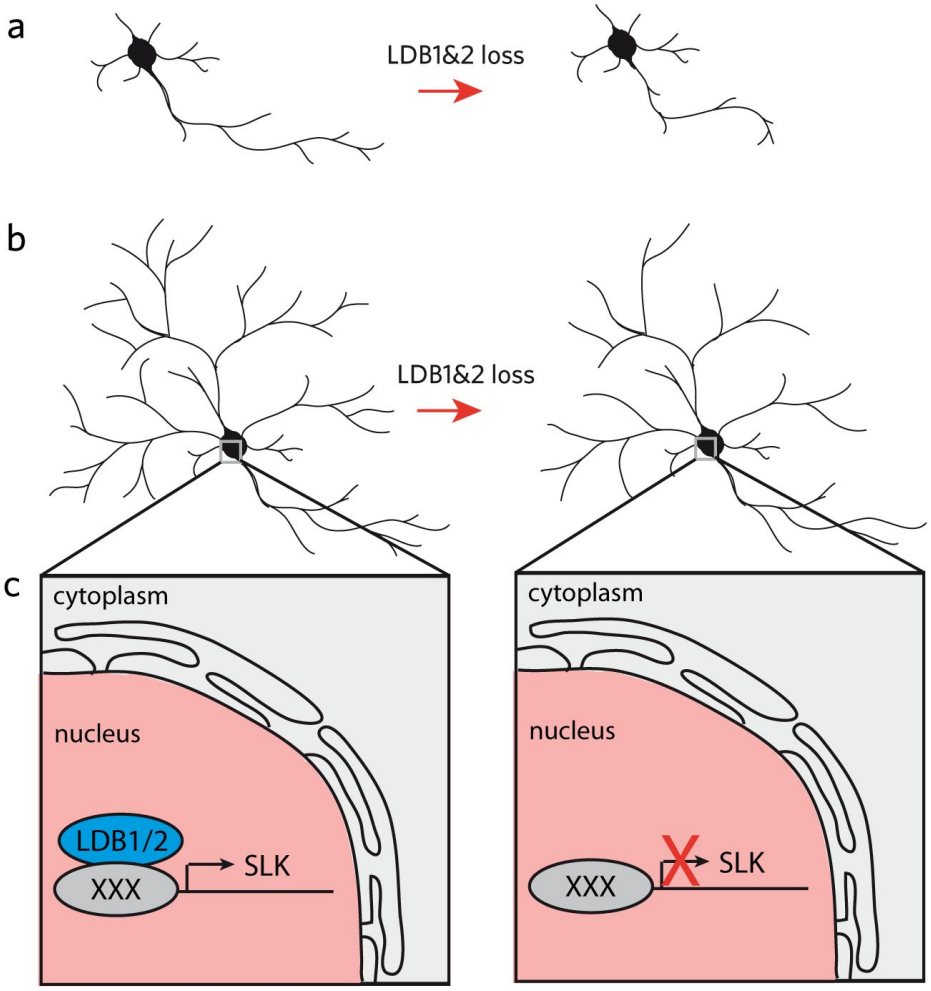

Figure 7.5: **LDB1 and LDB2 are needed for normal neurite growth**. (a) Upon LDB1 and LDB2 loss dysplastic neurons are formed, characterized by reduced axon length and (b) complexity of the dendritic arbor. (c) Possible mechanism of action of LDB1 and LDB2 to regulate neurite growth. In control cells, LDB proteins regulate *SLK* transcription that is needed for neurite development. Upon LDB1/2 loss *SLK* transcription is altered and thus, neurite development is impaired.

8 Abbreviations

4E-BP	Eukaryotic translation initiation factor 4E binding protein 1
AAV	Adeno-associated virus
acTubulin	Acetylated tubulin
Akt	Protein kinase B
AMPK	AMP-dependent protein kinase
AMOG	Adhesion molecule on glia
ANOVA	Analysis of variance
Arp2/3	Actin-related protein 2/3
ASD	Autism spectrum disease
ATH	AT1-46 homology domain
A.u.	Arbitrary units
BC	Balloon cell
BLBP	Brain lipid-binding protein
BME	Basal Medium Eagle
bp	Base pair
BRAF	proto-oncogene B-Raf or v-Raf murine sarcoma viral oncogene homolog B1
BSA	Bovine serum albumin
C2C12 cells	Murine myoblast cells
C57Bl/6	Black six mice
CamKII	Calcium-calmodulin kinase II
Cb	Collybistin
C. elegans	Caenorhabditis elegans
CD	Class of differentiation
Cdc42	Cell division control protein 42 homolog
CDK5	Cyclin-dependent kinase 5
cDNA	Complementary DNA
CMV	Cytomegalie virus
Cre	Cre recombinase
ct	Cycle threshold
Cux1	Cut-like homeobox 1
DCL	Doublecortin-like
DCX	Doublecortin
CNS	Central nervous system
DEPC	Diethylpyrocarbonate
DEPDC5	DEP domain containing protein 5

DIV	Day in vitro
DMEM	Dulbecco's Modified Eagle's Medium
DNA	Desoxyribonucleic acid
DNT	Dysembryoplastic neuroepithelial tumors
E	Embryonic day
ECM	Extracellular matrix
EDTA	Ethylenediaminetetraacetic acid
eIF4G	Eukaryotic initiation factor 4G
Emx1	Empty Spiracles Homeobox 1
F-actin	Filamentous actin
FAK	Focal adhesion kinase
FCS	Fetal calf serum
FCD	Focal cortical dysplasia
FingR	Fibronectin intrabodies generated with mRNA display
fl	flox
FoxP2	Forkhead box P2
Fw	Forward
GABA	Gamma-aminobutyric acid
GC	Giant cell
GDP	Guanosindiphosphat
GEF	Guanine exchange factors
GFAP	Glial Fibrillary Acidic Protein
GFP	Green fluorescent protein
GG	Ganglioglioma
GKC	Germinal center kinase
GLAST	Glutamate/aspartate transporter
GNT	Glioneuronal tumors
GTP	Guanosintriphosphat
h	Hour
HBSS	Hank's Buffered Salt Solution
HE	Hematoxylin & Eosin
HCl	Hydrochloride
HEK293T	Human embryonic kidney 293T
HEPES	4-(2-hydroxyethyl)-1-piperazineethanesulfonic acid
HRas	Transforming protein p21, Proto-oncogene
hrGFP	human renilla GFP
ICC	Immunocytochemistry
IHC	Immunohistochemistry
IMDM	Iscove's Modified Dulbecco's Medium
IPC	Intermediary progenitor cell
IR	Immunoreactivity
IUE	*In utero* electroporation

JNK1	Jun terminal kinase 1
kb	Kilobase pair
kg	Kilogram
KO	knockout
LB	Luria Broth
Ldb	Lim-domain binding
LEAT	Long-term epilepsy associated tumors
LKB	Liver kinase B1
LOH	Loss of heterozygosity
LRP12	Low-density lipoprotein receptor-related protein 12
M	Molar
MAP	Microtubule associated protein
MAPK	Mitogen activated protein kinase
MCD	Malformations of cortical development
MEM	Minimum essential medium
mEPSC	Miniature excitatory postsynaptic potential
mg	Milligramm
min	Minutes
mIPSC	Miniature inhibitory postsynaptic potential
ml	Milliliter
mM	Millimolar
mm	Millimeter
M-NAP	Microtubule and nuclear associated protein
mRNA	Messenger RNA
Mst3b	Mammalian Ste20-like kinase 3b
mTOR	mammalian target of rapamycin, mechanistic target of rapamycin
mut	Mutated
myr	Myristoylated
NEC	Neuroepithelial cells
NeuN	Neuronal Nuclei
NF	Neurofilament
NL2	Neuroligin 2
nM	Nanomolar
NMDAR	N-methyl-d-aspartate receptors
nm	Nanometer
n.s.	Not significant
OE	Overexpression
Otx1	Orthodenticle Homeobox 1
P	Postnatal day
PAK	p21-activated kinase
Pax6	Paired box gene 6
PBS	Phosphate buffered saline

PCR	Polymerase chain reaction
PDK1	3-phosphoinosi- tide-dependent protein kinase 1
pen/strep	Penicillin/streptomycin
PFA	Paraformaldehyde
Pfu	Pyrococcus furiosus
PI3K	Phosphatidylinositol 3-kinase
PI3P	Phosphatidylinositol 3-phosphate
pS6	Phosphorylated ribosomal protein S6
PSD	Postsynaptic density
PSD95	Postsynaptic density protein 95
PTEN	Phosphatase and tensin homolog
PTZ	Pentylenetetazole
Raf	Rapidly Accelerated Fibrosarcoma
Rac1	Ras-related C3 botulinum toxin substrate 1
Rev	Reverse
RFP, mRFP	Red fluorescent protein, monomeric
RGC	radial glia cell
Rheb	Ras-homolog expressed in brain
RhoA	Ras homolog gene family, member A
RNA	Ribonucleic acid
RNAi	RNA interference
RPM	Rounds per minute
S6	Ribosomal S6 protein
SDS	Sodium dodecyl sulfate
SDS PAGE	SDS polyacryalmid gel electrophoresis
sec	Second
SEM	Standard error of mean
SEGA	Subependymal giant cell astrocytomas
SH3	Src-homology 3
SLK	Ste20 like kinse
shRNA	Small hairpin RNA
SNP	Single nucleotide polymorphism
Ste20	Sterile 20
SVZ	Subventricular zone
TBC1D24	TBC1 domain family member 24
TBS	Tris-buffered saline
TBST	Tris-buffered saline and Ttriton X-100
TEMED	Tetramethylethylenediamine
Tbr1	T-Box/Brain-1
TSC	Tuberous sclerosis complex
VASP	Vasodilator-stimulated phosphoprotein
VZ	Ventricular zone

WHO	World health organization
WT	Wild type
µl	Microliter
µm	Micrometer

Bibliography

[1] Hui Yin, Y, Ahmad, N, & Makmor-Bakry, M. (2013) Pathogenesis of epilepsy: challenges in animal models. *Iranian journal of basic medical sciences* **16**, 1119–1132.

[2] Epilepsy Fact Sheet, W. (2016) <http://www.who.int/mediacentre/factsheets/fs999/en/>. p. cited on 01.03.2016.

[3] Berg, A. T, Berkovic, S. F, Brodie, M. J, Buchhalter, J, Cross, J. H, van Emde Boas, W, Engel, J, French, J, Glauser, T. A, Mathern, G. W, Moshé, S. L, Nordli, D, Plouin, P, & Scheffer, I. E. (2010) Revised terminology and concepts for organization of seizures and epilepsies: Report of the ILAE Commission on Classification and Terminology, 2005-2009. *Epilepsia* **51**, 676–685.

[4] Fisher, R. S, van Emde Boas, W, Blume, W, Elger, C, Genton, P, Lee, P, & Engel, J. J. (2005) Epileptic seizures and epilepsy: definitions proposed by the International League Against Epilepsy (ILAE) and the International Bureau for Epilepsy (IBE). *Epilepsia* **46**, 470–472.

[5] Lopes da Silva, F, Blanes, W, Kalitzin, S. N, Parra, J, Suffczynski, P, & Velis, D. N. (2003) Epilepsies as dynamical diseases of brain systems: basic models of the transition between normal and epileptic activity. *Epilepsia* **44 Suppl 12**, 72–83.

[6] Regesta, G & Tanganelli, P. (1999) Clinical aspects and biological bases of drug-resistant epilepsies. *Epilepsy Research* **34**, 109–122.

[7] Shorvon, S. D. (2011) The etiologic classification of epilepsy. *Epilepsia* **52**, 1052–1057.

[8] Blümcke, I, Vinters, H. V, Armstrong, D, Aronica, E, Thom, M, & Spreafico, R. (2009) Malformations of cortical development and epilepsies: neuropathological findings with emphasis on focal cortical dysplasia. *Epileptic Disorders* **11**, 181–193.

[9] Sisodiya, S. M, Fauser, S, Cross, J. H, & Thom, M. (2009) Focal cortical dysplasia type II: biological features and clinical perspectives. *Lancet Neurology* **8**, 830–843.

[10] Aronica, E, Becker, A. J, & Spreafico, R. (2012) Malformations of cortical development. *Brain pathology* **22**, 380–401.

[11] Thom, M, Blümcke, I, & Aronica, E. (2012) Long-term epilepsy-associated tumors. *Brain pathology* **22**, 350–379.

[12] Barkovich, A. J, Guerrini, R, Kuzniecky, R. I, Jackson, G. D, & Dobyns, W. B. (2012) A developmental and genetic classification for malformations of cortical development: update 2012. *Brain* **135**, 1348–1369.

[13] Blümcke, I & Wiestler, O. D. (2002) Gangliogliomas: an intriguing tumor entity associated with focal epilepsies. *Journal of Neuropathology & Experimental Neurology* **61**, 575–584.

[14] Fauser, S, Becker, A, Schulze-Bonhage, A, Hildebrandt, M, Tuxhorn, I, Pannek, H. W, Lahl, R,

Schramm, J, & Blümcke, I. (2004) CD34-immunoreactive balloon cells in cortical malformations. *Acta Neuropathologica* **108**, 272–278.

[15] Kam, R, Chen, J, Blümcke, I, Normann, S, Fassunke, J, Elger, C. E, Schramm, J, Wiestler, O. D, & Becker, A. J. (2004) The reelin pathway components disabled-1 and p35 in gangliogliomas–a mutation and expression analysis. *Neuropathol and applied neurobiology* **30**, 225–232.

[16] Boer, K, Troost, D, Timmermans, W, van Rijen, P. C, Spliet, W. G. M, & Aronica, E. (2010) Pi3K-mTOR signaling and AMOG expression in epilepsy-associated glioneuronal tumors. *Brain pathology* **20**, 234–244.

[17] Crino, P. B. (2011) mTOR: A pathogenic signaling pathway in developmental brain malformations. *Trends in Molecular Medicine* **17**, 734–742.

[18] Baybis, M, Yu, J, Lee, A, Golden, J. A, Weiner, H, McKhann, G, Aronica, E, & Crino, P. B. (2004) mTOR cascade activation distinguishes tubers from focal cortical dysplasia. *Annals of Neurology* **56**, 478–487.

[19] Miyata, H, Chiang, A. C. Y, & Vinters, H. V. (2004) Insulin signaling pathways in cortical dysplasia and TSC-tubers: tissue microarray analysis. *Annals of Neurology* **56**, 510–519.

[20] Lim, K. C & Crino, P. B. (2013) Focal malformations of cortical development: new vistas for molecular pathogenesis. *Neuroscience* **252**, 262–276.

[21] Lamparello, P, Baybis, M, Pollard, J, Hol, E. M, Eisenstat, D. D, Aronica, E, & Crino, P. B. (2007) Developmental lineage of cell types in cortical dysplasia with balloon cells. *Brain* **130**, 2267–2276.

[22] Hadjivassiliou, G, Martinian, L, Squier, W, Blümcke, I, Aronica, E, Sisodiya, S. M, & Thom, M. (2010) The application of cortical layer markers in the evaluation of cortical dysplasias in epilepsy. *Acta Neuropathologica* **120**, 517–528.

[23] Orlova, K. A, Tsai, V, Baybis, M, Heuer, G. G, Sisodiya, S, Thom, M, Strauss, K, Aronica, E, Storm, P. B, & Crino, P. B. (2010) Early progenitor cell marker expression distinguishes type II from type I focal cortical dysplasias. *Journal of Neuropathology & Experimental Neurology* **69**, 850–863.

[24] Aronica, E & Crino, P. B. (2014) Epilepsy related to developmental tumors and malformations of cortical development. *Neurotherapeutics* **11**, 251–268.

[25] Pitkänen, A, Lukasiuk, K, Dudek, F. E, & Staley, K. J. (2015) Epileptogenesis. *Cold Spring Harbor perspectives in medicine* **5**.

[26] Rakhade, S. N & Jensen, F. E. (2009) Epileptogenesis in the immature brain: emerging mechanisms. *Nature Reviews Neurology* **5**, 380–391.

[27] Pitkänen, A. (2010) Therapeutic approaches to epileptogenesis-hope on the horizon. *Epilepsia* **51 Suppl 3**, 2–17.

[28] Sierra, A, Gröhn, O, & Pitkanen, A. (2015) Imaging microstructural damage and plasticity in the hippocampus during epileptogenesis. *Neuroscience* **309**, 162–172.

[29] Pitkänen, A & Lukasiuk, K. (2011) Mechanisms of epileptogenesis and potential treatment targets. *The Lancet Neurology* **10**, 173–186.

[30] Aronica, E, Leenstra, S, van Veelen, C. W, van Rijen, P. C, Hulsebos, T. J, Tersmette, A. C, Yankaya, B, & Troost, D. (2001) Glioneuronal tumors and medically intractable epilepsy: a clinical study with long-term follow-up of seizure outcome after surgery. *Epilepsy Research* **43**, 179–191.

[31] Yang, I, Chang, E. F, Han, S. J, Barry, J. J, Fang, S, Tihan, T, Barbaro, N. M, & Parsa, A. T. (2011) Early surgical intervention in adult patients with ganglioglioma is associated with improved clinical seizure outcomes. *Journal of clinical neuroscience : official journal of the Neurosurgical Society of Australasia* **18**, 29–33.

[32] Englot, D. J, Berger, M. S, Barbaro, N. M, & Chang, E. F. (2012) Factors associated with seizure freedom in the surgical resection of glioneuronal tumors. *Epilepsia* **53**, 51–57.

[33] Giulioni, M, Gardella, E, Rubboli, G, Roncaroli, F, Zucchelli, M, Bernardi, B, Tassinari, C. A, & Calbucci, F. (2006) Lesionectomy in epileptogenic gangliogliomas: seizure outcome and surgical results. *Journal of clinical neuroscience : official journal of the Neurosurgical Society of Australasia* **13**, 529–535.

[34] van Breemen, M. S. M, Wilms, E. B, & Vecht, C. J. (2007) Epilepsy in patients with brain tumours: epidemiology, mechanisms, and management. *Lancet Neurology* **6**, 421–430.

[35] Rajneesh, K. F & Binder, D. K. (2009) Tumor-associated epilepsy. *Neurosurgical Focus* **27**, E4.

[36] Aronica, E, Redeker, S, Boer, K, Spliet, W. G. M, van Rijen, P. C, Gorter, J. A, & Troost, D. (2007) Inhibitory networks in epilepsy-associated gangliogliomas and in the perilesional epileptic cortex. *Epilepsy Research* **74**, 33–44.

[37] Luyken, C, Blümcke, I, Fimmers, R, Urbach, H, Elger, C. E, Wiestler, O. D, & Schramm, J. (2003) The spectrum of long-term epilepsy-associated tumors: long-term seizure and tumor outcome and neurosurgical aspects. *Epilepsia* **44**, 822–830.

[38] Giulioni, M, Marucci, G, Martinoni, M, Marliani, A. F, Toni, F, Bartiromo, F, Volpi, L, Riguzzi, P, Bisulli, F, Naldi, I, Michelucci, R, Baruzzi, A, Tinuper, P, & Rubboli, G. (2014) Epilepsy associated tumors: Review article. *World Journal of Clinical Cases* **2**, 623–641.

[39] Morris, H. H, Matkovic, Z, Estes, M. L, Prayson, R. A, Comair, Y. G, Turnbull, J, Najm, I, Kotagal, P, & Wyllie, E. (1998) Ganglioglioma and intractable epilepsy: clinical and neurophysiologic features and predictors of outcome after surgery. *Epilepsia* **39**, 307–313.

[40] Becker, A. J, Blümcke, I, Urbach, H, Hans, V, & Majores, M. (2006) Molecular neuropathology of epilepsy-associated glioneuronal malformations. *Journal of Neuropathology & Experimental Neurology* **65**, 99–108.

[41] Ortiz-González, X. R, Venneti, S, Biegel, J. A, Rorke-Adams, L. B, & Porter, B. E. (2011) Ganglioglioma arising from dysplastic cortex. *Epilepsia* **52**, e106–8.

[42] Blümcke, I, Giencke, K, Wardelmann, E, Beyenburg, S, Kral, T, Sarioglu, N, Pietsch, T, Wolf, H. K, Schramm, J, Elger, C. E, & Wiestler, O. D. (1999) The CD34 epitope is expressed in neoplastic and malformative lesions associated with chronic, focal epilepsies. *Acta Neuropathologica* **97**, 481–490.

[43] Zhu, J. J, Leon, S. P, Folkerth, R. D, Guo, S. Z, Wu, J. K, & Black, P. M. (1997) Evidence for clonal origin of neoplastic neuronal and glial cells in gangliogliomas. *American Journal of Pathology* **151**, 565–571.

[44] Gilmore, E. C & Herrup, K. (2000) Cortical development: receiving reelin. *Current Biology* **10**, R162–6.

[45] Homayouni, R & Curran, T. (2000) Cortical development: Cdk5 gets into sticky situations. *Current biology* **10**, R331–4.

[46] Senzaki, K, Ogawa, M, & Yagi, T. (1999) Proteins of the CNR family are multiple receptors for Reelin. *Cell*.

[47] Fassunke, J, Majores, M, Tresch, A, Niehusmann, P, Grote, A, Schoch, S, & Becker, A. J. (2008) Array analysis of epilepsy-associated gangliogliomas reveals expression patterns related to aberrant development of neuronal precursors. *Brain* **131**, 3034–3050.

[48] Aronica, E, Boer, K, Becker, A, Redeker, S, Spliet, W. G. M, van Rijen, P. C, Wittink, F, Breit, T, Wadman, W. J, Lopes da Silva, F. H, Troost, D, & Gorter, J. A. (2008) Gene expression profile analysis of epilepsy-associated gangliogliomas. *Neuroscience* **151**, 272–292.

[49] Aronica, E & Gorter, J. A. (2007) Gene expression profile in temporal lobe epilepsy. *The Neuroscientist* **13**, 100–108.

[50] Fernandez-Funez, P, Lu, C. H, Rincon-Limas, D. E, Garcia-Bellido, A, & Botas, J. (1998) The relative expression amounts of apterous and its co-factor dLdb/Chip are critical for dorso-ventral compartmentalization in the Drosophila wing. *The EMBO Journal* **17**, 6846–6853.

[51] Dougherty, M. J, Santi, M, Brose, M. S, Ma, C, Resnick, A. C, Sievert, A. J, Storm, P. B, & Biegel, J. A. (2010) Activating mutations in BRAF characterize a spectrum of pediatric low-grade gliomas. *Neuro Oncology* **12**, 621–630.

[52] Schindler, G, Capper, D, Meyer, J, Janzarik, W, Omran, H, Herold-Mende, C, Schmieder, K, Wesseling, P, Mawrin, C, Hasselblatt, M, Louis, D. N, Korshunov, A, Pfister, S, Hartmann, C, Paulus, W, Reifenberger, G, & von Deimling, A. (2011) Analysis of BRAF V600E mutation in 1,320 nervous system tumors reveals high mutation frequencies in pleomorphic xanthoastrocytoma, ganglioglioma and extra-cerebellar pilocytic astrocytoma. *Acta Neuropathologica* **121**, 397–405.

[53] Peyssonnaux, C & Eychène, A. (2001) The Raf/MEK/ERK pathway: new concepts of activation. *Biology of the cell* **93**, 53–62.

[54] Samadani, U, Judkins, A. R, Akpalu, A, Aronica, E, & Crino, P. B. (2007) Differential cellular gene expression in ganglioglioma. *Epilepsia* **48**, 646–653.

[55] Zheng, B, Jeong, J. H, Asara, J. M, Yuan, Y.-Y, Granter, S. R, Chin, L, & Cantley, L. C. (2009) Oncogenic B-RAF negatively regulates the tumor suppressor LKB1 to promote melanoma cell proliferation. *Molecular cell* **33**, 237–247.

[56] Prabowo, A. S, Iyer, A. M, Veersema, T. J, Anink, J. J, Schouten-van Meeteren, A. Y. N, Spliet, W. G. M, van Rijen, P. C, Ferrier, C. H, Capper, D, Thom, M, & Aronica, E. (2014) BRAF V600E mutation is associated with mTOR signaling activation in glioneuronal tumors. *Brain pathology* **24**, 52–66.

[57] Inoki, K, Li, Y, Xu, T, & Guan, K.-L. (2003) Rheb GTPase is a direct target of TSC2 GAP activity and regulates mTOR signaling. *Genes & Development* **17**, 1829–1834.

[58] Sarbassov, D. D, Ali, S. M, & Sabatini, D. M. (2005) Growing roles for the mTOR pathway. *Current Opinion in Cell Biology* **17**, 596–603.

[59] Orlova, K. A & Crino, P. B. (2010) The tuberous sclerosis complex. *Annals of the New York Academy of Sciences*.

[60] Costa-Mattioli, M & Monteggia, L. M. (2013) mTOR complexes in neurodevelopmental and neuropsychiatric disorders. *Nature Neuroscience* **16**, 1537–1543.

[61] Galanopoulou, A. S, Gorter, J. A, & Cepeda, C. (2012) Finding a better drug for epilepsy: the mTOR pathway as an antiepileptogenic target. *Epilepsia* **53**, 1119–1130.

[62] McDaniel, S. S & Wong, M. (2011) Therapeutic role of mammalian target of rapamycin (mTOR) inhibition in preventing epileptogenesis. *Neuroscience letters* **497**, 231–239.

[63] Vezzani, A. (2012) Before epilepsy unfolds: finding the epileptogenesis switch. *Nature Medicine* **18**, 1626–1627.

[64] Wong, M, Crino, P. B, Noebels, J. L, Avoli, M, Rogawski, M. A, Olsen, R. W, & Delgado-Escueta, A. V. (2012) mTOR and Epileptogenesis in Developmental Brain Malformations. *Jasper's Basic Mechanisms of the Epilepsies*.

[65] Chen, B, Tardell, C, Higgins, B, Packman, K, Boylan, J. F, & Niu, H. (2012) BRAFV600E negatively regulates the AKT pathway in melanoma cell lines. *PLoS ONE* **7**, e42598.

[66] Davies, H, Bignell, G. R, Cox, C, Stephens, P, Edkins, S, Clegg, S, Teague, J, Woffendin, H, Garnett, M. J, Bottomley, W, Davis, N, Dicks, E, Ewing, R, Floyd, Y, Gray, K, Hall, S, Hawes, R, Hughes, J, Kosmidou, V, Menzies, A, Mould, C, Parker, A, Stevens, C, Watt, S, Hooper, S, Wilson, R, Jayatilake, H, Gusterson, B. A, Cooper, C, Shipley, J, Hargrave, D, Pritchard-Jones, K, Maitland, N, Chenevix-Trench, G, Riggins, G. J, Bigner, D. D, Palmieri, G, Cossu, A, Flanagan, A, Nicholson, A, Ho, J. W. C, Leung, S. Y, Yuen, S. T, Weber, B. L, Seigler, H. F, Darrow, T. L, Paterson, H, Marais, R, Marshall, C. J, Wooster, R, Stratton, M. R, & Futreal, P. A. (2002) Mutations of the BRAF gene in human cancer. *Nature* **417**, 949–954.

[67] De Tommasi, A, Luzzi, S, D'Urso, P. I, De Tommasi, C, Resta, N, & Ciappetta, P. (2008) Molecular genetic analysis in a case of ganglioglioma: identification of a new mutation. *Neurosurgery* **63**, 976–980.

[68] Resta, N, Lauriola, L, Puca, A, Susca, F. C, Albanese, A, Sabatino, G, Di Giacomo, M. C, Gessi, M, & Guanti, G. (2006) Ganglioglioma arising in a Peutz-Jeghers patient: a case report with molecular implications. *Acta Neuropathologica* **112**, 106–111.

[69] Yang, H, Higgins, B, Kolinsky, K, Packman, K, Go, Z, Iyer, R, Kolis, S, Zhao, S, Lee, R, Grippo, J. F, Schostack, K, Simcox, M. E, Heimbrook, D, Bollag, G, & Su, F. (2010) RG7204 (PLX4032), a selective BRAFV600E inhibitor, displays potent antitumor activity in preclinical melanoma models. *Cancer Research* **70**, 5518–5527.

[70] Andermann, F. (2000) Cortical dysplasias and epilepsy: a review of the architectonic, clinical, and seizure patterns. *Advances in neurology* **84**, 479–496.

[71] Guerrini, R, Sicca, F, & Parmeggiani, L. (2003) Epilepsy and malformations of the cerebral cortex. *Epileptic Disorders* **5 Suppl 2**, S9–26.

[72] Abdel Razek, A. A. K, Kandell, A. Y, Elsorogy, L. G, Elmongy, A, & Basett, A. A. (2009) Disorders of cortical formation: MR imaging features. *American Journal of Neuroradiology* **30**, 4–11.

[73] Battal, B, Ince, S, Akgun, V, Kocaoglu, M, Ozcan, E, & Tasar, M. (2015) Malformations of cortical development: 3T magnetic resonance imaging features. *World Journal of Radiology* **7**, 329–335.

[74] Wong, M & Roper, S. N. (2015) Genetic animal models of malformations of cortical development and epilepsy. *Journal of Neuroscience Methods* **260**, 73–82.

[75] Blümcke, I, Thom, M, Aronica, E, Armstrong, D. D, Vinters, H. V, Palmini, A, Jacques, T. S, Avanzini, G, Barkovich, A. J, Battaglia, G, Becker, A, Cepeda, C, Cendes, F, Colombo, N, Crino, P, Cross, J. H, Delalande, O, Dubeau, F, Duncan, J, Guerrini, R, Kahane, P, Mathern, G, Najm, I, Özkara, Ç, Raybaud, C, Represa, A, Roper, S. N, Salamon, N, Schulze-Bonhage, A, Tassi, L, Vezzani, A, & Spreafico, R. (2011) The clinicopathologic spectrum of focal cortical dysplasias: a consensus classification proposed by an ad hoc Task Force of the ILAE Diagnostic Methods Commission. *Epilepsia* **52**, 158–174.

[76] Blümcke, I, Pieper, T, Pauli, E, Hildebrandt, M, Kudernatsch, M, Winkler, P, Karlmeier, A, & Holthausen, H. (2010) A distinct variant of focal cortical dysplasia type I characterised by magnetic resonance imaging and neuropathological examination in children with severe epilepsies. *Epileptic Disorders* **12**, 172–180.

[77] Crino, P. B, Nathanson, K. L, & Henske, E. P. (2006) The tuberous sclerosis complex. *New England Journal of Medicine* **355**, 1345–1356.

[78] Osborne, J. P, Fryer, A, & Webb, D. (1991) Epidemiology of tuberous sclerosis. *Annals of the New York Academy of Sciences* **615**, 125–127.

[79] Chu-Shore, C. J, Major, P, Camposano, S, Muzykewicz, D, & Thiele, E. A. (2010) The natural history of epilepsy in tuberous sclerosis complex. *Epilepsia* **51**, 1236–1241.

[80] Curatolo, P, Verdecchia, M, & Bombardieri, R. (2002) Tuberous sclerosis complex: a review of neurological aspects. *European Journal of Paediatric Neurology*.

[81] Prabowo, A. S, Anink, J. J, Lammens, M, Nellist, M, van den Ouweland, A. M. W, Adle-Biassette, H, Sarnat, H. B, Flores-Sarnat, L, Crino, P. B, & Aronica, E. (2013) Fetal brain lesions in tuberous sclerosis complex: TORC1 activation and inflammation. *Brain pathology* **23**, 45–59.

[82] Richardson, E. P. (1991) Pathology of tuberous sclerosis. Neuropathologic aspects. *Annals of the New York Academy of Sciences* **615**, 128–139.

[83] Crino, P. B. (2013) Evolving neurobiology of tuberous sclerosis complex. *Acta Neuropathologica* **125**, 317–332.

[84] Mizuguchi, M & Takashima, S. (2001) Neuropathology of tuberous sclerosis. *Brain and Development* **23**, 508–515.

[85] Grajkowska, W, Kotulska, K, Jurkiewicz, E, & Matyja, E. (2010) Brain lesions in tuberous sclerosis complex. Review. *Folia Neuropathol* **48**, 139–149.

[86] Kuzniecky, R. (2015) Epilepsy and malformations of cortical development: new developments. *Current Opinion in Neurology* **28**, 151–157.

[87] Crino, P. B. (2015) Focal Cortical Dysplasia. *Seminars in Neurology* **35**, 201–208.

[88] Schick, V, Majores, M, Engels, G, Spitoni, S, Koch, A, Elger, C. E, Simon, M, Knobbe, C, Blümcke, I, & Becker, A. J. (2006) Activation of Akt independent of PTEN and CTMP tumor-suppressor gene mutations in epilepsy-associated Taylor-type focal cortical dysplasias. *Acta Neuropathologica* **112**, 715–725.

[89] Schick, V, Majores, M, Engels, G, Hartmann, W, Elger, C. E, Schramm, J, Schoch, S, & Becker, A. J. (2007) Differential Pi3K-pathway activation in cortical tubers and focal cortical dysplasias with balloon cells. *Brain pathology* **17**, 165–173.

[90] Jansen, L. A, Mirzaa, G. M, Ishak, G. E, O'Roak, B. J, Hiatt, J. B, Roden, W. H, Gunter, S. A, Christian, S. L, Collins, S, Adams, C, Rivière, J.-B, St-Onge, J, Ojemann, J. G, Shendure, J, Hevner, R. F, & Dobyns, W. B. (2015) PI3K/AKT pathway mutations cause a spectrum of brain malformations from megalencephaly to focal cortical dysplasia. *Brain* **138**, 1613–1628.

[91] D'Gama, A. M, Geng, Y, Couto, J. A, Martin, B, Boyle, E. A, LaCoursiere, C. M, Hossain, A, Hatem, N. E, Barry, B. J, Kwiatkowski, D. J, Vinters, H. V, Barkovich, A. J, Shendure, J, Mathern, G. W, Walsh, C. A, & Poduri, A. (2015) Mammalian target of rapamycin pathway mutations cause hemimegalencephaly and focal cortical dysplasia. *Annals of Neurology* **77**, 720–725.

[92] Majores, M, Blümcke, I, Urbach, H, Meroni, A, Hans, V, Holthausen, H, Elger, C. E, Schramm, J, Galli, C, Spreafico, R, Wiestler, O. D, & Becker, A. J. (2005) Distinct allelic variants of TSC1 and TSC2 in epilepsy-associated cortical malformations without balloon cells. *Journal of Neuropathology & Experimental Neurology* **64**, 629–637.

[93] Lugnier, C, Majores, M, Fassunke, J, Pernhorst, K, Niehusmann, P, Simon, M, Nellist, M, Schoch, S, & Becker, A. (2009) Hamartin variants that are frequent in focal dysplasias and cortical tubers have reduced tuberin binding and aberrant subcellular distribution in vitro. *Journal of Neuropathology & Experimental Neurology* **68**, 1136–1146.

[94] Becker, A. J, Urbach, H, Scheffler, B, Baden, T, Normann, S, Lahl, R, Pannek, H. W, Tuxhorn, I, Elger, C. E, Schramm, J, Wiestler, O. D, & Blümcke, I. (2002) Focal cortical dysplasia of Taylor's balloon cell type: mutational analysis of the TSC1 gene indicates a pathogenic relationship to tuberous sclerosis. *Annals of Neurology* **52**, 29–37.

[95] Van Slegtenhorst, M, de Hoogt, R, Hermans, C, Nellist, M, Janssen, B, Verhoef, S, Lindhout, D, van den Ouweland, A, Halley, D, Young, J, Burley, M, Jeremiah, S, Woodward, K, Nahmias, J, Fox, M, Ekong, R, Osborne, J, Wolfe, J, Povey, S, Snell, R. G, Cheadle, J. P, Jones, A. C, Tachataki, M, Ravine, D, Sampson, J. R, Reeve, M. P, Richardson, P, Wilmer, F, Munro, C, Hawkins, T. L, Sepp, T, Ali, J. B, Ward, S, Green, A. J, Yates, J. R, Kwiatkowska, J, Henske, E. P, Short, M. P, Haines, J. H, Jozwiak, S, & Kwiatkowski, D. J. (1997) Identification of the tuberous sclerosis gene TSC1 on chromosome 9q34. *Science* **277**, 805–808.

[96] Carbonara, C, Longa, L, Grosso, E, Borrone, C, Garrè, M. G, Brisigotti, M, & Migone, N. (1994) 9q34 loss of heterozygosity in a tuberous sclerosis astrocytoma suggests a growth suppressor-like activity also for the TSC1 gene. *Human Molecular Genetics* **3**, 1829–1832.

[97] Sampson, J. R & Harris, P. C. (1994) The molecular genetics of tuberous sclerosis. *Human Molecular Genetics* **3 Spec No**, 1477–1480.

[98] Tyburczy, M. E, Dies, K. A, Glass, J, Camposano, S, Chekaluk, Y, Thorner, A. R, Lin, L, Krueger, D, Franz, D. N, Thiele, E. A, Sahin, M, & Kwiatkowski, D. J. (2015) Mosaic and intronic mutations in TSC1/TSC2 explain the majority of TSC patients with no mutation identified by conventional testing. *PLoS genetics* **11**, e1005637.

[99] Jones, A. C, Shyamsundar, M. M, Thomas, M. W, Maynard, J, Idziaszczyk, S, Tomkins, S, Sampson,

J. R, & Cheadle, J. P. (1999) Comprehensive mutation analysis of TSC1 and TSC2-and phenotypic correlations in 150 families with tuberous sclerosis. *American journal of human genetics* **64**, 1305–1315.

[100] Niida, Y, Lawrence-Smith, N, Banwell, A, Hammer, E, Lewis, J, Beauchamp, R. L, Sims, K, Ramesh, V, & Ozelius, L. (1999) Analysis of both TSC1 and TSC2 for germline mutations in 126 unrelated patients with tuberous sclerosis. *Human mutation* **14**, 412–422.

[101] Van Slegtenhorst, M, Verhoef, S, Tempelaars, A, Bakker, L, Wang, Q, Wessels, M, Bakker, R, Nellist, M, Lindhout, D, Halley, D, & van den Ouweland, A. (1999) Mutational spectrum of the TSC1 gene in a cohort of 225 tuberous sclerosis complex patients: no evidence for genotype-phenotype correlation. *Journal of Medical Genetics* **36**, 285–289.

[102] Napolioni, V, Moavero, R, & Curatolo, P. (2009) Recent advances in neurobiology of Tuberous Sclerosis Complex. *Brain and Development* **31**, 104–113.

[103] Dabora, S. L, Jozwiak, S, Franz, D. N, Roberts, P. S, Nieto, A, Chung, J, Choy, Y. S, Reeve, M. P, Thiele, E, Egelhoff, J. C, Kasprzyk-Obara, J, Domanska-Pakiela, D, & Kwiatkowski, D. J. (2001) Mutational analysis in a cohort of 224 tuberous sclerosis patients indicates increased severity of TSC2, compared with TSC1, disease in multiple organs. *American journal of human genetics* **68**, 64–80.

[104] Hung, C.-C, Su, Y.-N, Chien, S.-C, Liou, H.-H, Chen, C.-C, Chen, P.-C, Hsieh, C.-J, Chen, C.-P, Lee, W.-T, Lin, W.-L, & Lee, C.-N. (2006) Molecular and clinical analyses of 84 patients with tuberous sclerosis complex. *BMC Medical Genetics* **7**, 72.

[105] Sancak, O, Nellist, M, Goedbloed, M, Elfferich, P, Wouters, C, Maat-Kievit, A, Zonnenberg, B, Verhoef, S, Halley, D, & van den Ouweland, A. (2005) Mutational analysis of the TSC1 and TSC2 genes in a diagnostic setting: genotype–phenotype correlations and comparison of diagnostic DNA techniques in Tuberous Sclerosis Complex. *European Journal of Human Genetics* **13**, 731–741.

[106] Curatolo, P, Moavero, R, Roberto, D, & Graziola, F. (2015) Genotype/Phenotype Correlations in Tuberous Sclerosis Complex. *Seminars in pediatric neurology* **22**, 259–273.

[107] Green, A. J, Johnson, P. H, & Yates, J. R. (1994) The tuberous sclerosis gene on chromosome 9q34 acts as a growth suppressor. *Human Molecular Genetics* **3**, 1833–1834.

[108] Henske, E. P, Scheithauer, B. W, Short, M. P, Wollmann, R, Nahmias, J, Hornigold, N, Van Slegtenhorst, M, Welsh, C. T, & Kwiatkowski, D. J. (1996) Allelic loss is frequent in tuberous sclerosis kidney lesions but rare in brain lesions. *American journal of human genetics* **59**, 400.

[109] Chan, J. A, Zhang, H, Roberts, P. S, Jozwiak, S, Wieslawa, G, Lewin-Kowalik, J, Kotulska, K, & Kwiatkowski, D. J. (2004) Pathogenesis of tuberous sclerosis subependymal giant cell astrocytomas: biallelic inactivation of TSC1 or TSC2 leads to mTOR activation. *Journal of Neuropathology & Experimental Neurology* **63**, 1236–1242.

[110] Crino, P. B, Aronica, E, Baltuch, G, & Nathanson, K. L. (2010) Biallelic TSC gene inactivation in tuberous sclerosis complex. *Neurology* **74**, 1716–1723.

[111] Henske, E. P, Wessner, L. L, Golden, J, Scheithauer, B. W, Vortmeyer, A. O, Zhuang, Z, Klein-Szanto, A. J, Kwiatkowski, D. J, & Yeung, R. S. (1997) Loss of tuberin in both subependymal

giant cell astrocytomas and angiomyolipomas supports a two-hit model for the pathogenesis of tuberous sclerosis tumors. *American Journal of Pathology* **151**, 1639–1647.

[112] Feliciano, D. M, Su, T, Lopez, J, Platel, J.-C, & Bordey, A. (2011) Single-cell Tsc1 knockout during corticogenesis generates tuber-like lesions and reduces seizure threshold in mice. *Journal of Clinical Investigation* **121**, 1596–1607.

[113] Piedimonte, L. R, Wailes, I. K, & Weiner, H. L. (2006) Tuberous sclerosis complex: molecular pathogenesis and animal models. *Neurosurgical Focus* **20**, E4.

[114] Scheidenhelm, D. K & Gutmann, D. H. (2004) Mouse models of tuberous sclerosis complex. *Journal of child neurology* **19**, 726–733.

[115] Uhlmann, E. J, Apicelli, A. J, Baldwin, R. L, Burke, S. P, Bajenaru, M. L, Onda, H, Kwiatkowski, D, & Gutmann, D. H. (2002) Heterozygosity for the tuberous sclerosis complex (TSC) gene products results in increased astrocyte numbers and decreased p27-Kip1 expression in TSC2+/- cells. *Oncogene* **21**, 4050–4059.

[116] Qin, W, Chan, J. A, Vinters, H. V, Mathern, G. W, Franz, D. N, Taillon, B. E, Bouffard, P, & Kwiatkowski, D. J. (2010) Analysis of TSC cortical tubers by deep sequencing of TSC1, TSC2 and KRAS demonstrates that small second-hit mutations in these genes are rare events. *Brain pathology* **20**, 1096–1105.

[117] Tavazoie, S. F, Alvarez, V. A, Ridenour, D. A, Kwiatkowski, D. J, & Sabatini, B. L. (2005) Regulation of neuronal morphology and function by the tumor suppressors Tsc1 and Tsc2. *Nature Neuroscience* **8**, 1727–1734.

[118] Wong, M. (2009) Animal models of focal cortical dysplasia and tuberous sclerosis complex: recent progress toward clinical applications. *Epilepsia* **50 Suppl 9**, 34–44.

[119] Zhou, J, Blundell, J, Ogawa, S, Kwon, C.-H, Zhang, W, Sinton, C, Powell, C. M, & Parada, L. F. (2009) Pharmacological inhibition of mTORC1 suppresses anatomical, cellular, and behavioral abnormalities in neural-specific Pten knock-out mice. *Journal of Neuroscience* **29**, 1773–1783.

[120] Grote, A, Robens, B. K, Blümcke, I, Becker, A. J, Schoch, S, & Gembe, E. (2016) LRP12 silencing during brain development results in cortical dyslamination and seizure sensitization. *Neurobiology of Disease* **86**, 170–176.

[121] Marin-Valencia, I, Guerrini, R, & Gleeson, J. G. (2014) Pathogenetic mechanisms of focal cortical dysplasia. *Epilepsia* **55**, 970–978.

[122] Kellinghaus, C, Kunieda, T, Ying, Z, Pan, A, Lüders, H. O, & Najm, I. M. (2004) Severity of histopathologic abnormalities and in vivo epileptogenicity in the in utero radiation model of rats is dose dependent. *Epilepsia* **45**, 583–591.

[123] Takase, K.-i, Shigeto, H, Suzuki, S. O, Kikuchi, H, Ohyagi, Y, & Kira, J.-i. (2008) Prenatal freeze lesioning produces epileptogenic focal cortical dysplasia. *Epilepsia* **49**, 997–1010.

[124] Sancini, G, Franceschetti, S, Battaglia, G, Colacitti, C, Di Luca, M, Spreafico, R, & Avanzini, G. (1998) Dysplastic neocortex and subcortical heterotopias in methylazoxymethanol-treated rats: an intracellular study of identified pyramidal neurones. *Neuroscience letters* **246**, 181–185.

[125] Colacitti, C, Sancini, G, DeBiasi, S, Franceschetti, S, Caputi, A, Frassoni, C, Cattabeni, F, Avanzini, G, Spreafico, R, Di Luca, M, & Battaglia, G. (1999) Prenatal methylazoxymethanol treatment in

rats produces brain abnormalities with morphological similarities to human developmental brain dysgeneses. *Journal of Neuropathology & Experimental Neurology* **58**, 92–106.

[126] Moroni, R. F, Inverardi, F, Regondi, M. C, Pennacchio, P, Spreafico, R, & Frassoni, C. (2013) Genesis of heterotopia in BCNU model of cortical dysplasia, detected by means of in utero electroporation. *Developmental Neuroscience* **35**, 516–526.

[127] Moroni, R. F, Inverardi, F, Regondi, M. C, Watakabe, A, Yamamori, T, Spreafico, R, & Frassoni, C. (2009) Expression of layer-specific markers in the adult neocortex of BCNU-Treated rat, a model of cortical dysplasia. *Neuroscience* **159**, 682–691.

[128] Kwon, C.-H, Zhu, X, Zhang, J, & Baker, S. J. (2003) mTor is required for hypertrophy of Pten-deficient neuronal soma in vivo. *Proceedings of the National Academy of Sciences of the United States of America* **100**, 12923–12928.

[129] Ljungberg, M. C, Sunnen, C. N, Lugo, J. N, Anderson, A. E, & D'Arcangelo, G. (2009) Rapamycin suppresses seizures and neuronal hypertrophy in a mouse model of cortical dysplasia. *Disease Models & Mechanisms* **2**, 389–398.

[130] Yeung, R. S, Katsetos, C. D, & Klein-Szanto, A. (1997) Subependymal astrocytic hamartomas in the Eker rat model of tuberous sclerosis. *American Journal of Pathology* **151**, 1477–1486.

[131] Mizuguchi, M, Takashima, S, Yamanouchi, H, Nakazato, Y, Mitani, H, & Hino, O. (2000) Novel cerebral lesions in the Eker rat model of tuberous sclerosis: cortical tuber and anaplastic ganglioglioma. *Journal of Neuropathology & Experimental Neurology* **59**, 188–196.

[132] Uhlmann, E. J, Wong, M, Baldwin, R. L, Bajenaru, M. L, Onda, H, Kwiatkowski, D. J, Yamada, K, & Gutmann, D. H. (2002) Astrocyte-specific TSC1 conditional knockout mice exhibit abnormal neuronal organization and seizures. *Annals of Neurology* **52**, 285–296.

[133] Wong, M, Ess, K. C, Uhlmann, E. J, Jansen, L. A, Li, W, Crino, P. B, Mennerick, S, Yamada, K. A, & Gutmann, D. H. (2003) Impaired glial glutamate transport in a mouse tuberous sclerosis epilepsy model. *Annals of Neurology* **54**, 251–256.

[134] Jansen, L. A, Uhlmann, E. J, Crino, P. B, Gutmann, D. H, & Wong, M. (2005) Epileptogenesis and reduced inward rectifier potassium current in tuberous sclerosis complex-1-deficient astrocytes. *Epilepsia* **46**, 1871–1880.

[135] Zeng, L.-H, Ouyang, Y, Gazit, V, Cirrito, J. R, Jansen, L. A, Ess, K. C, Yamada, K. A, Wozniak, D. F, Holtzman, D. M, Gutmann, D. H, & Wong, M. (2007) Abnormal glutamate homeostasis and impaired synaptic plasticity and learning in a mouse model of tuberous sclerosis complex. *Neurobiology of Disease* **28**, 184–196.

[136] Zeng, L.-H, Rensing, N. R, Zhang, B, Gutmann, D. H, Gambello, M. J, & Wong, M. (2011) Tsc2 gene inactivation causes a more severe epilepsy phenotype than Tsc1 inactivation in a mouse model of tuberous sclerosis complex. *Human Molecular Genetics* **20**, 445–454.

[137] Magri, L, Cominelli, M, Cambiaghi, M, Cursi, M, Leocani, L, Minicucci, F, Poliani, P. L, & Galli, R. (2013) Timing of mTOR activation affects tuberous sclerosis complex neuropathology in mouse models. *Disease Models & Mechanisms* **6**, 1185–1197.

[138] Way, S. W, McKenna, J, Mietzsch, U, Reith, R. M, Wu, H. C.-J, & Gambello, M. J. (2009) Loss

of Tsc2 in radial glia models the brain pathology of tuberous sclerosis complex in the mouse. *Human Molecular Genetics* **18**, 1252–1265.

[139] Way, S. W, Rozas, N. S, Wu, H. C, McKenna, J, Reith, R. M, Hashmi, S. S, Dash, P. K, & Gambello, M. J. (2012) The differential effects of prenatal and/or postnatal rapamycin on neurodevelopmental defects and cognition in a neuroglial mouse model of tuberous sclerosis complex. *Human Molecular Genetics* **21**, 3226–3236.

[140] Meikle, L, Talos, D. M, Onda, H, Pollizzi, K, Rotenberg, A, Sahin, M, Jensen, F. E, & Kwiatkowski, D. J. (2007) A mouse model of tuberous sclerosis: neuronal loss of Tsc1 causes dysplastic and ectopic neurons, reduced myelination, seizure activity, and limited survival. *Journal of Neuroscience* **27**, 5546–5558.

[141] Meikle, L, Pollizzi, K, Egnor, A, Kramvis, I, Lane, H, Sahin, M, & Kwiatkowski, D. J. (2008) Response of a neuronal model of tuberous sclerosis to mammalian target of rapamycin (mTOR) inhibitors: effects on mTORC1 and Akt signaling lead to improved survival and function. *Journal of Neuroscience* **28**, 5422–5432.

[142] Ehninger, D, Han, S, Shilyansky, C, Zhou, Y, Li, W, Kwiatkowski, D. J, Ramesh, V, & Silva, A. J. (2008) Reversal of learning deficits in a Tsc2+/- mouse model of tuberous sclerosis. *Nature Medicine* **14**, 843–848.

[143] Fu, C, Cawthon, B, Clinkscales, W, Bruce, A, Winzenburger, P, & Ess, K. C. (2012) GABAergic interneuron development and function is modulated by the Tsc1 gene. *Cerebral Cortex* **22**, 2111–2119.

[144] Magri, L, Cambiaghi, M, Cominelli, M, Alfaro-Cervello, C, Cursi, M, Pala, M, Bulfone, A, Garcìa-Verdugo, J. M, Leocani, L, Minicucci, F, Poliani, P. L, & Galli, R. (2011) Sustained activation of mTOR pathway in embryonic neural stem cells leads to development of tuberous sclerosis complex-associated lesions. *Cell stem cell* **9**, 447–462.

[145] Carson, R. P, Van Nielen, D. L, Winzenburger, P. A, & Ess, K. C. (2012) Neuronal and glia abnormalities in Tsc1-deficient forebrain and partial rescue by rapamycin. *Neurobiology of Disease* **45**, 369–380.

[146] Goto, J, Talos, D. M, Klein, P, Qin, W, Chekaluk, Y. I, Anderl, S, Malinowska, I. A, Di Nardo, A, Bronson, R. T, Chan, J. A, Vinters, H. V, Kernie, S. G, Jensen, F. E, Sahin, M, & Kwiatkowski, D. J. (2011) Regulable neural progenitor-specific Tsc1 loss yields giant cells with organellar dysfunction in a model of tuberous sclerosis complex. *Proceedings of the National Academy of Sciences* **108**, E1070–9.

[147] Abs, E, Goorden, S. M. I, Schreiber, J, Overwater, I. E, Hoogeveen-Westerveld, M, Bruinsma, C. F, Aganović, E, Borgesius, N. Z, Nellist, M, & Elgersma, Y. (2013) TORC1-dependent epilepsy caused by acute biallelic Tsc1 deletion in adult mice. *Annals of Neurology* **74**, 569–579.

[148] Campbell, S. L, Buckingham, S. C, & Sontheimer, H. (2012) Human glioma cells induce hyperexcitability in cortical networks. *Epilepsia* **53**, 1360–1370.

[149] Kirschstein, T & Köhling, R. (2015) Animal models of tumour-associated epilepsy. *Journal of Neuroscience Methods* pp. 117–119.

[150] Jiang, X & Nardelli, J. (2016) Cellular and molecular introduction to brain development. *Neurobiology of Disease* **92**, 3–17.

[151] Paridaen, J. T. M. L, Wilsch-Bräuninger, M, & Huttner, W. B. (2013) Asymmetric inheritance of centrosome-associated primary cilium membrane directs ciliogenesis after cell division. *Cell* **155**, 333–344.

[152] Lui, J. H, Hansen, D. V, & Kriegstein, A. R. (2011) Development and evolution of the human neocortex. *Cell* **146**, 18–36.

[153] Borrell, V & Götz, M. (2014) Role of radial glial cells in cerebral cortex folding. *Current Opinion in Neurobiology* **27**, 39–46.

[154] Götz, M & Huttner, W. B. (2005) The cell biology of neurogenesis. *Nature Reviews Molecular Cell Biology* **6**, 777–788.

[155] Kriegstein, A, Noctor, S, & Martínez-Cerdeño, V. (2006) Patterns of neural stem and progenitor cell division may underlie evolutionary cortical expansion. *Nature Reviews Neuroscience* **7**, 883–890.

[156] Asami, M, Pilz, G. A, Ninkovic, J, Godinho, L, Schroeder, T, Huttner, W. B, & Götz, M. (2011) The role of Pax6 in regulating the orientation and mode of cell division of progenitors in the mouse cerebral cortex. *Development* **138**, 5067–5078.

[157] Meyer, G, Soria, J. M, Martínez-Galán, J. R, Martín-Clemente, B, & Fairén, A. (1998) Different origins and developmental histories of transient neurons in the marginal zone of the fetal and neonatal rat cortex. *The Journal of Comparative Neurology* **397**, 493–518.

[158] Noctor, S. C, Martínez-Cerdeño, V, Ivic, L, & Kriegstein, A. R. (2004) Cortical neurons arise in symmetric and asymmetric division zones and migrate through specific phases. *Nature Neuroscience* **7**, 136–144.

[159] Molyneaux, B. J, Arlotta, P, Menezes, J. R. L, & Macklis, J. D. (2007) Neuronal subtype specification in the cerebral cortex. *Nature Reviews Neuroscience* **8**, 427–437.

[160] Rakic, P. (2009) Evolution of the neocortex: a perspective from developmental biology. *Nature Reviews Neuroscience* **10**, 724–735.

[161] Luskin, M. B & Shatz, C. J. (1985) Studies of the earliest generated cells of the cat's visual cortex: cogeneration of subplate and marginal zones. *Journal of Neuroscience* **5**, 1062–1075.

[162] Supèr, H, Soriano, E, & Uylings, H. B. (1998) The functions of the preplate in development and evolution of the neocortex and hippocampus. *Brain research reviews* **27**, 40–64.

[163] Gressens, P. (2006) Pathogenesis of migration disorders. *Current Opinion in Neurology* **19**, 135–140.

[164] Marín, O, Valdeolmillos, M, & Moya, F. (2006) Neurons in motion: same principles for different shapes? *Trends in neurosciences* **29**, 655–661.

[165] LoTurco, J. J & Bai, J. (2006) The multipolar stage and disruptions in neuronal migration. *Trends in neurosciences* **29**, 407–413.

[166] Bahi-Buisson, N, Poirier, K, Fourniol, F, Saillour, Y, Valence, S, Lebrun, N, Hully, M, Bianco, C. F, Boddaert, N, Elie, C, Lascelles, K, Souville, I, LIS-Tubulinopathies Consortium, Beldjord, C, &

Chelly, J. (2014) The wide spectrum of tubulinopathies: what are the key features for the diagnosis? *Brain* **137**, 1676–1700.

[167] Fallet-Bianco, C, Laquerrière, A, Poirier, K, Razavi, F, Guimiot, F, Dias, P, Loeuillet, L, Lascelles, K, Beldjord, C, Carion, N, Toussaint, A, Revencu, N, Addor, M.-C, Lhermitte, B, Gonzales, M, Martinovich, J, Bessieres, B, Marcy-Bonnière, M, Jossic, F, Marcorelles, P, Loget, P, Chelly, J, & Bahi-Buisson, N. (2014) Mutations in tubulin genes are frequent causes of various foetal malformations of cortical development including microlissencephaly. *Acta neuropathologica communications* **2**, 69.

[168] Parnavelas, J. G. (2000) The origin and migration of cortical neurones: new vistas. *Trends in neurosciences* **23**, 126–131.

[169] Tanaka, D. H & Nakajima, K. (2012) Migratory pathways of GABAergic interneurons when they enter the neocortex. *European Journal of Neuroscience* **35**, 1655–1660.

[170] Welagen, J & Anderson, S. (2011) Origins of neocortical interneurons in mice. *Developmental Neurobiology* **71**, 10–17.

[171] Greig, L. C, Woodworth, M. B, Galazo, M. J, Padmanabhan, H, & Macklis, J. D. (2013) Molecular logic of neocortical projection neuron specification, development and diversity. *Nature Reviews Neuroscience* **14**, 755–769.

[172] Beierlein, M, Fall, C. P, Rinzel, J, & Yuste, R. (2002) Thalamocortical bursts trigger recurrent activity in neocortical networks: layer 4 as a frequency-dependent gate. *Journal of Neuroscience* **22**, 9885–9894.

[173] Feldmeyer, D. (2012) Excitatory neuronal connectivity in the barrel cortex. *Frontiers in neuroanatomy* **6**, 24.

[174] Lozovaya, N, Gataullina, S, Tsintsadze, T, Tsintsadze, V, Pallesi-Pocachard, E, Minlebaev, M, Goriounova, N. A, Buhler, E, Watrin, F, Shityakov, S, Becker, A. J, Bordey, A, Milh, M, Scavarda, D, Bulteau, C, Dorfmuller, G, Delalande, O, Represa, A, Cardoso, C, Dulac, O, Ben-Ari, Y, & Burnashev, N. (2014) Selective suppression of excessive GluN2C expression rescues early epilepsy in a tuberous sclerosis murine model. *Nature Communications* **5**, 4563.

[175] Giedd, J. (1999) Brain development, IX: human brain growth. *The American Journal of Psychiatry* **156**, 4.

[176] Wiggin, G. R, Fawcett, J. P, & Pawson, T. (2005) Polarity proteins in axon specification and synaptogenesis. *Developmental Cell* **8**, 803–816.

[177] Forscher, P & Smith, S. J. (1988) Actions of cytochalasins on the organization of actin filaments and microtubules in a neuronal growth cone. *Journal of Cell Biology* **107**, 1505–1516.

[178] Bradke, F & Dotti, C. G. (1999) The role of local actin instability in axon formation. *Science* **283**, 1931–1934.

[179] Witte, H & Bradke, F. (2008) The role of the cytoskeleton during neuronal polarization. *Current Opinion in Neurobiology* **18**, 479–487.

[180] Wickstead, B & Gull, K. (2011) The evolution of the cytoskeleton. *Journal of Cell Biology* **194**, 513–525.

[181] Ng, J, Nardine, T, Harms, M, Tzu, J, Goldstein, A, Sun, Y, Dietzl, G, Dickson, B. J, & Luo, L. (2002) Rac GTPases control axon growth, guidance and branching. *Nature* **416**, 442–447.

[182] Luo, L. (2000) Rho GTPases in neuronal morphogenesis. *Nature Reviews Neuroscience* **1**, 173–180.

[183] Chhabra, E. S & Higgs, H. N. (2007) The many faces of actin: matching assembly factors with cellular structures. *Nature Cell Biology* **9**, 1110–1121.

[184] Arber, S, Barbayannis, F. A, Hanser, H, Schneider, C, Stanyon, C. A, Bernard, O, & Caroni, P. (1998) Regulation of actin dynamics through phosphorylation of cofilin by LIM-kinase. *Nature* **393**, 805–809.

[185] Edwards, D. C, Sanders, L. C, Bokoch, G. M, & Gill, G. N. (1999) Activation of LIM-kinase by Pak1 couples Rac/Cdc42 GTPase signalling to actin cytoskeletal dynamics. *Nature Cell Biology* **1**, 253–259.

[186] Jaffe, A. B & Hall, A. (2005) Rho GTPases: biochemistry and biology. *Annual Review of Cell and Developmental Biology* **21**, 247–269.

[187] Hur, E.-M & Zhou, F.-Q. (2010) GSK3 signalling in neural development. *Nature Reviews Neuroscience* **11**, 539–551.

[188] Sapir, T, Sapoznik, S, Levy, T, Finkelshtein, D, Shmueli, A, Timm, T, Mandelkow, E.-M, & Reiner, O. (2008) Accurate balance of the polarity kinase MARK2/Par-1 is required for proper cortical neuronal migration. *Journal of Neuroscience* **28**, 5710–5720.

[189] Sapir, T, Shmueli, A, Levy, T, Timm, T, Elbaum, M, Mandelkow, E.-M, & Reiner, O. (2008) Antagonistic effects of doublecortin and MARK2/Par-1 in the developing cerebral cortex. *Journal of Neuroscience* **28**, 13008–13013.

[190] Kishi, M, Pan, Y. A, Crump, J. G, & Sanes, J. R. (2005) Mammalian SAD kinases are required for neuronal polarization. *Science* **307**, 929–932.

[191] Shelly, M, Cancedda, L, Heilshorn, S, Sumbre, G, & Poo, M.-m. (2007) LKB1/STRAD promotes axon initiation during neuronal polarization. *Cell* **129**, 565–577.

[192] Rehberg, K, Kliche, S, Madencioglu, D. A, Thiere, M, Müller, B, Meineke, B. M, Freund, C, Budinger, E, & Stork, O. (2014) The serine/threonine kinase Ndr2 controls integrin trafficking and integrin-dependent neurite growth. *Journal of Neuroscience* **34**, 5342–5354.

[193] Baas, P. W, Deitch, J. S, Black, M. M, & Banker, G. A. (1988) Polarity orientation of microtubules in hippocampal neurons: uniformity in the axon and nonuniformity in the dendrite. *Proceedings of the National Academy of Sciences of the United States of America* **85**, 8335–8339.

[194] Ferreira, A, Busciglio, J, & Cáceres, A. (1989) Microtubule formation and neurite growth in cerebellar macroneurons which develop in vitro: evidence for the involvement of the microtubule-associated proteins, MAP-1a, HMW-MAP2 and Tau. *Developmental brain research* **49**, 215–228.

[195] Zheng, Y, Wildonger, J, Ye, B, Zhang, Y, Kita, A, Younger, S. H, Zimmerman, S, Jan, L. Y, & Jan, Y.-N. (2008) Dynein is required for polarized dendritic transport and uniform microtubule orientation in axons. *Nature Cell Biology* **10**, 1172–1180.

[196] Sakakibara, A, Ando, R, Sapir, T, & Tanaka, T. (2013) Microtubule dynamics in neuronal morphogenesis. *Open Biology* **3**, 130061.

[197] Tessier-Lavigne, M & Goodman, C. S. (1996) The molecular biology of axon guidance. *Science* **274**, 1123–1133.

[198] Grueber, W. B, Jan, L. Y, & Jan, Y.-N. (2003) Different levels of the homeodomain protein cut regulate distinct dendrite branching patterns of Drosophila multidendritic neurons. *Cell* **112**, 805–818.

[199] Parrish, J. Z, Kim, M. D, Jan, L. Y, & Jan, Y.-N. (2006) Genome-wide analyses identify transcription factors required for proper morphogenesis of Drosophila sensory neuron dendrites. *Genes & Development* **20**, 820–835.

[200] Hand, R, Bortone, D, Mattar, P, Nguyen, L, Heng, J. I.-T, Guerrier, S, Boutt, E, Peters, E, Barnes, A. P, Parras, C, Schuurmans, C, Guillemot, F, & Polleux, F. (2005) Phosphorylation of Neurogenin2 specifies the migration properties and the dendritic morphology of pyramidal neurons in the neocortex. *Neuron* **48**, 45–62.

[201] Matthews, J. M, Bhati, M, Craig, V. J, Deane, J. E, Jeffries, C, Lee, C, Nancarrow, A. L, Ryan, D. P, & Sunde, M. (2008) Competition between LIM-binding domains. *Biochemical Society transactions* **36**, 1393–1397.

[202] Segawa, H, Miyashita, T, Hirate, Y, Higashijima, S, Chino, N, Uyemura, K, Kikuchi, Y, & Okamoto, H. (2001) Functional repression of Islet-2 by disruption of complex with Ldb impairs peripheral axonal outgrowth in embryonic zebrafish. *Neuron* **30**, 423–436.

[203] Zheng, Q, Schaefer, A. M, & Nonet, M. L. (2011) Regulation of C. elegans presynaptic differentiation and neurite branching via a novel signaling pathway initiated by SAM-10. *Development* **138**, 87–96.

[204] Zhong, Z, Ma, H, Taniguchi-Ishigaki, N, Nagarajan, L, Becker, C. G, Bach, I, & Becker, T. (2011) SSDP cofactors regulate neural patterning and differentiation of specific axonal projections. *Developmental Biology* **349**, 213–224.

[205] Leone, D. P, Panagiotakos, G, Heavner, W. E, Joshi, P, Zhao, Y, Westphal, H, & McConnell, S. K. (2016) Compensatory actions of Ldb adaptor proteins during corticospinal motor neuron differentiation. *Cerebral Cortex*.

[206] Asprer, J. S. T, Lee, B, Wu, C.-S, Vadakkan, T, Dickinson, M. E, Lu, H.-C, & Lee, S.-K. (2011) LMO4 functions as a co-activator of neurogenin 2 in the developing cortex. *Development* **138**, 2823–2832.

[207] Yogev, S & Shen, K. (2014) Cellular and molecular mechanisms of synaptic specificity. *Annual Review of Cell and Developmental Biology* **30**, 417–437.

[208] Hashimoto, K & Kano, M. (2013) Synapse elimination in the developing cerebellum. *Cellular and Molecular Life Sciences* **70**, 4667–4680.

[209] Kerrisk, M. E, Greer, C. A, & Koleske, A. J. (2013) Integrin $\alpha 3$ is required for late postnatal stability of dendrite arbors, dendritic spines and synapses, and mouse behavior. *Journal of Neuroscience* **33**, 6742–6752.

[210] Fiala, J. C, Feinberg, M, Popov, V, & Harris, K. M. (1998) Synaptogenesis via dendritic filopodia in developing hippocampal area CA1. *Journal of Neuroscience* **18**, 8900–8911.

[211] Ziv, N. E & Garner, C. C. (2004) Cellular and molecular mechanisms of presynaptic assembly. *Nature Reviews Neuroscience* **5**, 385–399.

[212] Lin, Y.-C & Koleske, A. J. (2010) Mechanisms of synapse and dendrite maintenance and their disruption in psychiatric and neurodegenerative disorders. *Annual Review of Neuroscience* **33**, 349–378.

[213] Fletcher, T. L, De Camilli, P, & Banker, G. (1994) Synaptogenesis in hippocampal cultures: evidence indicating that axons and dendrites become competent to form synapses at different stages of neuronal development. *Journal of Neuroscience* **14**, 6695–6706.

[214] Li, Z & Sheng, M. (2003) Some assembly required: the development of neuronal synapses. *Nature Reviews Molecular Cell Biology* **4**, 833–841.

[215] Arikkath, J & Reichardt, L. F. (2008) Cadherins and catenins at synapses: roles in synaptogenesis and synaptic plasticity. *Trends in neurosciences* **31**, 487–494.

[216] Yagi, T & Takeichi, M. (2000) Cadherin superfamily genes: functions, genomic organization, and neurologic diversity. *Genes & Development* **14**, 1169–1180.

[217] Aplin, A. E, Howe, A, Alahari, S. K, & Juliano, R. L. (1998) Signal transduction and signal modulation by cell adhesion receptors: the role of integrins, cadherins, immunoglobulin-cell adhesion molecules, and selectins. *Pharmacological reviews* **50**, 197–263.

[218] Krueger, D. D, Tuffy, L. P, Papadopoulos, T, & Brose, N. (2012) The role of neurexins and neuroligins in the formation, maturation, and function of vertebrate synapses. *Current Opinion in Neurobiology* **22**, 412–422.

[219] Yamauchi, T. (2002) Molecular constituents and phosphorylation-dependent regulation of the post-synaptic density. *Mass spectrometry reviews* **21**, 266–286.

[220] Okabe, S. (2007) Molecular anatomy of the postsynaptic density. *Molecular and cellular neurosciences* **34**, 503–518.

[221] Choii, G & Ko, J. (2015) Gephyrin: a central GABAergic synapse organizer. *Experimental and Molecular Medicine* **47**, e158.

[222] Allison, D. W, Chervin, A. S, Gelfand, V. I, & Craig, A. M. (2000) Postsynaptic scaffolds of excitatory and inhibitory synapses in hippocampal neurons: maintenance of core components independent of actin filaments and microtubules. *Journal of Neuroscience* **20**, 4545–4554.

[223] Ethell, I. M & Pasquale, E. B. (2005) Molecular mechanisms of dendritic spine development and remodeling. *Progress in Neurobiology* **75**, 161–205.

[224] Mei, L & Xiong, W.-C. (2008) Neuregulin 1 in neural development, synaptic plasticity and schizophrenia. *Nature Reviews Neuroscience* **9**, 437–452.

[225] Tyzio, R, Represa, A, Jorquera, I, Ben-Ari, Y, Gozlan, H, & Aniksztejn, L. (1999) The establishment of GABAergic and glutamatergic synapses on CA1 pyramidal neurons is sequential and correlates with the development of the apical dendrite. *Journal of Neuroscience* **19**, 10372–10382.

[226] Khazipov, R, Esclapez, M, Caillard, O, Bernard, C, Khalilov, I, Tyzio, R, Hirsch, J, Dzhala, V, Berger, B, & Ben-Ari, Y. (2001) Early development of neuronal activity in the primate hippocampus in utero. *Journal of Neuroscience* **21**, 9770–9781.

[227] Fritschy, J.-M, Harvey, R. J, & Schwarz, G. (2008) Gephyrin: where do we stand, where do we go? *Trends in neurosciences* **31**, 257–264.

[228] Tyagarajan, S. K & Fritschy, J.-M. (2014) Gephyrin: a master regulator of neuronal function? *Nature Reviews Neuroscience* **15**, 141–156.

[229] Kirsch, J & Betz, H. (1995) The postsynaptic localization of the glycine receptor-associated protein gephyrin is regulated by the cytoskeleton. *Journal of Neuroscience* **15**, 4148–4156.

[230] Bausen, M, Fuhrmann, J. C, Betz, H, & O'Sullivan, G. A. (2006) The state of the actin cytoskeleton determines its association with gephyrin: role of ena/VASP family members. *Molecular and cellular neurosciences* **31**, 376–386.

[231] Harvey, K, Duguid, I. C, Alldred, M. J, Beatty, S. E, Ward, H, Keep, N. H, Lingenfelter, S. E, Pearce, B. R, Lundgren, J, Owen, M. J, Smart, T. G, Luscher, B, Rees, M. I, & Harvey, R. J. (2004) The GDP-GTP exchange factor collybistin: an essential determinant of neuronal gephyrin clustering. *Journal of Neuroscience* **24**, 5816–5826.

[232] Papadopoulos, T, Eulenburg, V, Reddy-Alla, S, Mansuy, I. M, Li, Y, & Betz, H. (2008) Collybistin is required for both the formation and maintenance of GABAergic postsynapses in the hippocampus. *Molecular and cellular neurosciences* **39**, 161–169.

[233] Papadopoulos, T, Korte, M, Eulenburg, V, Kubota, H, Retiounskaia, M, Harvey, R. J, Harvey, K, O'Sullivan, G. A, Laube, B, Hülsmann, S, Geiger, J. R. P, & Betz, H. (2007) Impaired GABAergic transmission and altered hippocampal synaptic plasticity in collybistin-deficient mice. *The EMBO Journal* **26**, 3888–3899.

[234] Blundell, J, Tabuchi, K, Bolliger, M. F, Blaiss, C. A, Brose, N, Liu, X, Südhof, T. C, & Powell, C. M. (2009) Increased anxiety-like behavior in mice lacking the inhibitory synapse cell adhesion molecule neuroligin 2. *Genes, brain, and behavior* **8**, 114–126.

[235] Poulopoulos, A, Aramuni, G, Meyer, G, Soykan, T, Hoon, M, Papadopoulos, T, Zhang, M, Paarmann, I, Fuchs, C, Harvey, K, Jedlicka, P, Schwarzacher, S. W, Betz, H, Harvey, R. J, Brose, N, Zhang, W, & Varoqueaux, F. (2009) Neuroligin 2 drives postsynaptic assembly at perisomatic inhibitory synapses through gephyrin and collybistin. *Neuron* **63**, 628–642.

[236] Marco, E. J, Abidi, F. E, Bristow, J, & Dean, W. B. (2008) ARHGEF9 disruption in a female patient is associated with X linked mental retardation and sensory hyperarousal. *Journal of Medical Genetics*.

[237] Kalscheuer, V. M, Musante, L, Fang, C, Hoffmann, K, Fuchs, C, Carta, E, Deas, E, Venkateswarlu, K, Menzel, C, Ullmann, R, Tommerup, N, Dalprà, L, Tzschach, A, Selicorni, A, Luscher, B, Ropers, H.-H, Harvey, K, & Harvey, R. J. (2009) A balanced chromosomal translocation disrupting ARHGEF9 is associated with epilepsy, anxiety, aggression, and mental retardation. *Human mutation* **30**, 61–68.

[238] Dejanovic, B, Djémié, T, Grünewald, N, Suls, A, Kress, V, Hetsch, F, Craiu, D, Zemel, M, Gormley, P, Lal, D, EuroEPINOMICS Dravet working group, Myers, C. T, Mefford, H. C, Palotie, A, Helbig, I, Meier, J. C, De Jonghe, P, Weckhuysen, S, & Schwarz, G. (2015) Simultaneous impairment of neuronal and metabolic function of mutated gephyrin in a patient with epileptic encephalopathy. *EMBO Molecular Medicine* **7**, 1580–1594.

[239] Machado, C. O. F, Griesi-Oliveira, K, Rosenberg, C, Kok, F, Martins, S, Passos-Bueno, M. R, & Sertie, A. L. (2016) Collybistin binds and inhibits mTORC1 signaling: a potential novel mechanism contributing to intellectual disability and autism. *European Journal of Human Genetics* **24**, 59–65.

[240] Papadopoulos, T, Schemm, R, Grubmüller, H, & Brose, N. (2015) Lipid binding defects and perturbed synaptogenic activity of a Collybistin R290H mutant that causes epilepsy and intellectual disability. *Journal of Biological Chemistry* **290**, 8256–8270.

[241] Maćkowiak, M, Mordalska, P, & Wędzony, K. (2014) Neuroligins, synapse balance and neuropsychiatric disorders. *Pharmacological Reports* **66**, 830–835.

[242] Tyagarajan, S. K, Ghosh, H, Yévenes, G. E, Nikonenko, I, Ebeling, C, Schwerdel, C, Sidler, C, Zeilhofer, H. U, Gerrits, B, Muller, D, & Fritschy, J.-M. (2011) Regulation of GABAergic synapse formation and plasticity by GSK3beta-dependent phosphorylation of gephyrin. *Proceedings of the National Academy of Sciences* **108**, 379–384.

[243] Giesemann, T, Schwarz, G, Nawrotzki, R, Berhörster, K, Rothkegel, M, Schlüter, K, Schrader, N, Schindelin, H, Mendel, R. R, Kirsch, J, & Jockusch, B. M. (2003) Complex formation between the postsynaptic scaffolding protein gephyrin, profilin, and Mena: a possible link to the microfilament system. *Journal of Neuroscience* **23**, 8330–8339.

[244] Fuhrmann, J. C, Kins, S, Rostaing, P, El Far, O, Kirsch, J, Sheng, M, Triller, A, Betz, H, & Kneussel, M. (2002) Gephyrin interacts with Dynein light chains 1 and 2, components of motor protein complexes. *Journal of Neuroscience* **22**, 5393–5402.

[245] Zacchi, P, Antonelli, R, & Cherubini, E. (2014) Gephyrin phosphorylation in the functional organization and plasticity of GABAergic synapses. *Frontiers in cellular neuroscience* **8**, 103.

[246] Flores, C. E, Nikonenko, I, Mendez, P, Fritschy, J.-M, Tyagarajan, S. K, & Muller, D. (2015) Activity-dependent inhibitory synapse remodeling through gephyrin phosphorylation. *Proceedings of the National Academy of Sciences* **112**, E65–72.

[247] Dan, I, Watanabe, N. M, & Kusumi, A. (2001) The Ste20 group kinases as regulators of MAP kinase cascades. *Trends in Cell Biology* **11**, 220–230.

[248] Zhang, Y.-H, Hume, K, Cadonic, R, Thompson, C, Hakim, A, Staines, W, & Sabourin, L. A. (2002) Expression of the Ste20-like kinase SLK during embryonic development and in the murine adult central nervous system. *Developmental brain research* **139**, 205–215.

[249] Sabourin, L. A, Tamai, K, Seale, P, Wagner, J, & Rudnicki, M. A. (2000) Caspase 3 cleavage of the Ste20-related kinase SLK releases and activates an apoptosis-inducing kinase domain and an actin-disassembling region. *Molecular and Cellular Biology* **20**, 684–696.

[250] Sabourin, L. A & Rudnicki, M. A. (1999) Induction of apoptosis by SLK, a Ste20-related kinase. *Oncogene* **18**, 7566–7575.

[251] Hao, W, Takano, T, Guillemette, J, Papillon, J, Ren, G, & Cybulsky, A. V. (2006) Induction of apoptosis by the Ste20-like kinase SLK, a germinal center kinase that activates apoptosis signal-regulating kinase and p38. *The Journal of biological chemistry* **281**, 3075–3084.

[252] Burakov, A. V, Zhapparova, O. N, Kovalenko, O. V, Zinovkina, L. A, Potekhina, E. S, Shanina, N. A, Weiss, D. G, Kuznetsov, S. A, & Nadezhdina, E. S. (2008) Ste20-related protein kinase LOSK (SLK) controls microtubule radial array in interphase. *Molecular biology of the cell* **19**, 1952–1961.

[253] Wagner, S, Storbeck, C. J, Roovers, K, Chaar, Z. Y, Kolodziej, P, McKay, M, & Sabourin, L. A. (2008) FAK/src-family dependent activation of the Ste20-like kinase SLK is required for microtubule-dependent focal adhesion turnover and cell migration. *PLoS ONE* **3**, e1868.

[254] Wagner, S. M & Sabourin, L. A. (2009) A novel role for the Ste20 kinase SLK in adhesion signaling and cell migration. *Cell Adhesion & Migration* **3**, 182–184.

[255] Schaller, M. D. (2004) FAK and paxillin: regulators of N-cadherin adhesion and inhibitors of cell migration? *Journal of Cell Biology* **166**, 157–159.

[256] Wagner, S, Flood, T. A, O'Reilly, P, Hume, K, & Sabourin, L. A. (2002) Association of the Ste20-like kinase (SLK) with the microtubule. Role in Rac1-mediated regulation of actin dynamics during cell adhesion and spreading. *The Journal of biological chemistry* **277**, 37685–37692.

[257] Guilluy, C, Rolli-Derkinderen, M, Loufrani, L, Bourgé, A, Henrion, D, Sabourin, L, Loirand, G, & Pacaud, P. (2008) Ste20-related kinase SLK phosphorylates Ser188 of RhoA to induce vasodilation in response to angiotensin II Type 2 receptor activation. *Circulation research* **102**, 1265–1274.

[258] Zhapparova, O. N, Fokin, A. I, Vorobyeva, N. E, Bryantseva, S. A, & Nadezhdina, E. S. (2013) Ste20-like protein kinase SLK (LOSK) regulates microtubule organization by targeting dynactin to the centrosome. *Molecular biology of the cell* **24**, 3205–3214.

[259] Viswanatha, R, Ohouo, P. Y, Smolka, M. B, & Bretscher, A. (2012) Local phosphocycling mediated by LOK/SLK restricts ezrin function to the apical aspect of epithelial cells. *The Journal of Cell Biology* **199**, 969–984.

[260] Pytowski, B, Hicklin, D. J, Kornhaber, G, Dellaratta, D. V, & Witte, L. (1998) Identification and initial characterization of mSLK, a murine member of the STE20 family of kinases. *Archives of biochemistry and biophysics* **359**, 310–319.

[261] Quizi, J. L, Baron, K, Al-Zahrani, K. N, O'Reilly, P, Sriram, R. K, Conway, J, Laurin, A.-A, & Sabourin, L. A. (2013) SLK-mediated phosphorylation of paxillin is required for focal adhesion turnover and cell migration. *Oncogene* **32**, 4656–4663.

[262] O'Reilly, P. G, Wagner, S, Franks, D. J, Cailliau, K, Browaeys, E, Dissous, C, & Sabourin, L. A. (2005) The Ste20-like kinase SLK is required for cell cycle progression through G2. *The Journal of biological chemistry* **280**, 42383–42390.

[263] Storbeck, C. J, Wagner, S, O'Reilly, P, McKay, M, Parks, R. J, Westphal, H, & Sabourin, L. A. (2009) The Ldb1 and Ldb2 transcriptional cofactors interact with the Ste20-like kinase SLK and regulate cell migration. *Molecular biology of the cell* **20**, 4174–4182.

[264] Gross, G. G, Junge, J. A, Mora, R. J, Kwon, H.-B, Olson, C. A, Takahashi, T. T, Liman, E. R, Ellis-Davies, G. C. R, McGee, A. W, Sabatini, B. L, Roberts, R. W, & Arnold, D. B. (2013) Recombinant Probes for Visualizing Endogenous Synaptic Proteins in Living Neurons. *Neuron* **78**, 971–985.

[265] Kohrmann, M, Haubensak, W, Hemraj, I, Kaether, C, Lessmann, V. J, & Kiebler, M. A. (1999) Fast, convenient, and effective method to transiently transfect primary hippocampal neurons. *Journal of neuroscience research* **58**, 831–835.

[266] Louis, D. N, Ohgaki, H, Wiestler, O. D, Cavenee, W. K, Burger, P. C, Jouvet, A, Scheithauer, B. W, & Kleihues, P. (2007) The 2007 WHO classification of tumours of the central nervous system. *Acta Neuropathologica* **114**, 97–109.

[267] Sholl, D. A. (1953) Dendritic organization in the neurons of the visual and motor cortices of the cat. *Journal of anatomy* **87**, 387–406.

[268] Ristanović, D, Milošević, N. T, & Štulić, V. (2006) Application of modified Sholl analysis to neuronal dendritic arborization of the cat spinal cord. *Journal of Neuroscience Methods* **158**, 212–218.

[269] Robens, B. K, Grote, A, Pitsch, J, Schoch, S, Cardoso, C, & Becker, A. J. (2016) Minute amounts of hamartin wildtype rescue the emergence of tuber-like lesions in conditional Tsc1 ablated mice. *Neurobiology of Disease* **95**, 134–144.

[270] Racine, R. J. (1972) Modification of seizure activity by electrical stimulation. II. Motor seizure. *Electroencephalography and Clinical Neurophysiology* **32**, 281–294.

[271] Simeonova, I & Huillard, E. (2014) In vivo models of brain tumors: roles of genetically engineered mouse models in understanding tumor biology and use in preclinical studies. *Cellular and Molecular Life Sciences* **71**, 4007–4026.

[272] Rak, B, Szlufik, S, Grajkowska, W, Perek, D, Dembowska-Bagińska, B, Filipek, I, Daszkiewicz, P, Włodarski, P, & Jóźwiak, J. (2013) Upregulation of mitogen-activated protein kinase in ganglioglioma. *Folia Neuropathol* **51**, 283–289.

[273] Hengstschläger, M, Rodman, D. M, Miloloza, A, Hengstschläger-Ottnad, E, Rosner, M, & Kubista, M. (2001) Tuberous sclerosis gene products in proliferation control. *Mutation Research* **488**, 233–239.

[274] Feliciano, D. M, Lin, T. V, Hartman, N. W, Bartley, C. M, Kubera, C, Hsieh, L, Lafourcade, C, O'Keefe, R. A, & Bordey, A. (2013) A circuitry and biochemical basis for tuberous sclerosis symptoms: from epilepsy to neurocognitive deficits. *International Journal of Developmental Neuroscience* **31**, 667–678.

[275] Falace, A, Buhler, E, Fadda, M, Watrin, F, Lippiello, P, Pallesi-Pocachard, E, Baldelli, P, Benfenati, F, Zara, F, Represa, A, Fassio, A, & Cardoso, C. (2014) TBC1D24 regulates neuronal migration and maturation through modulation of the ARF6-dependent pathway. *Proceedings of the National Academy of Sciences* **111**, 2337–2342.

[276] Wong, M & Crino, P. B. (2012) Tuberous sclerosis and epilepsy: role of astrocytes. *Glia* **60**, 1244–1250.

[277] Mukhopadhyay, M, Teufel, A, Yamashita, T, Agulnick, A. D, Chen, L, Downs, K. M, Schindler, A, Grinberg, A, Huang, S.-P, Dorward, D, & Westphal, H. (2003) Functional ablation of the mouse Ldb1 gene results in severe patterning defects during gastrulation. *Development* **130**, 495–505.

[278] Kadrmas, J. L & Beckerle, M. C. (2004) The LIM domain: from the cytoskeleton to the nucleus. *Nature Reviews Molecular Cell Biology* **5**, 920–931.

[279] van Meyel, D. J, O'Keefe, D. D, Thor, S, Jurata, L. W, Gill, G. N, & Thomas, J. B. (2000) Chip is an essential cofactor for apterous in the regulation of axon guidance in Drosophila. *Development* **127**, 1823–1831.

[280] Chen, F, Becker, A. J, & LoTurco, J. J. (2014) Contribution of tumor heterogeneity in a new animal model of CNS tumors. *Molecular Cancer Research* **12**, 742–753.

[281] LoTurco, J, Manent, J.-B, & Sidiqi, F. (2009) New and improved tools for in utero electroporation studies of developing cerebral cortex. *Cerebral Cortex* **19 Suppl 1**, i120–5.

[282] Prabhakar, S, Goto, J, Zhang, X, Zuang, X, Sena-Esteves, M, Bronson, R, Brockmann, J, Gianni, D, Wojtkiewicz, G. R, Chen, J. W, Stemmer-Rachamimov, A, Kwiatkowski, D. J, & Breakefield, X. O. (2013) Stochastic model of Tsc1 lesions in mouse brain. *PLoS ONE* **8**, e64224.

[283] Major, P, Rakowski, S, Simon, M. V, Cheng, M. L, Eskandar, E, Baron, J, Leeman, B. A, Frosch, M. P, & Thiele, E. A. (2009) Are cortical tubers epileptogenic? Evidence from electrocorticography. *Epilepsia* **50**, 147–154.

[284] Carbonara, C, Longa, L, Grosso, E, Mazzucco, G, Borrone, C, Garrè, M. L, Brisigotti, M, Filippi, G, Scabar, A, Giannotti, A, Falzoni, P, Monga, G, Garini, G, Gabrielli, M, Riegler, P, Danesino, C, Ruggieri, M, Magro, G, & Migone, N. (1995) Apparent preferential loss of heterozygosity at TSC2 over TSC1 chromosomal region in tuberous sclerosis hamartomas. *Genes, Chromosomes and Cancer* **15**, 18–25.

[285] Lesma, E, Sirchia, S. M, Ancona, S, Carelli, S, Bosari, S, Ghelma, F, Montanari, E, Di Giulio, A. M, & Gorio, A. (2009) The methylation of the TSC2 promoter underlies the abnormal growth of TSC2 angiomyolipoma-derived smooth muscle cells. *The American journal of pathology* **174**, 2150–2159.

[286] Han, S, Santos, T. M, Puga, A, Roy, J, Thiele, E. A, McCollin, M, Stemmer-Rachamimov, A, & Ramesh, V. (2004) Phosphorylation of tuberin as a novel mechanism for somatic inactivation of the tuberous sclerosis complex proteins in brain lesions. *Cancer Research* **64**, 812–816.

[287] Franz, D. N, Belousova, E, Sparagana, S, Bebin, E. M, Frost, M, Kuperman, R, Witt, O, Kohrman, M. H, Flamini, J. R, Wu, J. Y, Curatolo, P, de Vries, P. J, Berkowitz, N, Anak, O, Niolat, J, & Jozwiak, S. (2014) Everolimus for subependymal giant cell astrocytoma in patients with tuberous sclerosis complex: 2-year open-label extension of the randomised EXIST-1 study. *The Lancet Oncology* **15**, 1513–1520.

[288] Manent, J.-B, Wang, Y, Chang, Y, Paramasivam, M, & LoTurco, J. J. (2009) Dcx reexpression reduces subcortical band heterotopia and seizure threshold in an animal model of neuronal migration disorder. *Nature Medicine* **15**, 84–90.

[289] Prabhakar, S, Zhang, X, Goto, J, Han, S, Lai, C, Bronson, R, Sena-Esteves, M, Ramesh, V, Stemmer-Rachamimov, A, Kwiatkowski, D. J, & Breakefield, X. O. (2015) Survival benefit and phenotypic improvement by hamartin gene therapy in a tuberous sclerosis mouse brain model. *Neurobiology of Disease* **82**, 22–31.

[290] Leemhuis, J, Boutillier, S, Barth, H, Feuerstein, T. J, Brock, C, Nürnberg, B, Aktories, K, & Meyer, D. K. (2004) Rho GTPases and phosphoinositide 3-kinase organize formation of branched dendrites. *The Journal of biological chemistry* **279**, 585–596.

[291] Newey, S. E, Velamoor, V, Govek, E.-E, & Van Aelst, L. (2005) Rho GTPases, dendritic structure, and mental retardation. *Journal of Neurobiology* **64**, 58–74.

[292] Reverte, C. G, Benware, A, Jones, C. W, & LaFlamme, S. E. (2006) Perturbing integrin function inhibits microtubule growth from centrosomes, spindle assembly, and cytokinesis. *Journal of Cell Biology* **174**, 491–497.

[293] Lo, S. H. (2006) Focal adhesions: what's new inside. *Developmental Biology* **294**, 280–291.

[294] Schneider, S, Weydig, C, & Wessler, S. (2007) Targeting focal adhesions:Helicobacter pylori-host communication in cell migration. *Cell Communication and Signaling* **6**, 2–2.

[295] Sahai, E & Marshall, C. J. (2003) Differing modes of tumour cell invasion have distinct requirements for Rho/ROCK signalling and extracellular proteolysis. *Nature Cell Biology* **5**, 711–719.

[296] Warren, M. S, Bradley, W. D, Gourley, S. L, Lin, Y.-C, Simpson, M. A, Reichardt, L. F, Greer, C. A, Taylor, J. R, & Koleske, A. J. (2012) Integrin β1 signals through Arg to regulate postnatal dendritic arborization, synapse density, and behavior. *Journal of Neuroscience* **32**, 2824–2834.

[297] Chen, L, Liao, G, Waclaw, R. R, Burns, K. A, Linquist, D, Campbell, K, Zheng, Y, & Kuan, C.-Y. (2007) Rac1 controls the formation of midline commissures and the competency of tangential migration in ventral telencephalic neurons. *Journal of Neuroscience* **27**, 3884–3893.

[298] Tang, J, Ip, J. P. K, Ye, T, Ng, Y.-P, Yung, W.-H, Wu, Z, Fang, W, Fu, A. K. Y, & Ip, N. Y. (2014) Cdk5-dependent Mst3 phosphorylation and activity regulate neuronal migration through RhoA inhibition. *Journal of Neuroscience* **34**, 7425–7436.

[299] Hur, E. M, Saijilafu, Lee, B. D, Kim, S. J, Xu, W. L, & Zhou, F. Q. (2011) GSK3 controls axon growth via CLASP-mediated regulation of growth cone microtubules. *Genes & Development* **25**, 1968–1981.

[300] Megías, M, Emri, Z, Freund, T. F, & Gulyás, A. I. (2001) Total number and distribution of inhibitory and excitatory synapses on hippocampal CA1 pyramidal cells. *Neuroscience* **102**, 527–540.

[301] Soykan, T, Schneeberger, D, Tria, G, Buechner, C, Bader, N, Svergun, D, Tessmer, I, Poulopoulos, A, Papadopoulos, T, Varoqueaux, F, Schindelin, H, & Brose, N. (2014) A conformational switch in collybistin determines the differentiation of inhibitory postsynapses. *The EMBO Journal* **33**, 2113–2133.

[302] Chiou, T.-T, Bonhomme, B, Jin, H, Miralles, C. P, Xiao, H, Fu, Z, Harvey, R. J, Harvey, K, Vicini, S, & De Blas, A. L. (2011) Differential regulation of the postsynaptic clustering of γ-aminobutyric acid type A (GABAA) receptors by collybistin isoforms. *Journal of Biological Chemistry* **286**, 22456–22468.

[303] Liang, J, Xu, W, Hsu, Y.-T, Yee, A. X, Chen, L, & Südhof, T. C. (2015) Conditional neuroligin-2 knockout in adult medial prefrontal cortex links chronic changes in synaptic inhibition to cognitive impairments. *Molecular Psychiatry* **20**, 850–859.

[304] Feng, G, Tintrup, H, Kirsch, J, Nichol, M. C, Kuhse, J, Betz, H, & Sanes, J. R. (1998) Dual requirement for gephyrin in glycine receptor clustering and molybdoenzyme activity. *Science* **282**, 1321–1324.

[305] Levy, J. M, Chen, X, Reese, T. S, & Nicoll, R. A. (2015) Synaptic Consolidation Normalizes AMPAR Quantal Size following MAGUK Loss. *Neuron* **87**, 534–548.

[306] Smith, K. R, Davenport, E. C, Wei, J, Li, X, Pathania, M, Vaccaro, V, Yan, Z, & Kittler, J. T. (2014) GIT1 and βPIX are essential for GABA(A) receptor synaptic stability and inhibitory neurotransmission. *Cell Reports* **9**, 298–310.

[307] Blümcke, I, Aronica, E, Urbach, H, Alexopoulos, A, & Gonzalez-Martinez, J. A. (2014) A neuropathology-based approach to epilepsy surgery in brain tumors and proposal for a new

terminology use for long-term epilepsy-associated brain tumors. *Acta Neuropathologica* **128**, 39–54.

[308] Thaler, J. P, Lee, S.-K, Jurata, L. W, Gill, G. N, & Pfaff, S. L. (2002) LIM factor Lhx3 contributes to the specification of motor neuron and interneuron identity through cell-type-specific protein-protein interactions. *Cell* **110**, 237–249.

[309] Matthews, J. M & Visvader, J. E. (2003) LIM-domain-binding protein 1: a multifunctional cofactor that interacts with diverse proteins. *EMBO reports* **4**, 1132–1137.

[310] Cross, A. J, Jeffries, C. M, Trewhella, J, & Matthews, J. M. (2010) LIM domain binding proteins 1 and 2 have different oligomeric states. *Journal of Molecular Biology* **399**, 133–144.

[311] Narkis, G, Tzchori, I, Cohen, T, Holtz, A, Wier, E, & Westphal, H. (2012) Isl1 and Ldb co-regulators of transcription are essential early determinants of mouse limb development. *Developmental Dynamics* **241**, 787–791.

[312] Goldberg, J. L. (2004) Intrinsic neuronal regulation of axon and dendrite growth. *Current Opinion in Neurobiology* **14**, 551–557.

[313] Wang, X, Kim, J. H, Bazzi, M, Robinson, S, Collins, C. A, & Ye, B. (2013) Bimodal control of dendritic and axonal growth by the dual leucine zipper kinase pathway. *PLoS Biology* **11**, e1001572.

[314] Wang, X, Sterne, G. R, & Ye, B. (2014) Regulatory mechanisms underlying the differential growth of dendrites and axons. *Neuroscience bulletin* **30**, 557–568.

9 Acknowledgements

Die Anfertigung dieser Doktorarbeit wäre nicht möglich gewesen ohne die großartige Unterstützung und Hilfe der verschiedensten Personen.

Zu aller erst möchte ich meinem Doktorvater Prof. Dr. Albert Becker dafür danken, dass ich an seinem Institut meine Doktorarbeit anfertigen und an diesem faszinierenden Thema arbeiten durfte. Danke für alle guten Ratschläge, Deinen inspirierenden Enthusiasmus und dass Du stets Geduld und Zeit für mich gefunden hast, um mir bei all meinen Fragen und Anliegen zu helfen. Darüber hinaus bin ich überaus dankbar für die Unterstützung und Förderung die Du mir entgegen gebracht hast, sowie die Möglichkeit mich zu einem eigenständigen Forscher zu entwickeln.

Ganz herzlich möchte ich mich bei Prof. Dr. Albert Haas bedanken, dass er die Aufgabe meines Zweitgutachters übernommen hat, sowie Prof. Dr. Frank Bradke und Prof. Dr. Gerd Bendas, dass Sie sich die Zeit genommen haben meinem Promotionskomitee beizutreten.

Desweiteren möchte ich Prof. Dr. Susanne Schoch-McGovern danken, die mit Ihrer Art sich für die Biologie zu begeistern, immer eine starke Motivationsquelle für mich war. Danke, für jeden guten Rat, für die Ideen, wissenschaftlichen Diskussionen und aufmunternde Worte wenn meine Experimente mal nicht so wollten wie ich.

Weiterhin möchte ich mich bei Prof. Dr. Heinz Beck für seine Unterstützung und Engagement bedanken unsere Forschung mit elektrophysiologischen Experimenten, vielen Ideen, Diskussionen und kritischem Lesen zu bereichern.

Ich möchte mich ebenfalls bei Prof. Dr. Dirk Dietrich bedanken der mich durch seine Ansichten und Fragen dazu gebracht hat Wissenschaft auch aus anderen Blickwinkeln zu betrachten.

Ein riesengroßer Dank geht an meinen Mann Carsten Robens ohne den ich erst gar nicht zur Wissenschaft gekommen wäre. Hättest Du mir nicht immer wieder geholfen meine eigenen Fähigkeiten zu sehen, mich mit Deinen liebevollen Worten durch frustrierende Phasen gebracht und mir mit deinen Physik- und Programmierskills beiseite gestanden, wäre meine Doktorarbeit sicherlich nicht so verlaufen wie sie es ist. Ich danke Dir, dass du für mich da bist und mir immer wieder neue Kraft und Ruhe gibst mich schweren Aufgaben zu stellen und sie als Herausforderung zu sehen.

Ich danke meiner Familie, Katharina, Elisabeth und Zbigniew Iwaniuk für das Leben, dass sie mir ermöglich haben. Ich danke Euch für eure aufmunternden Worte, permanente Unterstützung und diverse Filmabende, bei denen ich mich wieder fühlen konnte wie früher. Danke an Katharina, dass ich mich darauf verlassen konnte, dass meine große Schwester immer eine Antwort auf alle möglichen Fragen hat, ich mich jederzeit bei ihr ausweinen kann und sie Verständnis für manchmal vielleicht übertriebene kleine Weltuntergangsdramen hat.

Außerdem möchte ich auch meinen wunderbaren Kellerkinderkollegen danken.

Katrin die für mich unter Anedem durch ihren fürchterlich ansteckenden Enthusiasmus ein Vorbild ist, dass sie immer da war um über wissenschaftliche Fragestellungen zu diskutieren und Rat zu geben aber auch einfach weil sie mir als Büronachbarin und Freundin mit ihrer erfrischend anderen Art so ans Herz gewachsen ist.

J.Alex dafür, dass er nie müde geworden ist allen im Labor mit ihren technischen Problemen auszuhelfen und dabei trotzdem für den ein oder anderen Scherz (oder Klonierung) zu haben war.

Eva, Natascha, Silvia, Vanessa und Anne danke ich, dass sie mit ihrer fröhlichen, lieben und großherzigen Art das Leben im Labor so angenehm gemacht haben und mir geholfen haben meine Arbeit von Rechtschreib-fehlern und anderen Unannehmlichkeiten zu befreien. Danke liebe Natascha, dass Du mich in meinen letzten, stressigen Phasen der Doktorarbeit durch Deine Arbeit an hochkomplizierten, elektronischen Messgeräten so sehr entlastet hast.

Jule möchte ich dafür danken, dass sie mich durch ihre stetige Arbeit an Tieranträgen und Anliegen vor Arbeitslosigkeit bewahrt hat und dass sie durch ihre Keksklauerei verhindert hat, dass ich dick werde.

Alex Grote danke ich dafür, dass er mich in der hohen OP-Kunst unterwiesen hat und immer ein offenes Ohr für meine Problemchen hatte.

Ich danke Henning der mich mit seinen schlechten Witzen und Sprüchen an frustrierenden Tagen aufgeheitert hat und der mir im Laufe der Jahre ein guter Freund geworden ist.

Zudem danke ich noch Polina, Karen, Julia, Daniela, Lioba, Vivien, Indra, Ruth und besonders Sabine für eine schöne Arbeitsatmosphäre, ihre mentale sowie laborbezogene Unterstützung.

Zum Schluss möchte ich noch Sören, meinem besten Freund danken, dass er nun schon über 10 Jahre meine wuselig, hektische Art mit völlig entspannter Lässigkeit erträgt, immer zu mir steht und in allen Hinsichten ein echter Freund ist.